

**Blood Reaction Dynamics Under Shear Flow**

By

Jevgenia Zilberman-Rudenko

A DISSERTATION

Presented to the Department of Biomedical Engineering

of the Oregon Health & Science University

School of Medicine

in partial fulfillment of

the requirements for the degree of

Doctor of Philosophy

in Biomedical Engineering

March 2018

© Jevgenia Zilberman-Rudenko

All Rights Reserved

Department of Biomedical Engineering  
School of Medicine  
Oregon Health & Science University

---

CERTIFICATE OF APPROVAL

---

This is to certify that the Ph.D. Dissertation of  
Jevgenia Zilberman-Rudenko  
Blood Reaction Dynamics Under Shear Flow  
has been approved

---

Mentor: Owen J. T. McCarty, Ph.D.  
Professor of Biomedical Engineering

---

Member/Chair: András Gruber, M.D.  
Professor of Biomedical Engineering

---

Member: Martin A. Schreiber, M.D., F.A.C.S.  
Professor of Surgery

---

Member: William H. Fleming, M.D., Ph.D.  
Professor of Pediatrics and Medicine

---

Member: Monica T. Hinds, Ph.D.  
Professor of Biomedical Engineering

Dedicated to my husband, the dream-believer

## Acknowledgements

I am extremely thankful to the many people that challenged, inspired and supported me during the course of this work. There is not enough space in this dissertation to cover all aspects that I have learned and achieved during this dissertation thanks to the privilege of having these people in my life!

First and foremost, I would like to thank Dr. Owen J.T. McCarty for putting up with me and mentoring me through this process. Dr. McCarty is an expert in hemostasis and thrombosis, biorheology, imaging and assay development, who has been an incredible source of inspiration to me as an investigator and person. Dr. McCarty has been an incredible advisor to me throughout my graduate studies, and has been instrumental in my evolution as a scientist. I cannot thank you enough for the countless hours you have dedicated to help me improve and grow as a scientific and grant writer. I have further appreciated your support with my career development and many opportunities that you have allowed me to pursue, including but not limited to my trip to Johns Hopkins to learn new microfluidic techniques, my six-month research fellowship at the Scripps Research Institute, training of students and presenting at many national and international conferences. Your tireless work ethic, attention to detail and boundless energy have continually challenged and motivated me to strive for better. I am thankful and certain that the lessons I learned as part of the McCarty lab will set me for success in my next endeavors.

I have also been fortunate to receive guidance from a number of other members of Oregon Health & Science University faculty. In particular, I have learned a considerable amount from Dr. András Gruber, who possess a tremendous wisdom about science and medicine, a long history in coagulation research and pharmaceutical development as well as a keen understanding of unmet clinical need. Dr. Monica Hind has been my inspirations and a source of support for many years, including but not limited to my pre-dissertation, qualifier and this dissertation committee. Dr. Martin Schreiber is a surgeon-scientist who I aspire to become in a long term. I have learned a lot from Dr. Schreiber and his clinical research group, including nuances of trauma patient stabilization and basics of running a clinical research within a hospital. I am thankful to Dr. Harv Fleming for his enthusiasm, through-provoking questions and career advise as a



physician-scientists. I have had many memorable discussions with all of you and I truly appreciate your time, interest and effort in the critical review of this dissertation.

I would like to thank Erik Tucker, Jennifer Johnson, Christina Lorenz, Michael Wallisch, Florea Lupu (Oklahoma Medical Research Foundation), David Gailani (Vanderbilt), James Morrissey (University of Michigan), Stephanie Smith (University of Michigan) and Alvin Schmaier (Case Western Reserve University) for providing crucial reagents, thoughtful advice on my research and making translational research using non-human primates and mice a reality. I am thankful to Drs. Joseph Shatzel, Andrea Herzka, George Giraud, Frank Zhao, Megan Troxell, Michael Recht, Thomas Deloughery and Darlene Elias for teaching me about clinical research, care for the patients while mitigating risks of bleeding and thrombosis as well as work-life balance as a physician-scientist. Collectively, this incredible group of people have helped me understand how my experimental design impacts the translation of my work towards clinical outcomes and learn a tremendous amount!

My MD-PhD program and the office of graduate studies are supported by a wonderful group of people who made sure I had the support and structure throughout this endeavor. I extend my sincere thanks to Johanna Colgrove and Drs. David Jacoby, Daniel Marks, Allison Frye, Terry Morgan, Tom Scanlan, and Shoukhrat Mitalipov. Part of the reason of me joining the OHSU MD-PhD was meeting Drs. Jacoby and Fryer, a power couple who I admire as scientist as well as on a personal level.

Much of my work described in the future directions was built upon the many years of research done by groups at the Scripps Research Institute (Drs. John Griffin, Hiroshi Deguchi, Laurent Mosnier and Jose Fernandez) and the Johns Hopkins (Drs. Peter Searson and Andrew Wong). I truly appreciate these esteemed scientists for welcoming me into their scientific-homes and families and supporting my research and providing helpful insights as well as many opportunities to learn. A special thank you goes to Dr. Griffin who patiently introduced me into structure-function approach to therapy discovery, with whom I have bonded over our winding roads leading to career in research. Dr. Deguchi is an amazing MD-PhD scientist who I got a pleasure to closely work with and learn a tremendous amount from about translational

research from discovery to commercialization. Drs. Mosnier and Fernandez have been instrumental in the fibrinolysis work.

On a day-to-day basis, I was fortunate to conduct my research in a great working environment that results from working with great lab mates: Dr. Sandra Baker-Groberg, Laura Healy, Cristina Puy, Annachiara Mitrugno, Joanna Sylman, Jeevan Maddala, Rachel Rigg, Kevin Phillips, Joe Aslan, Toshiaki Shirai Maddie Midgett, Deirde Anderson, Patrick Journey, Kate Garland and Anne Rocheleau as well as all of the ‘baby’ future doctors, Chantal Wiesenekker, Anh Ngo, Stephanie Reitsma, Daniel Sallee, Graham Rykiel and Hari Lakshmanan. Sandra has facilitated my introduction to microfluidic perfusion studies. Cristina helped me find my dancing rhythm while navigating the complex networks of coagulation and life of FXI. Rachel has been a great help in editing my writing. I had a lot of fun exploring the world of biorheology and fibrin formation under shear flow with Jeevan, Joanna and Hari. We made and concurred platelet aggregates induced by cancer and inflammation with Aki and Annachiara. Laura, Annachiara and Anh would embrace me with sisterly love when I was hiding from the world. I will always cherish the moments of managing lab supplies and writing grants, as we learn all about inflammasome on the fly, with my trail mate, Laura. Our resident biochemistry guru, Jiaqing Pang, has been an incredible help with Western blots. Thank you all for being helpful and supportive co-workers my entire time at OHSU.

None of this would be possible without the tireless support of family and friends. I am thankful to my mom (Irina), dad (Aleksei), in-laws (Zinaida and Alik), all four of my sisters (Marina, Viktorija, Tatjana and Kristina) and grandparents for being unbelievably supportive, patient, and loving throughout the adventure of the past years even in the light of me not visiting them in Estonia for over 4 years. My friends have been a source of laughter and love, reminding me to always stay grounded. A special shout out goes to Kate Watson and her family for being a great support. Finally, I extend my deepest thanks to my husband, partner and best friend, Dmitriy, who has been incredibly flexible and patient with me throughout our moves around the country as we chase the magical path to my career as a physician-scientist. This dissertation is just as much yours as it is mine.

Thank you all!

# Table of Contents

|   |    |
|---|----|
| <b>Acknowledgements</b> .....   | 4  |
| <b>Table of Contents</b> .....  | 7  |
| <b>List of Figures</b> .....  | 15 |
| <b>List of Tables</b> .....   | 18 |
| <b>List of Abbreviations</b> .....  | 19 |
| <b>Abstract</b> .....   | 22 |
| <b>Chapter 1. Introduction</b> .....  | 24 |
| 1.1 <i>Synopsis</i> .....   | 24 |
| 1.2 <i>Blood biorheology and transport physics</i> .....                                      | 25 |
| 1.2.1    Poiseuille’s law and parabolic flow profile .....                                    | 25 |
| 1.2.2    Blood particles, Fåhræus and Linquist .....  | 26 |
| 1.2.3    Reynold’s number and flow type .....   | 27 |
| 1.2.4    Wall shear stress and shear rate.....  | 28 |
| 1.2.5    Thrombin mass transfer and Péclet number .....                                       | 29 |
| 1.3 <i>Coagulation overview</i> .....   | 31 |
| 1.3.1    Coagulation factors .....  | 32 |
| 1.3.2    Classic waterfall view of blood coagulation cascade .....                            | 33 |
| 1.3.3    Hemophilias, procoagulant defects and classic anticoagulants .....                   | 34 |
| 1.3.4    Classic clinical coagulation tests .....   | 37 |
| 1.3.5    Fibrinolysis basics and Thromboelastography (TEG).....                               | 38 |
| 1.3.6    Feedback loops, sepsis and development of alternative anti-coagulant therapies ..... | 41 |
| 1.4 <i>Platelet biology overview</i> .....  | 45 |
| 1.4.1    Platelet adhesion, tethering and aggregation .....                                   | 46 |

|   |  |           |
|---|--|-----------|
| 1.4.2   | Soluble platelet agonists.....                                     | 48        |
| 1.4.3   | Platelet secretion and platelet storage diseases .....             | 50        |
| 1.4.4   | Anti-platelet therapies .....                                      | 52        |
| 1.5   | <i>Vascular biology overview</i> .....                             | 53        |
| 1.5.1   | Endothelial cells overview .....                                   | 53        |
| 1.5.2   | Types of endothelial cells.....                                    | 53        |
| 1.5.3   | Blood-endothelium interface under shear flow .....                 | 54        |
| 1.5.4   | Endothelial damage and prothrombotic states.....                   | 56        |
| 1.5.5   | Utility of endothelialized microfluidic platform development ..... | 59        |
| 1.6   | <i>Thesis Overview</i> .....                                       | 60        |
| <b>Chapter 2. General Materials and Methods .....</b> |  | <b>62</b> |
| 2.1   | <i>Ethical Considerations</i> .....                                | 62        |
| 2.2   | <i>Common reagents</i> .....                                       | 63        |
| 2.3   | <i>Collection and utilization of human blood</i> .....             | 64        |
| 2.3.1   | Blood collection .....   | 64        |
| 2.3.2   | Platelet-rich and platelet-poor plasma preparation.....            | 64        |
| 2.3.3   | Washed platelet preparation .....                                  | 64        |
| 2.4   | <i>Closed system assays</i> .....                                  | 65        |
| 2.4.1   | Clotting assays .....  | 65        |
| 2.4.2   | Lipid vesicles .....   | 65        |
| 2.4.3   | Thrombin generation assay in fresh whole blood, PRP and PPP .....  | 65        |
| 2.4.4   | Activation of prothrombin by prothrombinase complex .....          | 66        |
| 2.4.5   | Plasma clot lysis .....  | 66        |
| 2.5   | <i>Open system assays</i> .....                                    | 67        |
| 2.5.1   | Ex vivo flow experiments .....                                     | 67        |
| 2.5.2   | Microscopy.....  | 67        |

|   |  |           |
|---|--|-----------|
| 2.5.3   | Western blots.....   | 68        |
| 2.5.4   | Capture of samples downstream from thrombus formation under shear flow.....                          | 68        |
| 2.5.5   | Fluorescence-activated cell sorting (FACS) of distal events.....                                     | 68        |
| 2.6   | <i>In vivo studies</i> .....   | 69        |
| 2.6.1   | Non-human primate model of thrombosis.....   | 69        |
| 2.6.2   | Assessment of distal platelet consumption in an in vivo thrombosis model.....                        | 69        |
| 2.6.3   | Non-human primate model of sepsis.....   | 70        |
| 2.6.4   | Mouse model of lethal pulmonary embolism.....  | 70        |
| <br>  |  |           |
| <b>Chapter 3. Dynamics of blood flow and thrombus formation in a multi-bypass microfluidic ladder network</b> |  | <b>72</b> |
| 3.1   | <i>Abstract</i> .....  | 72        |
| 3.2   | <i>Introduction</i> .....  | 73        |
| 3.3   | <i>Background</i> .....  | 74        |
| 3.4   | <i>Materials and Methods</i> .....   | 76        |
| 3.4.1   | Reagents.....  | 76        |
| 3.4.2   | Fabrication of mask and microfluidic device.....   | 76        |
| 3.4.3   | Coating of microfluidic devices with collagen and tissue factor.....                                 | 77        |
| 3.4.4   | Blood collection and preparation.....  | 77        |
| 3.4.5   | Ex vivo blood flow assay.....  | 78        |
| 3.4.6   | Modeling.....  | 78        |
| 3.4.7   | Statistical Analysis.....  | 83        |
| 3.5   | <i>Results</i> .....   | 83        |
| 3.5.1   | Modeling human blood flow and thrombus formation dynamics within a multi-bypass ladder network       | 83        |
| 3.5.2   | Prediction of thrombi formation within a ladder network: nucleation and evolution.....               | 84        |
| 3.5.3   | Temporal thrombus growth within a ladder network.....  | 86        |
| 3.5.4   | Prediction of the effect of thrombi formation propagation within a ladder network.....               | 87        |
| 3.5.5   | Prediction of the effect of the flow recirculation on platelet aggregation and fibrin formation..... | 89        |
| 3.5.6   | Effect of flow recirculation on platelet aggregation and fibrin formation.....                       | 90        |

|   |  |            |
|---|--|------------|
| 3.6   | <i>Discussion</i> .....  | 91         |
| <b>Chapter 4. Biorheology of platelet activation in the bloodstream distal to thrombus formation</b> .....  |  | <b>95</b>  |
| 4.1   | <i>Abstract</i> .....  | 95         |
| 4.2   | <i>Introduction</i> .....  | 96         |
| 4.3   | <i>Background</i> .....  | 96         |
| 4.4   | <i>Materials and Methods</i> .....   | 97         |
| 4.4.1   | Reagents .....   | 97         |
| 4.4.2   | Collection of human blood.....   | 98         |
| 4.4.3   | Clotting time assay .....  | 98         |
| 4.4.4   | Flow chamber assay .....   | 98         |
| 4.4.5   | Fluorescence Activated Cell Sorting (FACS)-analysis .....  | 100        |
| 4.4.6   | Simulation of thrombin mass transfer in flow distal to thrombus formation.....   | 100        |
| 4.4.7   | Statistical Analysis .....   | 101        |
| 4.5   | <i>Results</i> .....   | 102        |
| 4.5.1   | Development of a platform for the study of local and distal platelet activation.....   | 102        |
| 4.5.2   | Characterization of the effect of shear on platelet aggregation in the bloodstream.....                                      | 104        |
| 4.5.3   | Effect of distal residence time in flow on platelet activation in the bloodstream. ....                                      | 106        |
| 4.5.4   | Thrombin mass transfer in flow distal to thrombus formation. ....  | 108        |
| 4.5.5   | Characterization of inhibitors of the coagulation cascade. ....  | 110        |
| 4.5.6   | Study of local platelet deposition and aggregation on immobilized collagen. ....   | 110        |
| 4.5.7   | Study of distal platelet activation and microaggregate formation in the blood downstream of sites of thrombus formation..... | 112        |
| 4.6   | <i>Discussion</i> .....  | 114        |
| <b>Chapter 5. Coagulation factor XI promotes distal platelet activation and single platelet consumption in the bloodstream under shear flow</b> ..... |  | <b>116</b> |
| 5.1   | <i>Abstract</i> .....  | 116        |

|  |   |            |
|--|---|------------|
| 5.2  | <i>Introduction</i> .....   | 117        |
| 5.3  | <i>Background</i> .....   | 117        |
| 5.4  | <i>Materials and Methods</i> .....  | 118        |
| 5.4.1  | Reagents .....  | 118        |
| 5.4.2  | Blood collection, preparation of plasmas and clotting times.....  | 119        |
| 5.4.3  | Ex vivo flow experiments .....  | 119        |
| 5.4.4  | Microscopy.....   | 120        |
| 5.4.5  | Western blots.....  | 120        |
| 5.4.6  | FACS analysis.....  | 120        |
| 5.4.7  | In vivo thrombosis model.....   | 121        |
| 5.4.8  | Assessment of distal platelet consumption in in vivo thrombosis model .....                             | 121        |
| 5.4.9  | Data analysis .....   | 122        |
| 5.5  | <i>Results</i> .....  | 122        |
| 5.5.1  | Role of FXII and FXI in clotting times .....  | 122        |
| 5.5.2  | FXIa activity promotes local fibrin formation under shear .....   | 123        |
| 5.5.3  | Propagation of distal platelet activation and single platelet consumption under shear in flow .....     | 126        |
| 5.5.4  | FXIa activity promotes distal platelet activation and consumption in the presence of collagen and TF128 |            |
| 5.5.5  | Protection of 1A6-treated baboons from collagen-initiated distal single platelet consumption .....      | 132        |
| 5.6  | <i>Discussion</i> .....   | 133        |
| <br>   |   |            |
| <b>Chapter 6. Coagulation factor XII activity promotes platelet consumption in the presence of bacterial-type long-chain polyphosphate in blood flow <i>in vitro</i> and bacteria <i>in vivo</i></b> ..... |   | <b>136</b> |
| 6.1  | <i>Abstract</i> .....   | 136        |
| 6.2  | <i>Introduction</i> .....   | 137        |
| 6.3  | <i>Background</i> .....   | 137        |
| 6.4  | <i>Materials and Methods</i> .....  | 139        |
| 6.4.1  | Reagents .....  | 139        |

|  |   |            |
|--|---|------------|
| 6.4.2  | Development of an anti-factor XII function-blocking antibody.....   | 140        |
| 6.4.3  | Humanization of a function-blocking anti-factor XI antibody.....  | 141        |
| 6.4.4  | Enzyme-linked immunosorbent assay to quantify FXI(a) binding to (h)14E11.....   | 141        |
| 6.4.5  | Blood collection and preparation of plasmas .....   | 142        |
| 6.4.6  | Fibrin generation assay.....  | 142        |
| 6.4.7  | Clotting time assay.....  | 142        |
| 6.4.8  | Effects of 5C12 and CTI on FXIIa activity in vitro .....  | 143        |
| 6.4.9  | Ex vivo flow experiments .....  | 143        |
| 6.4.10   | Microscopy .....  | 143        |
| 6.4.11   | Western blots .....   | 144        |
| 6.4.12   | FACS analysis .....   | 144        |
| 6.4.13   | Mouse model of lethal pulmonary embolism .....  | 144        |
| 6.4.14   | Non-human primate model of sepsis .....   | 145        |
| 6.4.15   | Data analysis.....  | 145        |
| 6.5  | <i>Results</i> .....  | 146        |
| 6.5.1  | Long-chain polyP promotes platelet consumption in flowing blood.....  | 146        |
| 6.5.2  | Long-chain polyP promotes local thrombus formation on collagen surfaces.....  | 150        |
| 6.5.3  | Long-chain polyP promotes distal platelet activation and consumption in the blood flow downstream of sites of local thrombus formation..... | 153        |
| 6.5.4  | Long-chain polyP promotes distal platelet activation and consumption in the blood flow in a FXII-dependent manner .....                     | 155        |
| 6.5.5  | Long-chain polyP promotes platelet deposition and fibrin generation in vivo in a FXII-dependent manner                                      | 157        |
| 6.5.6  | Long-chain polyP-containing bacteria induce platelet and fibrinogen consumption in vivo in a FXIIa-dependent manner .....                   | 158        |
| 6.6  | <i>Discussion</i> .....   | 159        |
| <b>Chapter 7. Effect of pneumatic tubing system transport on stored platelet concentrate units .....</b> |   | <b>163</b> |



|       |  |     |
|-------|--|-----|
| 7.1   | <i>Abstract</i> .....  | 163 |
| 7.2   | <i>Introduction</i> .....  | 164 |
| 7.3   | <i>Background</i> .....  | 164 |
| 7.4   | <i>Materials and Methods</i> .....   | 166 |
| 7.4.1 | Materials and Reagents .....   | 166 |
| 7.4.2 | Procurement and handling of stored platelet concentrate units .....                              | 166 |
| 7.4.3 | Human whole blood collection and preparation of concentrated platelet rich plasma and serum..... | 168 |
| 7.4.4 | Preparation of washed platelets and supernatants from stored PC units or fresh cPRP .....        | 168 |
| 7.4.5 | Platelet activation and microaggregate detection .....   | 169 |
| 7.4.6 | Flow chamber assay .....   | 170 |
| 7.4.7 | Immunoblot determination of VWF.....   | 170 |
| 7.4.8 | Statistics .....   | 170 |
| 7.5   | <i>Results</i> .....   | 171 |
| 7.5.1 | Physical parameters of platelet concentrate sample handling .....                                | 171 |
| 7.5.2 | Effect of transport on platelet activation and aggregation.....                                  | 173 |
| 7.5.3 | Effect of PC unit supernatant on freshly prepared platelet activation and aggregation.....       | 175 |
| 7.5.4 | Effect of stored PC unit handling on platelet binding to collagen and VWF under shear.....       | 177 |
| 7.5.5 | Effect of PC unit handling on levels of platelet GPIb receptor and VWF forms .....               | 178 |
| 7.6   | <i>Discussion</i> .....  | 179 |

**Chapter 8. Design and utility of a point-of-care microfluidic platform to assess hematocrit and blood coagulation 182**

|     |                                    |     |
|-----|------------------------------------|-----|
| 8.1 | <i>Abstract</i> .....              | 182 |
| 8.2 | <i>Introduction</i> .....          | 183 |
| 8.3 | <i>Background</i> .....            | 183 |
| 8.4 | <i>Materials and Methods</i> ..... | 185 |
| 8.5 | <i>Results</i> .....               | 189 |

|  |   |            |
|--|---|------------|
| 8.5.1  | Design of a microfluidic platform for use with blood samples .....  | 189        |
| 8.5.2  | Microfluidic platform with anticoagulated whole human blood sample .....  | 190        |
| 8.5.3  | Estimation of microfluidic platform voltage sensitivity to hematocrit.....  | 191        |
| 8.5.4  | Sensitivity of the microfluidic platform to hematocrit .....  | 193        |
| 8.5.5  | Sensitivity of the microfluidic platform to coagulation.....  | 194        |
| 8.6  | <i>Discussion</i> .....   | 196        |
| <b>Chapter 9. Discussion and Future Directions .....</b> |   | <b>200</b> |
| 9.1  | <i>Discussion</i> .....   | 200        |
| 9.1.1  | Limitations .....   | 200        |
| 9.1.2  | Conclusions .....   | 202        |
| 9.2  | <i>Discovery of novel pro-coagulant and pro-thrombotic molecules</i> .....  | 207        |
| 9.2.1  | Prothrombotic skeletal muscle myosin directly enhances prothrombin activation by binding factors Xa and Va  | 208        |
| 9.2.2  | Role of cardiac myosin promoting thrombin generation and tissue plasminogen activator-induced plasma clot lysis.....  | 212        |
| 9.3  | <i>Development of microfluidic platforms to study blood reaction dynamics at the vessel wall</i> .....  | 216        |
| 9.3.1  | Removal of the C-terminal domains of ADAMTS13 by activated coagulation factor FXI induces platelet adhesion on endothelial cells under flow conditions..... | 216        |
| 9.3.2  | Development of a new 3D-endothelialized microfluidic model to study hemostasis.....   | 221        |
| <b>REFERENCES.....</b>                                   |   | <b>227</b> |
| <b>Biographical Sketch .....</b>                         |   | <b>270</b> |
| <b>Curriculum Vitae .....</b>                            |   | <b>271</b> |
| <b>RESEARCH PUBLICATIONS .....</b>                       |   | <b>273</b> |

## List of Figures

|  |     |
|--|-----|
| Figure 1.1 Schematic of a vessel with different spaces and aspects involved in perfusion maintenance and disturbance. .... | 24  |
| Figure 1.2 Parabolic flow profile of blood.....  | 26  |
| Figure 1.3 Role of blood components (blood coagulation factors and platelets) in hemostasis. ....                          | 31  |
| Figure 1.4 Classic view of generalized coagulation pathways. ....  | 33  |
| Figure 1.5 The fibrinolytic system and inhibition by TAFIa.....  | 38  |
| Figure 1.6 Thromboelastography (TEG) set up and read out.....  | 39  |
| Figure 1.7 Clinical thromboelastography (TEG) before and after Tranexamic acid intravenous (IV) infusion. ....             | 40  |
| Figure 1.8 Feedback loops and potential therapeutic targets.....   | 43  |
| Figure 1.9 Platelets in flowing blood.....   | 45  |
| Figure 1.10 Platelet structure.....  | 45  |
| Figure 1.11 Platelet adhesion and aggregation under shear flow. ....   | 46  |
| Figure 1.12 Platelet agonists.....   | 48  |
| Figure 1.13 Blood-endothelium interface.....   | 55  |
| Figure 3.1 Modeling human blood flow and thrombus formation dynamics within a multi-bypass ladder network .....            | 77  |
| Figure 3.2 Quantification of the spatial distribution of thrombus formation.....   | 78  |
| Figure 3.3 Prediction of thrombus formation within the ladder network: nucleation and evolution.....                       | 81  |
| Figure 3.4 Temporal thrombus growth within ladder network .....  | 86  |
| Figure 3.5 Prediction of the effect of thrombus formation within a ladder network .....                                    | 88  |
| Figure 3.6 Prediction of the effect of the flow recirculation on platelet aggregation and fibrin formation .....           | 89  |
| Figure 3.7 Effect of flow recirculation on platelet aggregation and fibrin formation.....                                  | 90  |
| Figure 3.8 An integrated approach to study thrombus formation within a microfluidic network. ....                          | 92  |
| Figure 4.1 The schematic of the flow chamber and FACS analysis.....  | 103 |
| Figure 4.2 Effect of shear on local platelet aggregate formation and distal platelet activation. ....                      | 105 |
| Figure 4.3 Effect of distal residence time in flow on platelet activation in the bloodstream. ....                         | 107 |
| Figure 4.4 Thrombin mass transfer in flow distal to thrombus formation. ....   | 109 |
| Figure 4.5 14E11, 1A6, and rivaroxaban prolonged the plasma clotting time.....   | 110 |

Figure 4.6 14E11, 1A6, and rivaroxaban did not affect local platelet aggregate formation under flow..... 111

Figure 4.7 FXI and FXa inhibitors abrogated distal platelet CD62P expression and microaggregate formation under shear..... 113

Figure 5.1 Role of FXII and FXI in clotting times. .... 122

Figure 5.2 FXIa activity promotes local fibrin formation under shear..... 124

Figure 5.3 FXIa activity promotes local thrombus formation in the presence of collagen and/or TF..... 125

Figure 5.4 Propagation of distal platelet activation and single platelet consumption under shear in flow. .... 126

Figure 5.5 Presence of collagen and TF promotes distal platelet consumption. .... 128

Figure 5.6 FXIa activity promotes distal platelet activation and consumption in the presence of collagen and / or low levels of TF..... 129

Figure 5.7 FXIa activity in local and distal platelet aggregation in the presence of VWF, Fibrinogen and Thrombin coated surfaces. .... 130

Figure 5.8 FXIa activity promotes distal platelet activation and consumption in the presence of collagen and TF under arterial shear rate. .... 131

Figure 5.9 Protection of 1A6-treated baboons from collagen-initiated distal single platelet consumption..... 132

Figure 6.1 Long-chain polyP promotes platelet consumption in flowing blood..... 147

Figure 6.2 Long-chain polyP promotes local thrombus formation on collagen surfaces. .... 149

Figure 6.3 Role of long-chain polyP in platelet aggregation on collagen and VWF under shear..... 151

Figure 6.4 Long-chain polyP as a surface activator of fibrin formation under shear..... 152

Figure 6.5 Long-chain polyP promotes fibrin formation and clotting of platelet poor plasma..... 152

Figure 6.6 Long-chain polyP promotes distal platelet activation and consumption in the blood flow downstream of sites of local thrombus formation. .... 154

Figure 6.7 Long-chain polyP promotes distal platelet activation and consumption in the blood flow in a FXII-dependent manner. .... 156

Figure 6.8 Long-chain polyP promotes platelet deposition and fibrin generation *in vivo* in a FXII-dependent manner. .... 157

Figure 6.9 Long-chain polyP-containing bacteria induce platelet and fibrinogen consumption *in vivo* in a FXIIa-dependent manner..... 158

Figure 6.10 Cartoon of Hypothesis. .... 161

|  |     |
|--|-----|
| Figure 7.1 A flow chart of an experimental PC unit handling procedure.....   | 167 |
| Figure 7.2 Physical parameters of PC unit handling. ....   | 172 |
| Figure 7.3 Fresh platelet activation and microaggregation.....   | 173 |
| Figure 7.4 Effect of transport on platelet activation and aggregation.....   | 174 |
| Figure 7.5 Effect of PC unit supernatant on fresh platelet activation and aggregation.....   | 176 |
| Figure 7.6 Effect of PC unit handling on platelet binding to collagen and VWF under shear.....   | 177 |
| Figure 7.7 Effect of PC unit handling on levels of platelet GPIb receptor and VWF forms. ....  | 178 |
| Figure 8.1 Design of a microfluidic platform for use with blood samples. ....  | 189 |
| Figure 8.2 Microfluidic platform with anticoagulated whole human blood sample. ....  | 190 |
| Figure 8.3 Estimation of microfluidic platform voltage sensitivity to hematocrit.....  | 192 |
| Figure 8.4 Sensitivity of the microfluidic platform to hematocrit.....   | 194 |
| Figure 8.5 Sensitivity of the microfluidic platform to coagulation. ....   | 195 |
| Figure 8.6 Schematic of possible blood measurements and result readouts. ....  | 198 |
| Figure 9.1 Fibrin deposition and platelet aggregation on myosin.....   | 209 |
| Figure 9.2 Skeletal muscle myosin promotes thrombin generation in platelet rich plasma and platelet poor<br>plasma. ....   | 210 |
| Figure 9.3 Anti-myosin antibody-induced reduction of thrombin peak values observed for acute trauma<br>coagulopathy plasmas and normal control plasmas following tissue factor/ $Ca^{2+}$ ion addition. .... | 211 |
| Figure 9.4 Thrombin generation can be driven by prothrombin activation on the surface of myosin which binds<br>FXa & FVa. ....   | 211 |
| Figure 9.5 Cardiac myosin promotes <i>ex vivo</i> thrombus formation in flowing blood. ....  | 213 |
| Figure 9.6 Cardiac myosin attenuates tPA-induced plasma clot lysis. ....   | 214 |
| Figure 9.7 Proteolysis of ADAMTS13 by FXIa. ....   | 217 |
| Figure 9.8 Spider <sup>JZR</sup> culture system. ....  | 218 |
| Figure 9.9 FXIa inhibits ADAMTS13 cleavage of VWF.....   | 219 |
| Figure 9.10 FXIa, thrombin and plasmin inhibit ADAMTS13 cleavage of VWF. ....  | 220 |
| Figure 9.11 Quantitative permeability studies.....   | 224 |
| Figure 9.12 The role of inflammation on platelet-endothelium interface under shear flow in 3D chamber .....  | 226 |

## List of Tables

|   |     |
|---|-----|
| Table 1.1 Fluid viscosity. ....   | 27  |
| Table 1.2 Velocity parameters in arteries and veins. ....   | 28  |
| Table 1.3 Hemodynamic and transport parameters in the human vasculature. ....                                       | 29  |
| Table 1.4 Causes of a prolonged prothrombin time (PT) and/or a prolonged activated thromboplastin time (aPTT). .... | 37  |
| Table 1.5 Primary content of platelet granules. ....  | 50  |
| Table 1.6 Overview of platelet storage diseases. ....   | 51  |
| Table 1.7 The effect of the physical biology of blood flow on the endothelium and platelets. ....                   | 58  |
| Table 7.1 Description of platelet concentrate samples used in the study. ....                                       | 168 |
| Table 7.2 Physical parameters of platelet concentrate sample handling. ....   | 171 |
| Table 9.1 Summary of perfusable endothelialized models. ....  | 222 |

## List of Abbreviations

|          |  |
|----------|--|
| ADAM10   | a disintegrin and metalloproteinase domain-containing protein 10       |
| ADAMTS13 | a disintegrin and metalloproteinase with a thrombospondin type 1 motif |
| ADP      | adenosine diphosphate  |
| AMB      | ambulatory (human courier) transport                                   |
| APC      | activated protein C  |
| aPTT     | activated partial thromboplastin time                                  |
| ATIII    | antithrombin   |
| ATP      | adenosine triphosphate   |
| BSA      | bovine serum albumin   |
| BSS      | Bernard-Soulier syndrome   |
| cAMP     | cyclic adenosine monophosphate   |
| CD62P    | P-selectin   |
| COX      | cyclooxygenase   |
| CPI      | carboxypeptidase inhibitor from tubers                                 |
| cPRP     | concentrated platelet-rich plasma                                      |
| CRP      | collagen-related peptide   |
| CTI      | corn trypsin inhibitor   |
| Da       | Dahmköhler number  |
| DIC      | Disseminated intravascular coagulation                                 |
| ECM      | extracellular matrix   |
| FACS     | fluorescence-activated cell sorting                                    |
| FII      | coagulation factor II (prothrombin)                                    |
| FIIa     | activated coagulation factor II (thrombin)                             |
| FV       | coagulation factor V (zymogen)   |
| FVa      | activated coagulation factor V   |

|        |  |
|--------|--|
| FVII   | coagulation factor VII (zymogen)                   |
| FVIIa  | activated coagulation factor VII                   |
| FVIII  | coagulation factor VIII (zymogen)                  |
| FVIIIa | activated coagulation factor VIII                  |
| FIX    | coagulation factor IX (zymogen)                    |
| FIXa   | activated coagulation factor IX                    |
| FX     | coagulation factor X (zymogen)                     |
| FXa    | activated coagulation factor X                     |
| FXI    | coagulation factor XI (zymogen)                    |
| FXIa   | activated coagulation factor XI                    |
| FXII   | coagulation factor XII (zymogen)                   |
| FXIIa  | activated coagulation factor XII                   |
| GPCR   | G-protein coupled receptor                         |
| GPIb   | glycoprotein Ib                                    |
| GPVI   | glycoprotein VI                                    |
| ICAM-1 | intercellular adhesion molecule 1 (CD54)           |
| ID     | immunodeficiency                                   |
| Ig     | immunoglobulin                                     |
| INR    | international normalized ratio of PT values        |
| ITAM   | immunoreceptor tyrosine-based activation motif     |
| MMP    | matrix metalloproteinase                           |
| PAR    | protease-activated receptor                        |
| PC     | platelet concentrate                               |
| PDGF   | platelet-derived growth factor                     |
| PDMS   | polydimethylsiloxane                               |
| PECAM  | platelet endothelial cell adhesion molecule (CD31) |



|                  |   |
|------------------|---|
| PF4              | platelet factor 4   |
| PGI <sub>2</sub> | prostacyclin  |
| PKC              | protein kinase C  |
| polyP            | polyphosphate   |
| PPACK            | Phe-Pro-Arg-chloromethylketone, protease inhibitor                      |
| PPP              | platelet-poor plasma  |
| PPXbd            | recombinant polyP-binding domain from <i>E. coli</i> exopolyphosphatase |
| PRP              | platelet-rich plasma  |
| PS               | phosphatidylserine  |
| PT               | prothrombin time  |
| PTS              | pneumatic tubing system   |
| TAFI             | thrombin-activateable fibrinolysis inhibitor                            |
| TEG              | thromboelastography   |
| TF               | tissue factor   |
| TNF $\alpha$     | tumor necrosis $\alpha$   |
| tPA              | tissue plasminogen activator  |
| TRAP-6           | thrombin receptor-activating peptide 6                                  |
| TxA <sub>2</sub> | thromboxane A <sub>2</sub>  |
| VCAM-1           | vascular cell adhesion protein 1  |
| VWF              | von Willebrand factor   |

## Abstract

### Blood Reaction Dynamics Under Shear Flow

Jevgenia Zilberman-Rudenko

Department of Biomedical Engineering  
School of Medicine  
Oregon Health & Science University

March 2018

Thesis Advisor: Owen J. T. McCarty, Ph.D.

The formation of a hemostatic plug to staunch blood loss at sites of vascular injury relies on the dynamical processes of activation of the coagulation cascade and platelet recruitment in the setting of the biorheology of blood flow. Thus, elucidation of the molecular mechanisms of thrombus formation *ex vivo* relies on the use of biomedical engineering principles to design platforms to study complex enzymatic reactions and cell biology under physiologically relevant shear flow conditions. The focus of this dissertation work is the development and testing of microfluidic platforms to study blood reaction dynamics in health and disease. The ultimate goal of this work is to expand our understanding of the (patho)physiology of thrombosis and hemostasis and determine how can we intervene with one without compromising the other.

In an intact healthy vessel, platelets travel within laminar flow in a quiescent form. Upon vessel injury, resting platelets are recruited to the exposed extracellular matrix under shear flow, followed by platelet adhesion and activation as part of the hemostatic plug formation. Aberrant geometries of extracorporeal blood oxygenators and thrombus formation within damaged vessels can change the biorheology of blood affecting distribution of blood components and reactants within the bloodstream and lead to platelet activation within flowing blood. In order to evaluate the effect of a thrombin generation at a local site of thrombus formation on a platelet activation in the blood flow distal to local site of thrombus formation, two novel *ex vivo* flow models were developed: (1) a microfluidic ladder network to mimic complexities of thrombus formation evolution in a multi-bypass system and (2) a

single channel flow model to mimic a local site of vascular injury in combination with the downstream collection of blood samples to allow for the analysis of distal platelet activation, microaggregate formation and single platelet consumption in flowing blood. Utilizing an integrated computational and experimental approach, the work herein shows that the initial local sites of thrombus formation promotes distal platelet activation, aggregation and consumption in a network geometry and in flowing blood in a shear- as well as residence time-dependent manner.

Thrombosis and hemostasis appear to separate mechanistically upstream of coagulation factor (F)XI, as FXI and FIX deficiency cause mild and severe hemophilia, respectively, while FXII deficiency is asymptomatic. FXI-deficient humans are largely protected from deep vein thrombosis and ischemic stroke. Furthermore, inhibition of FXI activation by activated FXII(a) improves survival in mice with peritoneal sepsis or listeriosis. Results described in this dissertation identify the role of FXI activation by FXIIa in thrombin generation and platelet aggregation at a local site of thrombus formation. Distal to the local site of thrombus formation, FXI activation by FXIIa promotes platelet activation and consumption in flowing blood. Moreover, FXII activity promotes platelet consumption in the presence of bacterial-type long-chain polyphosphate in blood flow *in vitro* and bacteria *in vivo*.

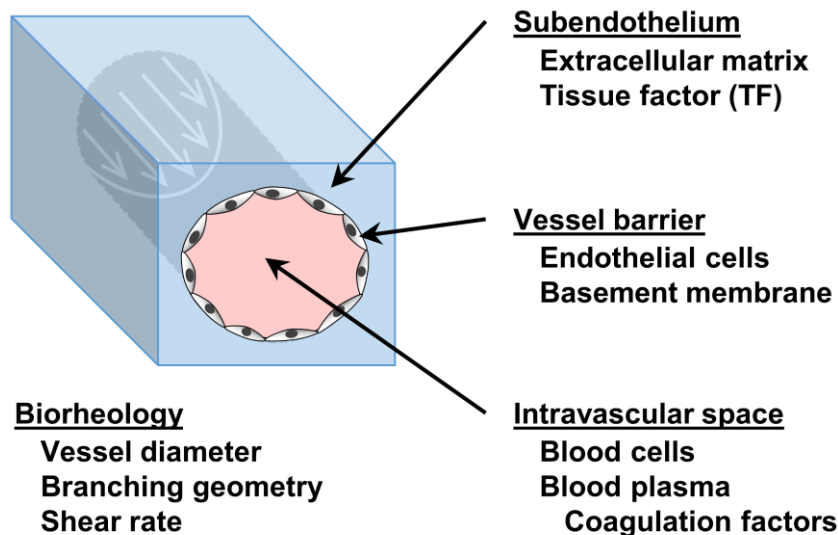
Clinically, it is important to be able to rapidly assess hemostasis in emergency situations as well as utilize effective therapeutic agents to mitigate bleeding and thrombotic risks. In order to facilitate mechanistic studies of platelet physiology in the context of blood flow, we have developed several computational and experimental approaches to study platelet and coagulation function under shear. In the last part of the dissertation we utilize tools developed to: (1) assess whether the mode of transport of platelet concentrate units within a hospital affects their function, as pertinent to their use in transfusion medicine, and (2) develop a new point-of-care microfluidic platform to assess clinically important blood parameters of hemostasis and thrombosis.

Collectively, this dissertation provides new study platforms and insights into the blood reaction dynamics under shear flow.

## Chapter 1. Introduction

### 1.1 Synopsis

Hemostasis is an active process between blood cells and blood plasma proteins under shear flow, resulting in thrombin generation, platelet activation and fibrin formation to generate a hemostatic plug that staunches blood loss following vessel injury. Thrombosis is a (patho)physiological process of blood reactions associated with life-threatening complications such as perfusion compromise. While the enzymatic reactions that mediate hemostasis are orchestrated outside the lumen of the blood vessel, including the subendothelium and endothelial layer, thrombosis reactions progress within the lumen of the blood vessel (Figure 1.1). The long-term goal of my work is to attain mechanistic understanding of these processes with the ultimate objective of identifying safe and efficacious therapeutic targets to maintain perfusion by preserving hemostasis while preventing thrombosis in select disease settings. In this chapter, we will explore fundamental aspects of blood biorheology, coagulation activation, platelet biology and endothelial cell function in the dynamic balance of hemostasis and thrombosis in select settings. The last section of this chapter (section 1.6) contains the overview of this thesis.



**Figure 1.1** Schematic of a vessel with different spaces and aspects involved in perfusion maintenance and disturbance.  
© Jevgenia Zilberman-Rudenko

## 1.2 Blood biorheology and transport physics

Consider a simple homogenous solution (sugar water) entering a circular pipe or a channel at a uniform velocity. Such fluid motion will be influenced by the diameter, geometry and surface of the pipe system, the pressure applied and a set viscosity of the fluid. Blood is a much more complex fluid that consists of a cell suspension in a viscous medium (plasma), all of which exist in a dynamic state of change depending on the different aspects affecting blood biorheology, blood cell deformability as well as pulsatile and circular pressure. This section will describe basics of blood biorheology concepts, all of which should be taken with the caveat of assumptions made to derive simplistic estimates of this intricate substance behavior in human vasculature. Note, the pulsatile flow of blood and blood cell deformability (specifically red blood cells, RBC) complicate all laws of biorheology described and as such are not taken into the account in the described relationships between physical parameters.

### 1.2.1 Poiseuille's law and parabolic flow profile

Assuming a blood entry at a uniform velocity and a no-slip condition, the fluid particles (blood cells; Section 1.2.2) in the layer in contact with the surface of the pipe (also known as boundary layer) tend to slow down or even stop due to friction experienced at the surface of the pipe (Section 1.2.3). The layers adjacent to the boundary layer will further gradually slow down as a result of inter-layer friction. Per Newton's First Law, the bulk flow rate through the pipe should remain constant, thus the velocity of the fluid at the center of the pipe has to increase proportionally (Figure 1.2).

This is the basis of the Poiseuille's law, which predicts that in a straight vessel (or a channel) with a uniform radius of  $r_i$ , the velocity profile of a fluid (e.g. blood) follows a parabolic distribution (Figure 1.2); where the velocity ( $v_r$ ) for different concentric 'layers' of blood is directly proportional to the pressure drop over the length of channel ( $\Delta P/l$ ), the radius ( $r_i$ ) of the channel, the location of 'layer' with respect to the center ( $r$ ) of the channel and reciprocal of the bulk viscosity ( $\mu$ ) of blood.

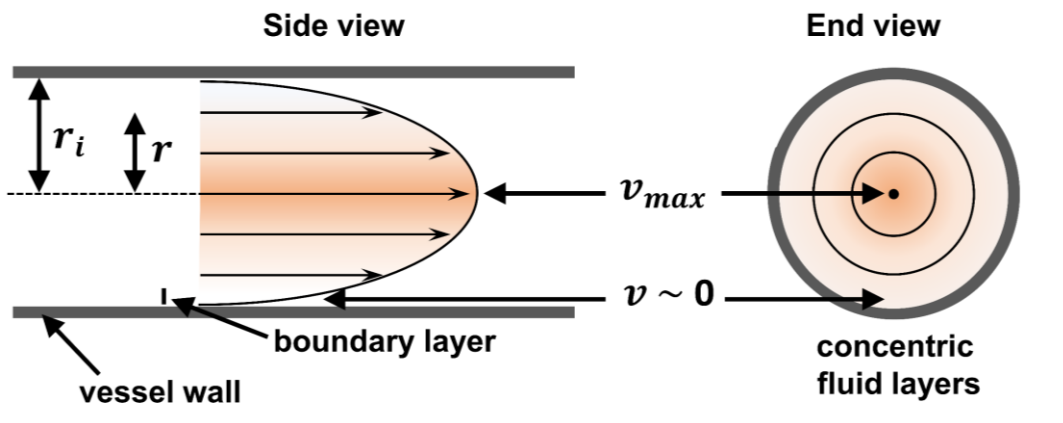
The Poiseuille's law assumes that blood is a Newtonian non-compressible fluid and thus can be described with the following equation[1,2]:

$$v_r = \frac{\Delta P (r_i^2 - r^2)}{4\mu l}$$

This predicts that the velocity of blood particles at the center of the channel is the fastest ( $v_{max}$ ):

$$v_{max} = (\Delta P/l) \cdot r_i^2/4\mu$$

The mean velocity, found at approximately  $0.7r_i$ , is  $\sim v_{max}/2$ . The steady bulk blood flow rate ( $Q$ ) is directly proportional to mean velocity and the cross-sectional area of the channel.



**Figure 1.2 Parabolic flow profile of blood.**

Figure adapted from Klabunde, Cardiovascular Physiology Concepts, 2nd ed., Lippincott Williams & Wilkins 2012.  
© Jevgenia Zilberman-Rudenko

### 1.2.2 Blood particles, Fåhræus and Linquist

The most abundant cell type (~99%) in the blood is the RBC. In humans, blood RBC content (hematocrit) ranges from 36-54 percent of blood volume, which translates to  $4.7-6.1 \times 10^6$  cells/ $\mu$ L.[3] RBCs play a critical role of supplying tissues with oxygen and nutrients as well as removal of the toxins (e.g. carbon dioxide). Human RBCs are anucleate corpuscles with a special biconcave disk shape with a diameter that ranges from 5.5 to 8.8  $\mu$ m and thickness of 2  $\mu$ m at the periphery and 1  $\mu$ m at the center.[4] This specific shape, elasticity and deformability, are important for RBC ability to circulate through the reticuloendothelial system and small diameter capillaries (< 3  $\mu$ m) as well as facilitate a radially-directed margination of platelets to the boundary layer (Figure 1.2) at the vessel wall.[5-8]

RBC flow within the bloodstream follows the Fåhræus effect, which predicts that, depending on the diameter of the vessel, RBCs will tend to migrate to the channel centerline and form a core that flows faster as compared to the rest of the blood and specifically plasma and platelets.[5–11] This behavior contributes to a special Fåhræus-Linquist effect that applies to vasculature of 10 – 300  $\mu\text{m}$ , which predicts that the viscosity of the blood is directly proportional to the diameter of the vessel. Thus, smaller vasculature such as capillaries and arterioles should have a lower apparent viscosity. Note, the majority of the *ex vivo* studies described in this dissertation will explore blood behavior in capillary channels of approximate diameter of 10 – 360  $\mu\text{m}$ .

### 1.2.3 Reynold's number and flow type

In laminar (from *Latin* ‘lami’ - thin layer or sheet) flow, the bulk flow rate ( $Q$ ) of the blood is directly proportional to the pressure gradient ( $\Delta P$ ). In turbulent flow, the flow rate is proportional to the square root of the pressure gradient. The turbulence of flow is predicted by the Reynolds number ( $Re$ ), a dimensionless quantity in fluid mechanics described with equation below:[12]

$$Re = \frac{\text{Inertial forces}}{\text{Viscous forces}} = \frac{\rho VD}{\mu}$$

where  $\rho$  is pressure ( $\text{N/m}^2$ ) applied and  $\mu$  is fluid bulk viscosity ( $\text{mPa}\cdot\text{s}$ ; Table 1.1).  $V$  and  $D$  are a fluid characteristic velocity and distance; which in a uniform solid pipe (or channel) translates to an average fluid velocity and the pipe (or channel) diameter, respectively.

The bulk viscosity of whole blood with a hematocrit of 45 percent is about four times higher than that of water (Table 1.1). Bulk viscosity of blood goes up with higher levels of hematocrit, which can be a contributing factor for thrombo-embolic complications and has been shown to associate with poor perfusion and oxygenation of heart muscle.[13]

| Fluid                                   | $\mu$<br>( $\text{mPa}\cdot\text{s}$ ) |
|---|--|
| Water (0°C)                             | 1.8                                    |
| Water (20°C)                            | 1.0                                    |
| Water (100°C)                           | 0.3                                    |
| Whole blood (37°C)<br>Hematocrit of 45% | ~4.0                                   |
| Blood plasma (37°C)<br>Hematocrit of 0% | ~1.5                                   |
| Engine oil (AE10)                       | ~200                                   |
| Air                                     | 0.018                                  |

**Table 1.1 Fluid viscosity.**  
© Jevgenia Zilberman-Rudenko

The laminar flow tends to be most prominent at low Reynolds numbers ( $< 2000$ ), whilst the turbulence of flow emerges at higher Reynolds numbers ( $> 4000$ ), with transitional flow in between.[14] For instance, blood flow may be more turbulent in a large diameter artery, such as an ascending aorta (Table 1.2 and Table 1.3), with a rapid flow in a patient with low hematocrit (anemia). Branching of vasculature with rapid changes in vessel diameter may also lead to disturbance in flow e.g., when a narrower vessel widens to a larger one. A vessel plaque or an atheroma that alters vessel diameter and malleability of a vessel may further cause turbulent flow. Generally, healthy arterioles and capillaries are assumed to have laminar flow (Table 1.2),[15] and as per Section 1.2.1 lower apparent viscosity.

| Vessel / Special condition | Peak velocity (cm/s) | Mean velocity (cm/s) | Reynolds # (peak) | Pulse propagation velocity (cm/s) |
|----------------------------|----------------------|----------------------|-------------------|-----------------------------------|
| <i>Ascending aorta</i>     | 20 – 290             | 10 – 40              | 4500              | 400 – 600                         |
| <i>Descending aorta</i>    | 25 – 250             | 10 – 40              | 3400              | 400 – 600                         |
| <i>Abdominal aorta</i>     | 50 – 60              | 8 – 20               | 1250              | 700 – 600                         |
| <i>Femoral artery</i>      | 100 – 120            | 10 – 15              | 1000              | 800 – 1030                        |
| <i>Carotid artery</i>      | 50 – 150             | 20 – 30              |                   | 600 – 1100                        |
| <i>Arteriole</i>           | 0.5 – 1.0            |                      | 0.09              |                                   |
| <i>Capillary</i>           | 0.02 – 0.17          |                      | 0.001             |                                   |
| <i>Inferior vena cava</i>  | 15 – 40              |                      | 700               | 100 - 700                         |

**Table 1.2 Velocity parameters in arteries and veins.**

Data adapted from Caro et al., *Cardiovasc Res* 1974. © Jevgenia Zilberman-Rudenko

#### 1.2.4 Wall shear stress and shear rate

At the boundary layer, the vessel wall will experience shearing deformation due to the interaction of a moving layer (blood) and a stationary layer (vessel wall). A type of frictional force exerted on a vessel wall by flowing blood is termed wall shear stress. Wall shear stress is directly proportional to fluid bulk viscosity ( $\mu$ ; Table 1.1) and steady bulk blood flow rate ( $Q$ ) and is inversely proportional to the radius ( $r_i$ ) of the channel to the third power. For this estimate, blood is assumed to act as Newtonian fluid with shear rate directly proportional to shear stress. The shear rate is defined as a ratio of fluid layer (‘moving plate’) velocity to the distance between the layer and the wall.



Under normal physiological conditions, wall shear stresses of human vasculature range from 1 to 60 dynes/cm<sup>2</sup>[2,5,16] and normal shear rate ranges from 20 to 2,000 s<sup>-1</sup> (Table 1.3).[1,2,5,17–19] Clinically, wall shear stress can be estimated by measuring blood flow using non-invasive imaging, such as ultrasound or magnetic resonance imaging. Shear stress plays a physiological role in the cardiovascular system by affecting (patho)physiologic gene expression and development of cardiovascular structures as well as blood-forming stem cells.[20,21]

| Vessel / Special condition | Shear rate (s <sup>-1</sup> ) | Shear stress (dyne/cm <sup>2</sup> ) | Diameter (mm) | Function   |
|----------------------------|-------------------------------|--------------------------------------|---------------|--|
| Ascending aorta            | 300                           | 2 – 10                               | 25            | Blood from heart   |
| Large arteries             | 300 – 800                     | 10 – 30                              | 1.0 – 4.0     | Distribution of oxygenated blood                           |
| Small arteries             |                               |                                      |               | Distribution and resistance (pressure and flow regulation) |
| Coronary artery (LCA/RCA)  | 300 – 1500                    | 10 – 60                              | 0.2 – 1.0     |  |
| Carotid artery             | 250                           | 10                                   |               |  |
| Arterioles                 | 500 – 1600                    | 20 – 60                              | 0.2 – 1.0     | Resistance   |
| Capillaries                | 200 - 2000                    | NA                                   | 0.006 – 0.010 | Gas exchange   |
| Post-capillary venules     | 50 – 200                      | 1 – 2                                | 0.01 – 0.20   | Exchange and collection                                    |
| Veins                      | 20 – 200                      | 0.8 – 8                              | 0.2 – 5.0     | Blood volume   |
| Coronary stenosis (LAD)    | 5000 – 100000                 |                                      |               |  |
| Deep vein thrombosis (DVT) | 0 – 200                       |                                      |               |  |

**Table 1.3 Hemodynamic and transport parameters in the human vasculature.**

Data adapted from Brass and Diamond, *J Thromb Haemost* 2016 and Klabunde, *Cardiovascular Physiology Concepts*, 2nd ed., Lippincott Williams & Wilkins 2012; LCA – left circumflex artery, RCA – right circumflex artery, LAD – left anterior descending artery. © Jevgenia Zilberman-Rudenko

In *ex vivo* flow experiments, to mimic a specific shear rate condition, shear rate is estimated by dividing average linear velocity of blood (derived from flow rate setting on a pump) and height of the microfluidic channel (space between two solid plates).

### 1.2.5 Thrombin mass transfer and Péclet number

The rate of platelet activation, aggregation and fibrin formation in an environment of flowing blood is a balance between the delivery of reactants (platelets and coagulation factors) to the local site of vascular injury relative to the rate of assembly and (in)activation of coagulation factors on the activated platelet surface.[22] The availability of soluble molecules, such as thrombin, at the site of the

local thrombus formation or in the bloodstream distal to sites of thrombus formation is dependent on the molecule mass transfer in flowing fluid.

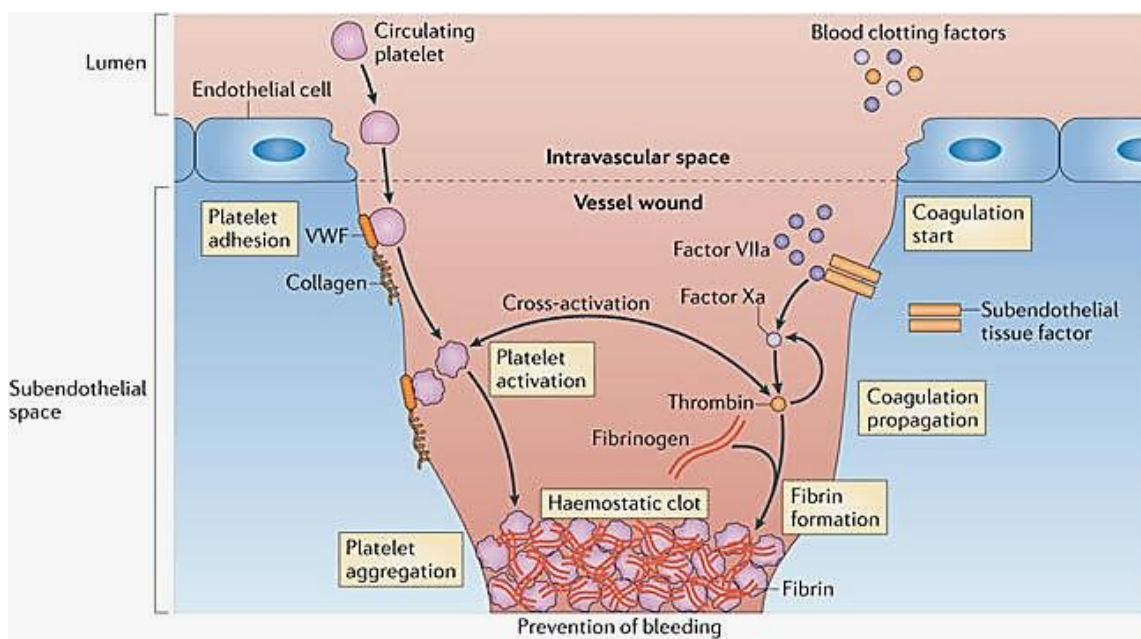
The Péclet number ( $Pe$ ), a dimensionless quantity that characterizes the relative importance of diffusion (molecule dispersal mostly perpendicular to velocity streamlines) to convection (molecule dispersal mostly parallel to/with velocity streamlines).[23–25] In a microfluidic platform, the Péclet number is directly proportional to a diameter of the channel multiplied by the corresponding fluid layer velocity and inversely proportional to the molecule diffusion coefficient. Diffusion dominates in settings where  $Pe < 1$ , whilst convection dominates in settings where  $Pe > 1$ . Applied experimental examples of this topic can be found in Chapter 3 and Chapter 4 of this dissertation.

The assumption of thrombin mass transfer relevance in vasculature is that thrombin remains active in the bloodstream. Thrombin is known to be rapidly inactivated by plasma inhibitors such as antithrombin (ATIII) and heparin cofactor II;[26–28] on the other hand, thrombin catalyzes its own feedback generation through activation of the coagulation factor XI (Section 1.3). Thus, these regulation pathways should be taken into account as appropriate.

### 1.3 Coagulation overview

One of the coagulation field pioneers, Earl W. Davie, PhD, refers to solidified blood clot formation as one of the most unusual and remarkable properties of blood.[29] Whole human blood is a suspension of blood cells (particles) and blood plasma (fluid). Blood plasma is packed with coagulation factors that upon activation can change the state of the fluid from liquid to nearly a solid in a process referred to as clotting. In this setting, plasma, platelets, vasculature and tissue molecules all collaborate to produce a clot in a regulated manner. For instance, activated (or damaged) platelets expose a membrane phospholipid, phosphatidylserine, which was shown to support clotting reactions.

The process of coagulation has been studied for centuries with initial discoveries starting in the mid- to late-1800s.[29–33] These discoveries led to a classic view of physiologic process of hemostasis where coagulation factors collaborate with platelets (Section 1.4) and vascular cells (Section 1.5) to form an extraluminal fibrin-rich platelet plug to staunch blood loss (Figure 1.3).[29,34] It was also discovered that the same players are involved in the pathological process of thrombosis whereby platelets and coagulation factors collaborate to make aggregates within the intravascular space associated with clinically significant thrombo-embolic complications.[35]



**Figure 1.3 Role of blood components (blood coagulation factors and platelets) in hemostasis.** Engelmann and Massberg., *Nat Rev Immunol* 2013; Reprinted with permission.

Distinction of these two processes, organ perfusion saving (hemostasis) vs. perfusion jeopardizing (thrombosis), has been the saga of many scientists from then on. This section will cover the basics of coagulation factors (section 1.3.1), the historic view of the coagulation cascade (section 1.3.2), hemophilias, procoagulant defects and standard anticoagulants (section 1.3.3), classic clinical coagulation tests (section 1.3.4), basics of fibrinolysis and thromboelastography (section 1.3.5) and, lastly, new findings altering the view of coagulation cascade and opening potential directions for the development of novel anticoagulants (section 1.3.6).

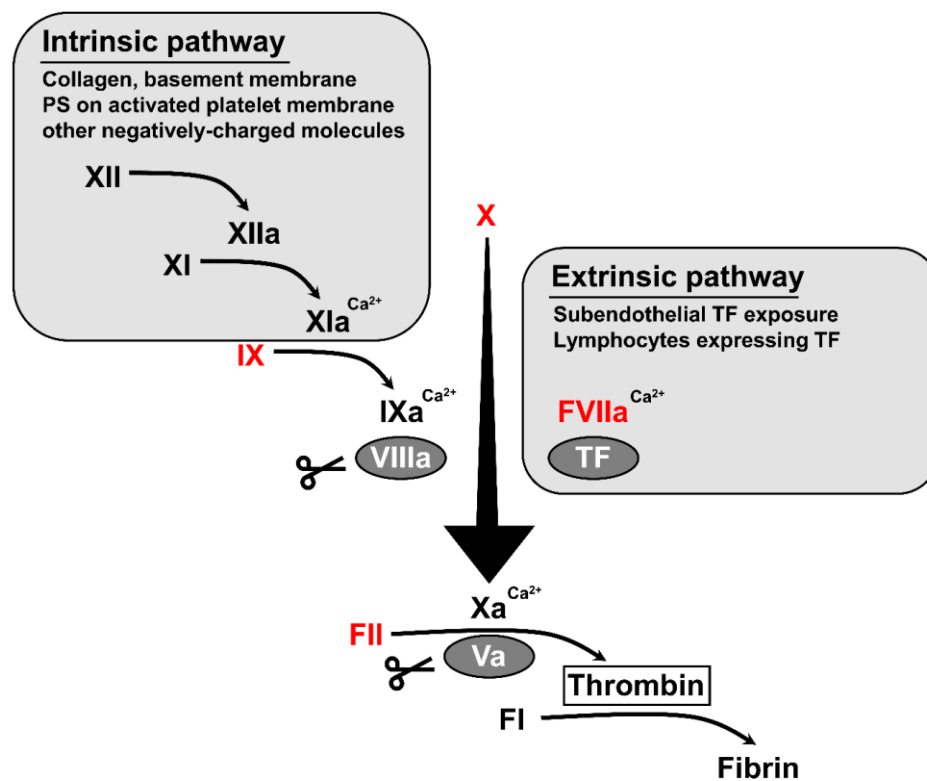
### 1.3.1 *Coagulation factors*

Each coagulation factor exists in blood as an inactive enzyme precursor (zymogen) denoted with a Roman numeral (e.g. coagulation factor XII, FXII). Most of the coagulation factors are serine proteases and thus, upon activation, these enzymes are able to activate the next respective zymogen in a “cascading” series of reactions (more on this in the next section 1.3.2). The activated coagulation factors are denoted with a lowercase ‘a’ (e.g. FXIIa).[36] Some special coagulation factors include tissue factor (TF or FIII), FV and FVIII which are glycoproteins that participate in reactions more as co-factors rather than enzymes.[29,36–38] Factor XIII is a transglutaminase that facilitates crosslinking and polymerization of activated fibrin monomers.[36] FI is fibrinogen.

All coagulation factors, except FVIII, are produced by liver. FVIII is manufactured by healthy endothelial cells. Coagulation factor function depends on a number of parameters and molecules. Vitamin K is generated in the small intestine and is reduced by hepatic (produced in liver) Vitamin K epoxide reductase. The reduced form of Vitamin K facilitates gamma-carboxylation of glutamic residues of FII (prothrombin), FVII, FIX, FX, protein C, S and Z, producing mature gamma-carboxyglutamic (GLA) domains which are responsible for these coagulation factors' ability to bind to phospholipids and calcium.[39,40]

### 1.3.2 Classic waterfall view of blood coagulation cascade

The classic view of the coagulation cascade contains two coagulation activation pathways (extrinsic and intrinsic) which converge into a common coagulation pathway and ultimately lead to thrombin generation and fibrin formation (Figure 1.4).[41] The extrinsic pathway is considered the principal pathway of coagulation activation *in vivo*.[42] The extrinsic pathway is initiated by tissue factor (TF) exposure in the presence of vessel injury or TF-bearing lymphocyte infiltration.[42–44] In the extrinsic pathway, coagulation factor VII (FVII) forms an activated complex with TF (FVIIa:TF) and activates coagulation factor X (FX). Coagulation FXa then binds prothrombin (FII) and FV forming the prothrombinase complex, cleaving prothrombin to thrombin. In the contact activation pathway, factor XII (FXII) is converted to activated protease FXIIa in the presence of negatively charged molecules.[45] FXIIa then catalyzes the activation of FXI, subsequently leading to activation of FIX and ultimately thrombin generation (Figure 1.4).



**Figure 1.4 Classic view of generalized coagulation pathways.**  
Adapted from Gailani and Renné, *ATVB* 2007; Factors in red have a GLA-domain and require reduced Vitamin K (Warfarin-sensitive); Filled ellipse around a factor denotes co-factor function; Scissors indicate targets of proteolytic regulation by APC.  
© Jevgenia Zilberman-Rudenko

Thrombin converts plasma soluble fibrinogen (FI) into an insoluble fibrin mesh by cleaving fibrin peptides A and B from fibrinogen (FI) thus revealing sites for fibrin polymerization by FXIII. Thrombin further promotes self-regulation by activating protein C, a process that is more efficient in the presence of endothelial thrombomodulin (TM; more in Section 1.5.3) and endothelial protein C receptors (EPCRs).[46,47] Activated protein C (APC) is a well-known cytoprotective protein, which among other things plays an important role in regulating coagulation.[48] Upon activation, APC acts as a serine protease and proteolytically inactivates FVa and FVIIIa (scissors; Figure 1.4).[49] A naturally occurring mutation, Factor V Leiden, protects FVa from being deactivated by APC putting patients with this mutation at thrombotic risk.[50,51]

Antithrombin (ATIII) is a naturally-occurring anticoagulant. ATIII is a serine protease that is produced by liver and circulates in plasma. ATIII inhibits thrombin, FXIIa, FXIa, FIXa, and FXa.[52] In the presence of heparin, ATIII is also able to inhibit the FVIIa:TF complex.[53,54] In the presence of heparin, the rate of ATIII-thrombin inactivation increases approximately 2000 to 4000 fold (to  $\sim 1.5 - 4 \times 10^7 \text{ M}^{-1} \text{ s}^{-1}$ ),[55–58] ATIII-FXa inhibition increases approximately 500 to 1000 fold,[55,58] and ATIII-FIXa inhibition increases approximately 1 million fold.[59]

### 1.3.3 *Hemophilias, procoagulant defects and classic anticoagulants*

Circulating plasma proteins play an important role in the delicate balance between hemostasis and thrombosis. Congenital deficiency of FVIII or FIX, hemophilia A and B respectively, both are associated with severe bleeding risks and require rather costly as well as sometimes dangerous therapeutic strategies. Coagulation factor replacement is the first line of treatment for hemophilia A and B, yet these have a risk for developing inhibitory antibodies.[60,61] Hemophilia A and B patients are affected early in life and amongst other things these patients undergo significant counseling and social adjustments to mitigate risks of bleeding e.g. due to a simple accident on a playground.

Congenital deficiency of FXI, also known as hemophilia C, typically causes mucosal bleeding symptoms or presents as increased bleeding in patients who have undergone a surgical procedure yet without significant correlation between remaining FXI levels and bleeding symptoms.[62] Notably, unlike hemophilia A and B, hemophilia C frequently remains undetected without provocation (e.g. dental extraction) and maybe only noted as a potential in the presence of an aberrant test result (Section 1.3.4 and Table 1.4) in an otherwise healthy individual. Congenital FXII deficiency is asymptomatic and presents with no bleeding diathesis except as marked on a coagulation test (Section 1.3.4 and Table 1.4)

Factor V Leiden is a hypercoagulable disorder due to mutation in FV making FVa resistant to inhibition by activated protein C.[50,51] Factor V Leiden mutation is autosomal dominant and is the most common hereditary coagulation disorder amongst ethnic Europeans.[63–65] Common presentation of Factor V Leiden is a woman with a history of unprovoked venous thromboembolism (VTE) during a pregnancy.[66]

There are a number of oral anticoagulants, colloquially known as blood thinners, that have been used clinically for mitigating the risk of thrombo-embolic complications, such as deep venous thrombosis (DVT) and pulmonary embolism (PE), in medically ill, postsurgical patients and patients with atrial fibrillation.[67,68] For the past fifty years, warfarin (Coumadin®) has remained as one of the most prescribed anticoagulants.[69] Similar to a well-known rodenticide (Coumarin), warfarin acts as a vitamin K reductase antagonist and thus affects maturation of FII, FVII, FIX, FX and protein C/S and Z GLA domains.

The variable pharmacokinetics and pharmacodynamics of warfarin make it somewhat challenging to maintain within a therapeutic range, which necessitates close monitoring of patients on warfarin (Table 1.4).[67–72] Besides mild to severe bleeding risks,[67,73,73–76] warfarin side-effects include a rare yet severe warfarin-induced skin necrosis, which has to do with an acquired protein C deficiency.[77] Most patients with non-valvular atrial fibrillation requiring long term anticoagulation

still receive warfarin. Warfarin effects can be reversed as needed for urgent procedures with vitamin K, fresh frozen blood plasma, prothrombin complex concentrates and recombinant factor

VII.[68,71,78,79]

Relatively new to the market, non-warfarin oral anticoagulants (NOACs) also known as direct oral anticoagulants (DOACs) are becoming more popular in the clinic. Dabigatran (Pradaxa®) is a direct thrombin inhibitor,[68,80,81] which has been approved for the reduction of risk of stroke and systemic embolism in patients with non-valvular atrial fibrillation for the treatment of DVT and PE in patients and for the reduction of the risk of recurrence of DVT and PE in previously treated patients.[82] Rivaroxaban (Xarelto®) and apixaban (Eliquis®) are both direct FXa inhibitors, which have been approved for stroke prevention in non-valvular atrial fibrillation as well as treatment and prophylaxis of VTE after elective major joint replacement surgery.[83,84] Fondaparinux (Arixtra®) is a synthetic pentasaccharide that acts as an indirect FXa and is administered via a subcutaneous injection. Fondaparinux has been shown beneficial for post-operative DVT prevention,[85–88] yet its use is limited due to the potential of bleeding.[85,89]

Heparin is another classic anticoagulant used in hospitals for prevention and mitigation of VTE. Heparin is a naturally occurring anticoagulant produced by basophils and mast cells.[90] Unfractionated heparin is made from porcine intestine and contains sulfated glycosaminoglycans of variable size.[91] Heparins act by enhancing ATIII activity (Section 1.3.2) and have been shown to be more effective than warfarin for post-operative prevention of VTE.[92–94] While overall safe, extended use of heparins (mostly of unfractionated type) can lead to a delay in fracture healing, osteoporosis and thrombocytopenia.[94–96] Low molecular weight heparins, such as enoxaparin (Lovenox®), have largely replaced unfractionated heparin use due to higher safety and ability to administer these via subcutaneous injection.[97]



### 1.3.4 Classic clinical coagulation tests

Clinical coagulation tests, such as the prothrombin time (PT) and activated partial thromboplastin time (aPTT) are frequently used to assess blood clotting function in patients. These tests are performed by assessing clotting of isolated platelet poor plasma (PPP) in the presence of known activators of coagulation cascade in a closed and mixed test system. For PT, the reaction is initiated via either the extrinsic pathway by a lipidated tissue factor (TF) or Innovin®. For aPTT, the reaction is initiated via the intrinsic pathway by silica or ellagic acid. Upon initiation, plasma gelation is detected once a steel bead suspended in the plasma stops moving and time to plasma gelation is marked. PT and aPTT times range between 11-14 seconds and 25-35 seconds, respectively. PT of an individual patient can further be expressed as the normalized ratio comparing the PT of a patient to the normal control in an international normalized ratio (INR); INR ranges 0.8 – 1.2.

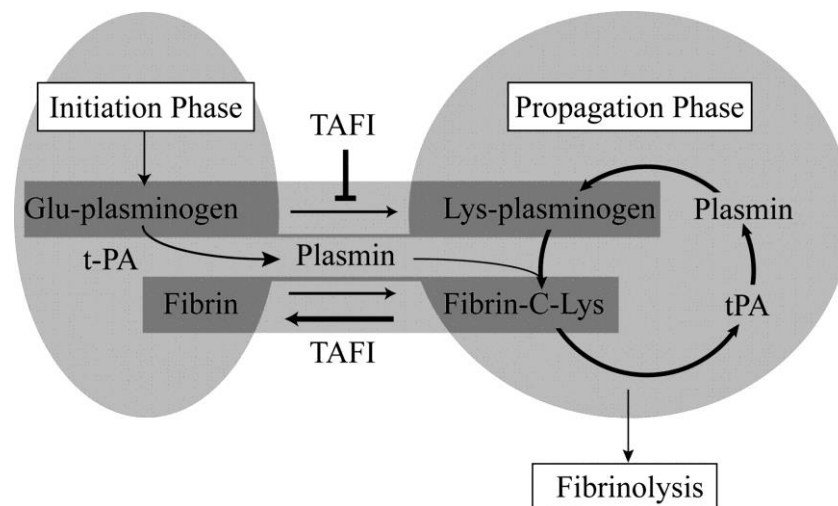
These tests can thus provide helpful information about defects in either extrinsic, intrinsic or common coagulation pathways by pinpointing specific coagulation factor deficiencies, disease progression or monitoring the drug effects of anticoagulant therapy (Table 1.4).

| Setting   | PT                  | aPTT       | Notes   |
|---|---------------------|------------|---|
| <i>Hemophilia A or B</i>                                | Normal              | Prolonged  | Congenital FVIII or FIX deficiency, severe bleeding   |
| <i>Hemophilia C</i>                                     | Normal              | Prolonged  | Congenital FXI deficiency, mild/provoked bleeding     |
| <i>FXII, PK, or HMWK deficit</i>                        | Normal              | Prolonged  | Asymptomatic, no bleeding diathesis                   |
| <i>Factor V Leiden</i>                                  | Normal              | Normal     | FV resistant to activated protein C                   |
| <i>Lupus 'anticoagulant'</i>                            | Normal              | Prolonged* | *associated with thrombosis rather than bleeding      |
| <i>VWF disease</i>                                      | Normal              | Prolonged  | FVIII is normally protected by VWF                    |
| <i>FVII deficiency</i>                                  | Prolonged           | Normal     | Rare, 1 : 500,000                                     |
| <i>Acquired FVII inhibitor</i>                          | Prolonged           | Normal     | Etiology varies                                       |
| <i>Warfarin<sup>PO</sup></i>                            | Prolonged           | Normal     | Inhibition or deficiency of reduced Vitamin K:        |
| <i>Malabsorption, liver disease</i>                     | Prolonged           | Normal     | immature FII, FVII, FIX, FX, protein C, S and Z       |
| <i>Liver failure</i>                                    | Prolonged           | Prolonged  | Deficiency of all coagulation factors                 |
| <i>Dabigatran<sup>PO</sup>, Argatroban<sup>PO</sup></i> | Prolonged           | Prolonged  | Direct thrombin inhibitor                             |
| <i>Rivaroxaban<sup>PO</sup>, Apixaban<sup>PO</sup></i>  | Prolonged           | Prolonged  | Direct FXa inhibitors                                 |
| <i>Fondaparinux<sup>SubQ</sup></i>                      | Prolonged           | Prolonged  | Indirect FXa inhibitor                                |
| <i>Heparin<sup>IV</sup>, Enoxaparin<sup>SubQ</sup></i>  | Normal <sup>‡</sup> | Prolonged  | ATIII enhancer: inhibits FIIa, FXIIa, FXIa, FIXa, FXa |

**Table 1.4 Causes of a prolonged prothrombin time (PT) and/or a prolonged activated thromboplastin time (aPTT).**  
 Data adapted from ©2018 UpToDate. Note: many anticoagulants affect common pathway factors and can prolong both the PT and the aPTT if present at high enough levels; Administration routes: PO – oral, IV – intravenous, SubQ – subcutaneous.  
<sup>‡</sup>- PT-reagents contain heparin-blocking agents. © Jevgenia Zilberman-Rudenko

### 1.3.5 Fibrinolysis basics and Thromboelastography (TEG)

Fibrinolysis is a regulatory process in blood by which formed fibrin-rich platelet aggregates are digested in vasculature.[98] Endothelial cells (Section 1.5) release tissue plasminogen activator (tPA) to initiate limited conversion of plasminogen into plasmin (Figure 1.5).[99] Plasmin then promotes the amplification of additional plasminogen conversion from inactive protein (plasminogen) to active protease (plasmin; Figure 1.5). A whole separate dissertation can be written on fibrinolysis and in fact has been by Dr. Laurent O. Mosnier, whom I got to work with during my recent fellowship at the Scripps Research Institute, La Jolla, CA (Section 9.2.2). Fibrinolysis is a highly regulated and complex process involving molecules and cells. To mention one, thrombin activatable fibrinolysis inhibitor (TAFIa) inhibits fibrinolysis by abrogating plasmin-mediated auto-feedback loops designed to generate a burst of plasmin formation. TAFIa achieves this by removing C-terminal lysine residues of fibrin which act as a template onto which both tPA and plasminogen bind thereby enhancing the catalytic efficiency of plasmin formation. Furthermore, TAFIa inhibits conversion of Glu-plasminogen to Lys-plasminogen, a better substrate for tPA.[99]

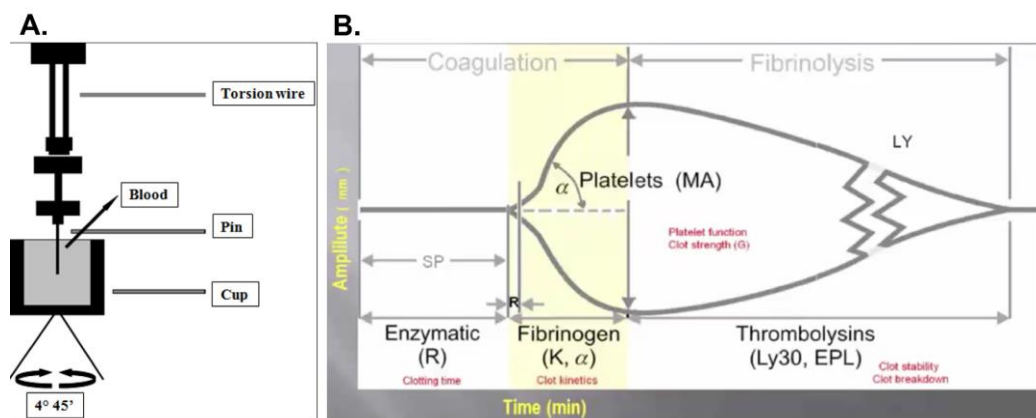


**Figure 1.5 The fibrinolytic system and inhibition by TAFIa.**

During the initiation phase of fibrinolysis, limited amounts of plasmin are generated. These small amounts of plasmin are not sufficient to degrade the fibrin clot but enable fibrinolysis to progress into its propagation phase. Plasmin promotes transition of fibrinolysis into the propagation phase by truncating Glu-plasminogen into Lys-plasminogen and by limited proteolysis of fibrin, thereby creating fibrin with C-terminal lysine residues (fibrin-C-Lys). Both of these positive feedback mechanisms are opposed by TAFIa. Subsequent plasmin-mediated proteolysis of the fibrin clot into soluble fibrin degradation products occurs on progression of fibrinolysis into the propagation phase. TAFIa inhibits fibrinolysis by opposing the transition of fibrinolysis into the progression phase. Mosnier and Bouma, *ATVB* 2006; Reprinted with permission.

In the clinic, fibrinolysis or thrombolysis can be initiated pharmacologically by infusion of tPA. The decision to incorporate this intervention into routine medical practice, however, includes a number of barriers and considerations (some of these will be described in section 9.2.2).[100,101] Inversely, hyperfibrinolysis (e.g. in the setting of disseminated consumptive coagulopathy, DIC, in sepsis or in some cases of severe trauma) can be reversed with antifibrinolytic therapies such as tranexamic acid (Lysteda®). Tranexamic acid was originally discovered in 1962 in Japan and has been in use in United States for over 20 years.[102] Tranexamic acid, a synthetic analog of amino acid lysine, acts by reversibly binding and saturating lysine receptors on plasminogen, thus preventing plasminogen and plasmin docking on fibrin (Figure 1.5).[103] Use of tranexamic acid has shown benefit in mitigating bleeding diathesis in patients with hemophilia or platelet storage defects,[104–106] and decreasing risk of death by halting bleeding post child birth[107] or traumas associated with severe bleeding.[108,109]

Thromboelastography (TEG) is a closed system method of testing viscoelastic properties of a clot. TEG has been primarily used in surgery and anesthesiology and is now becoming a standard of care test in some of the trauma centers to assess the aspects of the whole blood clot formation and lysis.[108,110] In a TEG test, a torsion wire suspends a pin immersed in the cup filled with whole blood and the viscoelastic clot measurements are taken as the cup rotates and reactions progress in the blood (Figure 1.6A).



**Figure 1.6 Thromboelastography (TEG) set up and read out.**  
Adapted from da Luz et al., *Scand J Trauma Resusc Emerg Med* 2013;

A typical TEG profile is shown in Figure 1.6B, where: R (min) is time of latency from the start of the test to initial fibrin formation; K (min) is the time it takes to achieve a certain level of clot strength (amplitude of 20 mm), angle ( $\alpha$ , degrees) measures the speed fibrin builds up and cross linking takes place, maximum clot amplitude (MA, mm) represents the ultimate strength of the fibrin clot and LY30 is the percentage decrease in the MA at 30 minutes post-MA and gives a measure of the degree of fibrinolysis.[111]

Figure 1.7 shows a real example of the clinical TEG utility; panel A shows a baseline TEG of a trauma patient with a suspected sepsis/DIC and panel B shows a TEG of the same patient after one

hour of tranexamic acid infusion (values for pertinent TEG measures are summarized in the table below graphs, with values out of range highlighted in red). In this example, the patient at baseline appears hypercoagulable (short R, steep angle) and hyperfibrinolytic (increased LY30) on TEG. The infusion of tranexamic acid corrects LY30 and potentially hyperfibrinolytic state[103] of the patient. Interestingly, infusion of a fluid furthermore stabilizes the procoagulant TEG-phenotype of the patients (R, K and angle change), which may suggest either basal hypercoagulability due to dehydration or dilutional coagulopathy after infusion. This patient received continuous monitoring for bleeding and clotting with repeated tests and exams at intensive care unit.

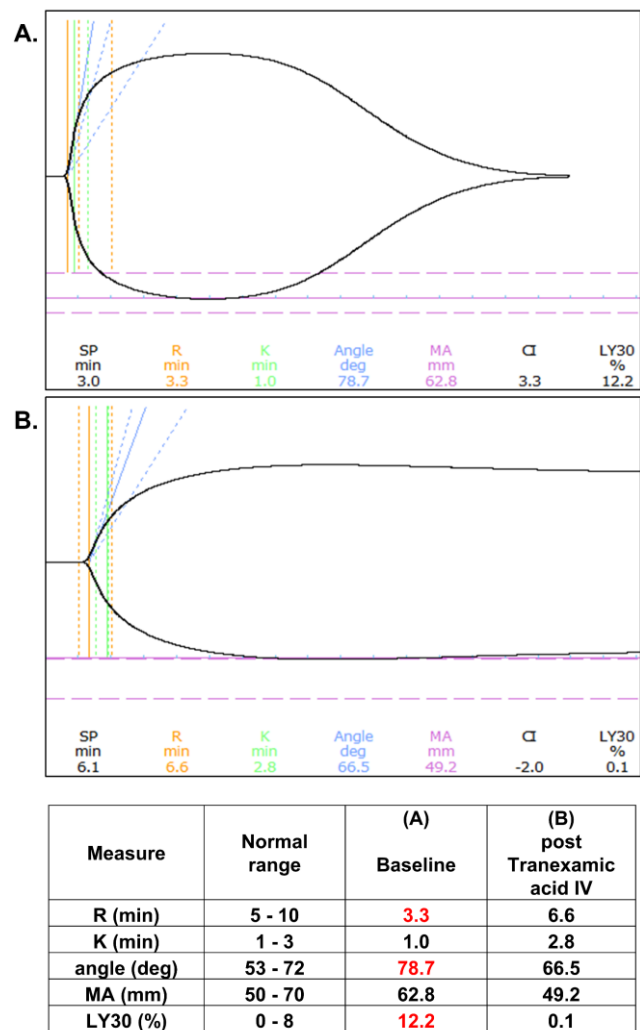


Figure 1.7 Clinical thromboelastography (TEG) before and after Tranexamic acid intravenous (IV) infusion.

© Jevgenia Zilberman-Rudenko

### 1.3.6 *Feedback loops, sepsis and development of alternative anti-coagulant therapies*

Thrombosis and hemostasis appear to separate mechanistically upstream of coagulation factor XI (FXI), as FXI and coagulation factor IX (FIX) deficiency cause mild and severe hemophilia, respectively, but coagulation factor XII (FXII) deficiency is asymptomatic. Clinically, congenital FXI deficiencies were reported to exhibit protection from ischemic stroke and exhibit a lower incidence of venous thromboembolism (VTE),[112,113] while elevated levels of FXI are an independent risk factor for VTE and ischemic stroke.[114,115]. Thus, inhibition of FXI activation by activated FXII(a) could help prevent thrombotic complications in settings where contact activation of the coagulation may be prevalent.

Both FXI and FXII facilitate clot formation through auxiliary mechanisms besides the well-established intrinsic or contact pathway (Section 1.3.2). For instance, FXIa is able to enhance thrombin generation independently of FXII when the extrinsic pathway of coagulation is initiated with small concentrations of TF.[116–118] More specifically, FXI can be feedback activated by thrombin and can also feedback to activate itself. Moreover, besides activating FIX, FXIa can directly activate FV and FVIII, weakly stimulate FX,[117,119,120] and inactivate tissue factor pathway inhibitor (TFPI), *in vitro*,[121] to promote thrombin generation. These alternative pathways may explain in part why mice lacking both FIX and FXI are more resistant to chemical injury-induced arterial thrombosis than mice deficient in FIX alone,[122] and why experimental thrombosis is reduced in mice lacking the contact pathway factors FXII, HK, PK, or FXI.[122]

Sepsis is an infection-induced systemic inflammatory response syndrome that typically progresses to insufficient organ perfusion and death within hours to days when left untreated.[123,124] Thirteen percent of the intensive care unit patients end up developing sepsis and about a quarter of these patients die after being subjected to a whirlwind of interventional procedures.[125,126] Mostly supportive treatment is complicated by fulminant disseminated intravascular consumptive coagulopathy (DIC), a deadly complication of sepsis characterized by concomitant thrombotic

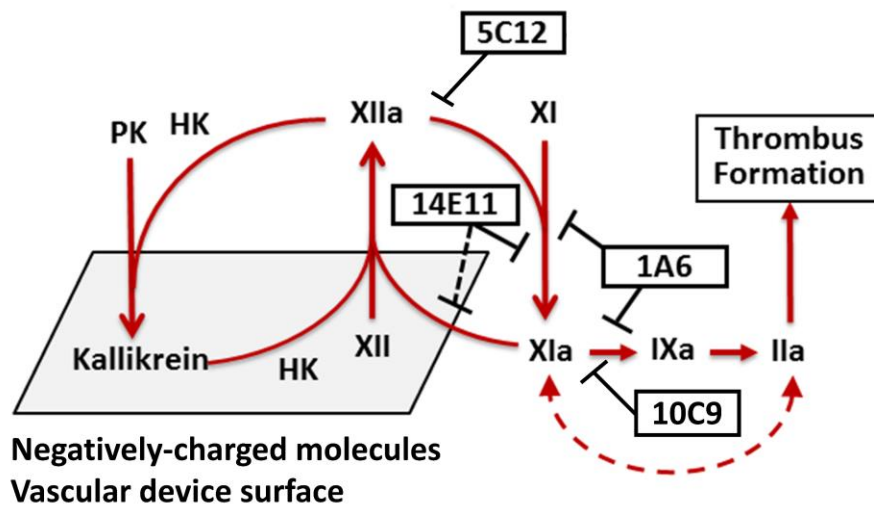
complications and bleeding due to thrombin generation amplification leading to platelet consumption.[127] In an attempt to both reduce pathologic thrombin generation and support the failing hemostatic system, patients are given transfusions of blood components combined with broad-spectrum anticoagulants (such as heparin; Section 1.3.3), which target all modes of thrombin generation; yet, this approach has not shown benefit in clinical trials.[128,129]

One of the therapies that was tried for sepsis was the recombinant form of activated protein C (APC). APC exerts its anticoagulant effects by proteolytically inactivating FVa and FVIIIa (Figure 1.4, section 1.3.2). Thus, by inhibiting these co-factor functions, APC limits the efficiency of thrombin generation by both coagulation pathways.[49] APC is also a well-known cytoprotective and anti-inflammatory protein and has been shown to stabilize endothelial cell junctions (section 1.5) important for maintenance of the blood-vessel barrier and to moderate levels of pro-inflammatory molecules such as histones.[48,130] APC showed promise in non-human primate models of sepsis where infusion of exogenous protein C was in the setting of *E. coli* infection.[131] In a double-blind clinical trial recombinant APC (Drotrecogin alfa or Xigris®) showed reduction in mortality with a slight increase in bleeding in patients with systemic inflammation and organ failure due to sepsis.[132] The potential of this trial led to the commercialization of APC by Eli Lilly and Company in 2001 under the brand name Xigris®. On October 25, 2011, Xigris® was withdrawn from the market due to the preliminary results of a large, multi-center clinical trial that demonstrated a lack of efficacy compared to placebo as well as an increased risk of bleeding.[133–135] One reason for the discrepancy between the initial clinical data and the PROWESS-SHOCK trial has been attributed to the reduced sepsis mortality due to better standards of care as well as poor inclusion selection by physicians. Nonetheless, systemic infusion of APC as a treatment for sepsis is no longer considered a clinically beneficial treatment strategy.

Our group has shown that FXI-deficiency or inhibition of FXI activation by FXIIa decreases inflammatory responses and platelet consumption as well as improves survival of mice with certain experimental infections, or at the least did not adversely affect the course of disease progression in the

presence of certain bacterial species.[136,137] Meanwhile, a broad-spectrum anticoagulant warfarin and Xigris® were detrimental in similar models of sepsis. Thrombin generation and fibrin formation are important for pathogen clearance. Our group found that fibrinogen-deficient mice, mice engineered to express low levels of TF or wild-type mice treated with warfarin all displayed reduced survival, increased bacterial burden, and exacerbated hemorrhagic pathology following intranasal challenge with *Yersinia pestis*; FXI deficiency did not result in survival benefit in *Y. pestis*-induced plagueas compared to wild-type mice.[138]

These and other findings are blurring the lines between the two classic coagulation pathways (Section 1.3.2) with FXI activation emerging as an important step for hemostasis and thrombosis, especially in the settings where blood gets exposed to foreign surfaces e.g. extracorporeal oxygenator networks. To further interrogate the FXIIa/FXIa axis in different settings, our group has developed a number of novel monoclonal antibodies (Figure 1.8).[139–141]



**Figure 1.8 Feedback loops and potential therapeutic targets.**

5C12 is a FXIIa active site domain-neutralizing antibody; 14E11 blocks FXI activation by FXIIa; 1A6 blocks both FXI activation by FXIIa and FIX activation by FXIa; 10C9 is a FXIa active site domain-neutralizing antibody.

© Jevgenia Zilberman-Rudenko

Using these novel tools, we found that FXI activation by FXIIa plays an important role in local thrombus formation and platelet activation and consumption in the bloodstream distal to site of thrombus formation under shear flow (more on this in Chapter 4 and Chapter 5). Inhibition of FXI

activation by FXIIa improves survival in mice with peritoneal sepsis or listeriosis[136] and prevents collagen-coated vascular graft occlusion in a non-human primate model of thrombosis.[142]

Furthermore, recently a clinical study demonstrated that reducing FXI levels with an anti-sense oligonucleotide served as an effective anticoagulation regimen for preventing postoperative VTE,[143] and one of our antibodies (humanized 14E11 or Xisomab) has shown significant benefit in an established model of bacterial sepsis in non-human primates[144] as well as has been approved for a phase 1 clinical trial (ClinicalTrials.gov Identifier: NCT03097341) with the future goal of preventing VTE in dialysis population. Together, these findings suggest that FXI activation by FXIIa may be an efficacious and safe target of anticoagulation in specific settings.

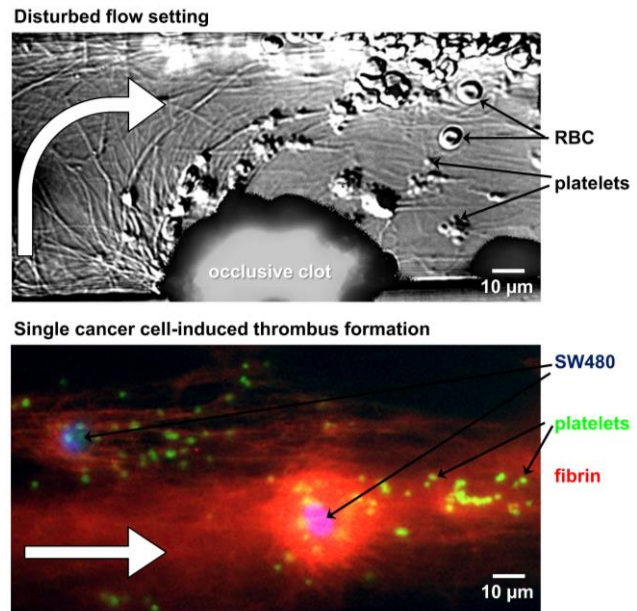


## 1.4 Platelet biology overview

Platelets are the second most abundant cells in the blood after red blood cells (RBCs; Section 1.2.1). Platelets serve an essential function in platelet plug formation during hemostasis. Platelets are discoid anucleate blood cells with a diameter of 2 to 4  $\mu\text{m}$ , which makes them the smallest cells in found in the blood (Figure 1.9).[145]

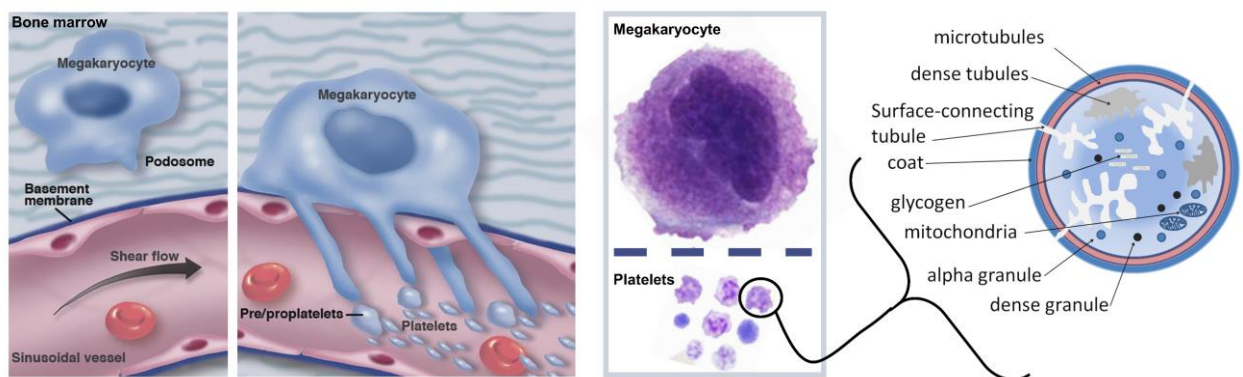
Platelets are produced in the bone marrow during the process of megakaryocyte fragmentation and platelet shedding into the bloodstream. During this process, megakaryocyte fragments (platelets) lose their

nucleus but retain other megakaryocyte structures, such as mitochondria, Golgi, lysosomes, glycogen stores, granules and microtubules as well as a rich repertoire of RNA and transcription factors (Figure 1.10).[146–148] In humans the blood concentration of platelets ranges from 150 to 350  $\times 10^9$  cells/L and newly shed platelets remain in circulation for 5 to 9 days.[149]



**Figure 1.9 Platelets in flowing blood.**

Top: Blood perfused through a ladder microfluidic network coated with collagen and platelet aggregates are visualized with differential interference contrast microscopy (Chapter 3). Bottom: Blood pretreated with PAR4 inhibitor (Section 1.5.2) and perfused past immobilized single-cell cancer (SW480) layer. Platelet aggregates are visualized with fluorescence microscopy. ©Jevgenia Zilberman-Rudenko



**Figure 1.10 Platelet structure.**

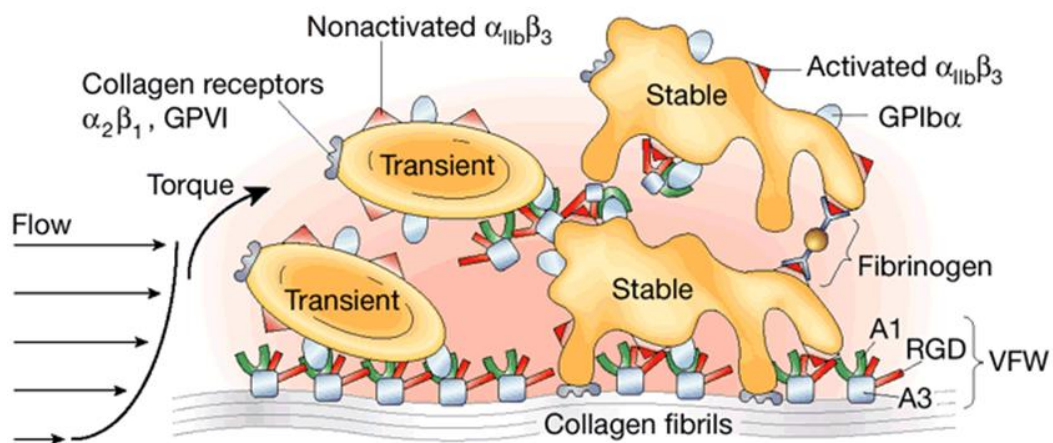
Figure adapted from French, Blood 2013. © Jevgenia Zilberman-Rudenko

### 1.4.1 Platelet adhesion, tethering and aggregation

Parts of section 1.5.1 was published in *Platelets* March 2017;28(5):449-456

Permission is not required by the publisher for this type of use.

Upon vessel injury, exposed extracellular matrix (ECM) proteins, such as fibrillar collagen, trigger a series of events that lead to the formation of a hemostatic plug to staunch blood loss.[150,151] The process of hemostasis depends on platelets tethering to the ECM in the presence of shear, leading to platelet adhesion, rapid cellular activation by contact with ECM proteins and release of soluble agonists (more on this in section 1.4.2) and accumulation of additional platelets (Figure 1.11).[152] ECM-bound von Willebrand factor (VWF) plays a critical role in initial platelet deposition via shear-dependent platelet receptor glycoprotein (GP)Ib binding to VWF.[153–155] Platelet receptor GPVI binds to collagen and mediates platelet activation via immunoreceptor tyrosine-based activation motif (ITAM) signaling within platelets leading to the release of secondary mediators and subsequent platelet aggregation. Upon platelet activation, platelets flip their membranes and expose P-selectin (CD62P) on their surface which, together with integrin  $\alpha_{IIb}\beta_3$  and fibrinogen, promotes platelet aggregation.[156]



**Figure 1.11 Platelet adhesion and aggregation under shear flow.**

Upon vessel injury, VWF binds to exposed collagens in the ECM and platelets tether to and transiently interact with VWF via GPIb. Stable adhesion occurs when GPVI and  $\alpha_2\beta_1$  interact with collagen at the site of injury.

Ruggeri, *Nature Medicine* 2002. Reprinted with permission.

The ability to conduct experiments under shear flow conditions allowed researchers to discriminate the roles of platelet receptors and proteins in the pathology of platelet dysfunction-related diseases, such as Bernard-Soulier syndrome (BSS). BSS is a bleeding diathesis disorder associated with a qualitative or quantitative deficiency in the platelet receptor GPIb, which binds VWF in a shear-dependent manner and thus is required for the initial step of platelet recruitment from the bloodstream during hemostasis in arteries and arterioles.[157] As platelets are able to bind to ECM proteins, such as collagen and laminin, via integrins  $\alpha_2\beta_1$  and  $\alpha_6\beta_1$ , respectively, and activate via the GPVI receptor under static conditions, the role of GPIb only became evident when experiments were performed under shear.[152,158,159] In particular, platelet recruitment to the endothelium was found to be mediated by the shear-dependent binding of the platelet receptor complex GPIb-IX-V with the A1 domain of VWF after VWF conformational activation.[155,160]

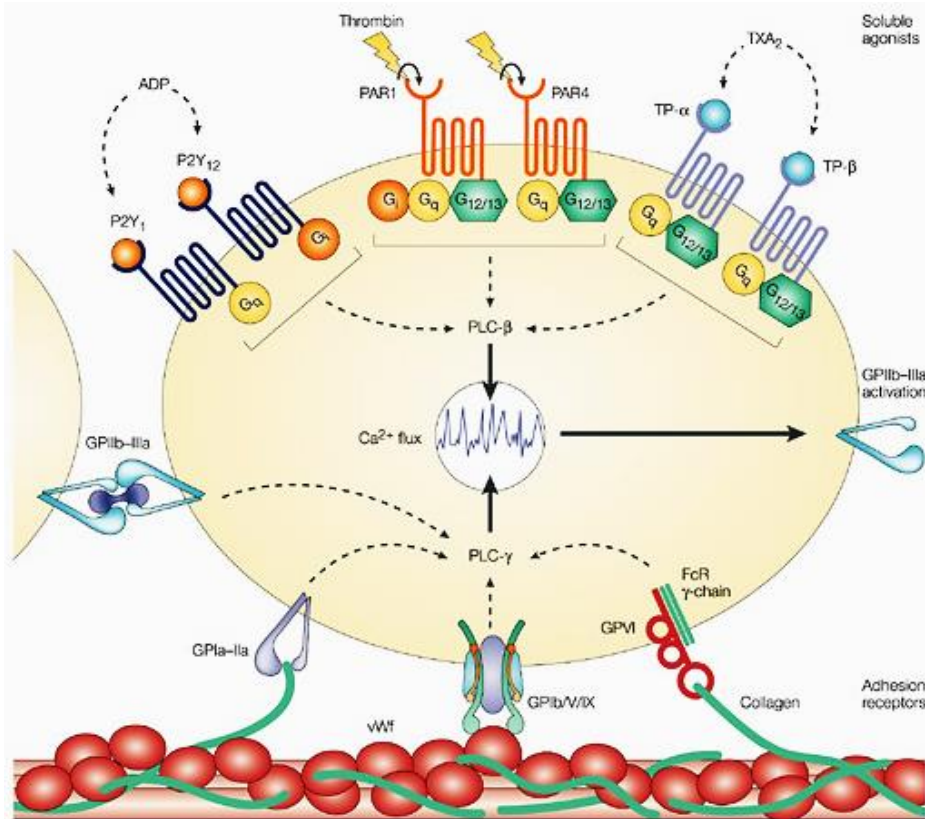
VWF monomers are stored in Weibel-Palade bodies of endothelial cells and  $\alpha$ -granules of platelets. VWF multimers are released upon cell activation by the serine protease thrombin, hormones or inflammatory cytokines.[161,162] Parallel-plate flow chamber studies showed that ultra-large multimer forms of VWF are efficiently processed and removed by the VWF-cleaving protease, ADAMTS13 (a disintegrin and metalloprotease thrombospondin type 1 motif, member 13), on cultured ECs under shear.[163,164] These studies provided a mechanism behind the thrombotic complications seen in patients with Thrombotic Thrombocytopenic Purpura (TTP), which is associated with conformational changes in ADAMTS13 and thus results in the persistence of ultra-large VWF multimers.[165] Imaging of activated VWF in endothelialized parallel-plate flow chamber studies, validated by studies in harvested vessels, is an example of the utility of microfluidic device technologies towards the development of non-invasive diagnostic approaches to assess disease states such as TTP.[166] Similar studies have revealed potential mechanisms of thrombotic complications in atherosclerosis, associated with platelet and EC activation and increased VWF expression.[167,168]

### 1.4.2 Soluble platelet agonists

Parts of 1.5.2 section was accepted for publication in *Platelets* 2018

Permission is not required by the publisher for this type of use.

Formation of initial platelet membrane tethers via GPIb-VWF is a transient and reversible phase of platelet aggregation. Tethers provide close physical proximity between platelets which can facilitate global platelet activation via autocrine and paracrine stimulation with soluble agonists, a required second step for stabilization of platelet aggregates via calcium-dependent assembly of  $\alpha_{IIb}\beta_3$  integrins (Figure 1.11 and Figure 1.12).[169] Notably, while each soluble agonist will be described separately, it is important to keep in mind that more often than not platelet stimulation occurs in a presence of a mixture of agonists with one frequently enhancing the other's effect.[170]



**Figure 1.12 Platelet agonists.**

Jacson and Schoenwaelder, *Nature Reviews Drug Discovery* 2003. Reprinted with permission.

Platelets become activated by serine proteases such as thrombin that cleave platelet protease-activated receptors (PARs) and initiate intracellular signaling pathways (Figure 1.12). Human platelets express PAR1 and PAR4, G-protein coupled receptors (GPCRs) that are activated by proteolytic cleavage of an extracellular N-terminal site to reveal a tethered peptide ligand bearing the sequence SFLLRN.[171] Subsequently, the ligand binds the receptor itself and initiates intracellular G-protein signaling.[172,173] Murine platelets lack PAR1 and instead depend on signaling of PAR4 with PAR3 acting as a co-factor, an important consideration for translating findings of *in vivo* mouse platelet research.[174,175] For *in vitro* experiments, a synthetic peptide comprising the SFLLRN sequence known as Thrombin Receptor Activating Peptide 6 (TRAP-6) is frequently utilized as a positive control.[176]

In humans, PAR1 and PAR4 activation leads to intracellular signaling cascades causing release of calcium stores, secretion of dense and alpha granule contents (Table 1.5 and Figure 1.12), and platelet shape change, culminating in platelet activation and stable platelet aggregate formation.[177] Structural differences between PAR1 and PAR4 result in differing outputs in platelet function. PAR1 contains a negatively-charged N-terminal sequence that binds the anion-binding exosite I of thrombin, which allosterically enhances thrombin's activity and enables it to activate both PAR1 and PAR4 while tethered to PAR1. PAR4 lacks this thrombin binding sequence, and higher concentrations of thrombin are required to activate PAR4 as compared to PAR1.[178,179]

Thrombin binds PAR1 transiently, causing robust platelet activation that is carefully constrained by rapid phosphorylation, internalization and degradation of the receptor.[180] PAR4 is also internalized to terminate its activity, but this internalization occurs via a different route than that of PAR1, in a manner hypothesized to enable prolonged signaling.[181] These differences in PAR4 vs. PAR1 result in a response to thrombin that is slower but more sustained over time, with varying functional effects, including roles in enhancing clot stability and procoagulant microparticle release that suggest a more pronounced effect of platelet PAR4 activity in thrombus formation.[182,183]

Adenosine diphosphate (ADP) is an essential platelet GPCR agonist. Non-metabolic ADP is released by activated platelets (Table 1.5) and promotes activation and recruitment of additional platelets by activating P2Y<sub>12</sub>. [177] Thromboxane A<sub>2</sub> (TXA<sub>2</sub>) is another GPCR agonist, produced by the conversion of arachidonic acid by cyclooxygenase and is released by activated platelets. TXA<sub>2</sub> can be mimicked with a commercially available TXA<sub>2</sub> analog (U46619). Epinephrine or adrenaline can also activate GPCR signaling in platelets in certain conditions.

5-hydroxytryptamine (5-HT), also known as serotonin, is a hormone implicated in depression. 5-HT has been shown to be a weak platelet aggregation on its own. 5-HT is released from activated platelets (Table 1.5) and supports platelet aggregation in the presence of thrombin, ADP or epinephrine. [184] Interestingly, cocaine has been shown to abrogate 5-HT reuptake leading to increased 5-HT levels and platelet aggregation, which may be in part responsible for cardiovascular complications in cocaine users. [185]

#### 1.4.3 Platelet secretion and platelet storage diseases

Platelet secretion is an essential part of platelet function. Platelet releasate content can vary depending on the context of platelet activation and include a mixture from >300 distinct molecules (Table 1.5). [186] Platelets primarily contain two types of granules, dense and alpha (α), and majority of the content of granules is synthesized in megakaryocytes prior to platelet shedding. Some select molecules, e.g. coagulation factor V and fibrinogen, are packaged into platelets by endocytosis. [187]

| Dense granules  | Alpha granules  |  |  |
|---|---|--|--|
| <i>Small molecules:</i><br>Serotonin (5-HT),<br>ADP,<br>Polyphosphate | <i>Hemostatic factors:</i><br>Coagulation Factor V,<br>VWF,<br>Fibrinogen | <i>Angiogenic factors:</i><br>Angiogenin,<br>VEGF                    | <i>Growth factors:</i> PDGF,<br>βFGF,<br>SDF1α |
|   | <i>Metalloproteases:</i><br>MMP2,<br>MMP9                                 | <i>Anti-angiogenic factors:</i><br>Angiostatin,<br>Platelet factor 4 | <i>Cytokines:</i><br>TNFα                      |

**Table 1.5 Primary content of platelet granules.**

©Jevgenia Zilberman-Rudenko

Clinically, platelet granule defects, also known as platelet storage pool diseases, arise due to a number of mechanisms and range in severity.[188] A brief summary of these is included in Table 1.6. Many of the platelet storage defects have a similar phenotype and non-specific findings, making it difficult to properly diagnose. Usually, the official diagnosis of a storage platelet disease is rather extensive and requires a number of studies, including flow cytometry and platelet aggregation.[104]

| Syndrome/Disorder                | Defect | Bleeding | Aggr. Defect             | Additional issues                          |
|----------------------------------|--------|----------|--------------------------|--|
| <i>Hermansky-Pudlak</i>          | Dense  | ++ / +++ | Low 2 <sup>nd</sup> wave | Oculocutaneous albinism, eye defects       |
| <i>Chediak-Higashi</i>           | Dense  | ++ / +++ | Low 2 <sup>nd</sup> wave | Partial albinism, ID, neurological         |
| <i>GrisCELLI</i>                 | Dense  | none / + | NA                       | Partial albinism (hair), ID, neurological  |
| <i>Gray platelet</i>             | Alpha  | + / ++   | Thrombin, collagen       | Myelofibrosis, empty granules              |
| <i>Quebec platelet</i>           | Alpha  | + / ++   | Epinephrine              | Low granule content                        |
| <i>Arthrogryposis</i>            | Alpha  | +        | ADP                      | Renal, cholestasis, ichthyosis, infections |
| <i>X-linked thrombocytopenia</i> | Both   | Both     | Low                      | β-thalassemia, erythropoietic porphyria    |
| <i>Wiskott-Aldrich</i>           | Both   | ++ / +++ | Low                      | Eczema, ID, autoimmunity                   |

**Table 1.6 Overview of platelet storage diseases.**

Data adapted from Sandrock and Zieger, *Transfusion and Hemotherapy* 2010.

Key: + - mild, ++ - moderate, +++ - severe. ID – immunodeficiency. ©Jevgenia Zilberman-Rudenko

While efficacy can vary, patients with these disorders receive common treatments, such as tranexamic acid, desmopressin/DDAVP, FVIIa, and platelet transfusions.[104–106] Tranexamic acid is an antifibrinolytic that inhibits the activation of plasminogen to plasmin – an active enzyme that breaks down a fibrin mesh (Section 1.3.5).[103] Desmopressin/DDAVP induces release of VWF from endothelial stores.[189] Sometimes, bone marrow transplantations is considered for very severe defects.[190]

#### 1.4.4 *Anti-platelet therapies*

There is a wide range of anti-platelet therapies that are currently used primarily for cardiovascular population. Aspirin irreversibly inhibits cyclooxygenase thus reducing TXA<sub>2</sub> synthesis.[191] Oral anti-platelet reagents such as ticlopidine (Ticlid®), clopidogrel (Plavix®) and prasugrel (Effient®) inhibit ADP-induced expression of  $\alpha_{IIb}\beta_3$ . [192] Abciximab (ReoPro®) inhibits  $\alpha_{IIb}\beta_3$  directly. Cangrelor (Kengreal®) is an intravenous drug of the same class as clopidogrel.

A dual anti-platelet therapy, aspirin and clopidogrel, is frequently prescribed to patients who have undergone balloon angioplasty and drug-eluting stent placement post heart attack.[193,194] These oral therapies are easily administered by patients at home and are usually continued for at least six months post procedure. However, the clopidogrel effect only lasts for a short period of time and some patients have shown resistance to this therapy. A relatively new P2Y<sub>12</sub> inhibitor, ticagrelor (Brilinta®), has shown superior efficacy in preventing myocardial infarction (MI) in patients post post-coronary artery stenting as well as lower bleeding incidences as compared to clopidogrel.[195]

Previously abciximab was the gold standard therapy used during balloon angioplasty and stent placement procedure. However, data from the use clopidogrel and cangrelor has led many to question the efficacy, safety and need for abciximab during the procedure.[196–199] In a recent trial, abciximab has shown to increase the incidence of thrombocytopenia and need for transfusions over Clopidogrel.[199] Since then, the 2016 American College of Cardiology/American Heart Association task force on clinical practice has issued a guideline to avoid use of abciximab in patients adequately preloaded with clopidogrel-class therapy.[193]

It should be noted that with use of any irreversible anti-platelet therapy it is important to remember that it will take about 5 to 9 days for the body to produced new platelets. The half-life of both aspirin and clopidogrel is about 1 full day. Thus, when stabilizing patients with traumatic injury to the head and a suspicion of a brain bleed, platelet transfusion may be considered.[200–202]



## 1.5 Vascular biology overview

Parts of Section 1.6 were published in *Platelets* March 2017;28(5):449-456

Permission is not required by the publisher for this type of use.

### 1.5.1 *Endothelial cells overview*

The luminal surface of blood vessels is lined with a confluent monolayer of endothelial cells (ECs), which under normal conditions governs blood flow dynamics including providing a barrier between blood and tissue and regulating platelet aggregation and thrombin generation in the bloodstream.[203,204] In turn, blood components, primarily platelets (Section 1.4) and coagulation factors such as thrombin (Section 1.3), regulate EC barrier integrity.

### 1.5.2 *Types of endothelial cells*

During embryogenesis, elaborated network of vascular beds develop that serve similar yet distinct functions (Table 1.3). Thus it is reasonable to expect that adult EC phenotypes vary according to the local requirements placed on it by individual organs and vasculature function.[205] The field of regenerative medicine has been invested in finding ECs appropriate for prosthetic organ development and have identified a few cells types which may serve as appropriate progenitors for EC-based therapeutics.[206] For instance, blood-derived endothelial colony forming cells (ECFCs) can be purified from a peripheral blood sample and, in trained hands, have shown capacity for expansion.[207]

In 1999 the common EC types used to study blood-endothelium interface were human umbilical vein ECs (HUVECs) and three immortalized EC lines (HMEC-1, ECV304 and EaHy926). All four express intercellular adhesion molecule-1 (ICAM-1), vascular cell adhesion molecule-1 (VCAM-1), E-selectin, major histocompatibility complex (MHC) class I and MHC class II, CD40, CD95 (fas) and lymphocyte function associated antigen-3 (LFA-3). HUVECs, HMEC-1 and EaHy926 express cell

adhesion molecule-1 (PECAM-1), while ECV304 is constitutively negative for PECAM-1. HUVECs are the most common type of ECs used in microfluidic studies. HUVECs are favored over immortalized endothelial cell lines as HUVECs were shown to appropriately express molecules upon stimulation with physiological cytokines, VCAM-1 and E-selectin in response to tumor necrosis factor-alpha (TNF- $\alpha$ ) and MHC class II antigens in response to interferon-gamma (IFN- $\gamma$ ).[208]

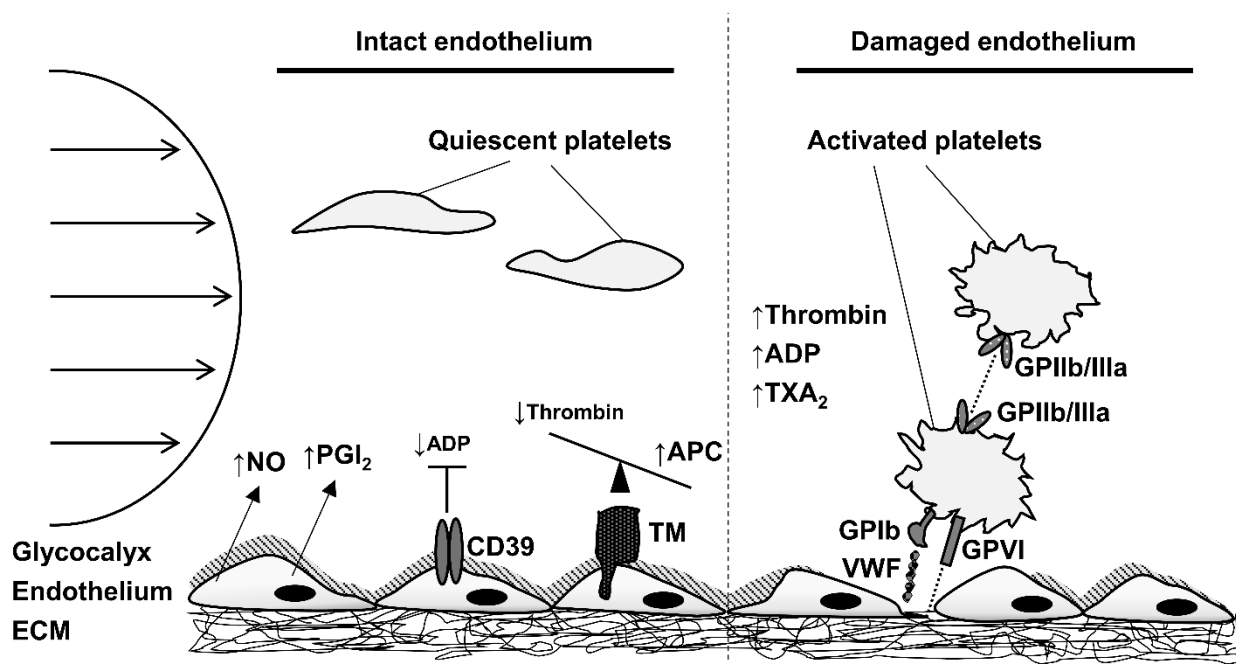
Several studies have shown that similarly to primary ECs isolated from the vasculature,[209] HUVECs respond to a gradient of wall shear stresses by changing their morphology,[210] alignment,[211,212] formation of cell-to-cell junctions,[213,214] and altering transcription profile.[215] Similar to Estrada et al.[216] and Urbaczek et al.,[217] in our hands (Section 9.3 and [218]), HUVECs cultured under shear arrived at a monolayer of ellipsoidal and aligned cells faster than HUVECs grown under static culturing conditions. Furthermore, HUVECs cultured under shear rearranged their cytoskeleton to transition from a cobblestone to an elongated formation similar to primary cells and promoted less adhesion to blood cells at baseline, in line with findings that this induced morphology of primary ECs reduced the inflammatory and immunogenic properties of ECs that are implicated in the development of atherosclerosis.[209]

These published reports and science forum discussions suggest that HUVECs may be a suitable cell line to study blood-endothelium interface as long as the culturing passage number of the cells is low and preferably does not exceed 3 passages in an effort to retain the activity of EC regulatory pathways, such as production of nitric oxide. Since 1999, several other types of ECs, such as human abdominal aorta EC (HAAEC) and human umbilical artery ECs (HUAECs) have become commercially available; however, these do not seem to be as popular for microfluidic studies.

### 1.5.3 *Blood-endothelium interface under shear flow*

Under physiologic laminar flow conditions, the ECs that comprise a healthy vessel lumen prevent activation and aggregation of platelets in the bloodstream through membrane endonucleotidases

(CD39/ATPase), which hydrolyze adenosine diphosphate (ADP) molecules released by activated platelets (Section 1.4.3), as well as by secreting prostacyclin (PGI<sub>2</sub>) and, perhaps the most effective platelet inhibitor, nitric oxide (NO; Table 1.7 and Figure 1.13).[219–223] Moreover, healthy endothelium efficiently inhibits generation of a potent platelet agonist, thrombin, through the catalysis of protein C to the anticoagulant serine protease, activated protein C (APC), in a thrombomodulin (TM)-dependent manner (Section 1.3.2).[224]



**Figure 1.13 Blood-endothelium interface.**

Under laminar flow, healthy endothelial cells prevent platelet adhesion and aggregation by secreting soluble nitric oxide (NO) and prostacyclin (PGI<sub>2</sub>). The surface of the endothelium is covered by anti-adhesive layer of glycocalyx and expresses endonucleases (CD39), which hydrolyzes adenosine diphosphate (ADP), and thrombomodulin (TM), which promotes reduction of thrombin and an increase in antithrombotic activated protein C (APC), all of which serve to maintain platelets in their quiescent state. Upon vessel injury, platelets are rapidly recruited to subendothelial extracellular matrix (ECM) proteins via platelet glycoprotein (GP)Ib binding to the adhesive protein von Willebrand factor (VWF). Platelets are activated downstream of the collagen receptor GPVI leading to glycoprotein IIb/IIIa (GPIIb/IIIa)-dependent aggregate formation to prevent blood loss. Activated platelets release adenosine diphosphate (ADP) and thromboxane (TXA<sub>2</sub>) and provide a surface for thrombin generation, all of which feedback to promote secondary recruitment and activation of platelets from the bloodstream to form a hemostatic plug. Zilberman-Rudenko et al., *Platelets* 2017. Permission is not required by the publisher for this type of use.

The roles of the pro/anticoagulants produced by the endothelium have been studied in reductionist approaches through, for example, the addition of a NO donor, soluble TM and other reagents in microfluidic platforms in order to study their individual roles in maintaining vessel patency

and platelets in a quiescent state.[225–227] Under physiologic conditions, the surface of the endothelium is covered by a glycosamino-glycan-rich layer, termed the glycocalyx, which facilitates EC mechanotransduction and expression of NO in a shear stress-dependent manner. Moreover, the glycocalyx serves as an antiadhesive barrier between the healthy vessel and cells in the bloodstream, including platelets and leukocytes (Figure 1.13).[228–230] Loss of the glycocalyx has been implicated in acute and chronic diseases, such as sepsis, atherosclerosis and diabetes, and is associated with thrombo-hemorrhagic complications.[231] The composition of the glycocalyx is dependent upon the physical biology of the vessel microenvironment including the cross-sectional area and shear rate.[228,232]

#### 1.5.4 *Endothelial damage and prothrombotic states*

The subendothelial compartment of the vessel is lined with extracellular matrix (ECM) proteins, such as collagen and laminin, which when exposed to the bloodstream upon injury to the EC layer or loss of homotypic EC intercellular gap junctions facilitates platelet recruitment, activation, aggregation and thrombin generation in a shear-dependent manner (Table 1.7).[233,234] Moreover, platelets can bind directly to activated ECs at sites of inflammation.[235] Under these conditions, activated ECs facilitate recruitment of platelets through the secretion of the adhesive protein von Willebrand factor (VWF), expression of tissue factor (TF), the initiator of the extrinsic cascade of coagulation (Section 1.3.2), and increased expression of E- and P-selectin, which facilitates recruitment of leukocytes in a PSGL-1-dependent manner.[236,237]

Thrombin acts as a direct activator of local EC signaling including promotion of platelet aggregation on the surface of the activated endothelium and activation of ADAM10 (A Disintegrin and metalloproteinase domain-containing protein 10)-dependent VE-cadherin proteolysis leading to endothelial cell dissociation and gap formation.[238,239] Disseminated loss of barrier and vascular

leak, a serious sequela of sepsis progression, leads to hypotension, hypoperfusion, tissue edema and multiorgan failure which are only temporarily attenuated with aggressive fluid resuscitation.[240,241]

Inflammation, endothelial injury and presence of microbial molecules lead to thrombin generation which then feeds back to activate the contact coagulation pathway via activation of FXI, leading to the amplification of thrombin generation and widespread platelet activation (Table 1.7).[44,242] The contact pathway can also be directly activated by the presence of negatively charged microbial molecules, such as polyphosphate (long-polyP), peptidoglycan (PGN) and endotoxin (LPS), which facilitate FXII autoactivation leading to activation of FXI,[243,244] and FXIa inhibition of endogenous EC anticoagulation mechanisms by cleaving tissue factor pathway inhibitor (TFPI), a reaction that is accelerated by the presence of platelet releasate to promote additional thrombin generation.[245,141,246] This potentially fatal spiral can progress to further endothelial damage, consumption of platelets and coagulation factors as well as ultimately multi-organ failure.

Platelets and ECs exhibit an intimate relationship required to maintain vessel integrity. Platelet binding to the vessel wall results from the release and polymerization of VWF, decrease in the glycocalyx layer or following fibrin deposition on activated ECs.[35] Inflammation and exposure of the vasculature to oxidative stress, via reactive oxygen species (ROS), has been shown to decrease TM production[247–249] and CD39 activity,[250] promote assembly of hyperadhesive VWF[247,251] and thus increase the recruitment of platelets.[252] Tissue necrosis factor  $\alpha$  (TNF $\alpha$ ), a prevalent cytokine associated with sepsis, has been shown to directly promote EC activation, decrease barrier function and increase procoagulant TF expression.[253,254]

Platelets have been shown to assist metastasis and the intravasation of tumor cells across the endothelial cell layer through the expression and secretion of lysyl oxidase (LOX) and matrix metalloproteinases (MMPs; Table 1.5 and Table 1.7).[255] Moreover, platelet granules contain an abundance of growth factors, such as VEGF and PDGF, which has been shown to promote tumor cell growth and angiogenesis *in vitro* and *in vivo*. [256–258] Furthermore, endothelial cell-bound platelets

have been shown to directly recruit circulating tumor cells, which may play a role of seeding of cancer cells in specific vascular beds.[258–261]

| Setting                                  | Endothelium   | Platelets   |
|--|---|---|
| Laminar flow, intact endothelial barrier | Anti-adhesive layer, glycocalyx[228–232]<br>CD39/ATPDase expression[219,222]<br>Soluble antiplatelet molecules: nitric oxide (NO) and prostacyclin (PGI <sub>2</sub> )[220–222]<br>Anticoagulants: thrombomodulin (TM) and activated protein C (APC)[224] | Circulate as quiescent surveyors of the vessel wall[237]  |
| Endothelial barrier damage               | Exposure of extracellular membrane (ECM) proteins: collagen, laminin, etc.[233,234]<br>Release of von Willebrand factor (VWF)[162]  | Adhesion to ECM proteins via GPIb and GPVI[152]<br>Platelet activation and release of ADP and TxA <sub>2</sub> [223]<br>Platelet aggregation via GPIIb/IIIa homodimers[152] |
| Perturbed flow                           | Development of gap-junction leak[262–264]<br>Decrease in NO and PGI <sub>2</sub> secretion[265]<br>Release of VWF[162,266]  | Shear-induced platelet activation[266–268]  |
| Inflammation Sepsis                      | TNF $\alpha$ -induced activation and TF surface expression[253,254]<br>ROS-mediated hyperadhesive VWF assembly[247,251] and TM inactivation[247–249]<br>CD39/ATPDase inactivation[250]  | ROS-induced platelet activation[252]<br>Thrombin-induced platelet activation[224]<br>Heterotypic platelet-leukocyte aggregate formation and adhesion to vessel wall[253]    |
| Tumor Metastasis                         | Similar phenomena associated with inflammation<br>+ Tumor cell-induced lysyl oxidase (LOX) and matrix metalloproteinases (MMPs) upregulation which facilitates intravasation[255]   | Binding and protection of circulating tumor cells (CTCs)[260,261]<br>Release of PDGF and VEGF[258]  |

**Table 1.7 The effect of the physical biology of blood flow on the endothelium and platelets.**  
Zilberman-Rudenko et al., *Platelets* 2017. Permission is not required by the publisher for this type of use.

### 1.5.5 *Utility of endothelialized microfluidic platform development*

The biophysical properties of blood flow play a key role in regulating the distribution of blood cells within the bloodstream,[237] maintenance of EC layer barrier integrity[262,263] and EC gene and protein expression profiles.[265] Platelet interactions with ECs and other cells in the vasculature are profoundly altered by blood flow dynamics (Section 1.4.1 and Table 1.7).[158,269,270] Thus, perfusable endothelialized microfluidic models hold potential for dynamic studies of the platelet-endothelium interface in health and disease states including evaluation of the efficacy and safety of pharmacological agents designed to treat or prevent cardiovascular diseases.

Our future work includes development and utilization of novel PDMS-based endothelialized microfluidic systems. In Chapter 9.3 we discuss results and directions of this ongoing effort which includes utilization of existing and production of new devices.

## 1.6 Thesis Overview

In this thesis, we examine broad as well as applied concepts of blood reaction dynamics under shear flow. The formation of a hemostatic plug to staunch blood loss at sites of vascular injury relies on the dynamical processes of platelet recruitment and activation of the coagulation cascade in the setting of the biorheology of blood flow.[5,6,271] Thus, elucidation of the molecular mechanisms of thrombus formation rely on the use of engineering principles to design platforms to study complex enzymatic reactions and cell biology under physiologically relevant shear flow conditions. The focus of this dissertation work was the development of microfluidic platforms to study and assess the dynamics of blood reactions in health and disease.

The field of blood biorheology science is a complex fusion of cell and molecular biology, biochemistry, engineering, fluid mechanics, material science and physics.[272–274] With the advent of new materials, fabrication processes and computation modeling approaches, microfluidic studies have expanded to tackling complex concepts of blood flow dynamics and its effects on coagulation processes and platelet function. In Chapter 3, we describe our work looking at the effect of specific microfluidic network geometry on dynamics of thrombus formation and evolution as pertinent to the design of microfluidic networks for exchange membrane geometry in extracorporeal oxygenator. In Chapter 4, we describe the development and utility of a novel flow setup to study the implications of local thrombus formation on distal platelet activation in different biorheological settings.

Coagulation FXII is an abundant protein in plasma, deficiency of which is clinically asymptomatic. FXII is activated in the presence of negatively charged proteins and activates FXI as part of the contact coagulation pathway leading to thrombin generation. FXI is furthermore activated by thrombin promoting thrombin generation amplification and, furthermore, activated FXI alters natural anticoagulation by proteolyzing tissue factor pathway inhibitor (TFPI). In Chapter 5, we use an *ex vivo* flow setup described in Chapter 4 and an *in vivo* model of non-human primate thrombosis to study the role of FXI activation by FXIIa and FXIa activity in platelet activation and consumption in



the bloodstream. Results of this study and our previous findings of FXI-deficiency being protective in thromboembolic complications in sepsis have prompted studies described in Chapter 6, where we again utilize of *ex vivo* and *in vivo* study approaches and platforms to interrogate potential therapeutic targets for finding a balance between hemostasis and thrombosis.

The ultimate goal of the efforts described within this dissertation is the development of clinically useful tools to assess blood reaction dynamics and identify druggable targets. The nature of this type of work in reality requires development of skills to interact with physicians, patients, hospital staff as well as manufacturing companies to properly design as well as develop products that would add value to medical practice. In the last two chapters of this dissertation, we describe collaborative work with clinical staff and manufacturing companies, where we apply lessons learned in the work described above to clinically relevant questions. In Chapter 7 we assess whether the mode of transport of platelet concentrate units within a hospital affects their function, which is of relevance to their use in transfusion medicine. In Chapter 8 we describe the development and a potential utility of a point-of-care microfluidic platform for whole blood analysis.

Chapter 9 contains discussion (section 9.1) of the limitations and conclusions of the work contained in this dissertation as well as the future directions (sections 9.2 - 9.3). In section 9.2, we describe our ongoing studies looking at novel pro-coagulant molecules such as skeletal and cardiac muscle myosin. In section 9.3, we describe development and utility of endothelialized microfluidic platforms to combine the study of platelet recruitment and activation of the coagulation cascade in the physiological context of vascular cells and shear.

## Chapter 2. General Materials and Methods

### 2.1 Ethical Considerations

All procedures performed in studies involving human participants were in accordance with the ethical standards of the institutional and/or national research committee and with the 1964 Helsinki declaration and its later amendments or comparable ethical standards. For all studies utilizing human blood, consent was obtained from healthy volunteers in accordance with an Oregon Health & Science University (OHSU) Internal Review Board (IRB)-approved protocol. No demographic data was collected on volunteers.

For studies with baboons (*Papio anubis*), the animals were housed and cared for at either the OHSU Oregon National Primate Research Center (ONPRC), a Category I facility and all experiments were approved by the OHSU West Campus Animal Care and Use Committee according to the *Guide for the Care and Use of Laboratory Animals* by the Committee on Care and Use of Laboratory Animals of the Institute of Laboratory Animal Resources, National Research Council (ISBN 0-309-05377-3, 1996). The Laboratory Animal Care and Use Program at the ONPRC is fully accredited by the Accreditation of Laboratory Animal Care (AAALAC) and has an approved assurance (no. A3304-01) for the care and use of animals from the Office for Protection from Research Risks at the National Institutes of Health.

For studies with mice, the animals were housed and cared for at the Case Western Reserve University (CWRU) Animal Resource Center (ARC), a Category I the American Association for AAALAC accredited facility. The CWRU ARC includes integrated a biohazard level 2/3 suite, high level rodent barrier, imaging suite, quarantine facilities, specific pathogen free and athymic rodent housing areas. All experiments were approved by the Case Western Institutional Animal Care and Use Committee (IACUC) according to the *Guide for the Care and Use of Laboratory Animals* by the Committee on Care and Use of Laboratory Animals of the Institute of Laboratory Animal Resources, National Research Council (ISBN 0-309-05377-3, 1996).

## 2.2 Common reagents

### *Agonists and Proteins*

Cross-linked collagen-related protein/CRP-XL was purchased from University of Cambridge (Cambridge, England). Thromboxane A<sub>2</sub> analog/U46619 and PAR-1 agonist/TRAP6 were from Tocris (Bristol, England). Epinephrine and fibrillar collagen were from Chrono-Log (Havertown, PA). Human VWF was from Haematologic Technologies, Inc (Essex Junction, VT). Fibrinogen was purchased from Enzyme Research Laboratories (South Bend, IN). Lipidated tissue factor (TF; Innovin<sup>®</sup> PT reagent) was purchased from Siemens (Munich, Germany). Ellagic acid (aPTT reagent) was purchased from Thermo Fisher (Waltham, MA). Polyphosphate molecules of the size produced by bacteria (long-chain polyP, >595 phosphate units in length) were prepared as described.[275]

### *Inhibitors and Function-blocking Antibodies*

Anti-factor XI function-blocking antibodies (1A6 and 14E11), factor XIa (10C9) and factor XIIa blocking antibodies (5C12) were generated as described.[139–141] Corn trypsin inhibitor (CTI) was purchased from Enzyme Research Laboratories (South Bend, IN). Hirudin was purchased from Hyphen Biomed (Neuville-sur-Oise, France). Phe-Pro-Arg-chloromethylketone (PPACK) was purchased from Santa Cruz (Dallas, TX). Recombinant polyP-binding domain from *Escherichia coli* polyphosphatase (PPXbd) was produced as described.[276]

### *Detection agents*

Rabbit anti-fibrinogen antibody was from Cappel MP Biomedicals, LLC, anti-rabbit-AF350 from Life technologies (Carlsbad CA). Anti-CD41-PE, anti-CD62P-APC and Cytotfix<sup>BD</sup> were from BD Pharmingen (Franklin Lakes, NJ). Anti-CD31-eFluor450 was from eBioscience (San Diego, CA). Anti-thrombin API (H-85), rabbit anti-human anti-VWF primary antibody and goat anti-human anti-Vinculin primary antibodies were purchased from Santa Cruz (Dallas, TX). Anti-integrin  $\alpha$ IIb from

Abnova (Taipei, Taiwan). Mouse anti-human anti-GPIIb/AK2 primary antibody was from GeneTex (Irvine, CA) and anti-mouse IgG -AF640 secondary was from Invitrogen (Carlsbad, CA). FXIIa chromogenic substrate S-2302 was purchased from Diapharma (West Chester, OH). SuperSignal West Dura Substrate was from Thermo Scientific (Waltham, MA).

All other reagents were from Sigma-Aldrich, Inc. or previously named sources.[245,277]

## **2.3 Collection and utilization of human blood**

### *2.3.1 Blood collection*

Venous whole blood was obtained from healthy volunteers in accordance with an Oregon Health & Science University (OHSU) Internal Review Board (IRB)-approved protocol. After sterilization of the decubitus field, blood was obtained by venipuncture with a 19G butterfly needle and manually drawn into either an empty syringe or a syringe with an appropriate anticoagulant.

### *2.3.2 Platelet-rich and platelet-poor plasma preparation*

Venous whole human blood was drawn into trisodium citrate (0.38% w/v). To isolate RBCs, whole blood was spun down at 1600 rpm for 10 minutes at RT in a Hermle Z300 centrifuge outfitted with rotor 221.12 V01 (Labnet, Edison, NJ). After the first spin, platelet rich plasma (PRP) was transferred into a new tube and, when appropriate, PRP was spun down again at 2500 rpm for 10 minutes to isolate platelet poor plasma (PPP).

### *2.3.3 Washed platelet preparation*

For washed platelet preparation, blood was drawn into 3.8% trisodium citrate 9:1 (v:v), and acid-citrate dextrose (ACD) was added at 1:10 (v:v). Platelet-rich plasma (PRP) was isolated by centrifugation at 200 g for 20 minutes, and platelets were separated from PRP at 1000 g for 10 minutes in the presence of prostacyclin (0.1 µg/ml). Platelets were resuspended in modified HEPES/Tyrode

buffer (129 mM NaCl, 0.34 mM Na<sub>2</sub>HPO<sub>4</sub>, 2.9 mM KCl, 12 mM NaHCO<sub>3</sub>, 20 mM HEPES, 1 mM MgCl<sub>2</sub>, pH 7.3, supplemented with 5 mM glucose), washed by centrifugation at 1000 g for 10 minutes, and resuspended again in modified HEPES/Tyrode buffer to the specified platelet count.

All blood products were used within 2 hours of the blood draw.

## **2.4 Closed system assays**

### *2.4.1 Clotting assays*

The activated partial thromboplastin time (aPTT) of human plasma were measured with a Trinity AMAX200 coagulation analyzer (Trinity Biotech, Bray, Ireland). Pooled human plasma was pretreated at 37°C for 10 min with 1A6, 14E11 or rivaroxaban, followed by incubation with aPTT reagent for 3 min at 37°C. Coagulation was then initiated by the addition of CaCl<sub>2</sub> (8.3 mM final), and clotting times were recorded.

### *2.4.2 Lipid vesicles*

Small unilamellar vesicles of phosphatidylcholine/phosphatidylserine (80% PC : 20% PS w/w) or (60% PC : 20% PS : 20% PE w/w) in 150 mM NaCl, 50 mM Tris, pH 7.4, Tris buffered saline (TBS) were prepared by sonication under a flow of nitrogen using a microtip sonicator.

### *2.4.3 Thrombin generation assay in fresh whole blood, PRP and PPP*

Plasma thrombin generation assays were performed as described[278,279] with some minor modifications. Freshly prepared whole blood (80 µL) or PRP and PPP from the same individual donor who provided whole blood (30 µl) was incubated with various concentration of myosin for 10 min at 37°C. Then, fluorogenic thrombin substrate solution (I-1140) with either tissue factor (Innovin, final 0.5 pM) containing 30 mM CaCl<sub>2</sub> or 30 mM CaCl<sub>2</sub> alone was added to the reaction mixture (total 110 µl) to initiate coagulation. Thrombin generation was followed continuously for 25 min using

SPECTRAmax GEMINI XS fluorometer (Molecular Devices, Sunnyvale, CA) with excitation and emission wavelengths set at 360 and 460 nm, respectively. The first derivative of fluorescence versus time was used to produce thrombin generation curves with the correction for substrate consumption and inner filter effect.[278,279] Results also included determination of lag time in minutes defined as the interval from the addition of substrate and CaCl<sub>2</sub> until the formation of 1 nM of thrombin and of area under the curve (AUC) defined as the sum of thrombin generated from 1 to 25 min (nM·min). Once-thawed pooled normal human (George King Bio Medical Inc., Overland Park, KS) (30 µl) were also tested for the plasma thrombin generation assay in the presence or absence of 4 µM PC/PS (80% : 20%) vesicles.

#### 2.4.4 *Activation of prothrombin by prothrombinase complex*

Cardiac myosin or skeletal muscle myosin were incubated with factor Va (5 nM, final) and factor Xa (0.2 nM, final) in TBS containing 0.5% BSA (TBBSA) with 5 mM CaCl<sub>2</sub>. Thrombin generation was initiated by the addition of prothrombin (0.75 µM, final, unless noted otherwise). The reaction was quenched by 10 mM EDTA, and the rate of thrombin formation was quantified by measuring thrombin concentration as the rate of substrate (Pefachrome TH) hydrolysis. In separate experiments, des-GLA-domain (DG)-factor Xa was used in place of factor Xa following the same protocols.

#### 2.4.5 *Plasma clot lysis*

Clot lysis was studied in a plasma system in which tPA-mediated fibrinolysis of a thrombin-induced clot is measured using turbidity as described earlier.[280,281] In short, a mixture of 100 µL of thrombin (5 nM, unless otherwise noted), calcium (17 mM, resulting in a free calcium concentration of 2.3 mM), phospholipid vesicles (60% PC : 20% PS : 20% PE; final concentration 10 µM) and tPA (100 ng/mL, unless otherwise noted) diluted with HEPES saline buffer (25 mM HEPES, 137 mM NaCl, 3 mM KCl, pH 7.4) 0.1% BSA was added to 100 µL citrated normal human pooled plasma, which was

pre-incubated for 30 min at 37°C in the presence of either control buffer (50 nM Tris, 600 mM NaCl) or myosin protein suspension in 50 nM Tris, 600 mM NaCl. After mixing, 100 µL of the reaction mixture was pipetted in a microtiter plate and then incubated at 37°C during which turbidity was measured over time at 405 nm in a Spectramax 340 kinetic microtiter plate reader (Molecular Devices Corporation, Menlo Park, CA, USA). The clot lysis time ( $t_{1/2}$ ) was defined as the time between the maximum turbidity and the midpoint of the maximum turbid-to-clear transition that characterizes the lysis of fibrin determined using an in house Lysis Analysis software developed by van de Poel et al.[282]

## 2.5 Open system assays

### 2.5.1 *Ex vivo flow experiments*

Glass capillary tubes/chambers (0.2×2×200 mm; VitroCom) were coated as described previously.[283] Surfaces were blocked with 5 mg/mL denatured bovine serum albumin (BSA) for 1 h prior to assembly into a flow system as shown in Figure 5.2A. Sodium citrate (0.38% w/v) anticoagulated whole blood was recalcified and perfused through the chamber for 10 min at an initial wall shear rate (300 or 1000 s<sup>-1</sup>).

### 2.5.2 *Microscopy*

After blood perfusion, glass capillaries were washed with phosphate-buffered saline (PBS) and HEPES/Tyrode buffer (136 mM NaCl, 2.7 mM KCl, 10 mM HEPES, 2 mM MgCl<sub>2</sub>, 0.1% BSA; pH7.4) containing 1.5% sodium citrate and 100 µM PPACK, followed by incubation with blocking buffer (1% BSA, 1% FCS in HEPES/Tyrode buffer) for 30 min. Glass capillaries were incubated with rabbit anti-serum against human fibrinogen (1:100) for 10 min and washed with PBS followed by an incubation with CD41-PE (1:50), CD62-FITC (1:50), and goat anti-rabbit Alexa Fluor 350 (1:500) in dark for 10

min. Glass capillaries were washed with PBS, fixed with paraformaldehyde (PFA 4%), and sealed with mounting media. Samples were analyzed on a Zeiss Axio Imager 2 microscope 6 (Carl Zeiss MicroImaging GmbH, Germany).

### 2.5.3 *Western blots*

Thrombi formed on collagen/TF were lysed for 5 min with 1× lysis buffer (10 mM Tris, 150 mM NaCl, 1 mM EGTA, 1 mM EDTA, 1% NP-40, 2 mM PMSF and 10 U DNase I) at 4°C, followed by treatment with 1 μM plasmin for 40 min at RT. Local fibrin deposition was evaluated by separating combined eluate samples on non-reducing SDS–PAGE gels, transferring to PVDF membrane and immunoblotting with rabbit anti-fibrinogen followed by anti-rabbit-HRP. Local platelet deposition and thrombin content was similarly evaluated by separating combined eluate samples on separate reducing SDS–PAGE gels and immunoblotting for CD41 or thrombin. Proteins were detected using ECL.

### 2.5.4 *Capture of samples downstream from thrombus formation under shear flow*

Flow chamber were coated as in Section 2.5.1 and integrated into flow system, Downstream samples were collected directly into 100 μM PPACK and 1.5% w/v sodium citrate (1 tube/min of perfusion) to final 50% dilution and evaluated using fluorescence-activated cell sorting (FACS). The initial shear rates were set by Harvard Apparatus PHD 2000 pump. Top loaded pump-driven syringes were connected to wells with blood via rubber washers which would disengage from the well upon pressure built up.

### 2.5.5 *Fluorescence-activated cell sorting (FACS) of distal events*

Pre- and post-chamber blood samples were collected into 100 μM PPACK and 1.5% w/v Na-citrate (1:1, v:v) and incubated with 1:50 dilution antibodies for 30 min at RT. Reactions were fixed by diluting 1:10 with RT 12.5% Cytofix<sup>BD</sup>. 10,000 single platelets were determined by a PE-conjugated



platelet marker CD41a and the characteristic forward and side-scatter scatter patterns via FACS (Canto II; BD Biosciences, Heidelberg, Germany). Platelet CD62P expression levels and single platelet consumption were determined as previously described.[284] Microaggregate formation was determined by the upshift in fluorescence intensity in CD31/CD41a double-positive events.

## **2.6 *In vivo* studies**

### *2.6.1 Non-human primate model of thrombosis*

Twenty four nonterminal studies were performed using twelve male baboons (*Papio anubis*, 9-11 kg). All studies were approved by the Institutional Animal Care and Use Committee of Oregon Health & Science University. Thrombosis experiments were conducted as previously described.[285,286] Briefly, a prosthetic vascular graft segments (4 mm internal diameter x 20 mm length, expanded-polytetrafluoroethylene; W. L. Gore & Associates, Flagstaff, AZ) coated with either collagen or BSA as control were acutely introduced into chronic femoral arteriovenous shunts as shown in Fig.6A, and exposed to blood flow. The flow rate through the graft was restricted to 100 mL/min (measured by the Transonics Systems flow meter, Ithaca, NY) by clamping the proximal shunt segment, thereby producing initial mean wall-shear rates of  $265 \text{ s}^{-1}$ . Local thrombus formation was assessed in real time with quantitative gamma camera imaging of radiolabeled platelet accumulation within the graft segment.

### *2.6.2 Assessment of distal platelet consumption in an in vivo thrombosis model*

Samples were collected distal to the graft from the bloodstream adjacent to the vessel wall (intraluminal boundary layer) into 3.8% w/v Na-citrate (1:9, v:v) before graft deployment (0 min), and then at 10 and 20 minutes. Blood was collected at a rate of 100  $\mu\text{L}/\text{min}$  during 10-minute intervals through a 0.64-mm id port located 10 mm distal to the graft as shown in Fig.6A. To maintain patency of the sampling port, PPACK (1 mM), which inhibits thrombin and other coagulation proteases,[287]

was infused at a rate of 20  $\mu\text{L}/\text{min}$  into a second 0.64-mm id port located 3 mm proximal to and in line with the collection port. Anticoagulant infusion and local blood sampling were regulated using syringe pumps (Harvard Apparatus, Holliston, MA). Platelet counts were determined using a micro-60 automated cell counter (Horiba ABX Diagnostics, Montpellier, France).

### 2.6.3 *Non-human primate model of sepsis*

*Papio anubis* baboons were dosed with a single 1 mg/kg intravenous bolus injection of anti-FXI antibody h14E11, 30 min before challenge. A lethal dose ( $1-2 \times 10^{10}$  cfu/kg) of *S. aureus* (strain B17266 Rosenbach, ATCC #49496) in 1.5 mL/kg sterile saline solution was infused intravenously over 2 hours (from  $T_0$  to  $T_{120}$  min). Blood samples were obtained at 0, 2, 4, 6 and 8 hours. Platelet levels were determined using a VetScan HM5 Hematology Analyzer (Abaxis). Whole blood samples were spun down to isolate plasma and plasma levels of fibrinogen levels were measured using a functional clotting assay developed by Clauss et al.[288]

### 2.6.4 *Mouse model of lethal pulmonary embolism*

Knockout (KO) mice were produced as described previously. In short, a B6/129 background was backcrossed 4 generations into C57BL/6 background.[289] These animals were mated with wild-type (WT) mice (C57BL/6, Jackson Laboratories) to make heterozygous animals and were re-derived into  $\text{Klkb1}^{-/-}$ .  $\text{Klkb1}^{-/-}$  mice and littermate WT colonies were maintained by brother/sister mating. Every 10 generations, the  $\text{Klkb1}^{-/-}$  mice are mated with C57BL/6J to re-derive KOs from the heterozygous mice. The genotyping of  $\text{Klkb1}^{-/-}$  mice was determined as described previously.[289]  $\text{FXII}^{-/-}$  mice (deficient in coagulation factor XII) in a C57BL/6J background were generously provided by Dr. Frank Castellino of the University of Notre Dame. Animal care and procedures were reviewed and approved by the Institutional Animal Care and Use Committees at Case Western Reserve University (CWRU) and performed in accordance with the guidelines of the American Association for Accreditation of

Laboratory Animal Care and the National Institutes of Health. Lung tissues were harvested, processed and stained with haematoxylin and eosin (H&E) stain to facilitate histopathologic studies. Images were obtained from a Leica SCN 400 Slide Scanner equipped with a Hamamatsu line sensor color camera and a 340/0.65 objective lens. The images were made through a 32 tube lens at 340 final magnification. Number of vessel occlusions quantified from H&E staining. Vessel occlusions per visual field were counted at 340.

### **Chapter 3. Dynamics of blood flow and thrombus formation in a multi-bypass microfluidic ladder network**

Jevgenia Zilberman-Rudenko, Joanna L. Sylman, Hari H. S. Lakshmanan,

Owen J. T. McCarty and Jeevan Maddala

This work was originally published by the Biomedical Engineering Society,

*Cellular and Molecular Biomedical Engineering*, 2017;10(1): 16-29.

with Editorial by Scott L. Diamond[290]

Permission is not required by the publisher for this type of use.

#### **3.1 Abstract**

The reaction dynamics of a complex mixture of cells and proteins, such as blood, in branched circulatory networks within the human microvasculature or extravascular therapeutic devices such as extracorporeal oxygenation machine (ECMO) remains ill-defined. In this report we utilize a multi-bypass microfluidics ladder network design with dimensions mimicking venules to study patterns of blood platelet aggregation and fibrin formation under complex shear. Complex blood fluid dynamics within multi-bypass networks under flow were modeled using COMSOL. Red blood cells and platelets were assumed to be non-interacting spherical particles transported by the bulk fluid flow, and convection of the activated coagulation factor II, thrombin, was assumed to be governed by mass transfer. This model served as the basis for predicting formation of local shear rate gradients, stagnation points and recirculation zones as dictated by the bypass geometry. Based on the insights from these models, we were able to predict the patterns of blood clot formation at specific locations in the device. Our experimental data was then used to adjust the model to account for the dynamical presence of thrombus formation in the biorheology of blood flow. The model predictions were then compared to results from experiments using recalcified whole human blood. Microfluidic devices were

coated with the extracellular matrix protein, fibrillar collagen, and the initiator of the extrinsic pathway of coagulation, tissue factor. Blood was perfused through the devices at a flow rate of 2  $\mu\text{L}/\text{min}$ , translating to physiologically relevant initial shear rates of 300 and 700  $\text{s}^{-1}$  for main channels and bypasses, respectively. Using fluorescent and light microscopy, we observed distinct flow and thrombus formation patterns near channel intersections at bypass points, within recirculation zones and at stagnation points. Findings from this proof-of-principle ladder network model suggest a specific correlation between microvascular geometry and thrombus formation dynamics under shear. This model holds potential for use as an integrative approach to identify regions susceptible to intravascular thrombus formation within the microvasculature as well as extravascular devices such as ECMO.

### **3.2 Introduction**

Use of hemodialyzers and extracorporeal membrane oxygenators improves patient survival and are therefore frequently used to maintain patients with kidney failure and/or acute respiratory distress syndrome despite significant thrombotic risks. These devices rely on evolving networks of exchange membranes [291,292] to promote efficient reagent exchange while reducing aberrant blood flow dynamics within complex geometries.[22,293] Studies in this chapter were designed to assess the kinetics of blood flow and thrombus formation within a specific multi-bypass channel network geometry in order to understand the role of specific flow patterns and geometry on blood cell transport and enzymatic coagulation dynamics in open (as supposed to closed) test systems.[6,294] In this chapter, we apply theory of biorheology and particle transport in fluids and utilize an integrated computational and experimental approach to predict and validate the role of microfluidic network geometry (and evolution of it in the presence of a thrombus formation) on thrombus nucleation and propagation. The findings and approach described herein provide a basis for rational exchange membrane microfluidic network design validation and improvement.

### 3.3 Background

Microfluidic flow chambers are powerful research tools as they require small amounts of blood samples to allow for investigation of blood cell-cell and cell-matrix interactions and thrombus formation under the dynamics of physiologically relevant levels of shear. Currently, the majority of microfluidic platforms used to assess thrombus formation rely on the coating of a single channel with extracellular matrix proteins, such as collagen, tissue factor (TF), or von Willebrand factor (VWF), to mimic a site of vascular injury.[272,294] These platforms have proven to be useful for the study of the biophysical and molecular mechanisms of thrombus growth at a fixed shear rate. Further, their utility has been demonstrated in studying complex shear-dependent interactions between platelets and vascular wall and diagnosing clotting disorders, such as VWF disease.[295,296] However, a single channel system fails to capture the complexities of branched vessel networks prevalent throughout the human circulatory system, or that exist in extravascular therapeutic device designs. In this report, we use a computational model to predict thrombus formation patterns within a multi-bypass network of channels. Our predictions were then tested experimentally following perfusion of recalcified human blood through the microfluidic device.

Within multi-bypass microfluidic geometries, whole blood is subject to complex flow dynamics. The presence of junctions and bifurcations in vascular networks can result in skewed velocity profiles, flow separation and secondary flows, attributed to sudden directional and dimensional changes within the channel network.[297,298] Subsequently, low flow regions develop, which allow for the accumulation of blood cells and accumulation of procoagulant proteases.[299] Moreover, blood leukocytes have been shown to preferentially adhere to surfaces downstream of channel bifurcations *in vitro* and *in vivo*.[300] Other flow disturbances imparted by complex geometries include stagnation points and fluid acceleration and deceleration, both of which have been associated with increased thrombus formation.[266,301]

The kinetics of thrombus formation within a multi-bypass channel geometry evolves over time as the blood flow is diverted due to the formation of an occlusive clot within the channel. Microvascular stenosis leads to a temporal increase in local shear rates, whereas occlusive thrombus formation leads to dramatic decreases in shear and local areas of blood stasis. Platelet adhesion and thrombin generation have been shown to increase within low shear zones at the downstream face of a forming thrombi.[301,302] Moreover, endothelial cells change their morphology and switch from an anticoagulant to a procoagulant phenotype within poststenotic zones, providing further evidence that the biorheology of blood flow is intimately related to the maintenance of blood vessel patency.[266,303]

Thrombus formation within a vessel network architecture can alter the distribution of blood cells within the bloodstream. In laminar blood flow, blood cells are distributed radially with platelets margined to the outer vessel wall and red blood cells (RBCs) preferentially comprising the inner core.[304–307] Shear rate has been shown to have a direct effect on blood viscosity due to an increase in RBC-RBC interactions, mediated by fibrinogen, occurring at shear rates below  $100 \text{ s}^{-1}$ .[308] In select regions of the branching vasculature, multiple and altered layers of RBCs and platelets have been observed to transiently divide the blood into relatively hemoconcentrated and hemodiluted streams, a phenomena know as plasma skimming.[309] For instance, organs containing microvessel channel networks, such as the spleen, placenta or the bone marrow exhibit high levels of plasma skimming,[310] which has been implicated to play a role in venous thrombosis in these vascular beds.[311,312]

This report describes a finite element simulation model of the biorheology of thrombus formation patterns within a multi-bypass microfluidic ladder network, which is subsequently validated with primary experiments using whole human blood. Our model predicts thrombus nucleation points at select regions of bifurcations, stagnation and recirculation based on velocity, shear rate and cell distribution profiles. Our model takes into account the effect of thrombus growth and thrombin

generation on blood flow within the ladder network. Overall, we demonstrate an integrated computational and experimental approach aimed to predict areas of thrombus formation within a branched microvascular geometry.

### **3.4 Materials and Methods**

#### *3.4.1 Reagents*

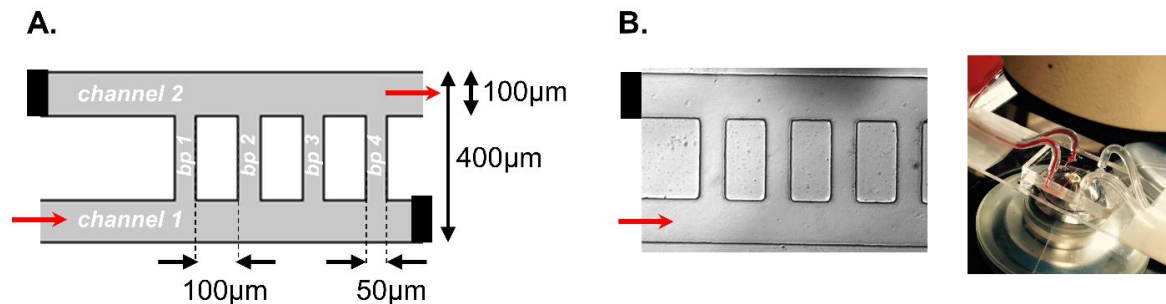
Dade<sup>®</sup> Innovin<sup>®</sup> was purchased from Siemens. All other materials were purchased from Sigma-Aldrich or previously cited sources.[313] Hepes-Tyrode buffer (129 mM NaCl, 20 mM HEPES, 12 mM NaHCO<sub>3</sub>, 2.9 mM KCl, 1 mM MgCl<sub>2</sub>, 0.34 mM Na<sub>2</sub>HPO<sub>4</sub>·12H<sub>2</sub>O; pH7.3) was modified with 0.045 g of glucose per 50 mL of buffer the day of experiment and kept in the 30°C bath until use.

#### *3.4.2 Fabrication of mask and microfluidic device*

The microfluidic ladder network was designed in AutoCAD to emulate the physiological parameters of postcapillary venules. The network was designed to consist of two sets of inlets and outlets entering two main channels (100 μm wide by 100 μm high) interconnected with ten equally spaced bypass channels (50 μm wide by 100 μm high); the first four bypasses are shown in Figure 3.1A. Paired contralateral inlets and outlets were stoppered and reopened at select iterations to achieve directional blood flow, originating from channel 1 and exiting from channel 2, while buffer was perfused from channel 2 to channel 1.

The mask was fabricated using standard photolithography and soft lithography techniques.[314,315] Our design was molded using a 10:1 ratio (w/w) of Sylgard<sup>®</sup> 184 polydimethylsiloxane (PDMS) polymer to curing agent. A BD-20AC Corona Treater (Electro-Technic products, Inc) was used to plasma bond PDMS molds onto microscopy slides. The final devices were assembled into the flow system as shown in Figure 3.1B.





**Figure 3.1 Modeling human blood flow and thrombus formation dynamics within a multi-bypass ladder network**  
 Parameters of a multi-bypass microfluidic ladder network device design (A) and an experimental prototype as visualized by differential interference contrast (DIC) microscopy (B). Network features two main channels and ten bypasses (bp 1-10); micrograph shows the first four bypasses. Black bars indicate a stoppered inlet and outlet; red arrows depict the direction of blood flow. Stoppered inlets and outlets were re-opened during the washing step.

### 3.4.3 Coating of microfluidic devices with collagen and tissue factor

Microfluidic devices were coated as previously described.[316] In short, devices were incubated with fibrillar collagen (150  $\mu\text{g}/\text{mL}$  in 10 mM acetic acid) for 1 hour with rotation at room temperature. Next, devices were rinsed with phosphate buffered saline (PBS) and incubated with a solution of Dade® Innovin® (0.1 nM tissue factor, TF, in ddH<sub>2</sub>O). Surfaces were then blocked with 5 mg/mL denatured bovine serum albumin (BSA) for 1 hour at room temperature. In parallel, control devices were incubated with appropriate dilution buffers, as described above, and blocked with BSA.

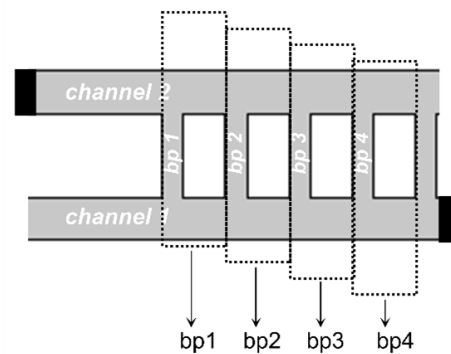
### 3.4.4 Blood collection and preparation

Whole blood was drawn by venipuncture from healthy adult volunteers into sodium citrate (0.38% w/v) in accordance with the Oregon Health & Science University Institutional Review Board. Blood was used within 2 hours of the blood draw. To allow detection of platelet-rich clot formation, blood was incubated with the mitochondrial dye 3,3'-Dihexyloxycarbocyanine Iodide (DiOC<sub>6</sub>; 2  $\mu\text{M}$  final). To initiate coagulation, blood was recalcified to a final concentration of 7.5 mM CaCl<sub>2</sub> and 3.5 mM MgCl<sub>2</sub> immediately prior to perfusion through the microfluidic device.

### 3.4.5 *Ex vivo blood flow assay*

Coated microfluidic devices were assembled into a pump-driven flow system. Modified HEPES-Tyrodes buffer was perfused through the device with a Harvard 2000 syringe pump in order to wet the channels and remove any air bubbles. We stoppered a contralateral channel inlet and outlet prior to perfusion of blood in order to reserve them for washing (inlet leading to channel 2 and outlet leaving channel 1; Figure 3.4A). DiOC<sub>6</sub>-stained sodium citrate (0.38% w/v) anticoagulated whole blood was recalcified and perfused through the coated microfluidic device at a flow rate of 2  $\mu\text{L}/\text{min}$ .

Real-time platelet aggregation was recorded using Zeiss Axio Imager 2 microscope (Carl Zeiss MicroImaging GmbH, Germany). After 30 min of blood perfusion, inlet and outlet channels were opened and networks were perfused with modified HEPES-Tyrodes buffer for an additional 20 min, followed by imaging with differential interference contrast and fluorescent light microscopy as previously described.[317] The surface areas of thrombi formed within each bypass and adjacent areas, as marked in Figure 3.2, were quantified using ImageJ and normalized per experiment to bypass 1. Average surface area fold changes and standard error means, SEM, were reported for 5 independent experiments (Figure 3.4D).



**Figure 3.2 Quantification of the spatial distribution of thrombus formation**

DiOC<sub>6</sub>-labeled whole human blood was perfused at a 2  $\mu\text{L}/\text{min}$  flow rate through a PDMS-ladder network coated with collagen and tissue factor; images of thrombus formation were recorded using differential interference contrast microscopy. The thrombus surface area was quantified for 5 experiments using ImageJ.

### 3.4.6 *Modeling*

#### 3.4.6.1 *Fluid dynamics*

The local hemodynamic environment was modeled using a commercial finite element software (COMSOL). The model included blood being perfused at a constant flow rate of 2  $\mu\text{L}/\text{min}$  through an inlet as shown in Figure 3.1. The exit pressure of the outlet was maintained at atmospheric pressure. At

these low flow rates, the Reynolds number (Re) is less than 1.  $Re < 1$  implies that the flow is viscous dominated, resulting in a creeping flow.

The Navier-Stokes modeling equations for incompressible creeping flow are given as follows:[318]

$$\rho \frac{\partial u(x, y)}{\partial t} = -\nabla p + \nabla \cdot (\mu (\nabla u + (\nabla u)^T))$$

where  $\rho$  is the density of blood cells, which was set at  $1060 \text{ kg/m}^3$ , P is pressure,  $t$  is time,  $\mu$  is the viscosity of blood, and  $u$  is the velocity profile.

Blood viscosity was estimated using a Power law which is given as follows:[319,320]

$$\mu = \lambda |\dot{\gamma}|^{n-1}$$

$$\lambda(\dot{\gamma}) = \mu_{\infty} + \Delta\mu \exp \left[ - \left( 1 + \frac{|\dot{\gamma}|}{a} \right) \exp \left( - \frac{b}{|\dot{\gamma}|} \right) \right]$$

$$n(\dot{\gamma}) = n_{\infty} - \Delta n \exp \left[ - \left( 1 + \frac{|\dot{\gamma}|}{c} \right) \exp \left( - \frac{d}{|\dot{\gamma}|} \right) \right]$$

where  $\mu_{\infty} = 0.035$ ,  $n_{\infty} = 1.0$ ,  $\Delta\mu = 0.25$ ,  $\Delta n = 0.45$ ,  $a = 50$ ,  $b = 3$ ,  $c = 50$  and  $d = 4$ .

The shear rate profile of the microfluidic network was modeled as follows:

$$\dot{\gamma} = \frac{1}{2} [\nabla u + (\nabla u)^T]$$

where  $\dot{\gamma}$  is the shear rate, and  $\nabla u$  is the gradient of the velocity. Using the above modeling equations, a velocity profile, shear rate and velocity streamlines were generated for the microfluidic network.

#### 3.4.6.2 Prediction of blood cell distribution

A particle-tracing module within COMSOL was used to predict the distribution of platelets and red blood cells (RBCs) within the channels. In the circulation, platelets marginate to preferentially populate a 2-5  $\mu\text{m}$  layer near the wall, whereas RBCs form a core in the center of the channel.

We modeled particle distribution changes within the complex geometry over time. Platelets and RBCs were modeled as spheres of 3.6  $\mu\text{m}$  and 8  $\mu\text{m}$  diameters, respectively, with a density of 1060

kg/m<sup>3</sup>. Particles with two different radii were released from the inlet at a predefined distribution: platelets were released with a normal distribution centered along the walls, whereas RBCs were released with a normal distribution at the center of the channel with a variance of 50 μm. The particle count ratio was set as 10 RBCs to 1 platelet and the RBC-core was set to occupy approximately 50% of the channel at the entrance, assuming a hematocrit of 0.5. The initial velocity of the particles at the inlet was set to be zero. Particles were transported by the viscous drag force on them due to the bulk flow.[318] As the particles moved through the channels, they were subject to a drag force, given as:

$$F = \frac{18\mu}{\rho_p d_p^2} m_p V_{rel},$$

where  $F$  is the drag force,  $\mu$  is the viscosity,  $\rho_p$  is the particle density,  $d_p$  is the particle diameter,  $V_{rel}$  is the relative velocity,  $m_p$  is the particle mass.[309] Particle trajectories were coupled to the continuous phase in a unidirectional manner.

#### *3.4.6.3 Prediction of thrombus nucleation points*

Initial thrombus nucleation points were predicted by integrating the blood flow velocity, shear rate, and blood cell distribution profiles as described above. The probability of a thrombus nucleating at a point within the network geometry was expected to increase with increased cell residence times, abrupt changes in shear and higher platelet counts.[6,304–307,321] Velocity streamline profiles initiated at the channel inlet predicted platelet residence times within the ladder network. Based on the assumption of a no-slip condition at the wall, the residence time was expected to be relatively higher near the walls of the channels as compared to the center of the channels, and reach infinity at the stagnation points created by the splitting of the bloodstream where the main channel and bypass intersection formed a right angle.

Based on the geometry, abrupt changes in the shear rate were expected immediately distal to the main channel intersection with bypasses.[322,323] The plasma skimming effect was assumed to

control the average number of platelets and RBCs present at each segment of the channel. Thrombus formation, modeled as solid spheres with a constant surface concentration of thrombin, was incorporated at these nucleation points (Figure 3.3E & F).

#### 3.4.6.4 Thrombin mass transfer

The mass transfer of thrombin within the microfluidic network was modeled to predict sites associated with increased thrombin levels. All clots were assumed to have thrombin surface concentrations of  $0.5 \text{ mol/m}^3$ . [324]

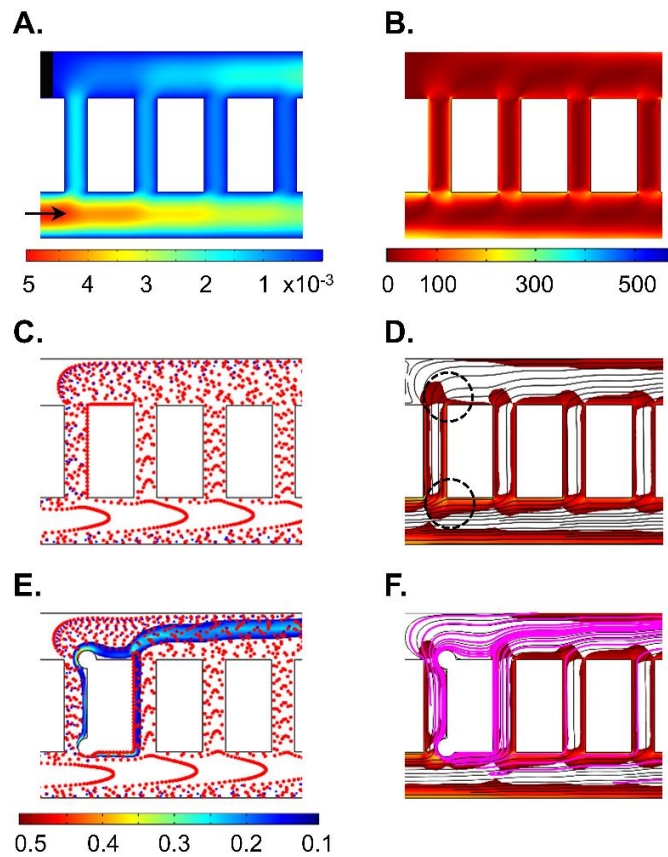
The equation used to obtain the concentration profiles is given below:

$$\nabla \cdot (-D_i \nabla C_i) + u \cdot \nabla C_i = 0$$

where  $D_i$  is the diffusivity of thrombin and was set at  $10 \text{ } \mu\text{m}^2/\text{s}$ , while  $u$  is the velocity profile in the network. [325] This equation along with the Navier-Stokes equation and continuity were solved simultaneously to obtain concentration and velocity profiles.

The Péclet number ( $LU/D$ ) of this flow was  $\gg 1$ , implying that the mass transfer of

thrombin within the bloodstream is expected to be largely dominated by convection as compared to diffusion. Therefore, the mass transfer of the most of the thrombin within bloodstream was expected to follow the streamlines as depicted in Figure 3.3F.



**Figure 3.3 Prediction of thrombus formation within the ladder network: nucleation and evolution**

Computer simulation of blood flow velocity profile (A;  $\mu\text{L}/\text{min}$ ), shear profile (B;  $\text{s}^{-1}$ ) and the initial blood cell distribution profile (C). A combination of velocity streamlines and shear rate gradient predicted a higher probability for the nucleation site for thrombus formation on the channel walls immediately downstream of intersections between main channels and bypasses (highlighted with black circles) (D). Computer simulations repeated in the presence of an obstruction to predict adjusted blood cell distribution profile during clot growth and thrombin convection  $\text{mol}/\text{m}^3$  (E) and combination of thrombin convection profile (purple) over bulk flow velocity streamlines and shear rate profile (F). Shear rates below  $30 \text{ s}^{-1}$  were subtracted from the shear rate heat maps on the overlays (D and F) for visibility of velocity streamlines.

#### *3.4.6.5 Prediction of the effect of thrombi formation propagation within ladder network*

Based on experimental observations of the thrombogenicity of collagen and TF-coated surfaces,[234,316] a simplified bypass-to-bypass thrombus propagation profile was developed and used to run simulations to study the dynamical effect of thrombus formation on the shear rate, platelet distribution and thrombin molar rate per bypass within the network. Simulations were performed for six scenarios corresponding to 0 – 30 min of perfusion time in 5 min steps. The thrombus formation within bypass 1 was expected to progress to 5%, 50% and 100% occlusion by 5, 10 and 15 min respectively. Geometric occlusion events were modeled as a pair of circular thrombi originating from the intersecting edges of each bypass with main channels 1 and 2. The bypass-to-bypass thrombus propagation relationship was set such as when the thrombus formation within the bypass ‘n’ reached 50% occlusion then the thrombus in bypass ‘n+1’ would reach 5% occlusion (Figure 3.5A).

Simulations for each metric per scenario were conducted at steady state. To estimate changes in the shear rate profile per bypass, a cut line method was used to monitor the changes in average shear rate as a function of occlusion percentage at each region marked by arrows (Figure 3.5B). The effect of sequential occlusion on the platelet trajectory was modeled by creating a particle counter at the exit of each bypass. The number of platelets travelled through each bypass were counted as a function of occlusion at the location indicated by arrows (Figure 3.5C). The sequential evolution of thrombus formation within the ladder network was expected to lead to dynamic changes in the thrombin flux in these bypasses and along the main channels. To estimate the amount of thrombin within the ladder network as a function of occlusion, a cut line method was used to calculate the average thrombin molar flow rate at regions indicated by arrows (Figure 3.5D).

### 3.4.7 *Statistical Analysis*

Data are shown as means  $\pm$  SEM. Statistical significance of differences between means was determined by ANOVA. If means were shown to be significantly different, multiple comparisons were performed by the Tukey test. Probability values of  $P < 0.05$  were selected to be statistically significant.

## 3.5 **Results**

### 3.5.1 *Modeling human blood flow and thrombus formation dynamics within a multi-bypass ladder network*

At sites of vascular injury, blood cells and proteins are subject to an evolving hemodynamic environment that determines the rate and morphology of thrombus formation. The goal of this project was to develop a computational model to predict the spatial and temporal dynamics of thrombus formation within a ladder network geometry. The prediction of the location and patterns of thrombus formation were then validated with primary experiments using whole human blood. We aimed to understand the contribution of complex branching and asymmetric geometries on thrombus initiation and propagation. Branching, stagnation points, and expansions were among the features of the microfluidic ladder channel. By having a multi-bypass model, we were able to study re-direction of flow from one bypass to the next as a result of the formation of an occlusive thrombus within the bypass channels. The microfluidic network ladder design in this report was designed to fall within the Stokes flow regime ( $Re \ll 1$ ) and therefore did not contain inertial driven features associated with larger diameter geometries (Figure 3.1).

### 3.5.2 Prediction of thrombi formation within a ladder network: nucleation and evolution

Four key parameters were simulated to predict the spatial and temporal dynamics of thrombus formation. These factors were: (i) blood flow velocity, (ii) shear rate gradient, (iii) blood cell distribution and (iv) thrombin convection profiles:

- (i) Blood flow velocity: Our COMSOL model predicted a series of stagnation points in which the blood velocity is close to zero and thus assumed to promote thrombus formation immediately downstream.[302] Formation of the stagnation points were predicted to occur at corners where the main channels intersect with bypass channels (Figure 3.2A).
- (ii) Shear rate gradient: Our model predicted a relative increase in local shear rates along the channel 1 wall and at corners at intersections between channel 1 and bypasses leading to channel 2 (Figure 3.2B). Thrombus formation was predicted to be favored near stagnation sites where the shear rate was predicted to undergo a rapid change in magnitude.[326] A combination of shear rate gradient and velocity profiles predicted a higher probability for nucleating thrombus formation on the channel walls immediately downstream of intersections between main channels and bypasses (Figure 3.2D; black circles).
- (iii) Blood cell distribution: Our model predicted that upwards of 50% of platelets were initially expected to separate into the first bypass (bp 1), due to the effect of plasma skimming (Figure 3.2C). Thus, the increased concentration of platelets in the first bypass was predicted to preferentially increase the rate of thrombus formation within the first bypass. Our model then predicted relatively decreased concentrations of platelets per unit volume in each subsequent bypass. However, as the flow rate decreased through the first bypass due to the formation of an occlusive thrombus within bp 1, the relative flow rate and



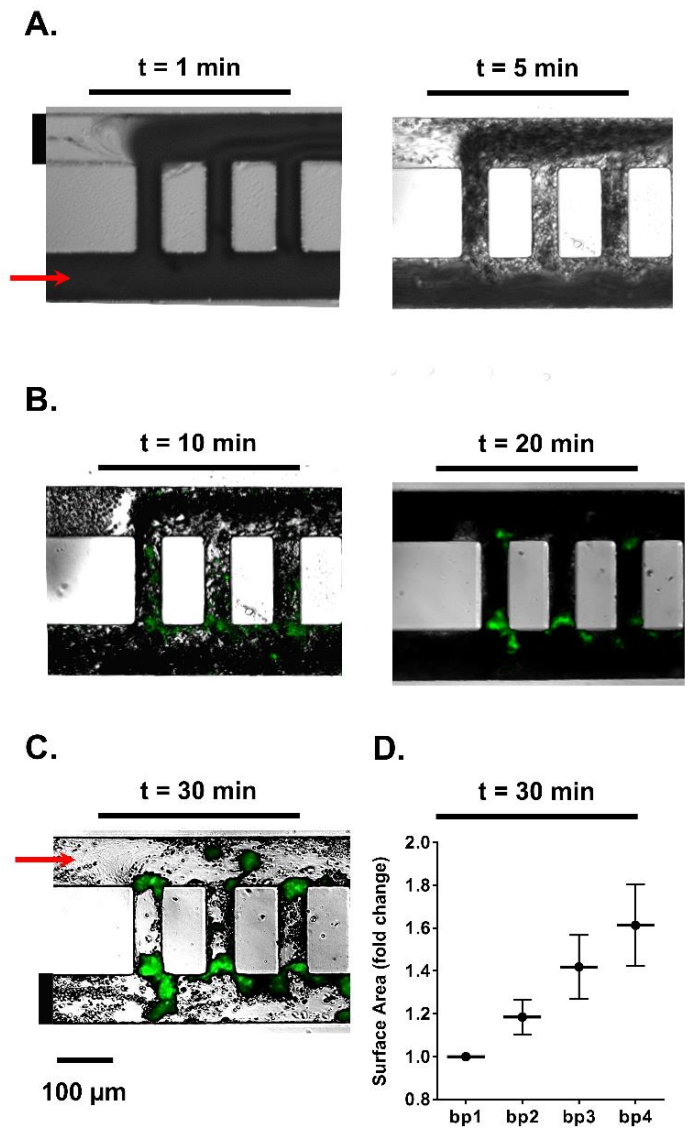
subsequent concentration of platelets was predicted to increase in the second bypass (bp 2), leading to an increased probability of thrombus formation in bp 2 as a function of time (Figure 3.2E).

- (iv) Thrombin convection: Nucleation of the initial site of thrombus formation, as predicted by blood velocity, shear gradient and cell distribution profile, was expected to serve as a local source of a thrombin generation. Thrombin is a potent serine protease with a diverse set of biological functions including the activation of platelets, activation of coagulation factors V, VIII and FXI, and cleavage of fibrinogen to form polymerized fibrin, all of which contribute to thrombus formation under flow.[327] Our model predicted that thrombin mass transfer in the bloodstream occurs via convection along the blood bulk flow (Figure 3.2F).

To summarize, our model predicted a higher probability of thrombus nucleation immediately downstream to locations in which the blood flow velocity is close to zero, and both shear gradients and platelet concentrations are higher as compared to the parameters found in the bulk bloodstream.

### 3.5.3 Temporal thrombus growth within a ladder network

We next studied the role of microfluidic channel geometry on platelet deposition and fibrin formation within a multi-bypass ladder network in an *ex vivo* blood flow assay. Platelet adhesion and aggregation were observed after the perfusion of recalcified whole human blood through the ladder network which was coated with collagen and tissue factor (Figure 3.4A). DiOC<sub>6</sub>-labeled (green) platelet aggregate formation was monitored in real-time using fluorescent light microscopy and revealed a pattern of increased platelet aggregate formation at the stagnation regions formed at intersection points between main channels and bypasses, starting at bypass 1 (Figure 3.4B). Moreover, after washing away non-adherent cells, an increase in the spatial distribution of fibrin was observed at the nucleation points and in regions where our model predicted transitions from high to low shear (Figure 3.4C).



**Figure 3.4 Temporal thrombus growth within ladder network** DiOC<sub>6</sub>-labeled whole human blood was perfused at a  $2 \mu\text{L}/\text{min}$  flow rate through a PDMS-ladder network coated with collagen and tissue factor; real-time images of thrombus formation were recorded using differential interference contrast (A) and fluorescence microscopy (B). Networks were subsequently washed with buffer for 20 min and re-imaged (C). Representative images shown,  $n=5$ . Total surface areas of thrombi per bypass were quantified and normalized to bp1 (D).

These experimental results validated the prediction of the thrombus nucleation at intersection points between the bypasses and main channels (Figure 3.2D). Quantitative analysis of the surface area of thrombi formed as a function of location demonstrated that thrombus formation occurred

sequentially from bypass 1 to bypass 2 and onwards to bypass 10, with preceding bypasses promoting larger thrombi formation, by surface area, in the subsequent bypass (Figure 3.4D).

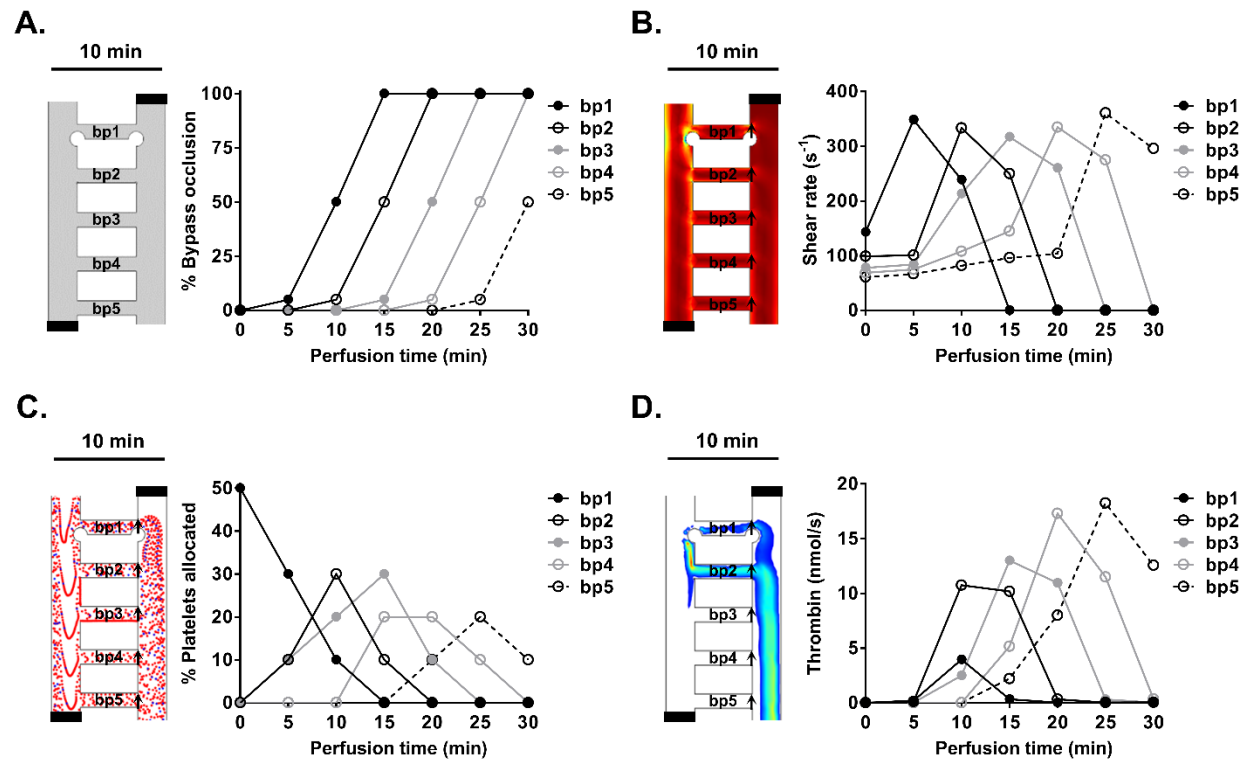
#### 3.5.4 *Prediction of the effect of thrombi formation propagation within a ladder network*

To predict the dynamical effect of thrombus formation on blood biochemistry within the microfluidic network, iterative simulations were performed and the effects of thrombus formation on shear, platelet distribution and thrombin molar rate were simulated at each bypass. Six separate scenarios with a set ratio of thrombus formation within bypasses were simulated. The scenario before blood entered a bypass, and thus prior to thrombus formation, was defined as a null scenario. Next, scenarios reflected thrombus growth within bypass 1 (bp1) in discrete time intervals of 5 minutes corresponding to 5%, 50% and 100% occlusion by 5, 10 and 15 min, respectively. For each scenario, a correlation between thrombus growth in a preceding and subsequent bypasses was set so that when a thrombus in bypass 'n' reached 50% occlusion, thrombus growth would commence in bypass 'n+1' and reach 5% occlusion (Figure 3.5A; Left panel shows simulation set up for a scenario at 10 min).

Our simulations showed that shear rate increases at bypass 1 (arrow) with 5% occlusion and start to fall at 50% occlusion as blood flow starts to redirect to and result in an increase in shear in the subsequent bypass (Figure 3.5B). Shear rate was expected to drop to zero once the bypass reached full occlusion. Our model predicted that platelet trajectories in the ladder network were sensitive to changes in the geometry due to thrombus formation. The sequential growth of thrombi was predicted to lead to increasing resistance in each bypass resulting in redirection of flow and platelets to subsequent bypasses.

Our model predicts that approximately half of the platelets will travel through bypass 1 prior to thrombus formation and that platelet concentrations within bypass 1 will decrease as the bypass starts to occlude, resulting in shunting of blood flow to downstream bypasses (Figure 3.5C). Our model predicted that the thrombin convection profile at each subsequent bypass would be higher than at the

previous bypass (Figure 3.5D). The presence of thrombi in an upstream bypass was predicted to serve as a surface for thrombin generation and convection into the blood flow. At complete occlusion of bypass 1, the overall molar flow rate of thrombin was expected to reach zero due to zero velocity.



**Figure 3.5 Prediction of the effect of thrombus formation within a ladder network**

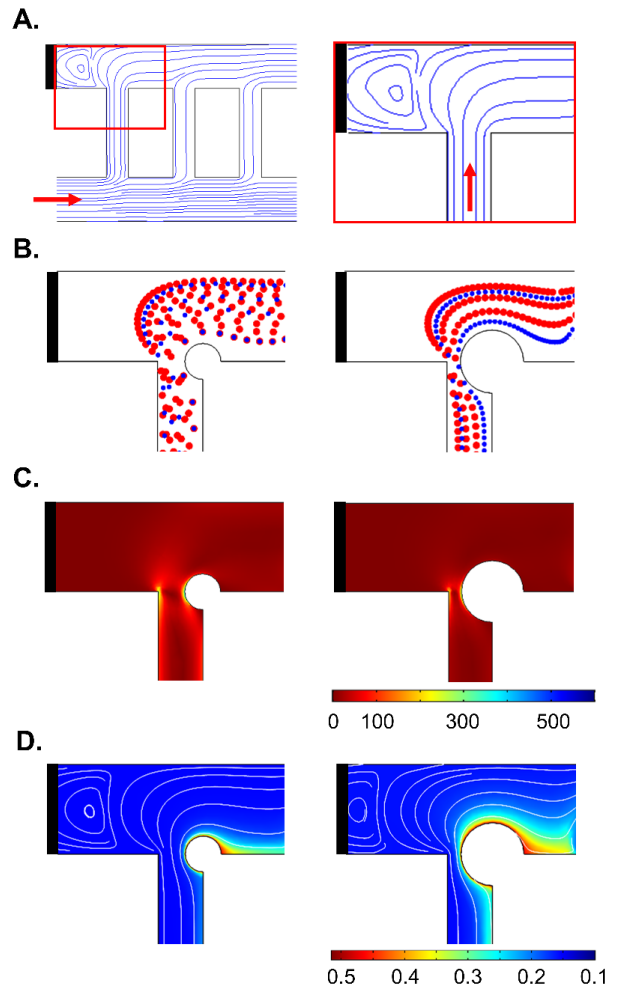
Computer simulations of the effects of thrombus formation on the dynamics of blood flow dynamics were performed at discrete time and bypass-to-bypass locations (A). The changes in shear profile (B;  $s^{-1}$ ), platelet distribution profile (C) and concentration profile of thrombin (D; nmol/s) at each bypass were calculated as a function of time. Arrows indicate regions of measurement integration.

### 3.5.5 Prediction of the effect of the flow recirculation on platelet aggregation and fibrin formation

In addition to predicting stagnation points and rapidly changing shear gradients within our ladder network, our model also predicted formation of a recirculation zone at the stoppered inlet of channel 2 due to the flow obstruction at the entrance of blood into the channel 2 from channel 1 via the first bypass, bp 1 (Figure 3.6A).

As the blood circulates through the first bypass, the boundary between the plasma layer and the no-flow zone moves along the direction of the plasma layer, thus creating a recirculation zone in the no-flow region. Our model predicted that platelets entering the recirculation zone would be exposed to lower levels of shear, and therefore would be less likely to aggregate as compared to the corners of the t-branch between bp 1 and channel 2, where platelets were predicted to experience the greatest acceleration in the change in shear (Figure 3.6B & C).

A decrease in flow rate was predicted to occur as the channel was occluded with a growing thrombus, resulting in partial flow redistribution to the other channels. The shear rate in the obstructed section of bp 1 was predicted to significantly increase due to the decrease in cross-sectional area. Our model predicted an increase in convection of thrombin into the recirculation zone as a function of obstructive thrombus formation as a combined result of the increased rate of thrombin generation at

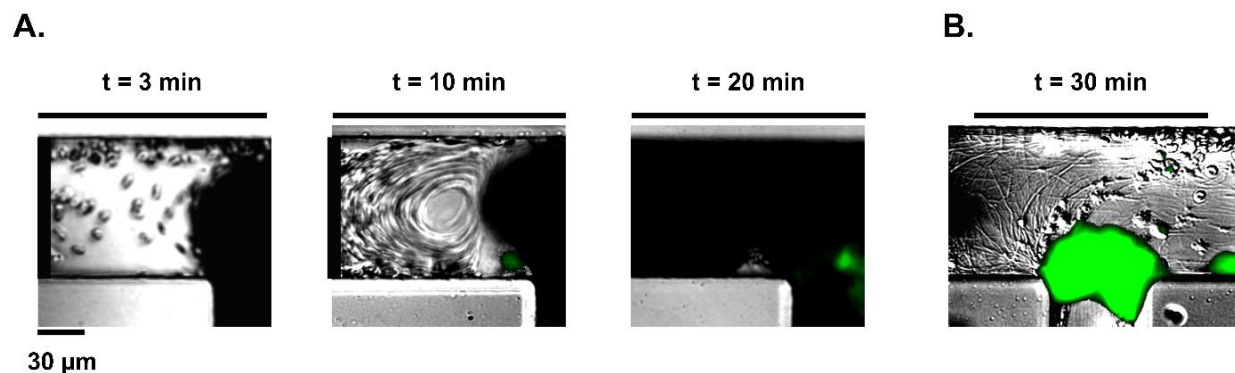


**Figure 3.6 Prediction of the effect of the flow recirculation on platelet aggregation and fibrin formation**  
Computer simulation of the streamlines of the bulk blood flow through the network ladder predicts a flow distortions at the intersection of the first bypass (bp 1; resulting in a zone of recirculation), at the stoppered channel (black bar), and at channel 2 (A). Simulation of blood cell transport during thrombus formation: < 50% of bypass obstruction, left, and > 50% bypass obstruction, right (B); shear rate profile (C) and thrombin convection profile mol/m<sup>3</sup> (D) within these regions.

the site of thrombus formation, an increase in plasma recirculation and reduced elimination by convection (Figure 3.6D).

### 3.5.6 *Effect of flow recirculation on platelet aggregation and fibrin formation*

To examine the role of blood flow recirculation on platelet aggregation and fibrin formation, a second set of contralateral inlet and outlet channels was stoppered (inlet leading to channel 2 and outlet leaving channel 1), after equilibration of the microfluidic network with buffer and before addition of recalcified whole human blood; this introduced a blood flow recirculation zone immediately next to the first bypass (bp 1). Upon blood entry into the first bypass from channel 1, blood flow was diverted into channel 2 by the pull of a syringe pump connected to the outlet (Figure 3.7A). Within minutes, we observed the transfer of blood cells from the blood bulk flow into the recirculation zone. A robust degree of fibrin formation was observed within the recirculation zone, while interestingly, we observed little platelet deposition or aggregation within the recirculation zone (Figure 3.7B). Fibrin strands were formed in the direction of the predicted stream lines of blood flow within the recirculation zone.



**Figure 3.7 Effect of flow recirculation on platelet aggregation and fibrin formation**

Dynamics of whole human blood flow at the intersection where the first bypass meets a stoppered channel, creating a recirculation zone (black bar); platelet aggregation was recorded using differential interference contrast and fluorescence microscopy in real time (A) while fibrin was imaged following a washing step (B). Representative images shown, n = 3.

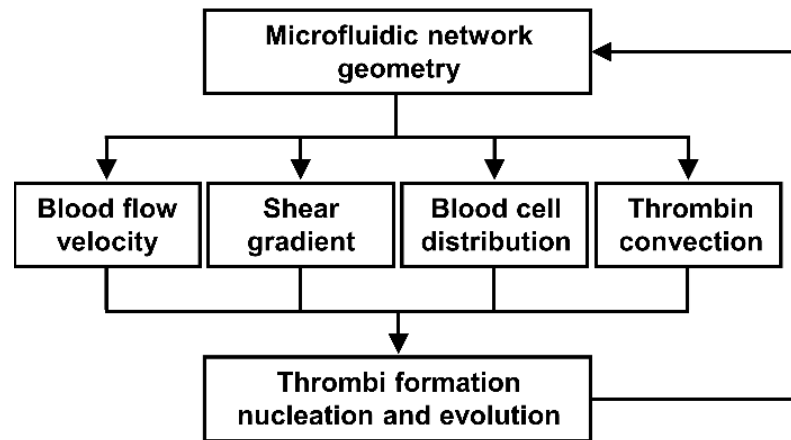
### 3.6 Discussion

Microfluidic devices have provided benefit in acting as a platform for understanding the mechanisms underlying the processes of occlusive thrombus formation within the vasculature and have potential for development as point-of-care therapeutic devices.[295,296,328–330] Notably, development of microfluidic oxygenator units to promote gas exchange has been of significant interest in the field.[331–335] Microfluidic networks may have utility in extracorporeal devices to trap bubbles and emboli as well as measure levels of reagents and toxins.[336–339] However, the role of the microfluidic network geometry in the thrombogenicity of devices such as extracorporeal oxygenation machine (ECMO), left ventricular assist devices, and nanomembrane hemodialysis cassettes is not well defined.[330,340,341]

An integrated approach of studying blood flow and thrombus formation within microfluidic networks in the presence of coagulation may be useful in understanding how the physical biology of a microfluidic device promotes thrombus formation, which may help in the development of safer therapeutic device designs. Moreover, this approach may further help predict the risk of thrombus formation within physiological microvascular network geometries found in human organs, such as the spleen, placenta, kidney and brain.[310,342,343] In this report, we have described a proof-of-principle integrated approach of studying blood flow and thrombus formation patterns in a multi-bypass microfluidic ladder network as summarized in Figure 3.8.

Incorporating computer simulation and experimental design, we were able to characterize the spatial and temporal distribution of platelet aggregation and fibrin formation as a function of the biorheological parameters of blood flow velocity and shear gradients and platelet and RBC distribution. We were able to determine how the initial conditions evolved as a function of sequential occlusive thrombus formation in bypasses within our ladder network. Our integrated approach utilized fundamental fluid dynamics principles to solve the effect of an evolving channel geometry due to the formation of an occlusive thrombus within the bypass geometry. Our approach can be used to develop

generalizable predictions of sites of thrombus formation within microfluidic network geometries. Our findings suggest that the rate of thrombus formation is enhanced in zones of prolonged platelet residence times and rapid shear gradients, blood compositions favoring platelet enrichment, and sites with elevated thrombin concentrations.



**Figure 3.8 An integrated approach to study thrombus formation within a microfluidic network.**

Integrated approach of creating simulations of blood flow velocity, shear and blood cell distribution profiles to predict the site of thrombus formation. Modeling was repeated to account for the dynamical response of blood rheology and thrombin generation as a function of temporal thrombus formation.

Our microfluidic ladder network was comprised of T-junctions connecting two parallel main channels and bypasses with 90 degree angles. Sharp angle bends were previously shown to cause skewed velocity flow profiles, decreases in velocity at fixed pressure drops as well as flow separation and recirculation zones, particularly in high Reynolds number flow.[344–346] Finite element simulations of a Newtonian fluid flow at different angle bifurcations have shown that for a fixed pressure drop, the variation of the bifurcation angle from 60 to 120 degrees resulted in an average velocity reduction of 1-4% compared to a channel with no bend, with laminar flow being maintained at a low Reynolds number.[346] Moreover, flow simulations of non-Newtonian power-law fluids encountering a 90 degree bifurcation have shown that recirculation zones and flow separations should not form when the Reynolds number is below 5.[347] In our setup we perfused whole blood, simulated



as a power law fluid with index  $n \leq 1$ , through a microfluidic network with Reynolds numbers below 1, and observed no turbulence in the flow field imparted by the sharp angle. However, we did note asymmetry in the velocity profile that could potentially influence thrombi formation. Our future work will look to incorporate quantitative methods to record blood cell flow in real time in order to validate the predicted flow profiles through the network geometry.

This report focused on thrombus formation patterns within the Stokes flow regime (Reynolds number;  $Re \ll 1$ ) and simplification of classifying blood cells as particles with constant diameters. Future work will focus on improving our model to predict the dynamics of thrombus formation in larger channels, with larger Reynolds numbers, which would need to take into account contributions from inertial flows and recirculation zones at sharp angles.[347] Furthermore, in certain vessel geometries, inherent blood cell shape and deformability would be expected to play an important role.[348–350] Another limitation of our model was the assumption that thrombin remained active in the bloodstream and that mass transfer via convection from upstream thrombi within the network contributed to the downstream flux of thrombin within subsequent bypasses. Thrombin is known to be rapidly inactivated by plasma inhibitors such as antithrombin (ATIII) and heparin cofactor II;[26–28] on the other hand, thrombin catalyzes its own feedback generation through activation of the coagulation factor XI. Our future work will focus on incorporating the kinetic parameters of thrombin generation and inactivation into our model of thrombin formation and downstream propagation within a ladder network. Our goal is to integrate this approach to predict the prothrombotic phenotype of specific vascular beds, such as encountered in the brain and lung, as well as extending our models to study the flow patterns within extravascular devices, such as ECMO.

Geometric factors of a bypass significantly influence thrombus formation, notably in complex configurations found in artificial flow networks. Extravascular therapeutic devices such as ECMO are used to pump and oxygenate a patient's blood during heart or lung surgery / failure. In veno-arterial ECMO, blood is oxygenated while it travels from a femoral vein into an artificial membrane lung

consisting of a branched network of thousands of small tubes before returning to the circulation via a femoral artery.[351] The blood flow within network is affected by changes in dimension, disturbances in the tubing such as stagnation points and stenoses, branching channels, and curved geometries. Our model and experimental data identify stagnation points and large shear gradients as regions of increased thrombogenicity. Along these lines, large expansions or contractions associated with rapid flow acceleration and deceleration have been shown to influence platelet aggregation both *in vitro* and *in vivo*. [266,301] Moreover, curved channels have been shown to cause velocity profile shifts resulting in secondary flow and exhibit increased potential as sites of thrombus formation.[352,353]

In conclusion, current ECMO designs require a systemic anticoagulant such as heparin to maintain patency, putting the patient at risk for serious bleeding complications. A better understanding of the thrombogenic profile of devices that contain ladder networks may help in optimizing geometric designs to decrease thrombin generation, thus lowering the risk of device failure due to occlusive thrombus formation.

## **Chapter 4. Biorheology of platelet activation in the bloodstream distal to thrombus formation**

Jevgenia Zilberman-Rudenko, Asako Itakura, Jeevan Maddala, Sandra M. Baker-Groberg, Ralf Vetter, Erik I. Tucker, András Gruber, Christoph Gerdes, Owen J.T. McCarty

This work was originally published by the Biomedical Engineering Society,

*Cellular and Molecular Biomedical Engineering*, 2016;9(4):496-508.

Permission is not required by the publisher for this type of use.

### **4.1 Abstract**

Thrombus growth at the site of vascular injury is mediated by the sequential events of platelet recruitment, activation and aggregation concomitant with the initiation of the coagulation cascade, resulting in local thrombin generation and fibrin formation. While the biorheology of a localized thrombus formation has been well studied, it is unclear whether local sites of thrombin generation propagate platelet activation within the bloodstream. In order to study the physical biology of platelet activation downstream of sites of thrombus formation, we developed a platform to measure platelet activation and microaggregate formation in the bloodstream. Our results show that thrombi formed on collagen and tissue factor promote activation and aggregation of platelets in the bloodstream in a convection-dependent manner. Pharmacological inhibition of the coagulation factors (F) X, XI or thrombin dramatically reduced the degree of distal platelet activation and microaggregate formation in the bloodstream without affecting the degree of local platelet deposition and aggregation on a surface of immobilized collagen. Herein we describe the development and an example of the utility of a platform to study platelet activation and microaggregate formation in the bloodstream (convection-limited regime) relative to the local site of thrombus formation.

## 4.2 Introduction

In this chapter we build on observations described in Chapter 3 to develop an *ex vivo* flow model to mimic a local site of vascular injury in combination with the downstream collection of blood samples to allow for the analysis of distal platelet activation, microaggregate formation and single platelet consumption in flowing blood. We use an integrated approach of computational simulation and experimental data to assess effects of shear and residence time distal to thrombus formation on platelet activation and consumption in flowing blood. This study demonstrates the utility of a measurement platform to assess platelet activation and microaggregate formation in solution downstream of sites of thrombus formation under shear flow. This work further prompts subsequent studies described in Chapter 5 to understand the role of specific coagulation factors in the distal effects of thrombus formation, which may lead to the development of safer and more effective antithrombotic agents.

## 4.3 Background

Platelets and coagulation factors contribute to both hemostasis, a physiological response to staunch blood loss from an injured vessel, and thrombosis, a pathological development of a clot that obstructs the vessel lumen. At sites of vessel injury, circulating platelets are rapidly recruited to the exposed extracellular matrix under shear flow, followed by platelet activation.[354] Platelet activation triggers the surface expression of CD62P (P-selectin) from  $\alpha$ -granules, and expression of active glycoprotein (GP) IIb/IIIa, by which platelets can form homotypic aggregates via fibrinogen binding. In parallel, the exposure of blood to tissue factor (TF) or negatively charged surfaces induces activation of extrinsic and intrinsic coagulation pathways, respectively, leading to thrombin generation and fibrin formation. Contact with negatively charged surfaces induces autoactivation of the zymogen coagulation factor XII (FXII).[355] Activated FXII (FXIIa) is a serine protease that converts coagulation factor XI (FXI) to the activated form of FXI (FXIa). Subsequently, FXIa activates factor

IX (FIX), which in turn activates factor X (FX). Activated FX (FXa) then converts prothrombin to thrombin. In addition to fibrin formation and platelet activation, thrombin can mediate feedback activation of FXI to perpetuate its own generation.[139] Thrombin converts fibrinogen to fibrin, and cleaves platelet protease-activated receptors (PARs). The complex mass of fibrin and activated platelets forms the basis of a hemostatic plug or, under pathological conditions, a thrombus that obstructs blood flow.

The rate of platelet activation, aggregation and fibrin formation in a fluid shear environment (i.e., flowing blood) is a balance between the delivery of reactants (platelets and coagulation factors) to the local site of vascular injury relative to the rate of assembly and (in)activation of coagulation factors on the activated platelet surface.[22] The biorheology of local thrombus formation has been extensively studied *in silico*, *in vitro* and *in vivo*. [356] However, the process by which local generation of thrombin at sites of thrombus formation promotes the activation of the coagulation cascade and platelets in the bloodstream is ill-defined. The aim of this study was to develop a platform to define the physical biology of platelet activation and microaggregate formation in the bloodstream distal to sites of local thrombus formation. An improved understanding of platelet activation and aggregate formation in the bloodstream may lead to the identification of antithrombotic targets that prevent distal platelet activation in the bloodstream without affecting local hemostasis.

## **4.4 Materials and Methods**

### **4.4.1 Reagents**

Fibrillar collagen reagent was purchased from Nycomed Austria GmbH (Linz, Austria). The tetrapeptide Gly-Pro-Arg-Pro-OH fibrin polymerization inhibitor, Pefabloc® FG (GPRP) was purchased from Pentapharm (Basel, Switzerland). Serine protease inhibitor Phe-Pro-Arg-chloromethylketone (PPACK) was purchased from Santa Cruz and tissue factor (TF, Dade Innovin) was purchased from Siemens. Murine monoclonal anti-FXI antibodies 1A6 and 14E11 were cloned,

expressed and purified as described.[139] The antibody 14E11 blocks the kininogen-binding region on the apple 2 (A2) domain and inhibits the activation of FXI by FXIIa.[140] The antibody 1A6 blocks the FIX-binding region on the A3 domain of FXI and inhibits FIX activation by FXIa.[140] The direct inhibitor of activated factor X (FXa), rivaroxaban, and thrombin inhibitor, melagatran, were provided from the manufacturer Bayer HealthCare AG. Rivaroxaban binds reversibly to FXa via the S1 and S4 pockets and inhibits FXa serine protease activity.[357] PE-conjugated mouse anti-human CD41a and CD61a, and APC-conjugated mouse human anti-CD62P was purchased from BD Biosciences (Heidelberg, Germany). Thrombin receptor activator peptide-6 (TRAP-6) was purchased from Bachem (Bubendorf, Switzerland). The partial thromboplastin time (aPTT) reagent, STA C. K. Prest 5 was purchased from Diagnostica STAGO (Asnières-sur-Seine, France). TriniCLOT calcium chloride was purchased from Trinity Biotech (Bray, Ireland). All other reagents were from Sigma-Aldrich (St. Louis, MO, USA) or previously named sources.[234,358]

#### 4.4.2 *Collection of human blood*

Human venous blood was drawn by venipuncture from healthy adult volunteers in accordance with the Oregon Health & Science University institutional review board. Blood was taken into 3.8% (w/v) sodium citrate using a ratio of 1 part citrate: 9 parts blood and immediately used for experiments.

#### 4.4.3 *Clotting time assay*

The activated partial thromboplastin time (aPTT) of human plasma were measured with a Trinity AMAX200 coagulation analyzer (Trinity Biotech, Bray, Ireland). Pooled human plasma was pretreated at 37°C for 10 min with 1A6, 14E11 or rivaroxaban, followed by incubation with aPTT reagent for 3 min at 37°C. Coagulation was then initiated by the addition of CaCl<sub>2</sub> (8.3 mM final), and clotting times were recorded.

#### 4.4.4 *Flow chamber assay*

The volume and surface area of platelet proximal aggregates were measured as previously described.[283] Briefly, glass capillary tubes (0.2 × 2 mm, VitroCom, Mountain Lakes, NJ, USA)

were coated with collagen (150 µg/ml) for 1 hr at room temperature, washed and incubated with tissues factor (TF, 0.1 nM) for additional hour, when indicated. Surfaces were blocked with 5 mg/ml denatured bovine serum albumin (BSA) for 1 hr prior to assembly into a flow system on the stage of a Zeiss microscope (Carl Zeiss, Thornwood, NY). Citrate-anticoagulated whole blood was incubated with the fibrin polymerization inhibitor, tetrapeptide Gly-Pro-Arg-Pro-OH (GPRP; 3 mM final) prior to the incubation with vehicle, 1A6 (1-50 µg/ml), 14E11 (1-50 µg/ml), or rivaroxaban (30-300 nM) for 10 min at 37°C. Blood was re-calcified to final of 7.5 mM CaCl<sub>2</sub>, 3.5 mM MgCl<sub>2</sub> immediately prior to perfusion over the collagen/TF-coated slide at a set initial shear for 5-10 min. The capillary tubes containing platelet aggregates were washed for 5 min with modified Hepes/Tyrode buffer (129 mM NaCl, 12 mM NaHCO<sub>3</sub>, 2.9 mM KCl, 20 mM HEPES, 1 mM MgCl<sub>2</sub>, 0.34 mM Na<sub>2</sub>HPO<sub>4</sub>·12H<sub>2</sub>O, 5.6 mM glucose; pH 7.3) at the same shear rate to remove unbound blood components.

The samples were fixed with 4% paraformaldehyde for image analysis. Z-stack images from three random fields of view (215 µm × 160 µm) were processed for each sample and taken from the surface of the slide to 5 µm above the platelet aggregate. For the data presentation, the volume histograms used 150 µm<sup>3</sup> size bins, while the surface area histogram used 40 µm<sup>2</sup> size bins, as previously described.[317] For the measurement of distal platelet activation in the presence of pharmacological antagonists, glass slides (Menzel-Gläser SUPERFROST 76 × 26 mm; Gerhard Menzel GmbH, Braunschweig, Germany) were coated with collagen (150 µg/ml) overnight at 4°C, followed by blocking with BSA prior to assembly into a flow system on the stage of a Zeiss microscope. Whole blood downstream of the flow chamber was collected into modified Hepes/Tyrode buffer containing 100 mM PPACK and 3.8% (v/w) sodium citrate at 1 min intervals. In parallel, whole blood was sampled from the upstream of the flow chamber and treated with buffer control (vehicle) or TRAP-6 (10 µg/ml) for 5 min.

#### 4.4.5 Fluorescence Activated Cell Sorting (FACS)-analysis

Blood samples collected from the upstream and downstream of the flow chamber were diluted with modified Hepes/Tyrode buffer containing 100 mM PPACK and 3.8% (v/w) sodium citrate and incubated with antibodies for 20 min. To stop antibody-labeling reactions, samples were diluted 1:10 with CellWash/Permafix (BD Biosciences). 10,000 single platelets were determined by a PE-conjugated platelet marker (CD41a or CD61a) and the characteristic forward and side-scatter patterns via flow cytometry (FACS). Platelet CD62P expression levels, microaggregate formation and single platelet consumption were determined as previously described.[284]

#### 4.4.6 Simulation of thrombin mass transfer in flow distal to thrombus formation

The distribution of thrombin in the bloodstream distal to the local site of thrombus formation was modeled using COMSOL with a single activated platelet as a source of initial thrombin concentration. The activated platelet is assumed to generate thrombin flux with a constant surface concentration of 0.5 mol/m<sup>3</sup>. [324] Platelets' diameter was set to 3.6 μm and platelets were assumed to move with the bulk blood flow at approximately 10-15 μm from the wall surface of a 1.0 mm diameter channel. Our model assumes that the neighboring platelets get rapidly activated and degranulate immediately due to the change in thrombin flux. [359]

This phenomena was incorporated in the model by giving a time delay in thrombin generation from the adjacent platelets. The time delay is estimated by calculating the time taken for the thrombin to reach the adjacent platelets, less than 1 second. The activated platelets also contribute to the overall thrombin concentration with the same boundary condition as the first platelet. The equation used to obtain the thrombin concentration profiles in flow was:

$$\frac{\partial c_i}{\partial t} = \nabla \cdot (D_i \nabla C_i) - u \cdot \nabla C_i$$

The boundary condition on the first activated platelet (p1) was set as:  $C_{s,p1} = 0$  at  $t = 0$  and  $0.5 \frac{mol}{m^3} \forall t > 0$  and for the rest of the platelets the same boundary condition was applied after a



delay (i.e.  $0 \forall t < \delta$  and  $0.5 \frac{mol}{m^3} \forall t > \delta$ ). In the above equation,  $D_i$  is the diffusivity of thrombin and is taken as  $10 \mu m^2/s$  and  $u$  is the velocity profile in the network.[325] This equation along with the Navier Stokes equation and continuity were solved simultaneously to obtain thrombin concentration and velocity profiles at 62.25, 250, 1000 and 4000  $s^{-1}$  shear rates.

Peclet number ( $LU/D$ ) of this flow was  $\gg 1$ , which implies that mass transfer was dominated by convection compared to diffusion resulting in thrombin distribution mostly along the stream lines of the bulk flow. Based on this hypothesis it can be predicated that lower flow rates will have thicker ‘plumes’ of thrombin near the walls of the channel compared to higher flow rates, resulting in a higher level of platelet aggregation in the bloodstream at lower flow rates.

#### 4.4.7 *Statistical Analysis*

Data are shown as means  $\pm$  SEM. Statistical significance of differences between means was determined by ANOVA. If means were shown to be significantly different, multiple comparisons were performed by the Tukey test. Probability values of  $P < 0.05$  were selected to be statistically significant.

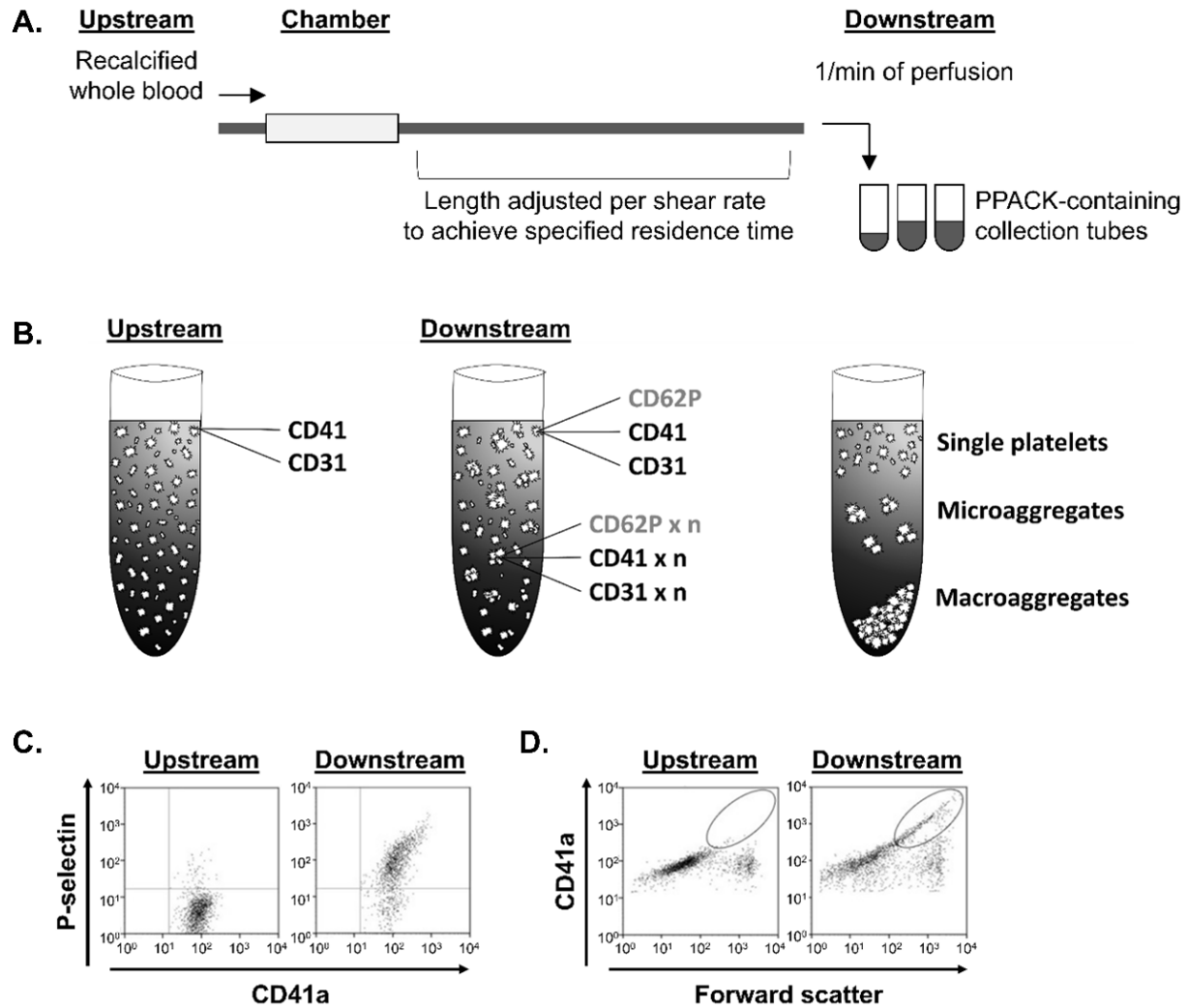
## 4.5 Results

### 4.5.1 *Development of a platform for the study of local and distal platelet activation.*

To investigate and characterize the biorheology of platelet activation in the bloodstream distal to sites of thrombus formation on collagen and tissue factor (collagen/TF)-coated surfaces as compared to control surfaces coated with bovine serum albumin (BSA control), we developed a FACS-based assay to measure platelet activation and microaggregate formation in downstream samples (Figure 4.1A).

Following perfusion of recalcified whole-blood through the flow chamber, downstream samples were collected at 1 min intervals and analyzed for platelet P-selectin (CD62P) expression as well as platelet-platelet aggregation. We utilized the fibrin-polymerization inhibitor, GPRP, in order to focus our current study on single platelet recruitment and platelet-platelet aggregation in the absence of extensive fibrin formation. This is a limitation of the current study, as fibrin is known to serve as a sink for thrombin. Single platelets in the bloodstream samples were detected by the combination of light scattering and PE-CD41/CD61 (GPIIb/IIIa) fluorescence. Quantification of the percentage of platelet activation was achieved by creating a gate around platelets with CD62P expression above the threshold on CD62P/CD41a scatter plots and normalizing events within gate to total CD41a-positive events (Figure 4.1B).

To quantify platelet microaggregate formation in the blood downstream of the collagen/TF or BSA-coated flow chamber, CD41a/forward scatter plots were generated and CD41a-positive events with increased forward scatter and mean fluorescence intensity were defined as platelet microaggregates and reported as events versus  $10^4$  single platelets (Figure 4.1C). This measurement platform allowed for the study of the effect of the local activation of the coagulation cascade on the activation of platelets in the bloodstream.



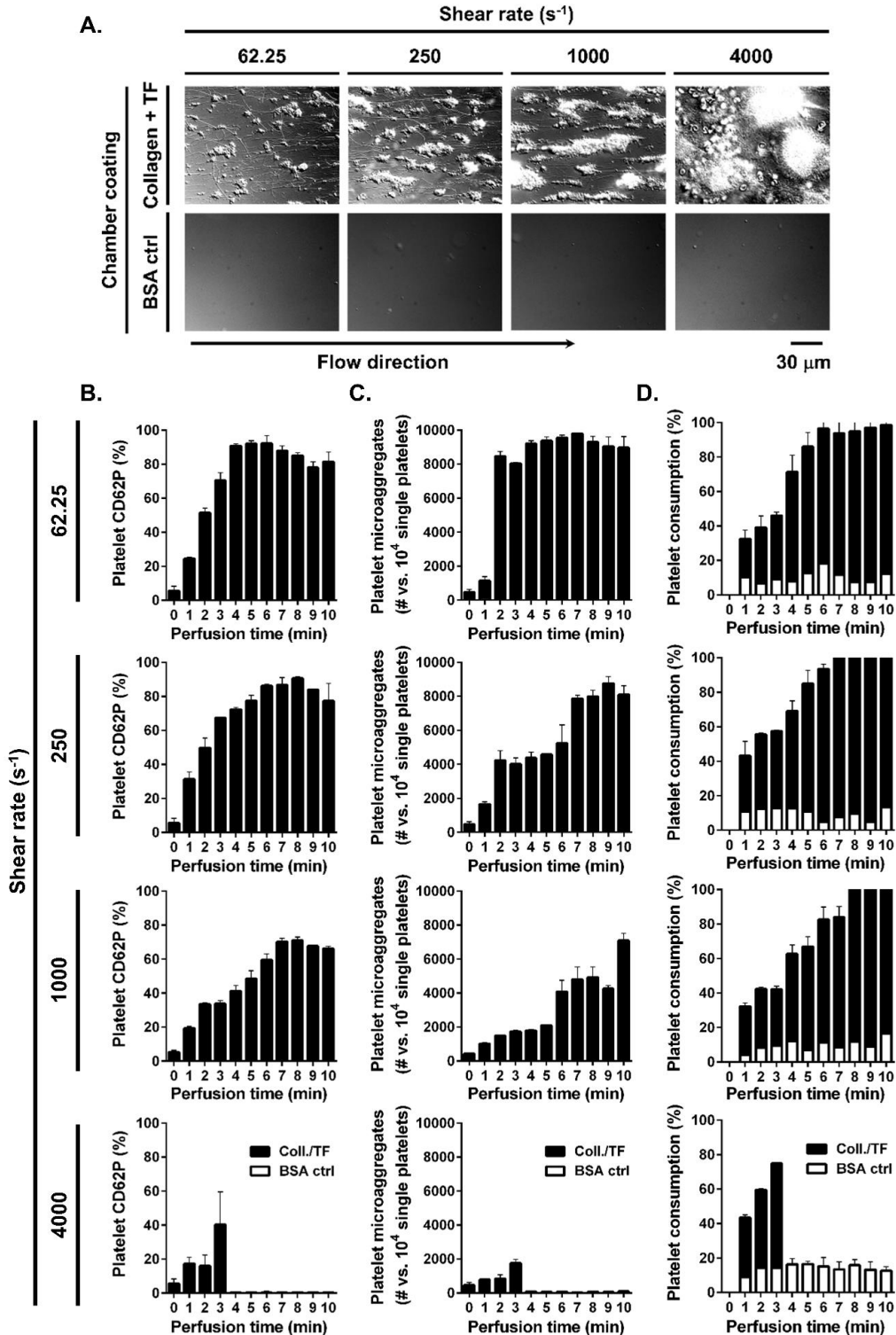
**Figure 4.1 The schematic of the flow chamber and FACS analysis.**

lood samples were taken before the blood perfusion (upstream) or at distal site to a collagen and tissue factor-coated flow (downstream) and analyzed by FACS. (B) Platelet activation and microaggregate formation as well as total single platelet (single platelet integration into forming microaggregates and precipitating out of blood macroaggregates) were assessed. were labeled for constitutively expressed platelet CD41a or CD31 and P-selectin (CD62P) expressed on activated platelets. (C) Platelet activation was determined by a dot plot with PE-CD41a and APC-CD62P fluorescence. (D) Platelet microaggregate n was defined by CD41a mean fluorescence intensity and size (forward scatter) shift, as indicated by the region marked with the ated platelets before (upstream; left) and after (downstream; right) perfusion over a collagen-coated surface are shown.

#### 4.5.2 *Characterization of the effect of shear on platelet aggregation in the bloodstream.*

To investigate and characterize the effect of shear on the biorheology of platelet aggregation in the bloodstream, we first looked at local thrombus formation on surfaces of immobilized collagen and tissue factor (collagen/TF) as compared to control surfaces coated with bovine serum albumin (BSA control). We observed increased platelet recruitment to collagen/TF-coated surfaces as compared to BSA control-coated surfaces. Platelet aggregation within 10 minutes of blood perfusion increased as a function of shear rate, with the lowest degree of local platelet aggregation observed at  $62.25 \text{ s}^{-1}$  and the greatest degree of local platelet aggregation observed at  $1000 \text{ s}^{-1}$ . Of note, flow chambers coated with collagen/TF completely occluded after 3 minutes of blood perfusion at a shear rate of  $4000 \text{ s}^{-1}$  (Figure 4.2A).

Our goal was to develop a measurement platform to study platelet activation and microaggregate formation in the bloodstream relative to the local site of thrombus formation. We found that platelet CD62P expression and aggregation dramatically increased in whole blood samples collected 15 seconds (residence time in flow) downstream of the site of thrombus formation on collagen/TF as compared to BSA control-coated surfaces at all shear rates tested ( $62.25$ ,  $250$ ,  $1000$  and  $4000 \text{ s}^{-1}$ ; Figure 4.2B-D). Maximal platelet activation was achieved sooner at lower shear rates, with  $92 \pm 1.9\%$  platelets activated by 5 min at  $62.25 \text{ s}^{-1}$ ,  $90 \pm 1.2\%$  by 8 min at  $250 \text{ s}^{-1}$  and  $71 \pm 2.0\%$  by 8 min at  $1000 \text{ s}^{-1}$ , while  $40 \pm 19.4\%$  of platelets were activated by 3 min at  $4000 \text{ s}^{-1}$  just prior to chamber occlusion. Per 10000 single platelets,  $9714 \pm 27$  platelets formed microaggregates by 7 min at  $62.25 \text{ s}^{-1}$ ,  $8714 \pm 393$  by 9 min at  $250 \text{ s}^{-1}$ ,  $7050 \pm 421$  by 10 min at  $1000 \text{ s}^{-1}$  and  $1689 \pm 220$  by 3 min at  $4000 \text{ s}^{-1}$ . Total single platelet consumption was achieved by 7 min at  $62.25 \text{ s}^{-1}$ , while both  $250 \text{ s}^{-1}$  and  $1000 \text{ s}^{-1}$  had  $2 \pm 0.4\%$  of single platelets remaining by 10 min of perfusion;  $40 \pm 0.6\%$  of single platelets remained in samples distal to local thrombus formation at  $4000 \text{ s}^{-1}$  prior to chamber occlusion by 3 min.



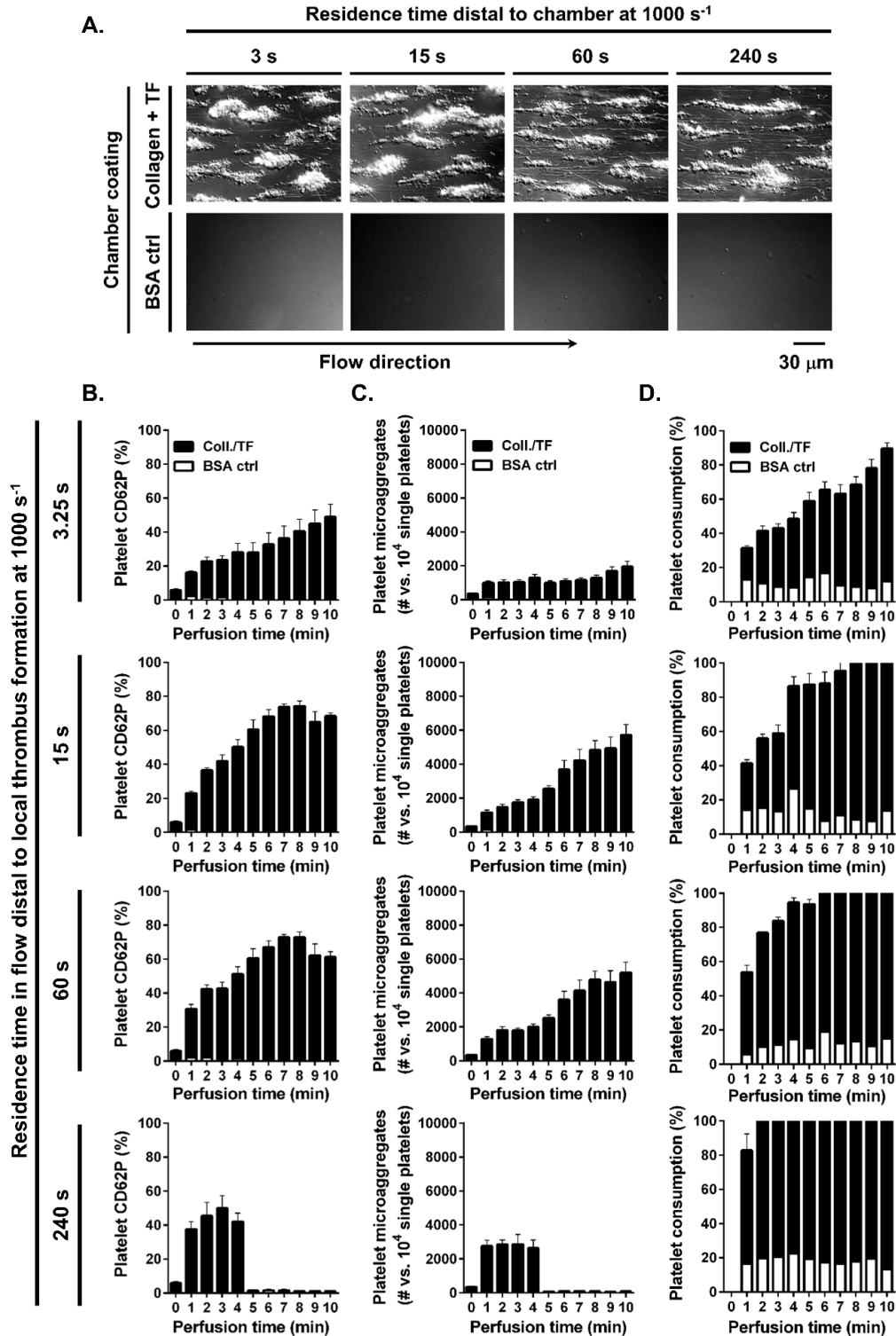
**Figure 4.2 Effect of shear on local platelet aggregate formation and distal platelet activation.**

Recalcified whole blood was perfused over collagen/TF or BSA-coated control surfaces for 10 min at 62.25, 250 or 1000  $s^{-1}$  shear rate and for 3 min (collagen/TF-coated chambers occluded by 3 min of perfusion) at 4000  $s^{-1}$  shear rate. (A) Final local platelet aggregates formed were evaluated by differential interference contrast microscopy. Samples were collected distally at each minute of perfusion after 15 s of residence time in flow and (B) distal platelet activation, (C) microaggregate formation and (D) single platelet consumption were quantified by FACS. Images and histograms are representative from each 3 fields of view from two different blood donors.

#### 4.5.3 *Effect of distal residence time in flow on platelet activation in the bloodstream.*

We next investigated the effect of blood residence time in flow distal to the local site of thrombus formation on platelet activation and aggregation in the bloodstream. We found that the local thrombus formation on surfaces of immobilized collagen and tissue factor (collagen/TF) and BSA control surfaces at  $1000\text{ s}^{-1}$  shear rate were not affected by addition of tubing downstream of the chambers (Figure 4.3A). We found that platelet CD62P expression and aggregation dramatically increased in whole blood as a function of residence time in flow downstream of the site of thrombus formation on collagen/TF as compared to BSA control surface (Figure 4.3B-D). Maximal platelet activation was achieved faster at longer residence times. For a distal residence time of 3.25 s, 10 min of local thrombus formation (perfusion time) was required to achieve activation of  $47\pm 7.7\%$  of the platelets in the bloodstream.

For a distal residence time of 15, 60 and 240 s, 8, 7 and 3 min of perfusion time was required to achieve activation of  $73\pm 3.0\%$ ,  $72\pm 1.6\%$ , and  $49\pm 7.5\%$  of the platelets in the bloodstream, respectively. Per 10000 single platelets,  $1874\pm 312$  platelets formed microaggregates following 10 min of perfusion for a residence time of 3.25 s,  $5671\pm 625$  platelets formed microaggregates by 10 min for a residence time of 15 s,  $5164\pm 606$  platelets formed microaggregates by 10 min for a residence time of 60 s, and  $2782\pm 582$  platelets formed microaggregates by 3 min for a residence time of 240 s of blood residence in flow. Single platelet consumption increased as a function of residence time, with  $78\pm 3.3\%$  of single platelets being consumed following 10 min of perfusion for a residence time of 3.25 s, whereas  $99\pm 0.1\%$  of single platelets were consumed following 10 min of perfusion for residence times of either 15 s or 60 s, and  $100\pm 0.5\%$  of single platelets were consumed by 4 min after 240 s of residence time.



**Figure 4.3 Effect of distal residence time in flow on platelet activation in the bloodstream.**

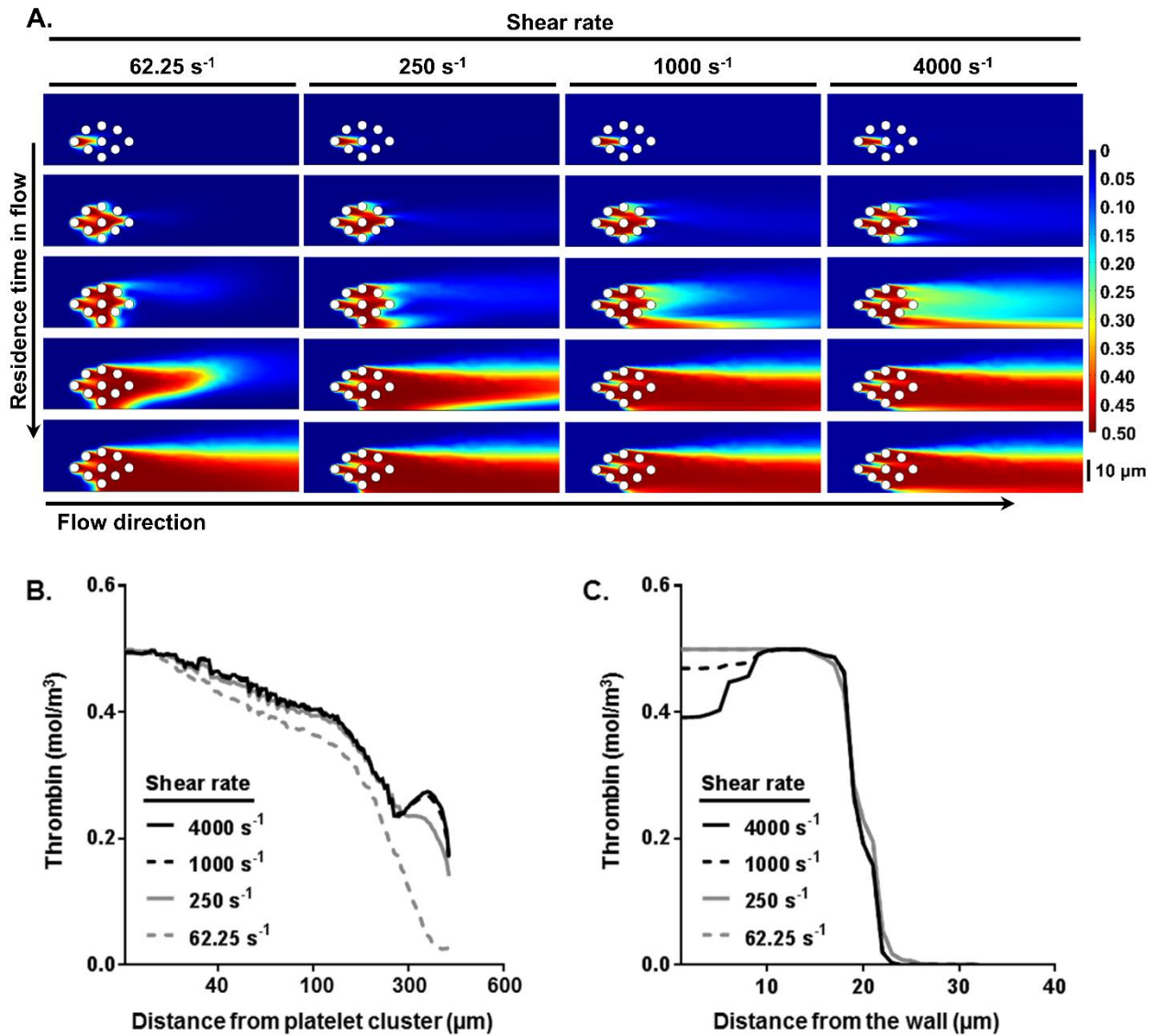
Recalcified whole blood was perfused over collagen/TF or BSA-coated control surfaces for 10 min at 1000 s<sup>-1</sup> shear rate. (A) Local platelet aggregates formed after 10 min of blood perfusion were evaluated by differential interference contrast (DIC) microscopy. Samples were collected distally to local thrombus formation after 3.25, 15, 60 or 240 s of residence time in flow and (B) distal platelet activation, (C) microaggregate formation and (D) single platelet consumption over perfusion time (min) were assessed by FACS. Images and histograms are representative from each 3 fields of view from four different blood donors.

#### 4.5.4 *Thrombin mass transfer in flow distal to thrombus formation.*

Finite element simulations of thrombin mass transfer using COMSOL was used to study the effect of inlet shear rate and residence time on thrombin generation in the bloodstream distal to sites of local thrombus formation. We hypothesized that the level of platelet aggregate formation in the bloodstream would increase as a function of residence time. Our model incorporated the following steps: (i) thrombin mass transfer within the bloodstream from a single activated platelet towards quiescent platelets, and (ii) the transport of non-activated platelets towards increasing concentrations of thrombin within the bloodstream, resulting in platelet activation. Therefore, our model predicts that platelet aggregation in the bloodstream is proportional to the area of thrombin concentration plume generated by a cluster of activated platelets present in the blood flow along with the residence time of this cluster.

Our model predicted that thrombin concentrations reach steady state both axially and radially within 15 seconds of residence time in flow at different shear rates (Figure 4.4A). Our simulations predicted that thrombin mass transfer in the bloodstream is dominated by convection and follows bulk flow. Thus, after 15 seconds of residence time in flow, the thrombin concentration profile in the axial direction starting from the platelet cluster would distribute farther at higher shear rates (Figure 4.4B). We used our model to estimate the mass transfer of thrombin 20  $\mu\text{m}$  downstream of platelet clusters as a function of radius from the wall to the center of the channel. Our simulations predicted that higher shear rates lead to a moderately lower initial radial diffusion profile compared to lower shear rates (Figure 4.4C). Our model predicted that the probability of platelet activation in the bloodstream increases as a function of residence time.





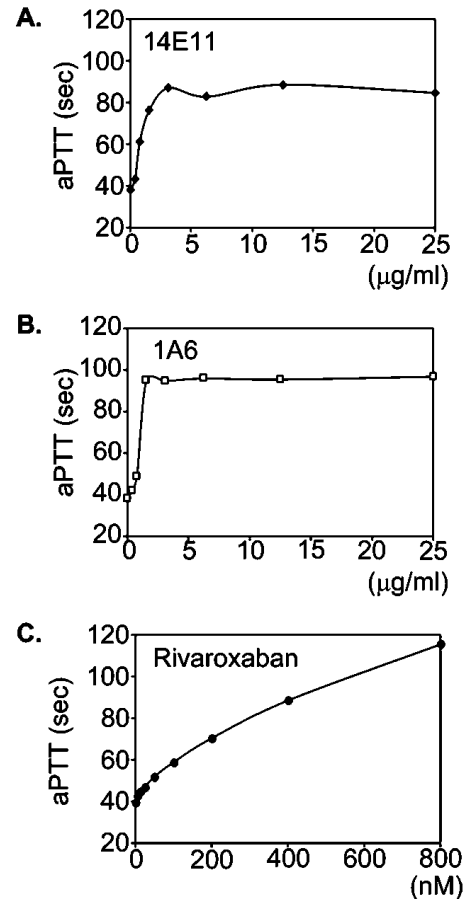
**Figure 4.4 Thrombin mass transfer in flow distal to thrombus formation.**

Thrombin distribution (mol/m<sup>3</sup>) in the bloodstream distal to local thrombus formation at increasing shear rates was simulated using COMSOL (A) over different residence time in flow; final residence time shown is 15 s. Predictions of (B) axial thrombin distribution from a platelet cluster in flow and (C) radial thrombin distribution from the wall to the channel center at different set shear rates after 15 s of residence time in flow.

#### 4.5.5 Characterization of inhibitors of the coagulation cascade.

We first verified the anticoagulant activity of pharmacological inhibitors of the coagulation cascade in an aPTT clotting assay using pooled platelet-poor human plasma. In this study we utilized the function-blocking FXI antibodies, 14E11 and 1A6, and the direct FXa inhibitor, rivaroxaban. 14E11 inhibits FXI activation by FXIIa, and 1A6 blocks FIX activation by FXIa and FXI activation by FXIIa.[141] Rivaroxaban reversibly binds to FXa via the S1 and S4 pockets and inhibits FXa serine protease activity.[357] The maximum aPTT prolongation with 14E11 and 1A6 was observed at the concentrations above 3  $\mu\text{g/ml}$  (Figure 4.5A & B). Both 14E11 and 1A6 doubled the clotting time at a concentration of 1-2  $\mu\text{g/ml}$ .

The maximal inhibition of clotting time observed with 1A6 (95 s) was somewhat longer than with 14E11 (85 s). The FXa inhibitor rivaroxaban inhibited clotting in a concentration-dependent manner, doubling the aPTT at 300 nM (Figure 4.5C). No saturating effect was observed for rivaroxaban up to a concentration of 800 nM.

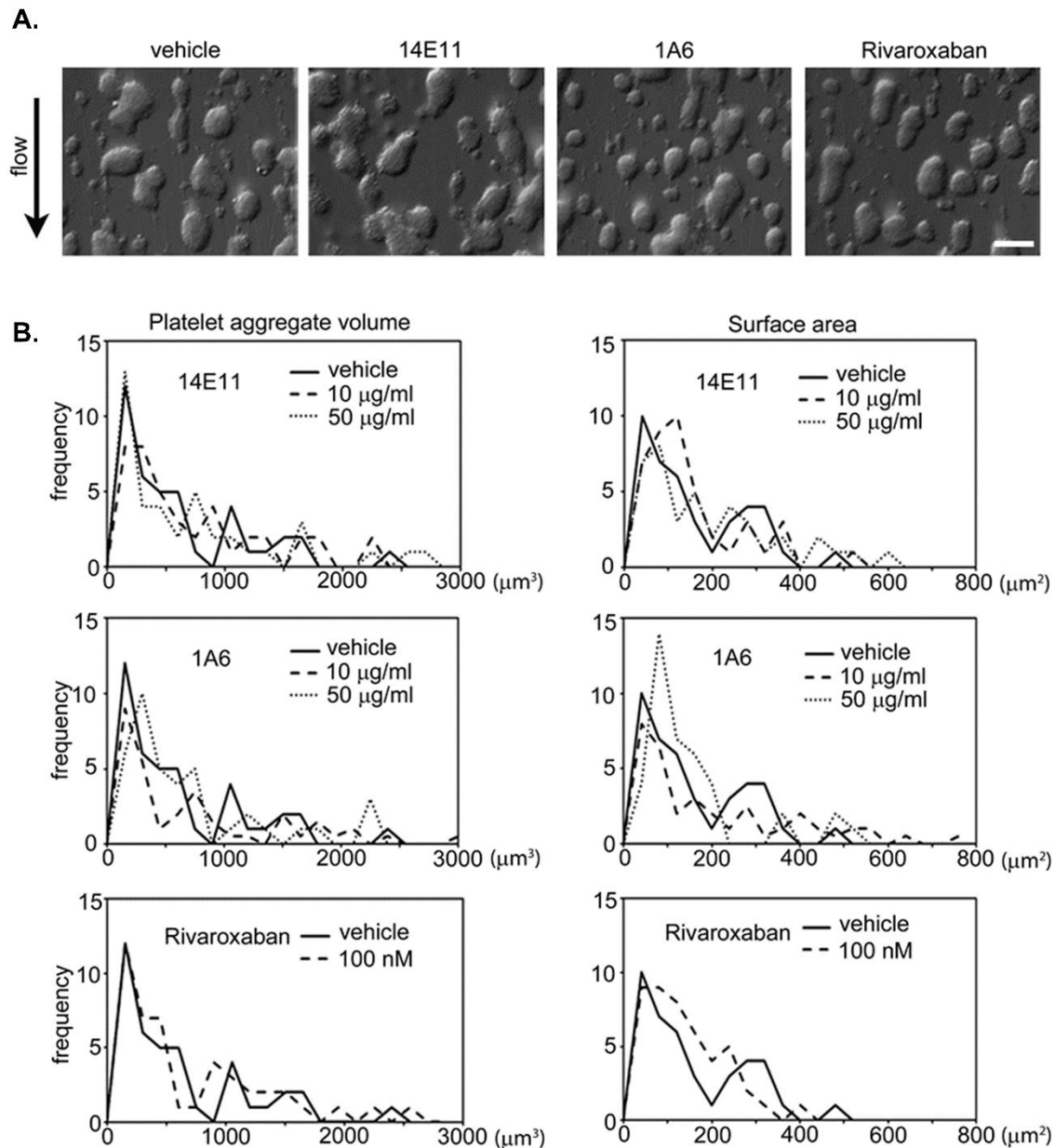


**Figure 4.5 14E11, 1A6, and rivaroxaban prolonged the plasma clotting time.** Pooled human plasma was incubated with increasing concentrations of (A) 14E11, (B) 1A6 or (C) rivaroxaban for 10 min and aPTT was recorded, as described in Methods.

#### 4.5.6 Study of local platelet deposition and aggregation on immobilized collagen.

Next, we investigated platelet adhesion and aggregation on immobilized collagen in a flow chamber system in the presence of pharmacological agents targeting intrinsic or extrinsic coagulation pathway. We observed platelet recruitment to collagen-coated surfaces under arterial shear conditions ( $1000 \text{ s}^{-1}$ ; Figure 4.6A).

As expected, the presence of the anti-FXI antibodies, 14E11 or 1A6, or FXa-inhibitor rivaroxaban did not alter the volume or surface coverage of platelet aggregates as compared to vehicle-treated controls (Figure 4.6B).



**Figure 4.6 14E11, 1A6, and rivaroxaban did not affect local platelet aggregate formation under flow.**

Recalcified whole blood was perfused over collagen-coated surfaces at  $1000 \text{ s}^{-1}$  shear rate. (A) Platelet aggregates formed on collagen surfaces in the presence of 14E11 (50  $\mu\text{g/ml}$ ), 1A6 (50  $\mu\text{g/ml}$ ) or rivaroxaban (100 nM). (B) Aggregate volume (left) and surface area (right) in the presence of 14E11 (top), 1A6 (middle) or rivaroxaban (bottom) at indicated concentrations. Images and histograms are representative from each 3 fields of view from two different blood donors. Scale bar = 20  $\mu\text{m}$ .

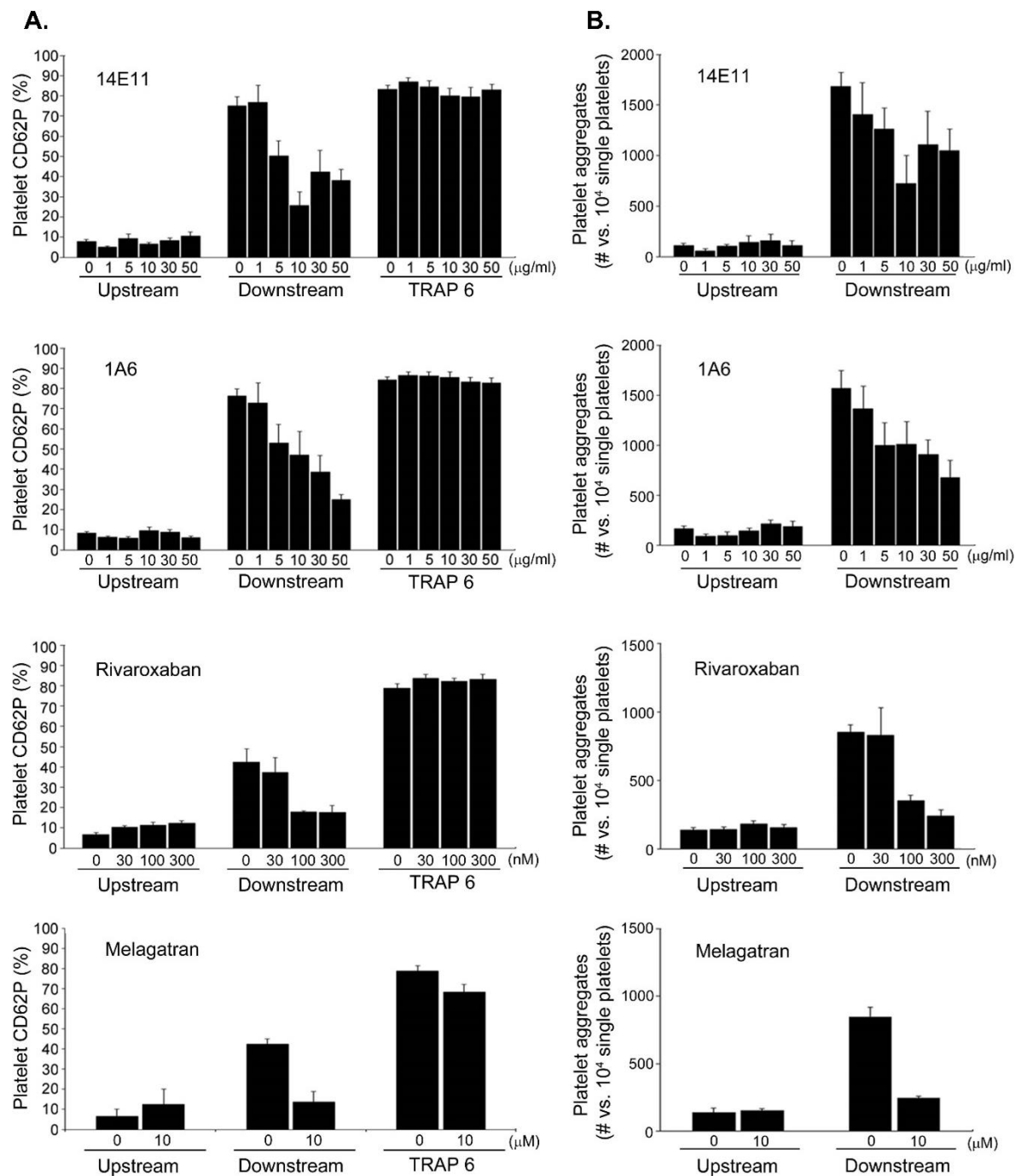
#### 4.5.7 *Study of distal platelet activation and microaggregate formation in the blood downstream of sites of thrombus formation.*

We found that platelet CD62P expression dramatically increased in whole blood downstream of the site of thrombus formation on surfaces of immobilized collagen with maximal CD62P expression reaching  $7.8 \pm 1.0\%$  upstream vs.  $75.1 \pm 4.5\%$  downstream of the flow (Figure 4.7A). We next investigated the role of contact activation of the coagulation cascade in promoting distal platelet activation. Treatment of blood with the function-blocking FXI-antibody, 14E11, inhibited CD62P expression, with the maximum inhibitory effect of 14E11 recorded at  $10 \mu\text{g/ml}$  ( $75.1 \pm 4.5\%$  vs.  $25.6 \pm 6.7\%$  in the presence of PBS or 14E11, respectively).

The function-blocking FXI-antibody, 1A6, reduced CD62P expression in a concentration-dependent manner and reached a maximum inhibition at  $50 \mu\text{g/ml}$  ( $76.3 \pm 3.5\%$  vs.  $24.8 \pm 2.6\%$  in the presence of PBS or 1A6, respectively). Platelet CD62P levels were reduced in the presence of the FXa-inhibitor  $100 \text{ nM}$  rivaroxaban by over 50% ( $42.4 \pm 6.6\%$  vs.  $17.8 \pm 0.67\%$  in the presence of DMSO or rivaroxaban, respectively).

Moreover, treatment of blood with the direct thrombin inhibitor, melagatran, was found to inhibit platelet CD62P expression to basal levels ( $45.0 \pm 4.9\%$  vs.  $13.7 \pm 2.2\%$  in the presence of DMSO or melagatran, respectively). Treatment of whole blood with the TRAP-6 induced comparable levels of platelet CD62P expression in the presence of vehicle, 14E11, 1A6, rivaroxaban, or melagatran.

We next analyzed downstream samples for the presence of platelet microaggregates. Previous studies have shown that FACS-analysis of whole blood samples can detect platelet microaggregates based on their characteristic forward scatter and fluorescence profiles,[360,361] although these and other studies were confined to the study of platelet activation and aggregation in closed systems.



**Figure 4.7 FXI and FXa inhibitors abrogated distal platelet CD62P expression and microaggregate formation under shear.** Whole blood, treated with 14E11, 1A6, rivaroxaban or melagatran at indicated concentrations, was perfused over a collagen-coated chambers immediately after recalcification; PBS or DMSO was used as vehicle. In parallel, whole blood samples were collected after treatment with vehicle or inhibitor, and incubated with TRAP-6 (10  $\mu\text{g/ml}$ ) or vehicle for 5 min. Data are reported as (A) mean  $\pm$  SEM percentage of CD62P-positive platelets, or (B) mean  $\pm$  SEM platelet microaggregate count versus  $10^4$  gated single platelets in gated population of at least three experiments. The maximal CD62P expression levels or microaggregate counts after 5 mins of perfusion are shown in the graphs for each treatment.

As shown in Figure 4.7, our platform was used to measure the formation of platelet microaggregates in the bloodstream sampled distal to the site of thrombus formation (~1500 or 850 aggregates/ $10^4$  single platelets in PBS or DMSO, respectively). We found that platelet microaggregate formation was significantly decreased by over 50% in the presence of the function-blocking FXI antibodies, 14E11 or 1A6, and by over 70% in the presence of the FXa inhibitor rivaroxaban or direct thrombin inhibitor melagatran as compared to vehicle (Figure 4.7B). Taken together, we demonstrate the utility of a measurement platform to study the effects of local activation of the coagulation cascade on the promotion of distal platelet activation and microaggregate formation in the bloodstream.

#### **4.6 Discussion**

At sites of vessel injury, thrombin generation is reaction rate limited by the conversion of zymogens to active enzymes following the assembly of coagulation factor complexes on the activated platelet surface.[6] The supply of reactants in the form of quiescent platelets and coagulation factors is in excess due to blood flow to the growing hemostatic plug. Thus, the ratio of the reaction rate to the convective mass transport rate, as defined by the Damköhler number ( $Da$ ), is high ( $Da > 1$ ).[22] Thus, for reactions catalyzed by the activated platelet surface within the growing hemostatic plug, such as the FXa and thrombin generation, the flow time scale is the rate limiting step as compared to the chemical time scale. Model systems have shown that the activation of FX under shear flow increases with the one-third power of shear rate, in agreement with a convection-limited reaction.[305] Meanwhile, the process of local thrombus formation at sites of vessel injury is sensitive to the presence of cofactors that form the tenase and prothrombinase complexes to drive thrombin generation, such as the coagulation (F) factors IX and VIII, respectively, as evidenced by the bleeding phenotype observed for patients with a deficiency or dysfunction of FIX or FVIII.[362]

In contrast, free-flowing platelets within the bloodstream present a unique 3-dimensional spatial distribution as compared to platelets recruited and bound to a growing thrombus on the blood vessel wall. We have previously shown that the physical parameter of spatial separation, defined as the cubic root of the volume per cell, provides a measure of the average linear separation between nearest neighbor cells, and dominates the control of coagulation kinetics for cells in flow.[363] Our previous work demonstrated that the spatial separation of procoagulant surfaces in the circulation, as calculated from carrier count of either TF-coated beads or TF-expressing cells, strongly correlated with their procoagulant and prothrombotic activity.[363] The results presented in the current study suggest that the probability of platelet activation in the bloodstream increases as a function of residence time distal to sites of thrombus formation. Moreover, our work suggests that activation of the coagulation factors XI and X play a key role in promoting thrombin generation, platelet activation and microaggregate formation in the bloodstream.[316]

## **Chapter 5. Coagulation factor XI promotes distal platelet activation and single platelet consumption in the bloodstream under shear flow**

Jevgenia Zilberman-Rudenko, Asako Itakura, Chantal P. Wiesenekker, Ralf Vetter, Coen Maas, David Gailani, Erik I. Tucker, András Gruber, Christoph Gerdes, Owen J. T. McCarty

This work was originally published by the American Heart Association, *Arteriosclerosis, Thrombosis, and Vascular Biology*, 2016;36(3):510-517.

Permission is not required by the publisher for this type of use.

### **5.1 Abstract**

*Objective:* Coagulation factor XI (FXI) has been shown to contribute to thrombus formation on collagen or tissue factor (TF)-coated surfaces *in vitro* and *in vivo* by enhancing thrombin generation. Whether the role of the intrinsic pathway of coagulation is restricted to the local site of thrombus formation is unknown. This study was aimed to determine whether FXI could promote both proximal and distal platelet activation and aggregate formation in the bloodstream.

*Approach and Results:* Pharmacological blockade of FXI activation or thrombin activity in blood did not affect local platelet adhesion, yet reduced local platelet aggregation, thrombin localization and fibrin formation on immobilized collagen and TF under shear flow, *ex vivo*. Downstream of the thrombus formed on immobilized collagen or collagen and 10 pM TF, platelet CD62P expression and microaggregate formation and progressive platelet consumption were significantly reduced in the presence of FXI-function blocking antibodies or a thrombin inhibitor in a shear rate- and time-dependent manner. In a non-human primate model of thrombus formation, we found that inhibition of FXI reduced single platelet consumption in the bloodstream distal to a site of thrombus formation.

*Conclusions:* This study demonstrates that the FXI-thrombin axis contributes to distal platelet activation and procoagulant microaggregate formation in the blood flow downstream of the site of



thrombus formation. Our data highlights FXI as a novel therapeutic target for inhibiting distal thrombus formation without affecting proximal platelet adhesion.

## 5.2 Introduction

Studies in this chapter utilize an *ex vivo* flow system described in Chapter 4 and examine the role of coagulation factor (F)XI in platelet activation and consumption in the bloodstream distal from a site of thrombus formation. The results demonstrate that activation of the FXI axis plays a key role in distal platelet activation and microaggregate formation in solution downstream of thrombus formation under both venous and arterial shear flow. In addition to its anticoagulant role, pharmacological targeting of FXI may be useful in mitigating platelet activation and therefore prevent platelet-driven amplification of platelet aggregate and thrombi formation in prothrombotic conditions involving direct contact pathway agonists and widespread vascular injury.

## 5.3 Background

Platelets and coagulation factors are two essential components of hemostasis. Upon vessel injury, resting platelets are immediately recruited to the exposed extracellular matrix under shear flow, followed by platelet adhesion and activation.[354] Platelet activation triggers the surface expression of CD62P (P-selectin) from  $\alpha$ -granules, and the conversion of integrin  $\alpha$ IIb $\beta$ 3 to its active conformation, potentiating homotypic aggregate formation via fibrinogen binding. In parallel, activation of the coagulation cascade leads to thrombin generation, which cleaves fibrinogen to fibrin to stabilize the hemostatic plug. Thrombin is also able to activate platelets through protease-activated receptors (PARs) and thus accelerate the activation of both hemostatic components.

Coagulation factor XI (FXI) participates in the intrinsic pathway, whereby activated FXI (FXIa) triggers the downstream activation of factor IX (FIX), which in turn activates factor X (FX). FXa then converts prothrombin to thrombin. Thrombin can directly activate FXIa to perpetuate its own

generation, thereby creating a procoagulant feedback loop of thrombin generation driven by FXI-thrombin axis.[139,364,365] To date, however, it is not clear whether the FXI-thrombin axis facilitates platelet activation and consumption in blood flow under prothrombotic conditions.

The aim of this study was to define the role of the FXI-thrombin axis in promoting platelet activation and aggregation at the site of, and distal to, thrombus formation under shear flow. We show that inhibition of FXIIa activation of FXI or thrombin activity abrogated platelet CD62P expression and microaggregate formation under both venous and arterial shear flows downstream of the site of thrombus formation on collagen and 10 pM TF. *In vivo*, inhibition of FXI also reduced single platelet consumption in the bloodstream distal to a site of thrombus formation. These results provide the first evidence of a role for FXI in mediating platelet activation and platelet aggregate formation downstream of the site of thrombus formation.

## **5.4 Materials and Methods**

### *5.4.1 Reagents*

Anti-factor XI antibodies 1A6, 14E11 and 10C9 were generated as described.[139–141] Plasmin and corn trypsin inhibitor (CTI) were from Enzyme Research Laboratories, Inc., hirudin from Hypen Biomed, Phe-Pro-Arg-chloromethylketone (PPACK) from Santa Cruz, fibrillar collagen from Chrono-Log Corp, lipidated tissue factor (TF; Dade<sup>®</sup> Innovin<sup>®</sup> PT reagent) from Siemens, and ellagic acid (aPTT reagent) from Pacific Haemostasis. Rabbit anti-fibrinogen antibody was from Cappel MP Biomedicals, LLC, anti-rabbit-AF350 from Life technologies, anti-CD41-PE and anti-CD62P-APC were from BD Pharmingen, CD31-eFluor450 was from eBioscience. Anti-thrombin API (H-85) antibody was from Santa Cruz Biotech and anti-integrin  $\alpha$ IIb from Abnova. FXI- and FXII-depleted plasmas were from Haematologic Technologies Inc. All other reagents were from Sigma-Aldrich, Inc. or previously named sources.[245]

#### 5.4.2 *Blood collection, preparation of plasmas and clotting times*

Human venous blood was drawn by venipuncture from healthy adult volunteers into sodium citrate in accordance with the OHSU Institutional Review Board. Platelet-poor plasma (PPP) was prepared by centrifugation of citrated whole blood (in 0.32% w/v sodium citrate) from three separate donors at  $2150\times g$  for 10 min. Further centrifugation of the plasma fractions at  $2150\times g$  for 10 min yielded PPP, which was then pooled and stored at  $-80^{\circ}\text{C}$  until use.

Clotting times of human whole blood or PPP were measured with a KC4 Coagulation Analyzer (Trinity Biotech PLC, Bray, Ireland). Samples were pretreated at room temperature (RT) for 3 min with blocking FXI antibodies 1A6 (50  $\mu\text{g}/\text{mL}$ ), 14E11 (50  $\mu\text{g}/\text{mL}$ ), 10C9 (50  $\mu\text{g}/\text{mL}$ ), FXII inhibitor CTI (40  $\mu\text{g}/\text{mL}$ ), or thrombin inhibitor hirudin (25  $\mu\text{g}/\text{mL}$ ) followed by incubation with activated partial thromboplastin time (aPTT) or prothrombin time (PT) reagent at  $37^{\circ}\text{C}$ , and clotting time was recorded. For aPTT assays, coagulation was initiated by the addition of  $\text{Ca}^{2+}$  (16.6 mM final). In select experiments, FXI- or FXII-depleted plasmas were used.

#### 5.4.3 *Ex vivo flow experiments*

Glass capillary tubes/chambers (0.2 $\times$ 2 $\times$ 200 mm; VitroCom) were coated as described previously.[283] Surfaces were blocked with 5 mg/mL denatured bovine serum albumin (BSA) for 1 h prior to assembly into a flow system as shown in Figure 5.2A. Sodium citrate (0.38% w/v) anticoagulated whole blood was recalcified and perfused through the chamber for 10 min at an initial wall shear rate (300 or 1000  $\text{s}^{-1}$ ). Downstream samples were collected directly into 100  $\mu\text{M}$  PPACK and 1.5% w/v sodium citrate (1 tube/min of perfusion) to final 50% dilution and evaluated using fluorescence-activated cell sorting (FACS). The initial shear rates were set by Harvard Apparatus PHD 2000 pump. Top loaded pump-driven syringes were connected to wells with blood via rubber washers which would disengage from the well upon pressure built up.

#### 5.4.4 *Microscopy*

After blood perfusion, glass capillaries were washed with phosphate-buffered saline (PBS) and Hepes/Tyrode buffer (136 mM NaCl, 2.7 mM KCl, 10 mM Hepes, 2 mM MgCl<sub>2</sub>, 0.1% BSA; pH7.4) containing 1.5% sodium citrate and 100 μM PPACK, followed by incubation with blocking buffer (1% BSA, 1% FCS in Hepes/Tyrode buffer) for 30 min. Glass capillaries were incubated with rabbit anti-serum against human fibrinogen (1:100) for 10 min and washed with PBS followed by an incubation with CD41-PE (1:50), CD62-FITC (1:50), and goat anti-rabbit Alexa Fluor 350 (1:500) in dark for 10 min. Glass capillaries were washed with PBS, fixed with paraformaldehyde (PFA 4%), and sealed with mounting media. Samples were analyzed on a Zeiss Axio Imager 2 microscope 6 (Carl Zeiss MicroImaging GmbH, Germany)

#### 5.4.5 *Western blots*

Thrombi formed on collagen/TF were lysed for 5 min with 1× lysis buffer (10 mM Tris, 150 mM NaCl, 1 mM EGTA, 1 mM EDTA, 1% NP-40, 2 mM PMSF and 10 U DNase I) at 4°C, followed by treatment with 1 μM plasmin for 40 min at RT. Local fibrin deposition was evaluated by separating combined eluate samples on non-reducing SDS–PAGE gels, transferring to PVDF membrane and immunoblotting with rabbit anti-fibrinogen followed by anti-rabbit-HRP. Local platelet deposition and thrombin content was similarly evaluated by separating combined eluate samples on separate reducing SDS–PAGE gels and immunoblotting for CD41 or thrombin. Proteins were detected using ECL.

#### 5.4.6 *FACS analysis*

Pre- and post-chamber blood samples were collected into 100 μM PPACK and 1.5% w/v Na-citrate (1:1, v:v) and incubated with 1:50 dilution antibodies for 30 min at RT. Reactions were fixed by diluting 1:10 with RT 12.5% Cytifix<sup>BD</sup>. 10,000 single platelets were determined by a PE-conjugated platelet marker CD41a and the characteristic forward and side-scatter scatter patterns via FACS (Canto II; BD Biosciences, Heidelberg, Germany). Platelet CD62P expression levels and single platelet

consumption were determined as previously described.[284] Microaggregate formation was determined by the upshift in fluorescence intensity in CD31/CD41a double-positive events.

#### 5.4.7 *In vivo thrombosis model*

Twenty four nonterminal studies were performed using twelve male baboons (*Papio anubis*, 9-11 kg). All studies were approved by the Institutional Animal Care and Use Committee of Oregon Health & Science University. Thrombosis experiments were conducted as previously described.[285,286] Briefly, a prosthetic vascular graft segments (4 mm internal diameter x 20 mm length, expanded-polytetrafluoroethylene; W. L. Gore & Associates, Flagstaff, AZ) coated with either collagen or BSA as control were acutely introduced into chronic femoral arteriovenous shunts as shown in Fig.6A, and exposed to blood flow. The flow rate through the graft was restricted to 100 mL/min (measured by the Transonics Systems flow meter, Ithaca, NY) by clamping the proximal shunt segment, thereby producing initial mean wall-shear rates of  $265 \text{ s}^{-1}$ . Local thrombus formation was assessed in real time with quantitative gamma camera imaging of radiolabeled platelet accumulation within the graft segment.

#### 5.4.8 *Assessment of distal platelet consumption in in vivo thrombosis model*

Samples were collected distal to the graft from the bloodstream adjacent to the vessel wall (intraluminal boundary layer) into 3.8% w/v Na-citrate (1:9, v:v) before graft deployment (0 min), and then at 10 and 20 minutes. Blood was collected at a rate of 100  $\mu\text{L}/\text{min}$  during 10-minute intervals through a 0.64-mm id port located 10 mm distal to the graft as shown in Figure 5.4A. To maintain patency of the sampling port, PPACK (1 mM), which inhibits thrombin and other coagulation proteases,[287] was infused at a rate of 20  $\mu\text{L}/\text{min}$  into a second 0.64-mm id port located 3 mm proximal to and in line with the collection port. Anticoagulant infusion and local blood sampling were regulated using syringe pumps (Harvard Apparatus, Holliston, MA). Platelet counts were determined using a micro-60 automated cell counter (Horiba ABX Diagnostics, Montpellier, France).

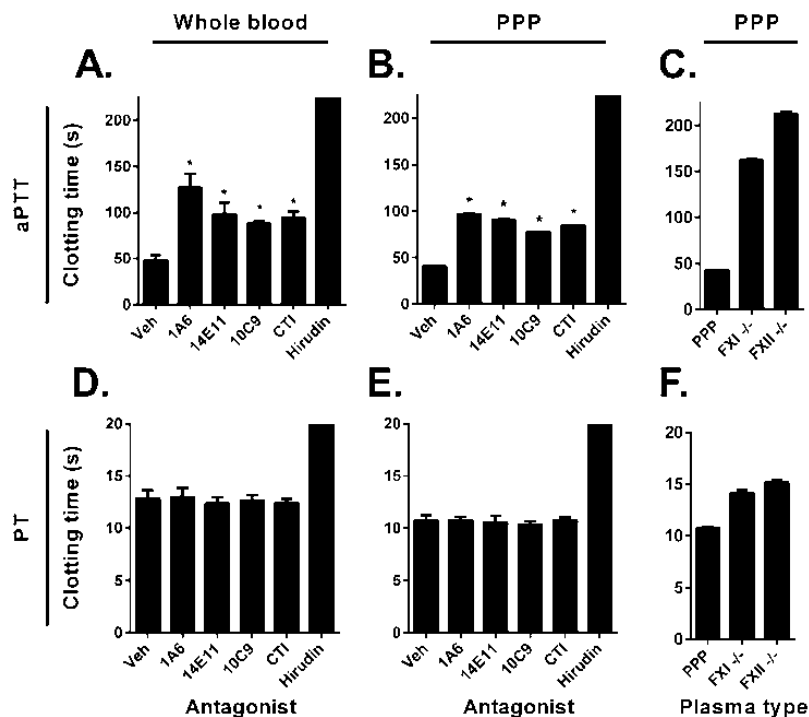
### 5.4.9 Data analysis

Data are shown as mean±SEM. Statistical significance of differences between means was determined by ANOVA. If means were shown to be significantly different, multiple comparisons were performed by the Tukey test. Probability values of  $P < 0.05$  were selected to be statistically significant.

## 5.5 Results

### 5.5.1 Role of FXII and FXI in clotting times

Our initial experiments were designed to evaluate the anticoagulant activity of FXI function-blocking antibodies, FXII inhibitor (CTI) and thrombin inhibitor (hirudin) in recalcified whole blood and platelet-poor plasma (Figure 5.1). Inhibition of FXI activation by FXIIa and FIX activation by FXIa with the function-blocking FXI-antibody (FXI-Ab 1A6) nearly tripled the aPTT in whole blood ( $47.8 \pm 5.6$  s) to  $126.9 \pm 15$  s.



**Figure 5.1 Role of FXII and FXI in clotting times.**

Recalcified whole blood (A, D), pooled human plasma (PPP; B, E) or coagulation-factor depleted plasma (C, F) was incubated with indicated FXI function blocking antibody, FXII inhibitor (CTI) or direct thrombin inhibitor (hirudin). aPTT (A-C) or PT (D-F) was recorded as described in Methods. \*indicates significantly different,  $p < 0.05$ , clotting time vs. vehicle (mean±SEM).

Inhibition of FXI activation by FXIIa (FXI-Ab 14E11) or the neutralization of the FXIa active site (FXI-Ab 10C9) or inhibition of FXII activity (CTI) prolonged aPTT to  $98.3 \pm 12.2$  s,  $87.9 \pm 3.3$  s, and  $94.2 \pm 6.9$  s, respectively (Figure 5.1A). As expected, none of the inhibitors, except for the direct thrombin inhibitor (hirudin), were able to prolong PT in whole blood (Figure 5.1D). Similar results were seen in aPTT and PT assays using platelet-poor pooled human plasma (Figure 5.1B&E).

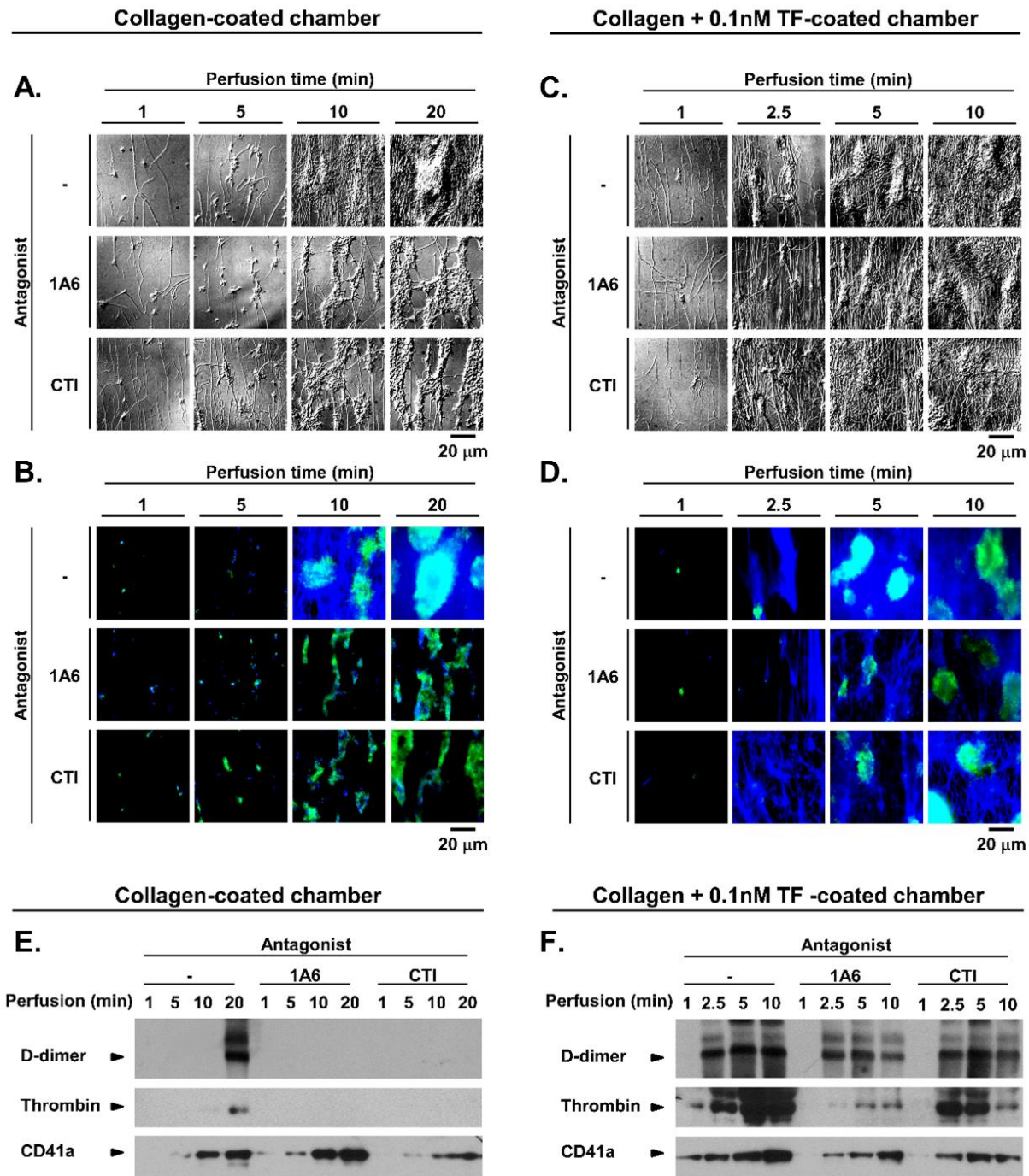
Moreover, aPTTs were prolonged to  $162.3 \pm 1.9$  and  $212.6 \pm 2.4$  s using FXI- and FXII-immuno-depleted plasmas, respectively (Figure 5.1C), while PTs were slightly prolonged to  $14.1 \pm 0.3$  s and  $15.2 \pm 0.1$  s, respectively (Figure 5.1F).

### 5.5.2 *FXIa activity promotes local fibrin formation under shear*

We next studied the role of FXI activation in local platelet deposition and fibrin formation under physiologically relevant shear flow conditions. Robust platelet adhesion, aggregation and fibrin formation was observed following the perfusion of recalcified whole blood over surfaces coated with collagen (Figure 5.2A&B).

Both the rate and the extent of fibrin formation were enhanced on surfaces coated with collagen and tissue factor (TF; 0.01–0.1 nM), as visually recorded using differential interference contrast and fluorescence microscopy (Figure 5.2C&D and Figure 5.3A&B). TF alone (0.01–0.1 nM) yielded robust fibrin networks largely absent of platelets (Figure 5.3A&B). Inhibition of FXI activation by FXIIa and FIX activation by FXIa with FXI-Ab 1A6, or inhibition of FXIIa activity with CTI, decreased fibrin formation on collagen or surfaces coated with collagen and 0.01 nM TF or TF alone (Figure 5.2A&B and Figure 5.3A&B). Hirudin prevented fibrin formation on all surfaces, while CTI had no effect on surfaces coated with collagen and 0.1 nM (Figure 5.2C&D).

These results were confirmed by analyzing the degree of fibrin formation and platelet deposition by Western blotting following clot lysis with plasmin for the fibrin degradation product, D-dimer, and the CD41a platelet surface marker (Figure 5.2E&F and Figure 5.3C).

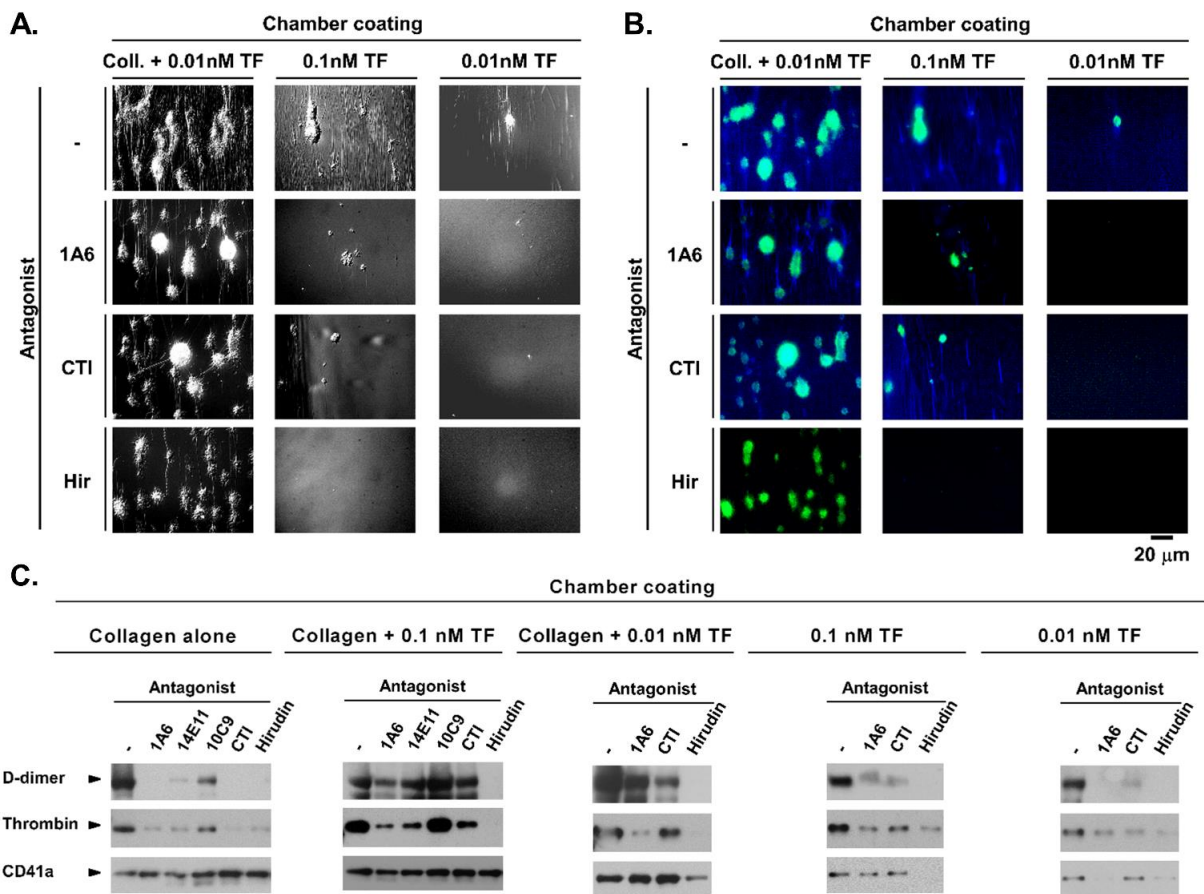


**Figure 5.2 FXIa activity promotes local fibrin formation under shear.**

Recalcified whole blood was perfused over collagen (A&B) or collagen and 0.1nM TF (C&D) for indicated times at a shear rate of  $300 \text{ s}^{-1}$ . Images of local thrombi formed at each time point in the presence of vehicle control,  $50 \mu\text{g/mL}$  1A6 or  $40 \mu\text{g/mL}$  CTI were recorded using differential interference contrast (A&C) or fluorescent light microscopy (B&D) after staining for fibrin (blue) and P-selectin (green). In parallel experiments, thrombi were lysed and immunoblotted for the fibrin degradation product, D-dimer, thrombin and the platelet surface receptor, CD41a (E&F).



Interestingly, we were able to detect thrombin in local thrombus lysates, and found that the increasing levels of clot-bound thrombin correlated with D-dimer levels. We found that inhibition of FXI activation by FXIIa with 14E11 reduced fibrin formation on collagen alone, while neither 14E11 nor the FXIa active site domain-neutralizing antibody, 10C9, affected fibrin formation on surfaces coated with collagen and 0.1 nM TF and 0.01 nM TF (Figure 5.3C). Control experiments using the thrombin inhibitor, hirudin, were shown to eliminate fibrin formation and the presence of clot-bound thrombin on all surfaces.

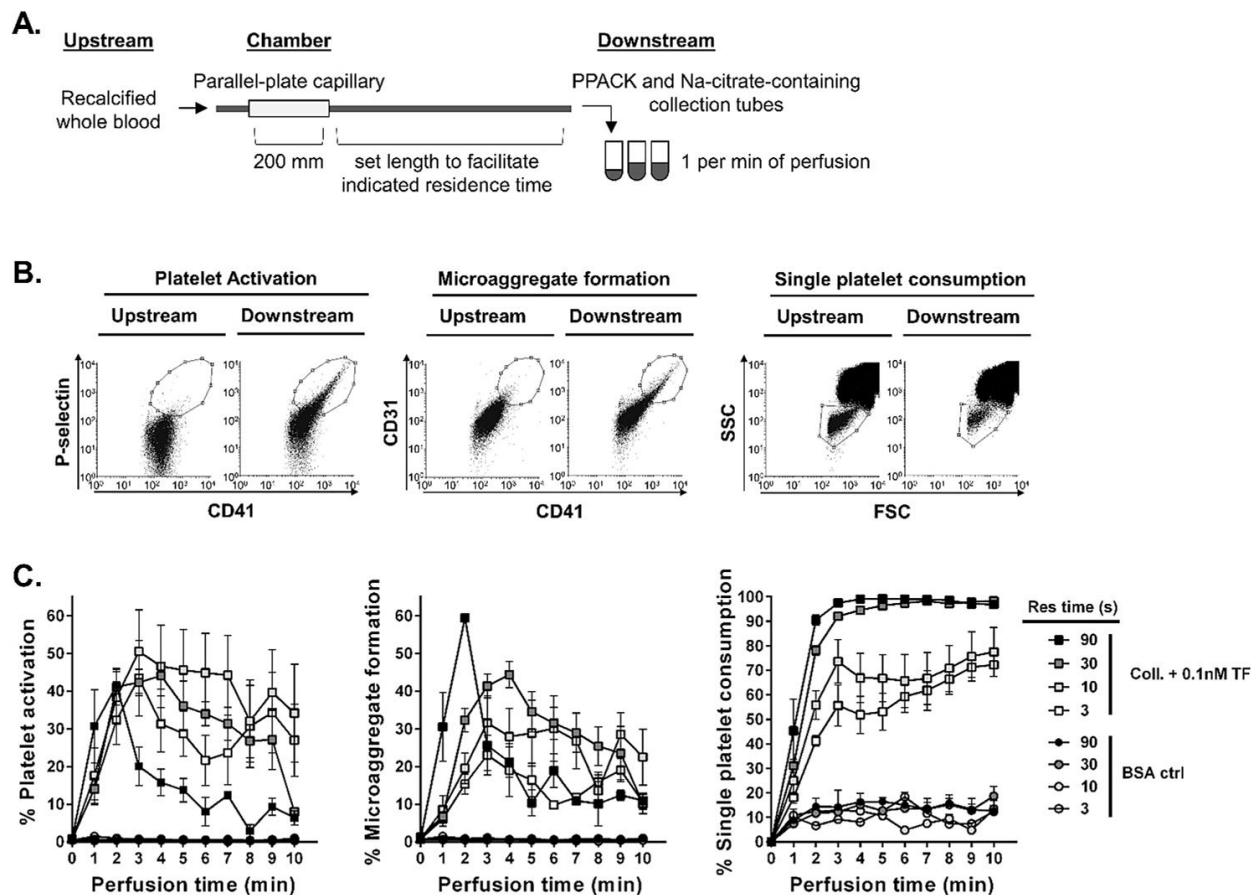


**Figure 5.3 FXIa activity promotes local thrombus formation in the presence of collagen and/or TF.**

Recalcified whole blood pretreated with either vehicle, 1A6, CTI or hirudin was perfused over chambers coated with collagen, collagen + 0.01 – 0.1 nM TF or 0.01 – 0.1 nM TF alone at shear rate of 300  $s^{-1}$ . Images of local thrombi formed at final 10 min of perfusion were recorded using differential interference contrast (A) or fluorescent light microscopy (B) after staining for fibrin (blue) and P-selectin (green). Local thrombi formed within chamber by 20 min of perfusion on collagen alone or by 10 min of perfusion on collagen and TF or TF alone were lysed and immunoblotted for the fibrin degradation product, D-dimer, thrombin and the platelet surface receptor, CD41a (C).

### 5.5.3 Propagation of distal platelet activation and single platelet consumption under shear in flow

We next designed a platform to determine whether local fibrin formation and thrombin generation at sites of thrombus formation promoted distal platelet activation and aggregate formation in the bloodstream. As shown in Figure 5.4A, a set length of tubing was added downstream of the chamber to allow platelets to react in flow for a set time (residence time) prior to being collected at 1 min intervals into tubes containing PPACK and sodium citrate.



**Figure 5.4 Propagation of distal platelet activation and single platelet consumption under shear in flow.**

Recalcified whole blood was perfused through a 200 mm chamber (coated with either BSA or 150  $\mu\text{g}/\text{mL}$  collagen + 0.1 nM TF) before being collected downstream after indicated residence time in flow (A). Downstream samples were collected into a reaction quenching solution at 1 min intervals, immunostained and evaluated by FACS flow cytometry for percent platelet activation (CD41a+/CD62P+ events), platelet microaggregate formation (high fluorescence intensity CD41a+/CD31+ events) and single platelet consumption (loss of single platelet population gate on FSC by SSC scatter). Representative raw FACS scatter plots (B) and quantification of distal samples (C), upstream sample (0 min) and TRAP-6-treated positive control (D) for at least three experiments are reported (mean $\pm$ SEM).

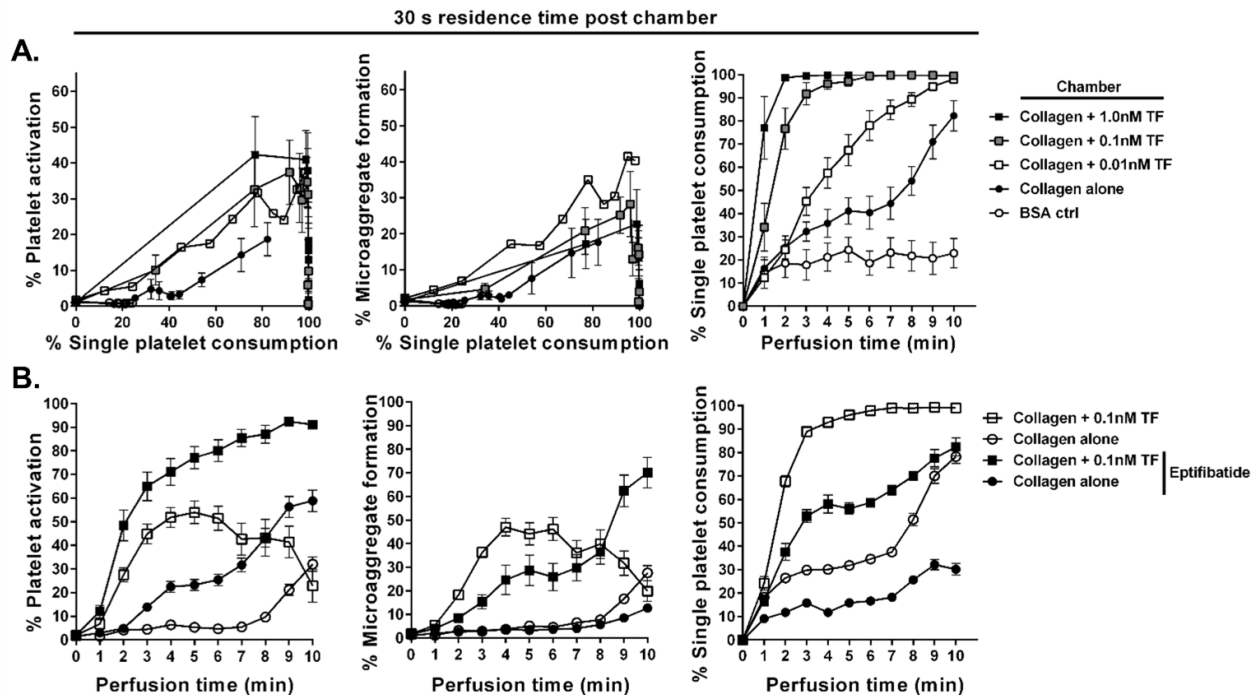
Distal single platelet consumption (reduction of single platelet population in the bloodstream), platelet activation (CD62P expression), and platelet microaggregate formation in solution (CD41a/CD31 high positive) was quantified using flow cytometry (Figure 5.4B). In parallel, untreated upstream samples were collected and analyzed to define the baseline parameters (time = 0 min), or stimulated with thrombin receptor activator peptide-6 (TRAP 6) to induce maximal platelet activation or microaggregate formation as a positive control ( $94.3 \pm 0.3\%$  P-selectin activation,  $47.6 \pm 2.4\%$  microaggregate formation, and  $77.2 \pm 3.6\%$  single platelet consumption; mean  $\pm$  SEM).

Our results show that platelet P-selectin expression, microaggregate formation and single platelet consumption increased as a function of residence time in whole blood samples downstream of chambers coated with collagen and 0.1 nM TF (Figure 5.4). In contrast, an increase in platelet activation, microaggregate formation or single platelet consumption was not observed downstream of BSA-coated chambers.

At a set residence time of 30 sec, we observed an increase in platelet activation, microaggregate formation and single platelet consumption as a function of perfusion times downstream of chambers coated with collagen (Figure 5.5A). The inclusion of 0.01–1.0 nM TF with collagen coatings significantly increased both the rate and extent of platelet activation and microaggregate formation. It should be noted that the presence of TF dramatically increased the rate of single platelet consumption, resulting in over a 95% loss of single platelets by 8, 4 and 2 min for 0.01 nM, 0.1 nM and 1 nM TF, respectively, leading to grossly visible insoluble clot formation in flow in the distal samples. A drop in the percent of activated platelets and microaggregates was observed at these time points, reflective of the consumption of single platelets and microaggregates into downstream clots.

Inhibition of platelet GPIIb-IIIa homodimer formation with eptifibatide increased circulating levels of single activated platelets and decreased microaggregate formation and single platelet consumption downstream of collagen-coated chambers.

Similarly, the prevention of clot formation in solution downstream of collagen with 0.1 nM TF-coated chambers with eptifibatide resulted in a continued increase in circulating activated platelet levels beyond 4 min and attenuated both microaggregate formation and single platelet consumption, presumably sustained by fibrin agglutination (Figure 5.5B).



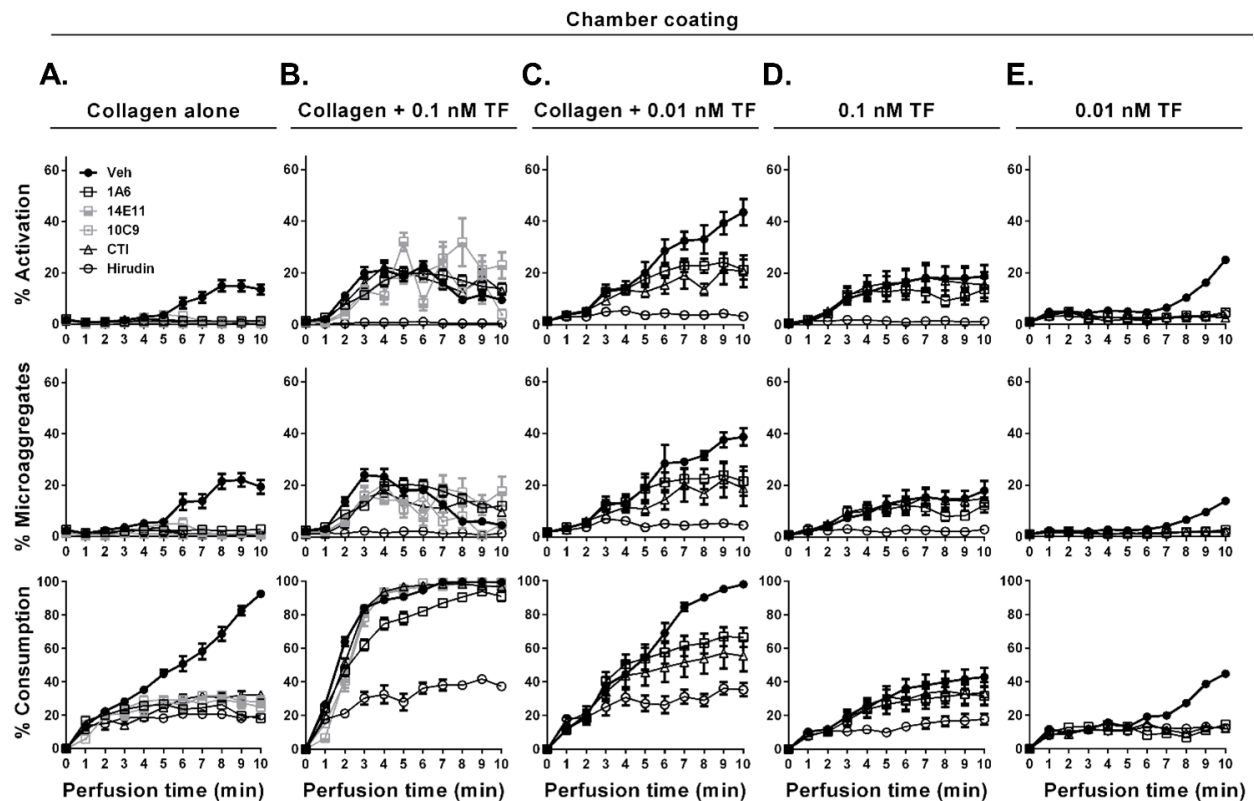
**Figure 5.5 Presence of collagen and TF promotes distal platelet consumption.**

Recalcified whole blood was perfused through a 200 mm chamber (coated with either BSA, collagen or collagen + 0.01 – 1.0 nM TF) and allowed to react in flow for 30 sec (residence time) before being collected into a reaction quenching solution at 1 min intervals. Quantification of platelet activation, microaggregate formation and single platelet consumption using FACS (A) for at least five experiments are reported (mean±SEM). In parallel experiments, whole blood was pretreated with a GPIIb-IIIa inhibitor, Eptifibatide (B).

#### 5.5.4 FXIa activity promotes distal platelet activation and consumption in the presence of collagen and TF

To examine the role of FXI activation in promoting distal platelet activation, whole blood was pretreated with the function-blocking FXI antibodies (1A6, 14E11 or 10C9), FXIIa inhibitor (CTI) or the thrombin inhibitor (hirudin) prior to perfusion through flow chambers coated with either collagen, TF, a combination of collagen and TF (0.01–0.1 nM), fibrinogen, thrombin, or VWF. Distal samples

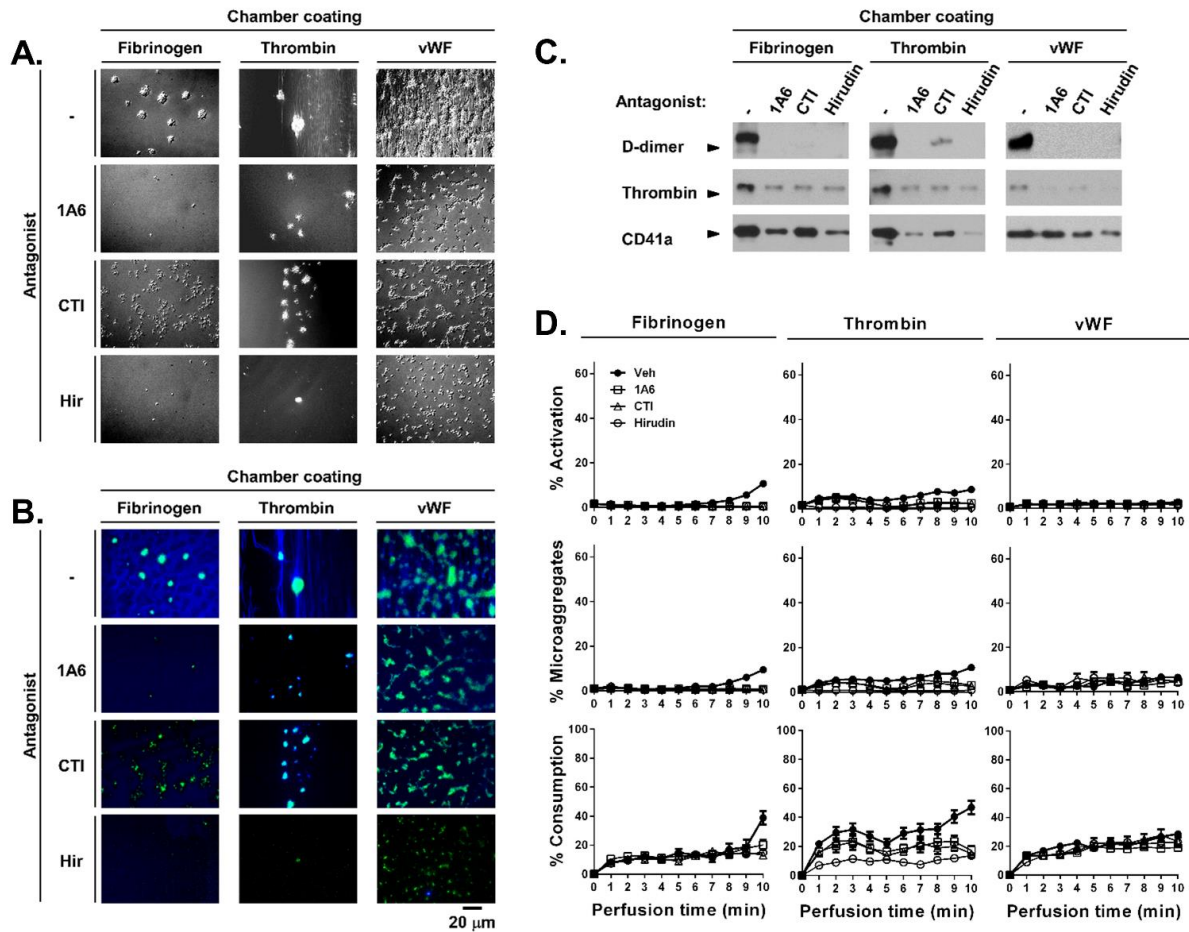
were collected downstream after 30 sec of residence time. We found that collagen, whether alone or in combination with TF, promoted the greatest degree of distal platelet activation and consumption as compared to TF alone, fibrinogen, thrombin or VWF (Figure 5.6 & Figure 5.7).



**Figure 5.6 FXIa activity promotes distal platelet activation and consumption in the presence of collagen and / or low levels of TF.**

Recalcified whole blood pretreated with either vehicle, 1A6, 14E11, 10C9, CTI or hirudin was perfused over chambers coated with collagen, collagen + 0.01 – 0.1 nM TF, or 0.01 – 0.1 nM TF alone at shear rate of  $300 \text{ s}^{-1}$ . Samples were collected downstream of the chamber; distal microaggregate formation and single platelet consumption was assessed by FACS (A-E). Results (mean $\pm$ SEM) from at least 4 experiments.

Our results show that inhibition of FXIIa activation of FXI, FXIa activation of FIX and FXIa activity with 14E11, 1A6 and 10C9, respectively, or FXIIa activity with CTI eliminated platelet activation, microaggregate formation and single platelet consumption downstream of collagen-coated chambers (Figure 5.6A). Exposure of blood to collagen in combination with increasing concentrations of TF drastically accelerated the rate and the extent of distal platelet activation, microaggregate formation and consumption (Figure 5.6B&C).



**Figure 5.7 FXIa activity in local and distal platelet aggregation in the presence of VWF, Fibrinogen and Thrombin coated surfaces.**

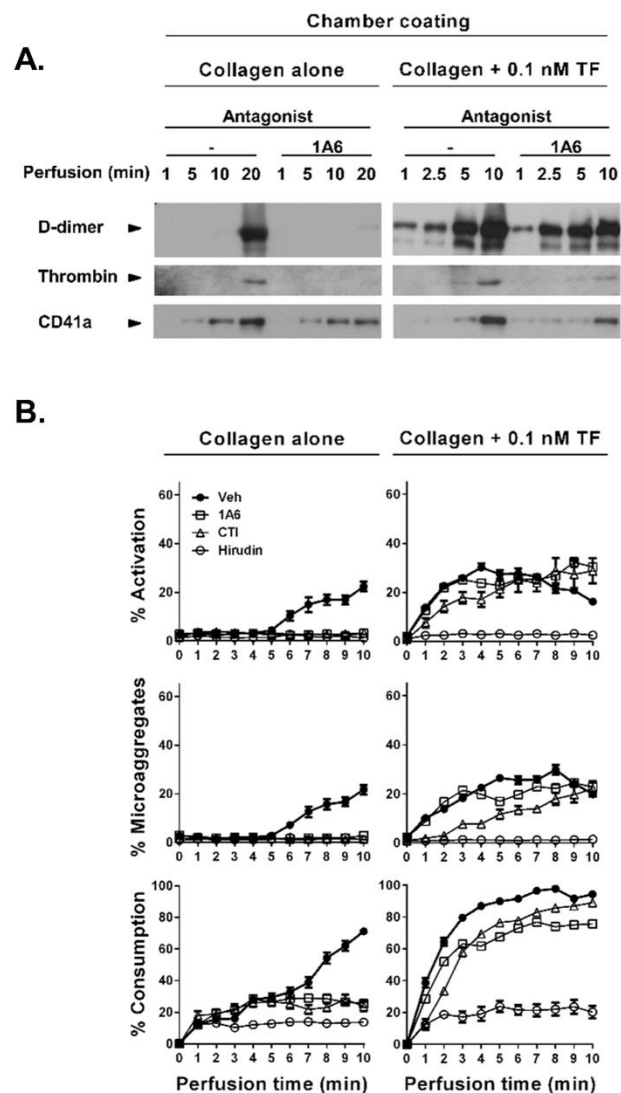
Recalcified whole blood pretreated with either vehicle, 1A6, CTI or hirudin was perfused over chambers coated fibrinogen, thrombin or with von Willebrand Factor (VWF) at shear rate of  $300 \text{ s}^{-1}$ . Images of local thrombi formed by 10 minutes of perfusion were recorded using differential interference contrast (A) or fluorescent light microscopy (B) after staining for fibrin (blue) and P-selectin (green). In parallel experiments, thrombi were lysed and immunoblotted for the fibrin degradation product, D-dimer, thrombin and the platelet surface receptor, CD41a (C). Samples were collected downstream of the chamber; distal microaggregate formation and single platelet consumption was assessed by FACS (D). Results (mean $\pm$ SEM) from at least 4 experiments.

In contrast to collagen alone, only the FXI inhibitor 1A6 attenuated the rate of platelet consumption in the presence of higher levels TF (0.1 nM), while both 1A6 and CTI were able to significantly reduce the rate of platelet consumption in the presence of lower levels of TF (0.01 nM; Figure 5.6D&E).

Hirudin dramatically reduced the degree of distal platelet activation, microaggregate formation and single platelet consumption regardless of local TF concentration.

A similar mechanism was observed when the shear rate was increased to 1000 s<sup>-1</sup> (Figure 5.8A&B).

These results suggest a role for the contact activation pathway in the initial amplification of thrombin generation downstream of sites of thrombus formation under flow.



**Figure 5.8 FXIa activity promotes distal platelet activation and consumption in the presence of collagen and TF under arterial shear rate.**

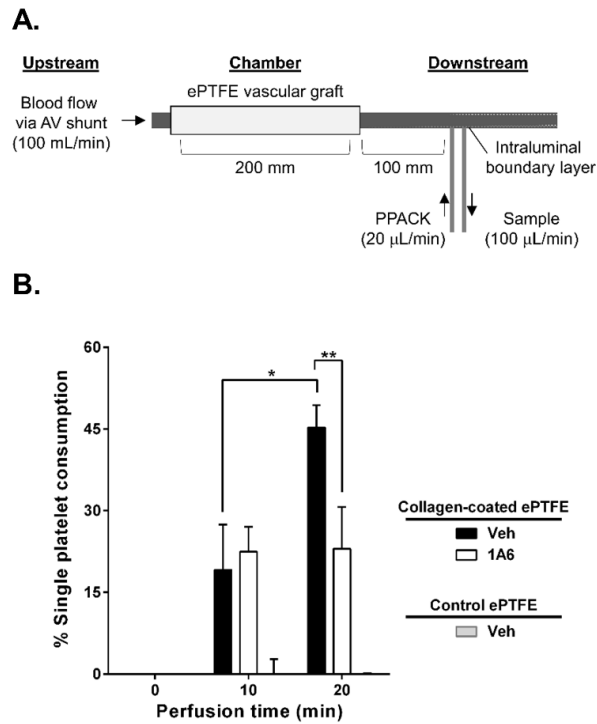
Recalcified whole blood pretreated with either vehicle, 1A6, CTI or hirudin was perfused over chambers coated with collagen or collagen + 0.1 nM TF at shear rate of 1000 s<sup>-1</sup>. Local thrombi formed within chamber at indicated perfusion times were lysed and immunoblotted for the fibrin degradation product, D-dimer, thrombin and the platelet surface receptor, CD41a (A). Samples were collected downstream of the chamber; distal microaggregate formation and single platelet consumption was assessed by FACS (B). Results (mean±SEM) from at least 4 experiments.

### 5.5.5 Protection of 1A6-treated baboons from collagen-initiated distal single platelet consumption

To examine the role of FXI activation in promoting distal platelet consumption in non-human primate baboon model, blood was collected distally from acutely introduced collagen-coated or control BSA-coated grafts in animals with chronic high flow arteriovenous shunts (Figure 5.9A). In line with the results shown in Figure 5.5A, exposure of blood to collagen *in vivo* accelerated the rate and the extent of distal single platelet consumption as compared to BSA controls.

Our data demonstrates that inhibition of FXI activity with 1A6 treatment reduced distal single platelet consumption at 20 min of perfusion by fifty percent ( $p = 0.0180$ ,  $n = 6$ ; Figure 5.9B). Taken together with our previous studies

demonstrating that inhibition of FXI prevented occlusion of collagen-coated grafts in a non-human primate model of thrombosis without increasing bleeding times,[142] our data provides rationale for the development of anti-FXI therapeutics for the prevention of thrombotic distal complications.



**Figure 5.9 Protection of 1A6-treated baboons from collagen-initiated distal single platelet consumption.**

4-mm internal diameter expanded-polytetrafluoroethylene (ePTFE) vascular graft was deployed into a chronic high flow arteriovenous (AV) shunt in healthy baboons. ePTFE was coated with either BSA or collagen and blood samples were drawn from the intraluminal coagulation marker concentration boundary layer by a syringe pump 1 cm downstream from acutely developing thrombi. 1 mM PPACK anticoagulant was infused at 1/5<sup>th</sup> of the sample extraction rate 3 mm proximal to the sample port to prevent the sample port from occluding during the 1-hour study. Blood flow through the graft was maintained at a fixed rate of 100 mL/min for the entirety of each study by proximal clamping (A). Quantification of the six separate animal experiments for each treatment (mean±SEM) are reported (B). Significant rise in percent single platelet consumption immediately distal to collagen-coated ePTFE was seen between 10 to 20 min of perfusion in control animals (\*,  $p = 0.0283$ ;  $n = 6$ ). 1A6-treated baboons maintained same single platelet levels at 20 min as at 10 min of perfusion ( $p = 0.9530$ ;  $n = 6$ ) significantly different from control at 20 min of perfusion (\*\*,  $p = 0.0180$ ;  $n = 6$ ).



## 5.6 Discussion

Coagulation FXI is an intrinsic pathway enzyme with an elusive role in normal hemostasis and mounting evidence for roles in thrombosis. Clinically, FXI deficiency is associated with only mild and injury-related bleeding, whilst elevated levels of FXI are associated with an increased risk for thrombotic complications.[366–368] Patients deficient in the other members of the contact pathway, namely FXII and prekallikrein, do not exhibit bleeding complications, suggesting that FXI may play a role in hemostasis through feedback activation by thrombin.[243,369–371] Moreover, activated FXI is able to activate FIX, FX, FV, and FVIII, bind platelets and inhibit tissue factor pathway inhibitor (TFPI).[245,246,372,373] FXI therefore acts to amplify thrombin via multiple pathways, providing rationale for the inhibition of FXI-mediated thrombin generation as an antithrombotic therapy design. For instance, a phase 2 clinical trial reducing FXI levels using FXI-antisense oligonucleotide demonstrated decreased incidence of deep venous thrombosis (DVT) after knee replacement surgery. While the study showed that reduction of FXI levels prevented venous thrombosis, translational approaches targeted at FXI may sacrifice the hemostatic function of FXI, increasing the risk of bleeding.[374,375] Thus, a better understanding of the role of FXI in thrombosis and hemostasis is required for the rational development of agents that target specific enzymatic functions of FXI, balancing safety with efficacy.

The biophysics of thrombus formation at a site of vascular injury has been well described,[272,376,377] in which blood flow dictates the transport kinetics of blood cells and coagulation factors to the site of injury, and thrombin generation is rate limited by the assembly and sequential activation of coagulation factors on the surface or activated platelets. Thus, the Damköhler number ( $Da$ ), which is the ratio of the rate of reaction to the rate of transport,[22] is high ( $Da > 1$ ). In contrast, within the bloodstream, the kinetics of platelet activation and thrombin generation are diffusion limited, as platelets in the bloodstream experience limited relative blood flow, as cells in suspension are transported by viscous forces within the bloodstream, resulting in a low  $Da$  ( $< 1$ ). Our

study demonstrates that FXI plays a differential role in promoting thrombin generation, platelet activation and aggregate formation in the bloodstream (diffusion-limited regime) relative to the site of thrombus formation (transport-limited regime).

Previously, we have demonstrated that inhibition of FXI activation by FXIIa is protective in a non-human primate model of local thrombus formation specifically due to a decrease in local thrombin generation and fibrin formation.[140,142,378] However, the mechanism by which the FXIa-thrombin axis may contribute to formation of platelet aggregates in flowing blood and distal microvascular occlusions under proximal procoagulant conditions has not been explored. In this study we investigated downstream changes in platelets in whole blood following passage through collagen- or collagen and TF-coated flow chambers. Our results demonstrate that local thrombus formation on immobilized collagen and TF potentiated platelet activation in the bloodstream, resulting in the rapid formation of platelet aggregates in the bloodstream, which may hold potential to occlude downstream vessels. This process of distal platelet activation was directly dependent on thrombin activity. Inhibition of FIX activation by FXIa with the FXI-Ab 1A6 was protective against distal single platelet consumption in the bloodstream both *in vitro* and *in vivo*, providing an additional role for FXI in thrombotic complications.

It has been established that the health of microvessels plays an important role in maintaining unobstructed blood flow to organs. Aging vessels are stiffer and more tortuous due to many factors including atherosclerosis plaque buildup, hypertension-driven vessel wall remodeling, smoking and diabetes, which predispose them to aberrant blood flow, platelet activation and thrombosis.[379] The physical biology of the microvasculature promotes increased platelet-platelet and platelet-endothelial cell interactions.[380,381] Additionally, the reduced flow rates within venules serves to increase the residence time of circulating platelets within these vascular beds. In patients, introduction of a vascular injury, such as a surgical incision during a joint replacement followed by stasis due to patient immobility post-operation, may result in a local burst of thrombin generation.[382,383]

Under conditions described above, our findings would suggest that FXI-dependent thrombin amplification and activation of platelets potentiates platelet microaggregate formation which may then occlude the microvascular networks. Our results demonstrate that activation of the FXI axis plays a key role in distal platelet activation and microaggregate formation in solution downstream of thrombus formation under both venous and arterial shear flow. Thus, in addition to its anticoagulant role, pharmacological targeting of FXI may be useful in mitigating platelet activation and therefore prevent platelet-driven amplification of platelet aggregate and thrombi formation in prothrombotic conditions involving direct contact pathway of the coagulation agonists (including artificial surfaces) and widespread vascular injury.

**Chapter 6. Coagulation factor XII activity promotes platelet consumption in the presence of bacterial-type long-chain polyphosphate in blood flow *in vitro* and bacteria *in vivo***

Jevgenia Zilberman-Rudenko, Stephanie E. Reitsma, Cristina Puy, Rachel A. Rigg,

Stephanie A. Smith, Erik I. Tucker, Robert Silasi, Coen Maas, Rolf T. Urbanus, David Gailani, James

H. Morrissey, András Gruber, Florea Lupu, Alvin H. Schmaier, Owen J. T. McCarty

Chapter 6. was submitted to the American Heart Association Society,

*Arteriosclerosis, Thrombosis, and Vascular Biology*, as response to reviewers

**6.1 Abstract**

*Background:* Terminal complications of bacterial sepsis include development of disseminated intravascular consumptive coagulopathy. Bacterial constituents, including long-chain polyphosphates (polyP), have been shown to activate the contact pathway of coagulation in plasma. Recent work shows that activation of the contact pathway in flowing whole blood can promote thrombin generation and platelet activation and consumption distal to thrombus formation *ex vivo* and *in vivo*.

*Aim:* Determine whether presence of long-chain polyP in the bloodstream promotes platelet activation and consumption in a coagulation factor (F)XII-dependent manner.

*Methods/Results:* Long-chain polyP promoted platelet P-selectin expression, microaggregate formation and platelet consumption in flowing whole blood in a contact activation pathway-dependent manner. Moreover, long-chain polyP accelerated fibrin formation on immobilized collagen surfaces under shear flow in a FXI-dependent manner. Distal to the site of thrombus formation, platelet consumption was dramatically enhanced in the presence of long-chain polyP in the blood flow in a FXI- and FXII-dependent manner. In a murine model, long-chain polyP promoted platelet deposition and fibrin generation in a FXII-dependent manner. Lastly, in a non-human primate model of bacterial sepsis, pretreatment of animals with an antibody blocking FXI activation by FXIIa diminished LD<sub>100</sub> *S. aureus*-induced platelet and fibrinogen consumption.

*Conclusions:* This study demonstrates that bacterial-type long-chain polyP promotes platelet activation in a FXII-dependent manner in flowing blood, which may contribute to sepsis-associated thrombotic processes, consumptive coagulopathy and thrombocytopenia.

## **6.2 Introduction**

While inflammation and vasoregulatory abnormalities dominate the clinical presentation of severe sepsis, excessive activation of the blood coagulation cascade associated with the development of fulminant disseminated intravascular coagulopathy (DIC) remains a common cause of sepsis-related mortality.[127,384,385] DIC is a thrombo-hemorrhagic complication that compromises organ perfusion and physiological response of hemostasis by causing thrombotic occlusion of blood vessels and consumptive coagulopathy, respectively. In this chapter, we use closed and open experimental platforms to study the role of FXIIa activity in the presence of bacterial-type long-chain polyphosphates (polyP). This work shows that FXIIa activity promotes platelet consumption in the presence of long-chain polyP in the blood flow *in vitro* and bacteria *in vivo*. This research may aid in the identification of potential mechanisms by which components of the contact activation pathway of coagulation influence the host response to infection by triggering thrombin generation and systemic platelet activation and consumption.

## **6.3 Background**

Sepsis is an infection-induced systemic inflammatory response syndrome that can progress into terminal hypotension, insufficient organ perfusion and death within hours to days when left untreated.[126] Some forms of sepsis are accompanied by disseminated intravascular coagulopathy (DIC), a thrombo-hemorrhagic complication that aggravates poor tissue perfusion by causing thrombotic occlusion of blood vessels and severe bleeding due to consumptive coagulopathy.[386] At present, DIC, which is a prevalent cause of sepsis-associated mortality, has no disease-specific

effective FDA-approved antithrombotic treatment. There is a clear need for a better understanding of the molecular basis of sepsis/SIRS in order to develop safe and effective therapies to improve clinical outcomes.

Several lines of evidence suggest that components of the contact activation pathway of coagulation influence the host response to infection by triggering thrombin generation.[387] It has been proposed that during sepsis, exposure of blood to foreign materials, including components of pathogens (e.g., long-chain polyphosphates (polyP)), leads to FXII autoactivation and the reciprocal activation of prekallikrein and FXII, which is accelerated in the presence of high molecular weight kininogen.[45,388–391] FXIIa promotes coagulation by activating FXI, termed the intrinsic pathway of coagulation. The resulting thrombin generation drives platelet activation and fibrin formation, which may contribute to the innate immune response to select pathogens. However, with escalating intravascular coagulation, the endogenous regulators of coagulation are eventually overwhelmed, leading to vessel occlusion, hypoperfusion, and organ damage.[130,392] Hemostatic blood components are consumed in the process, and a hemorrhagic disorder is superimposed on the thrombotic condition.

Epidemiological data show that FXI deficiency in humans is thromboprotective,[368,393] while experimental induction of contact activation of coagulation *in vivo* can imitate thrombo-hemorrhagic and other sepsis-associated complications.[140] Specifically, FXI activation by FXIIa has been shown to promote thrombin generation and contribute to local platelet activation and consumption of platelets in the bloodstream distal to sites of thrombus formation under shear flow *ex vivo* and *in vivo*.[277,313] Conversely, inhibition of FXI activation by FXIIa has been shown to attenuate coagulopathy development and promote survival in mice with polymicrobial sepsis[394] as well as prevent collagen-coated vascular graft occlusion in a primate model of thrombosis.[142] It is unclear whether bacterial components such as long-chain polyP are capable of promoting systemic thrombin generation in the circulating blood.

Inorganic polyP molecules consist of tens to thousands of negatively charged phosphate groups which can be introduced into the bloodstream by activated platelets (short-chain polyP)[395] or a variety of microorganisms (long-chain polyP).[396] Synthesized or purified polyP molecules are able to promote fibrin formation by directly activating FXII and enhancing activation of FV[397,398] with higher potency at increased polyP polymers lengths.[275] Long-chain polyP has also been shown to accelerate FXIa activation by both FXIIa and thrombin as well as prothrombin activation by FXIIa independent of FXI.[141,276]

In this study, we used closed and open systems to determine whether long-chain polyP is capable of promoting platelet consumption and coagulopathy in flowing blood. We employed the FXIIa inhibitor corn trypsin inhibitor (CTI), a novel anti-FXIIa-blocking antibody, 5C12, and three monoclonal anti-FXI antibodies: 14E11, which blocks FXI activation by FXIIa; 1A6, which blocks both FXI activation by FXIIa and FXIa activation of FIX, and 10C9, which is a FXIa active site domain-neutralizing antibody. Our results demonstrate that long-chain polyP can promote platelet deposition, activation, aggregation and consumption in the bloodstream in a FXII-dependent manner *in vitro* and *in vivo*. Furthermore, in a non-human primate model of bacterial sepsis, pretreatment of animals with humanized 14E11 to block FXI activation by FXIIa diminished LD<sub>100</sub> *S. aureus*-induced platelet and fibrinogen consumption.

These results suggest that neutralization of FXII activation in the bloodstream may represent a useful approach to preventing coagulopathy in conditions where significant levels of long-chain polyP are present.

## **6.4 Materials and Methods**

### **6.4.1 Reagents**

Anti-factor XI function-blocking antibodies 1A6, 14E11 and 10C9 were generated as described.[139–141] Corn trypsin inhibitor (CTI) was from Enzyme Research Laboratories, Inc.,

hirudin from Hyphen Biomed, Phe-Pro-Arg-chloromethylketone (PPACK) from Santa Cruz, fibrillar collagen from Chrono-Log Corp, lipidated tissue factor (TF; Innovin<sup>®</sup> PT reagent) from Siemens and ellagic acid (aPTT reagent) from Pacific Haemostasis. Rabbit anti-fibrinogen antibody was from Cappel MP Biomedicals, LLC, anti-rabbit-AF350 from Life technologies, anti-CD41-PE and anti-CD62P-APC were from BD Pharmingen, CD31-eFluor450 was from eBioscience. Anti-thrombin API (H-85) antibody was from Santa Cruz Biotech and anti-integrin  $\alpha$ IIb from Abnova. FXIIa chromogenic substrate S-2302 was purchased from Diapharma. Polyphosphate molecules of the size produced by bacteria (long-chain polyP, >595 phosphate units in length) were prepared as described.[275] Recombinant polyP-binding domain from *Escherichia coli* polyphosphatase (PPXbd) was produced as described.[276] All other reagents were from Sigma-Aldrich, Inc. or previously named sources.[245,277]

#### 6.4.2 *Development of an anti-factor XII function-blocking antibody*

The function-blocking anti-factor XII antibody 5C12 was produced using a similar approach as described previously.[399] In short, the murine FXII null genotype (C57Bl/6 background)[244] was crossed onto the Balb-C background through 7 generations. FXII-deficient Balb-C mice were given 25  $\mu$ g of a mixture of human and murine FXII and FXIIa by intraperitoneal injection in Freund complete adjuvant on day 0 and Freund incomplete adjuvant on day 28. Hybridomas were screened using a solid phase enzyme-linked immunosorbent assay (ELISA) against human FXII, and those that showed binding were subcloned twice by limiting dilution. 5C12 was the clone that produced the most potent neutralizing antibody, as measured by prolongation of the activated partial thromboplastin clotting time of normal human plasma. The cell line producing 5C12 was grown in a CL1000 bioreactor according to the manufacturer's protocol (Integra Biosciences), and the antibody was purified from the media using cation exchange and protein A chromatography.



#### 6.4.3 *Humanization of a function-blocking anti-factor XI antibody*

The murine monoclonal antibody 14E11 was generated by immunizing FXI-deficient Balb-C mice with recombinant mouse FXI. 14E11 was selected for further study based on its ability to prolong the aPTT in mammalian plasmas. 14E11 exerts its anticoagulant activity in part by binding to the FXI A2 domain and preventing assembly of the contact activation complex, composed of high molecular weight kininogen (HK), prekallikrein, and FXIIa, and inhibits FXI activation by FXIIa. The humanized form of this antibody (h14E11) was produced by complementarity determining region (CDR)-grafting (Antitope, Ltd.) from the precursor murine monoclonal antibody 14E11. Subsequently, h14E11 was manufactured using fed-batch fermentation of h14E11-expressing CHO DUKX B11 cells in a 1000 L bioreactor, followed by protein A affinity purification, viral inactivation at low pH, two polishing chromatography steps, followed by nanofiltration and formulation.

#### 6.4.4 *Enzyme-linked immunosorbent assay to quantify FXI(a) binding to (h)14E11*

FXI or FXIa (2 mg/mL, 100 mL/well) in 50 mM Na<sub>2</sub>CO<sub>3</sub> pH 9.6 were incubated overnight at 4°C in Immulon® 2HB microtiter plates (Thermo Scientific). Wells were blocked with 150 mL phosphate buffered saline (PBS) with 2% BSA for one hr at RT. 100 mL biotinylated 14E11, or h14E11 (100 to 10<sup>-7</sup> mM) in 90 mM HEPES pH 7.2, 100 mM NaCl, 0.1% BSA, 0.1% Tween-20 (HBS) was added and incubated for 90 min at RT. After washing with PBS-0.1% Tween-20 (PBST), 100 mL streptavidin-HRP (Thermo Scientific, 1:8000 dilution in HBS) was added and incubated at RT for 90 min. After washing, 100 mL Substrate Solution (12 mL 30 mM citric acid, 100 mM Na<sub>2</sub>HPO<sub>4</sub> pH 5.0, 1 tablet OPD, 12 mL 30% H<sub>2</sub>O<sub>2</sub>) was added. Reactions were stopped after 10 min with 50 mL 2.5M H<sub>2</sub>SO<sub>4</sub>. Absorbance at 495 nm was measured on a SpectroMax 340 microplate reader (Molecular Devices). Apparent K<sub>d</sub> values (nM) were calculated by plotting the dose-response data against the log<sub>10</sub> of the antibody concentration and fitting data to a four-parameter logistic curve. The apparent K<sub>d</sub> of h14E11 for human FXI and FXIa = 3.656 nM and 1.383 nM, respectively; the apparent K<sub>d</sub> of 14E11 for human FXI and FXIa = 0.431 nM and 0.152 nM, respectively.

#### 6.4.5 *Blood collection and preparation of plasmas*

Human venous blood was drawn by venipuncture from healthy adult volunteers into sodium citrate in accordance with the OHSU Institutional Review Board. Platelet-poor plasma (PPP) was prepared by centrifugation of citrated whole blood (in 0.32% w/v sodium citrate) from three separate donors at  $2150\times g$  for 10 min. Further centrifugation of the plasma fractions at  $2150\times g$  for 10 min yielded PPP, which was then pooled and stored at  $-80^{\circ}\text{C}$  until use.

#### 6.4.6 *Fibrin generation assay*

Solutions containing human PPP were incubated with vehicle or long-chain polyP (33, 100 or 300  $\mu\text{M}$ ) at  $37^{\circ}\text{C}$  for 10 min. Parallel reactions were performed in the presence of FXI function-blocking antibodies 1A6 (50  $\mu\text{g}/\text{mL}$ ) or 14E11 (50  $\mu\text{g}/\text{mL}$ ), the FXII inhibitor CTI (40  $\mu\text{g}/\text{mL}$ ), the thrombin inhibitor hirudin (40  $\mu\text{g}/\text{mL}$ ) or PPXbd (250  $\mu\text{g}/\text{mL}$ ). Fibrin generation was initiated with addition of either 25 mM  $\text{CaCl}_2$  alone or together with 100 pM human  $\alpha$ -thrombin. Changes in solution turbidity (A405) in clear flat-bottom polystyrene wells (Greiger) at  $37^{\circ}\text{C}$  were monitored by using a Tecan microplate reader (TECAN devices). The concentration of PPP was maintained at 33% final v/v in all conditions. The long-chain polyP was diluted in buffer containing 25 mM HEPES and 150 mM NaCl with 1% BSA (pH 7.4). The time interval required for the solution turbidity to reach the half-maximal value was defined as  $T_{\text{half-max}}$  as described previously.[246]

#### 6.4.7 *Clotting time assay*

Clotting times of PPP or whole blood were measured with a KC4 Coagulation Analyzer (Trinity Biotech PLC, Bray, Ireland). Samples were pretreated with FXI function-blocking antibodies 1A6 (50  $\mu\text{g}/\text{mL}$ ) or 14E11 (50  $\mu\text{g}/\text{mL}$ ), the FXII inhibitor CTI (40  $\mu\text{g}/\text{mL}$ ), the thrombin inhibitor hirudin (40  $\mu\text{g}/\text{mL}$ ) or PPXbd (250  $\mu\text{g}/\text{mL}$ ) and incubated with vehicle or long-chain polyP (33, 100 or 300  $\mu\text{M}$ ) at  $37^{\circ}\text{C}$  for 3 min. Clotting was initiated with addition of either 25 mM  $\text{CaCl}_2$  alone or together with 100 pM human  $\alpha$ -thrombin at  $37^{\circ}\text{C}$ , and clotting time was recorded. The concentration of PPP and whole blood was maintained at 33% and 66% final v/v, respectively, in all conditions.

#### 6.4.8 *Effects of 5C12 and CTI on FXIIa activity in vitro*

Effect of anti-factor FXIIa reagents was measured as described previously.[141,399] In short, after preincubation with either control buffer or different concentrations of 5C12 or CTI for 10 min at RT, human purified FXII (50 nM) was incubated with high molecular weight kininogen (HK; 12.5 nM), prekallikrein (PK; 12.5 nM) and long-chain polyP (10  $\mu$ M). After 1 hour samples were removed and quenched with polybrene (6  $\mu$ g/mL final; Sigma-Aldrich) to neutralize long-chain polyP and with soybean trypsin inhibitor (50  $\mu$ g/mL final; Sigma-Aldrich) to inactivate kallikrein. FXIIa activity was quantified by measuring rates of chromogenic substrate S-2302 (500  $\mu$ M; Diapharma) conversion by FXIIa at 405 nm. Rates of S-2302 FXIIa hydrolysis were converted to FXIIa concentrations using a standard curve and normalized to control buffer condition.

#### 6.4.9 *Ex vivo flow experiments*

Glass capillary tubes/chambers (0.2 $\times$ 2 $\times$ 200 mm; VitroCom) were coated as described previously.[277] Surfaces were blocked with 5 mg/mL denatured bovine serum albumin (BSA) for 1 h prior to assembly into a flow system. Sodium citrate (0.38% w/v) anticoagulated whole blood was recalcified and perfused through the chamber for 10 min at an initial wall shear rate of 300 s<sup>-1</sup>. Downstream samples were collected directly into 100  $\mu$ M PPACK and 1.5% w/v sodium citrate (1 tube/min of perfusion) to final 50% dilution and evaluated using fluorescence-activated cell sorting (FACS).

#### 6.4.10 *Microscopy*

After blood perfusion, glass capillaries were washed with phosphate-buffered saline (PBS) and HEPES/Tyrode buffer (136 mM NaCl, 2.7 mM KCl, 10 mM HEPES, 2 mM MgCl<sub>2</sub>, 0.1% BSA; pH7.4) containing 1.5% sodium citrate and 100  $\mu$ M PPACK, followed by incubation with blocking buffer (1% BSA, 1% FCS in HEPES/Tyrode buffer) for 30 min. Glass capillaries were incubated with rabbit anti-serum against human fibrinogen (1:100) for 10 min and washed with PBS followed by an incubation with CD41-PE (1:50), CD62-FITC (1:50), and goat anti-rabbit Alexa Fluor 350 (1:500) in dark for 10

min. Glass capillaries were washed with PBS, fixed with paraformaldehyde (PFA 4%), and sealed with mounting media. Samples were analyzed on a Zeiss Axio Imager 2 microscope 6 (Carl Zeiss MicroImaging GmbH, Germany).

#### 6.4.11 *Western blots*

Thrombi formed on collagen/TF were lysed for 5 min with 1× lysis buffer (10 mM Tris, 150 mM NaCl, 1 mM EGTA, 1 mM EDTA, 1% NP-40, 2 mM PMSF and 10 U DNase I) at 4°C, followed by treatment with 1 μM plasmin for 40 min at RT. Local fibrin deposition was evaluated by separating combined eluate samples on non-reducing SDS–PAGE gels, transferring to PVDF membrane and immunoblotting with rabbit anti-fibrinogen followed by anti-rabbit-HRP. Local platelet deposition and thrombin content was similarly evaluated by separating combined eluate samples on separate reducing SDS–PAGE gels and immunoblotting for CD41 or thrombin. Proteins were detected using ECL.

#### 6.4.12 *FACS analysis*

Pre- and post-chamber blood samples were collected into 100 μM PPACK and 1.5% w/v Na-citrate (1:1, v:v) and incubated with 1:50 dilution antibodies for 30 min at RT. Reactions were fixed by diluting 1:10 with RT 12.5% Cytofix<sup>BD</sup>. 10,000 single platelets were determined by a PE-conjugated platelet marker CD41a and the characteristic forward- and side-scatter scatter patterns via FACS (Canto II; BD Biosciences, Heidelberg, Germany). Platelet CD62P expression levels and single platelet consumption were determined as described previously.[277,284,313] Microaggregate formation was determined by the upshift in fluorescence intensity in CD31/CD41a double-positive events.

#### 6.4.13 *Mouse model of lethal pulmonary embolism*

Knockout (KO) mice were produced as described previously. In short, a B6/129 background was backcrossed 4 generations into C57BL/6 background.[289] These animals were mated with wild-type (WT) mice (C57BL/6, Jackson Laboratories) to make heterozygous animals and were re-derived into *Klkb1*<sup>-/-</sup>. *Klkb1*<sup>-/-</sup> mice and littermate WT colonies were maintained by brother/sister mating. Every 10

generations, the *Klkb1*<sup>-/-</sup> mice are mated with C57BL/6J to re-derive KOs from the heterozygous mice. The genotyping of *Klkb1*<sup>-/-</sup> mice was determined as described previously.[289] FXII<sup>-/-</sup> mice (deficient in coagulation factor XII) in a C57BL/6J background were generously provided by Dr. Frank Castellino of the University of Notre Dame. Animal care and procedures were reviewed and approved by the Institutional Animal Care and Use Committees at Case Western Reserve University (CWRU) and performed in accordance with the guidelines of the American Association for Accreditation of Laboratory Animal Care and the National Institutes of Health. Lung tissues were harvested, processed and stained with haematoxylin and eosin (H&E) stain to facilitate histopathologic studies. Images were obtained from a Leica SCN 400 Slide Scanner equipped with a Hamamatsu line sensor color camera and a 340/0.65 objective lens. The images were made through a 32 tube lens at 340 final magnification. Number of vessel occlusions quantified from H&E staining. Vessel occlusions per visual field were counted at 340.

#### 6.4.14 *Non-human primate model of sepsis*

*Papio anubis* baboons were dosed with a single 1 mg/kg intravenous bolus injection of anti-FXI antibody h14E11, 30 min before challenge. A lethal dose ( $1-2 \times 10^{10}$  cfu/kg) of *S. aureus* (strain B17266 Rosenbach, ATCC #49496) in 1.5 mL/kg sterile saline solution was infused intravenously over 2 hours (from T<sub>0</sub> to T<sub>120</sub> min). Blood samples were obtained at 0, 2, 4, 6 and 8 hours. Platelet levels were determined using a VetScan HM5 Hematology Analyzer (Abaxis). Whole blood samples were spun down to isolate plasma and plasma levels of fibrinogen levels were measured using a functional clotting assay developed by Clauss et al.[288]

#### 6.4.15 *Data analysis*

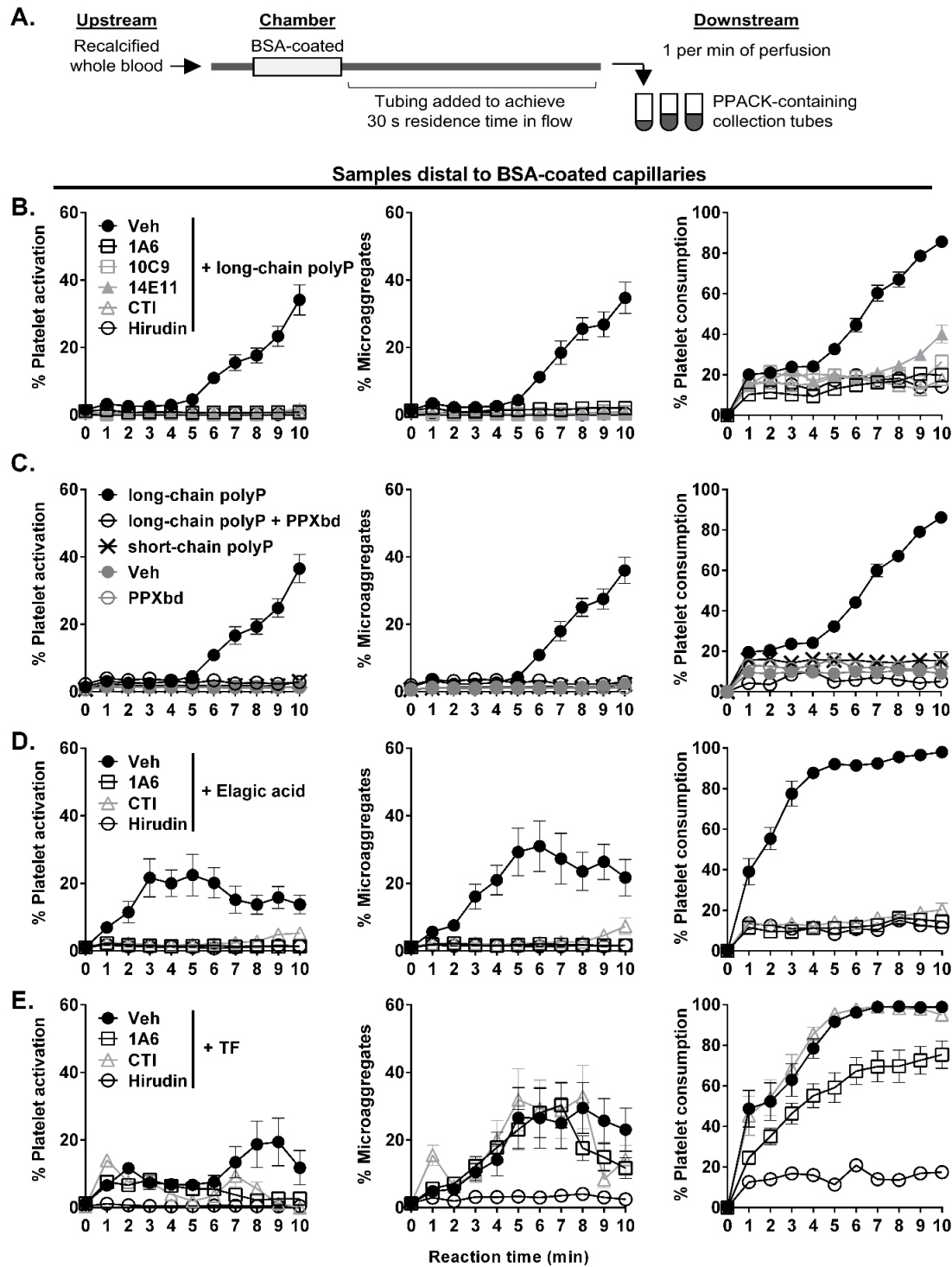
Data are shown as means  $\pm$  SEM. Statistical significance of differences between means was determined by ANOVA. If means were shown to be significantly different, multiple comparisons were performed by the Tukey test. Probability values of  $P < 0.05$  were selected to be statistically significant. Apparent K<sub>d</sub> values (nM), for comparison of 14E11 and h14E11, were calculated by

plotting the dose response data against the  $\log_{10}$  of the antibody concentration. The data was then fit to a four-parameter logistic curve and the Kd was calculated using GraphPad Prism.

## **6.5 Results**

### *6.5.1 Long-chain polyP promotes platelet consumption in flowing blood*

Our initial set of experiments examined whether soluble long-chain polyP promotes platelet activation in flowing blood. As shown in Figure 6.1A, recalcified whole blood was perfused through an inert (BSA-coated) flow chamber and tubing for a total residence time of 30 seconds before being collected downstream at 1 min intervals into tubes containing serine protease inhibitor (PPACK) and sodium citrate. Single platelet consumption (reduction of single platelet population in the bloodstream quantitated on FSC by SSC plot), platelet activation (CD62P expression), and platelet microaggregate formation in solution (CD41a/CD31 high positive) was quantified using flow cytometry as described previously.[277,313]



**Figure 6.1 Long-chain polyP promotes platelet consumption in flowing blood.**

Recalcified whole blood was perfused through BSA-coated chambers for indicated reaction times at  $300 \text{ s}^{-1}$  shear rate. Downstream samples were collected into solution containing serine protease inhibitor (PPACK) at 1 min intervals as shown in schematic (A), immunostained and evaluated by FACS flow cytometry for percent platelet activation (% CD41a+/CD62P+ vs. CD41a+ total events), platelet microaggregate formation (high fluorescence intensity CD41a+/CD31+ events) and single platelet consumption (loss of single platelet population gate on FSC by SSC scatter plots). Prior to recalcification, blood was pretreated with long-chain polyP (B), ellagic acid (D) or tissue factor (TF; E) and either vehicle or anti-FXI antibodies (1A6, 10C9 or 14E11), FXIIa inhibitor (CTI) or thrombin inhibitor (hirudin). In parallel experiments, blood was pretreated with either control buffer, long- or short-chain polyP in the presence of vehicle (filled) or 250  $\mu\text{g}/\text{mL}$  PPXbd (hollow; C). Results shown as mean  $\pm$  SEM from at least three experiments.

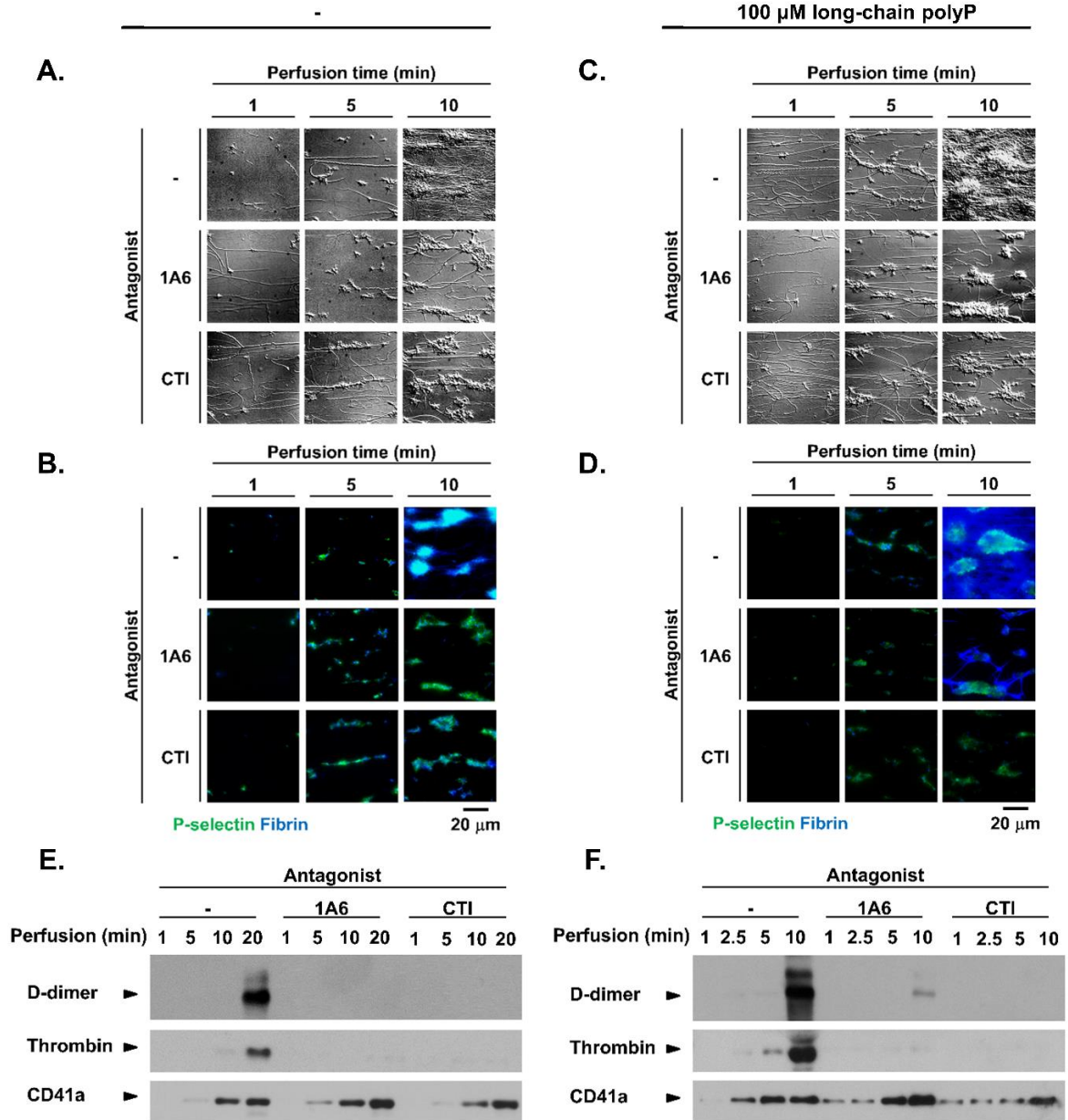
Our results show that addition of 100  $\mu$ M long-chain polyP to whole blood resulted in a robust increase in platelet activation (>30% CD62P expression), microaggregate formation and single platelet consumption (>80%) in the blood flow (Figure 6.1B), while platelets remained quiescent under control conditions (Figure 6.1C). Platelet activation, aggregate formation and consumption in the blood flow induced by long-chain polyP was abrogated by treatment of whole blood with either a FXIa active site domain-neutralizing antibody, 10C9, the anti-FXI antibody 1A6, which inhibits FXI activation by FXIIa and FIX activation by FXIa, the anti-FXI antibody 14E11, which inhibits FXI activation by FXIIa and conversely activation of FXII by FXIa, the FXIIa inhibitor corn trypsin inhibitor CTI, or the direct thrombin inhibitor, hirudin (Figure 6.1B).

We next pretreated blood with recombinant exopolyphosphatase binding domain (PPXbd), which competitively inhibits polyphosphate binding, to validate a role for long-chain polyP in promoting platelet activation in the blood flow. Our results show that the presence of PPXbd completely neutralized the effect of long-chain polyP to basal levels of platelet activation, aggregate formation and consumption (Figure 6.1C). In contrast, pretreatment of blood with recombinant short-chain polyP of the size secreted by platelets or PPXbd alone did not promote platelet activation, aggregate formation or consumption above baseline levels. Taken together, our results suggest that long-chain polyP promotes platelet activation and consumption in the bloodstream in a contact activation pathway-dependent manner.

Lastly, we used known activators of the contact pathway (ellagic acid) or the extrinsic pathway, tissue factor (TF) in our system to validate the role of activation of FXII or FVII, respectively, in promoting platelet consumption in blood flow (Figure 6.1D&E). Our results show that ellagic acid promoted platelet activation, aggregation and consumption in flowing blood, which was eliminated in the presence of CTI, 1A6 or hirudin. In contrast, the ability of TF to promote robust platelet aggregate formation or consumption was insensitive to CTI, while inhibition of FXI activation with 1A6 reduced the effect of TF on platelet consumption.



Collagen-coated capillaries



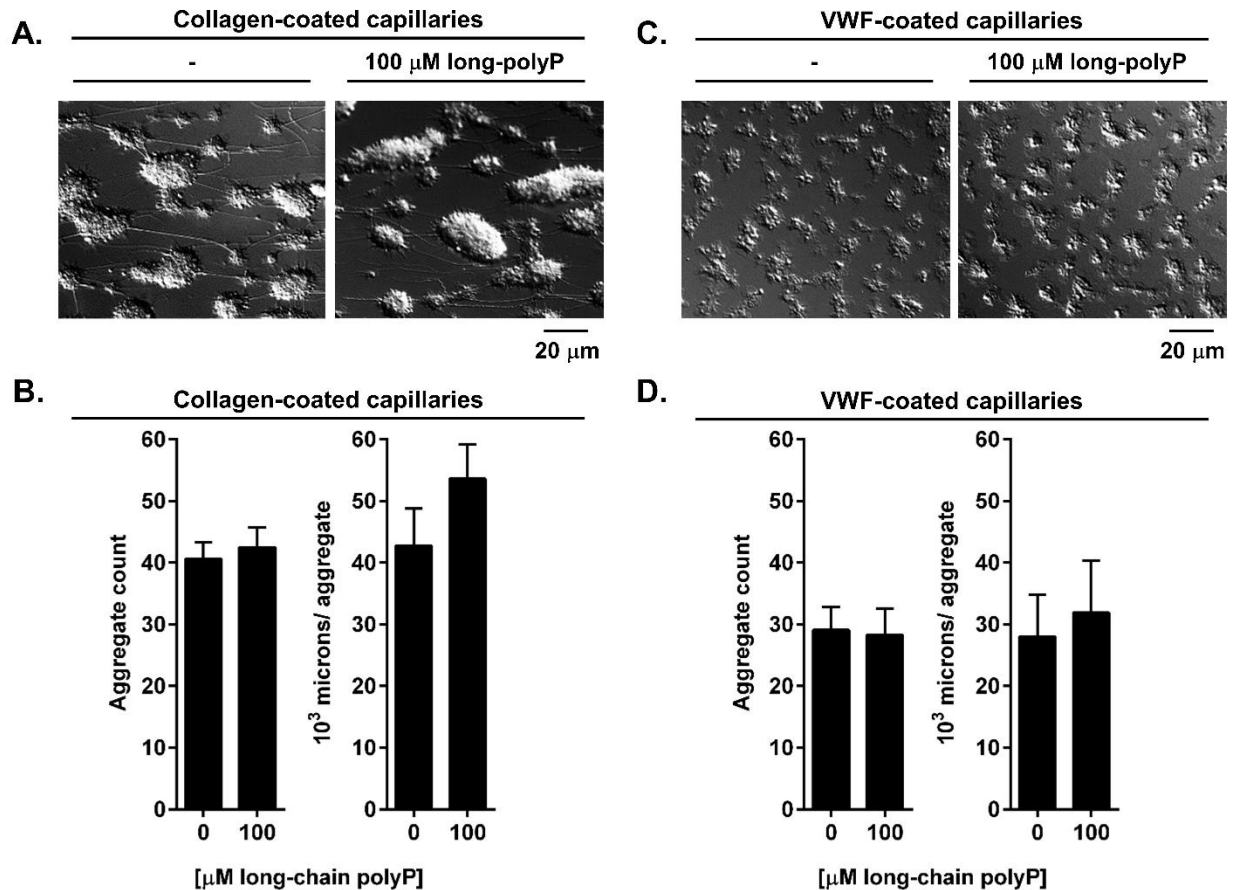
**Figure 6.2 Long-chain polyP promotes local thrombus formation on collagen surfaces.**

Recalcified whole blood was perfused over collagen-coated chambers for indicated perfusion times at  $300 \text{ s}^{-1}$  shear rate. Images of local thrombi formed at each perfusion time point in the presence of control buffer (-), 50  $\mu\text{g}/\text{mL}$  1A6 or 40  $\mu\text{g}/\text{mL}$  CTI were recorded using differential interference contrast (A) or fluorescent light microscopy (B) after staining for fibrin (blue) and P-selectin (green). In select experiments, whole blood was pretreated with 100  $\mu\text{M}$  long-chain polyP prior to re-calcification and perfusion over collagen-coated chambers (C) and (D). In parallel experiments, thrombi formed in the presence of control buffer (E) or 100  $\mu\text{M}$  long-chain polyP (F) by corresponding perfusion time points were subjected to detergent lysis and plasmin digest and immunoblotted for fibrin degradation product, D-dimer, thrombin and platelet surface receptor, CD41a. Representative images and blots for at least four separate experiments are shown.

### 6.5.2 *Long-chain polyP promotes local thrombus formation on collagen surfaces*

We next studied whether long-chain polyP has an effect on local platelet deposition and fibrin formation on collagen under shear flow conditions. Citrated whole blood was incubated with either vehicle or long-chain polyP prior to recalcification and perfusion over collagen-coated surfaces. Under vehicle conditions, we observed a time-dependent increase in the degree of platelet adhesion, aggregation, activation and fibrin formation on collagen (Figure 6.2A&B). The extent of fibrin formation was enhanced in the presence of soluble long-chain polyP, as visualized using differential interference contrast and fluorescence microscopy (Figure 6.2C&D). Long-chain polyP decreased the time required before detectable levels of d-dimer, clot-bound thrombin and platelets were observed in the formed thrombi, as measured by Western blot following lysis and plasmin digestion (Figure 6.2E&F). Blockade of FXI activation with 1A6 or inhibition of FXIIa activity with CTI nearly eliminated fibrin formation both in the presence or absence of long-chain polyP, while the degree of platelet deposition as measured by CD41a via Western blot remained fairly consistent under all conditions. Along these lines, in the absence of coagulation, platelet adhesion and aggregation on either collagen or immobilized von Willebrand factor (VWF) under flow was unaffected by the presence of long-chain polyP (Figure 6.3).

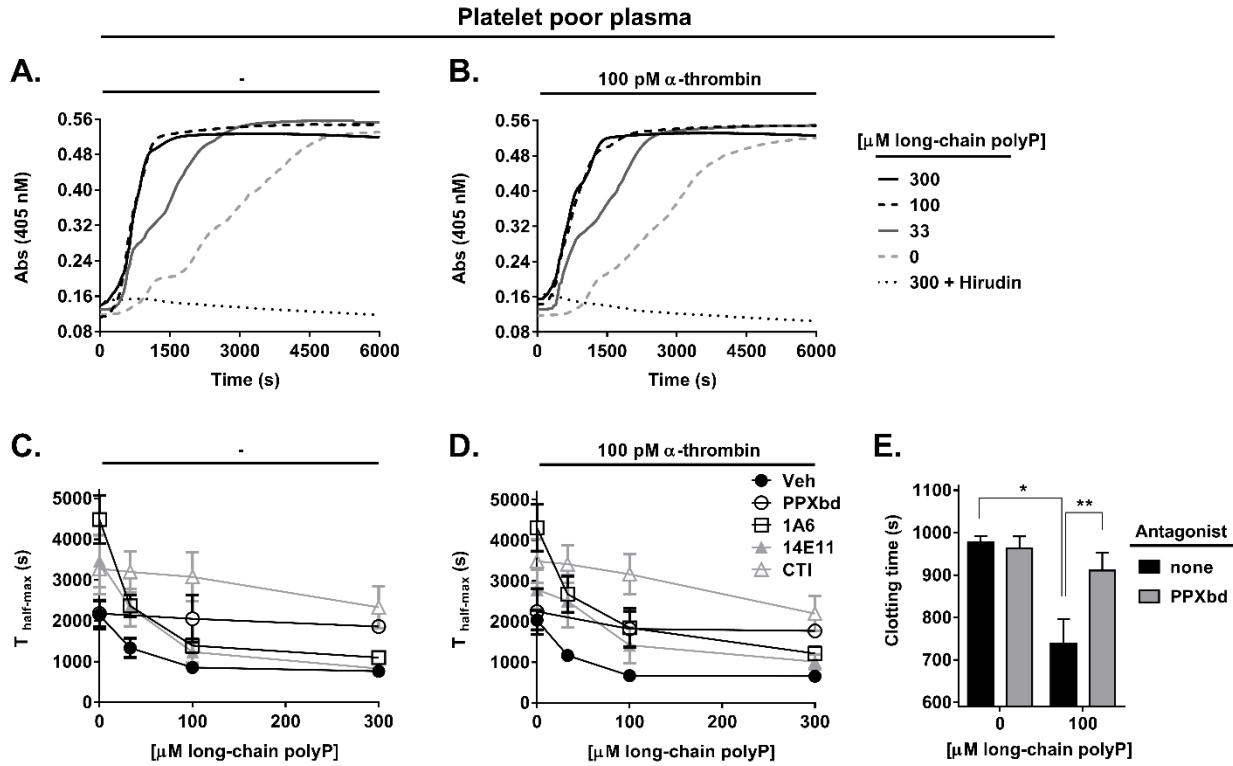
Conversely, in a closed system, we found that long-chain polyP promoted fibrin formation in a dose-dependent manner, decreasing the time required to reach half maximal fibrin levels ( $T_{\text{half-max}}$ ) from  $2140s \pm 346s$  under vehicle conditions to  $1332s \pm 236s$ ,  $854s \pm 138s$  and  $763s \pm 95s$  in the presence of 33, 100 and 300  $\mu\text{M}$  long-chain polyP, respectively (Figure 6.5A). The effect of long-chain polyP on fibrin formation was reversed by CTI or PPXbd (Figure 6.5B). Taken together, our results suggest that long-chain polyP promotes thrombin generation to enhance local fibrin formation at sites of thrombus formation in a contact activation pathway-dependent manner.



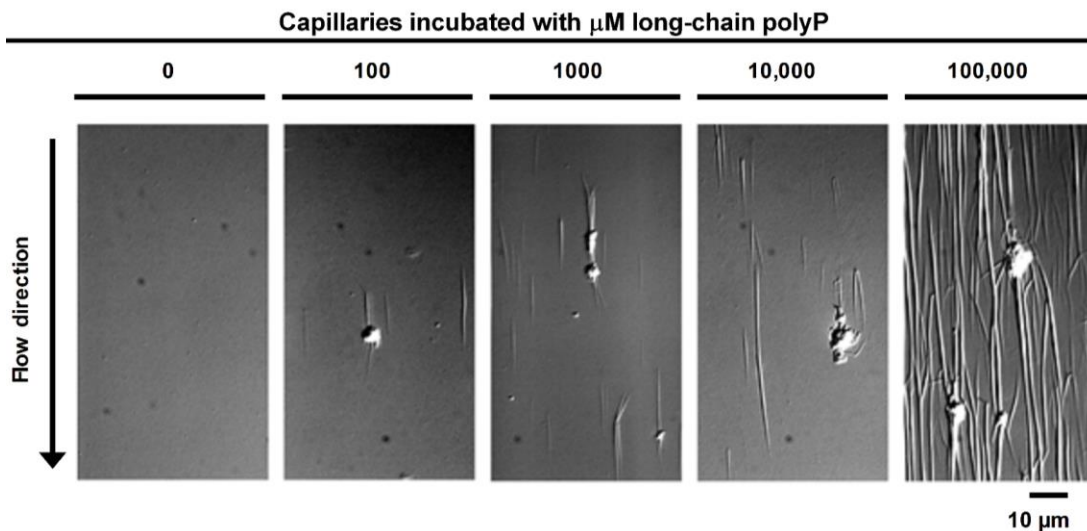
**Figure 6.3 Role of long-chain polyP in platelet aggregation on collagen and VWF under shear.**

Citrated and hirudinized whole blood was pretreated with vehicle (-) or 100  $\mu\text{M}$  long-chain polyP prior to recalcification and perfusion through surfaces of immobilized collagen (A) or VWF (C) at 300  $\text{s}^{-1}$  shear rate. Images of local platelet aggregates formed by 10 min of perfusion time were recorded using differential interference contrast. Quantification of aggregate count and average aggregate size ( $10^3$  microns/aggregate) on collagen (B) or VWF (D) for at least 5 independent experiments is represented as mean  $\pm$  SEM. No significant difference in the presence of long-chain polyP was found compared to vehicle.

Long-chain polyP was also able to serve as a direct surface activator for fibrin formation under shear. When long-chain polyP was immobilized onto a surface, the rate and extent of fibrin formation formed following perfusion of recalcified whole blood increased with increasing concentrations of immobilized long-chain polyP under shear flow (Figure 6.4). Notably, perfusion of recalcified whole blood past surfaces of increasing levels of immobilized myosin yielded enhanced levels of fibrin formation without significant increase in platelet deposition.



**Figure 6.5 Long-chain polyP promotes fibrin formation and clotting of platelet poor plasma.** Citrated platelet poor plasma (PPP) was incubated for 10 min at 37 °C with indicated levels of long-chain polyP in the presence of either vehicle control or 40  $\mu\text{g}/\text{mL}$  direct thrombin inhibitor (hirudin). Fibrin formation, measured by turbidity change at 405 nm, was initiated with recalcification (A) or recalcification and supplementation with 100 pM  $\alpha$ -thrombin (B). The time interval required for the turbidity of the recalcified PPP, pretreated with vehicle, 250  $\mu\text{g}/\text{mL}$  polyphosphate inhibitor (PPXbd), 50  $\mu\text{g}/\text{mL}$  FXI function-blocking antibodies (1A6 or 14E11) or 40  $\mu\text{g}/\text{mL}$  FXII inhibitor (CTI) in the presence of vehicle (C) or 100 pM  $\alpha$ -thrombin (D), to reach the half-maximal absorbance value was reported as  $T_{\text{half-max}}$ . Citrated PPP in the presence of vehicle or 250  $\mu\text{g}/\text{mL}$  polyphosphate inhibitor (PPXbd) was incubated for 3 min at 37 °C with 100  $\mu\text{M}$  long-chain polyP prior to recalcification to initiate clotting (E). Significant differences in clotting times, for at least 4 separate experiments, are indicated with \* and \*\* having p values of 0.004 and 0.043 respectively.

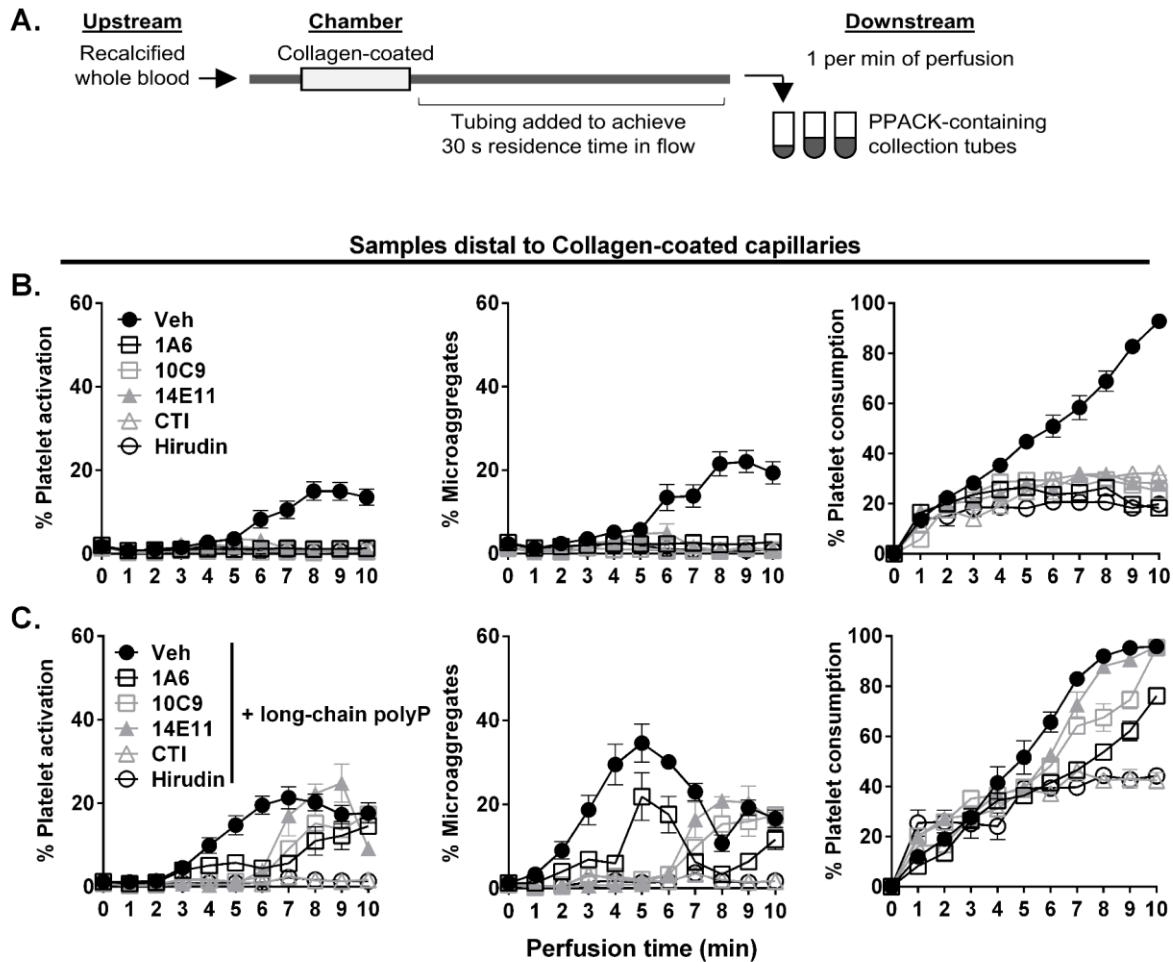


**Figure 6.4 Long-chain polyP as a surface activator of fibrin formation under shear.** Capillaries were incubated with different levels of long-chain polyP (0 – 100,000  $\mu\text{M}$ ), blocked with BSA and perfused with recalcified whole blood at 300  $\text{s}^{-1}$  shear rate for 10 min.

### 6.5.3 *Long-chain polyP promotes distal platelet activation and consumption in the blood flow downstream of sites of local thrombus formation*

Our previous work identified a role for FXI in promoting distal platelet activation downstream of sites of local thrombus formation. We next designed experiments to determine whether the presence of long-chain polyP would increase the rate and extent of downstream platelet activation in a FXII-dependent manner. As shown in Figure 6.6A, the outflowing blood was collected 30 sec downstream of a collagen-coated chamber. Our results show that platelet P-selectin expression and microaggregate formation increased as a function of time in whole blood samples downstream of collagen-coated chambers, reaching a maximum of 90% single platelet consumption by 10 min of perfusion in the presence of vehicle (Figure 6.6B). In accord with our previous findings, pretreatment of blood with the anti-FXI mAbs 14E11, 1A6 or 10C9 or the FXIIa inhibitor CTI eliminated downstream platelet activation and microaggregate formation and reduced single platelet consumption.

The presence of long-chain polyP significantly increased the rate of distal platelet activation, microaggregate formation and single platelet consumption in the blood flow downstream of the local site of thrombus formation (Figure 6.6C). For instance, the extent of microaggregate formation increased over 3-fold in the presence of long-chain polyP after 5 min relative to vehicle, while long-chain polyP decreased the time required to achieve a 95% loss of single platelets in the blood flow from 10 min down to 8 min. An initial inhibition of platelet activation and microaggregate formation was observed when blood was pretreated with the anti-FXI mAbs 14E11, 1A6 or 10C9, while only CTI and hirudin were able to eliminate platelet activation and microaggregate formation over the full 10 mins of observation.



**Figure 6.6 Long-chain polyP promotes distal platelet activation and consumption in the blood flow downstream of sites of local thrombus formation.**

Experimental set up schematic (A). Recalcified whole blood was perfused over collagen-coated chambers at  $300 \text{ s}^{-1}$  shear rate. Downstream samples were collected into solution containing serine protease inhibitor (PPACK) at 1 min intervals (perfusion time), immunostained and evaluated by flow cytometry (FACS). Percent platelet activation, platelet microaggregate formation and single platelet consumption in samples distal to thrombus formation on collagen-coated surfaces in the presence of vehicle control, 1A6, 10C9, 14E11, CTI or hirudin were quantified (B). In parallel experiments whole blood was pretreated with  $100 \mu\text{M}$  long-chain polyP prior to re-calcification and perfusion over collagen-coated chambers (C). Representative means  $\pm$  SEM for at least four separate experiments are shown.

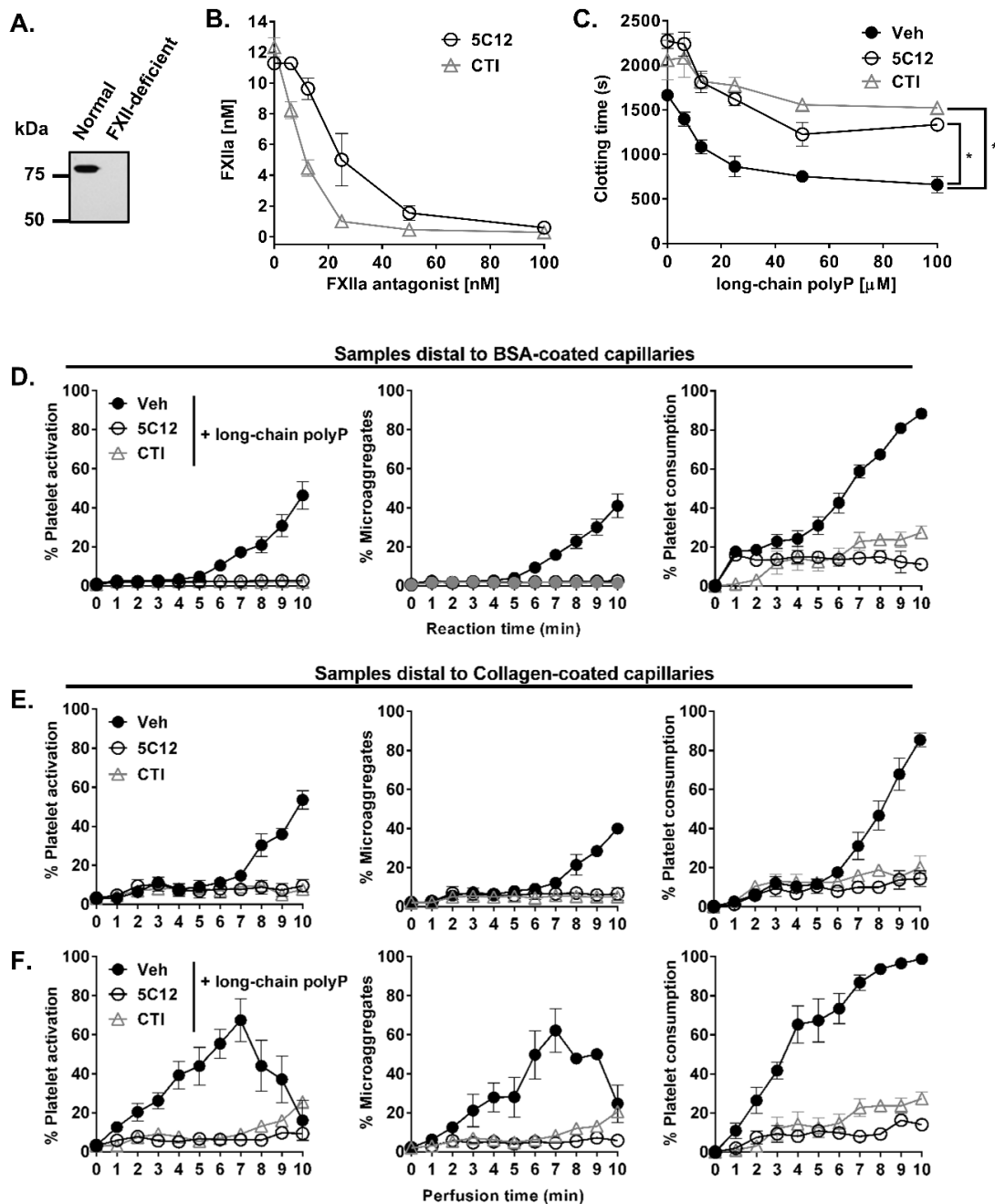
Taken together, our results suggest that long-chain polyP promotes distal platelet activation and consumption in the bloodstream downstream of sites of active thrombus formation in a contact activation pathway-dependent manner.

#### 6.5.4 *Long-chain polyP promotes distal platelet activation and consumption in the blood flow in a FXII-dependent manner*

Corn trypsin inhibitor (CTI) has classically been used as a FXIIa inhibitor. However, CTI has also been shown as a weak competitive inhibitor of FXIa.[400,401] Moreover, the inhibitory effect of CTI of FXIIa activity is transient as it forms a one-to-one complex with FXIIa or trypsin.[402] We therefore created an anti-FXII mAb, 5C12, to use as a tool to mechanistically define the role of the contact activation pathway in the ability of long-chain polyP to promote distal platelet activation and consumption.

We found that 5C12 bound human FXII in plasma (Figure 6.7A), and blocked the ability of long-chain polyP to activate FXII in a purified system consisting of human FXII, high molecular weight kininogen (HK) and prekallikrein (PK), as measured by quantifying FXIIa activity normalized to baseline using a chromogenic assay (Figure 6.7B). In recalcified plasma, 5C12 inhibited the ability of 100  $\mu$ M long-chain polyP to promote clotting to the same degree as CTI (Figure 6.7C).

We next evaluated the effect of 5C12 on platelet activation induced by long-chain polyP in our flow assay. Our data show that 5C12 eliminated the ability of long-chain polyP to promote platelet activation, microaggregate formation or consumption when blood was perfused either through an inert BSA-coated chamber or over a collagen-coated surface to induce a local site of thrombus formation (Figure 6.7D-F). These results provide evidence that long-chain polyP promotes distal platelet activation and consumption in the blood flow and downstream of sites of active thrombus formation in a FXII-dependent manner.



**Figure 6.7 Long-chain polyP promotes distal platelet activation and consumption in the blood flow in a FXII-dependent manner.**

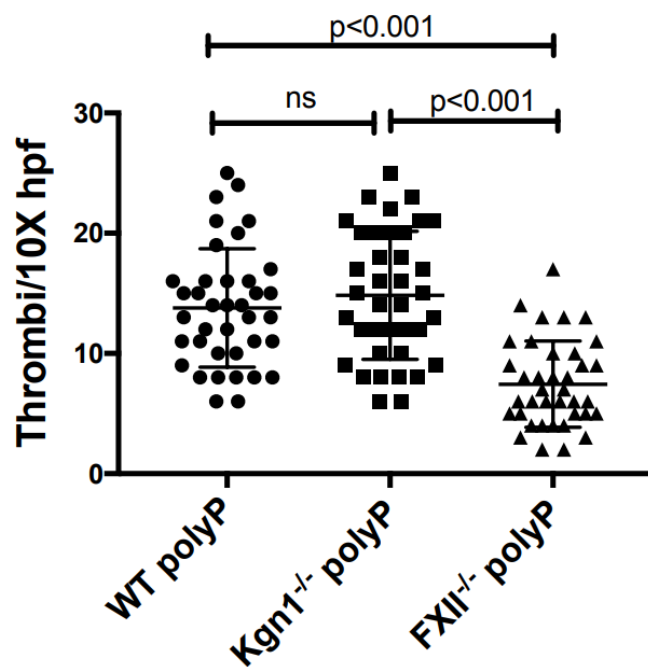
Characterization of the anti-FXII mAb, 5C12, showing that 5C12 binds to FXII from human plasma (A). Human recombinant FXII was preincubated with high molecular weight kinogen (HK), prekallikrein (PK) and long-chain polyP in the presence of increasing concentrations of 5C12 or CTI and levels of activated FXII were quantified using a chromogenic assays (B). Citrated platelet poor plasma (PPP) was pretreated with vehicle, 40  $\mu$ g/mL FXIIa inhibitor (CTI) or 50  $\mu$ g/mL anti-FXII mAb (5C12) and incubated for 3 min at 37 °C with either control buffer or indicated levels of long-chain polyP prior to recalcification to initiate clotting (C). Significant differences in clotting time, in the presence of 100  $\mu$ M long-chain polyP, for at least 3 separate experiments, are indicated with \* with having p values < 0.05. Activation, microaggregate formation and consumption of platelets was measured in recalcified flowing whole blood pretreated with either vehicle, 5C12, CTI or 14E1 in the presence of long-chain polyP (D). Role of FXII in platelet consumption distal to thrombus formation was assessed in the presence of either vehicle (E) or long-chain polyP (F). Representative means  $\pm$  SEM for at least three separate experiments are shown.



6.5.5 Long-chain polyP promotes platelet deposition and fibrin generation *in vivo* in a FXII-dependent manner

We next designed experiments to determine whether long-chain polyP induced platelet activation and fibrin formation in the bloodstream *in vivo*. A bolus of long-chain polyP was injected into a cohort of wild-type (WT), FXII-deficient ( $FXII^{-/-}$ ), prekallikrein-deficient ( $Klkbl^{-/-}$ ) or high molecular weight kininogen-deficient ( $Kgn1^{-/-}$ ) mice.

Our data show that the degree the extent of platelet deposition and fibrin formation observed in the lung tissue was markedly reduced for  $FXII^{-/-}$  mice as compared to WT or  $Kgn1^{-/-}$  mice (Figure 6.8). These studies indicate that presence of long-chain polyP in the bloodstream promotes platelet activation and fibrin generation *in vivo* in a FXII-dependent manner.

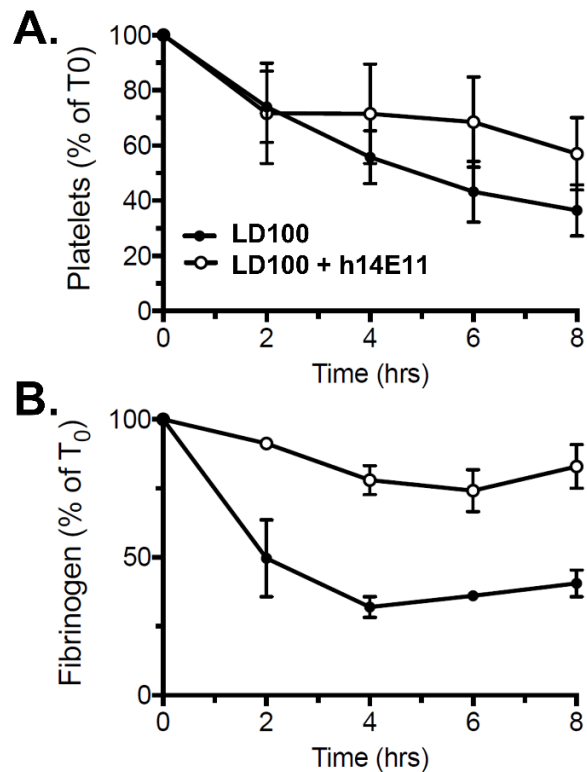


**Figure 6.8 Long-chain polyP promotes platelet deposition and fibrin generation *in vivo* in a FXII-dependent manner.** Lung sections from long-chain polyP-challenged wild type (WT),  $Kgn1^{-/-}$  and  $FXII^{-/-}$  mice were stained with H&E. Number of vessel occlusions per visual field were quantified. Mean  $\pm$  standard error of the mean (SEM) of 100 fields per group are shown. \*Significant difference ( $P < .05$ ) among the groups on 1-way analysis of variance (ANOVA).

6.5.6 Long-chain polyP-containing bacteria induce platelet and fibrinogen consumption *in vivo* in a FXIIa-dependent manner

In a proof-of-concept *in vivo* experiment, we examined whether inhibition of the ability of FXIIa to activate FXI could reduce consumption of platelets and fibrinogen in an established model of long-chain polyP-containing bacterial sepsis in baboons, *Papio anubis* (Figure 6.9). In this model, animals were challenged with heat-inactivated *Staphylococcus aureus* (*S. aureus*), a pathogenic bacterium known to contain polyP,[403,404] to a lethal dose (LD<sub>100</sub>) of  $1-2 \times 10^{10}$  colony forming units (cfu)/kg. Half an hour prior to bacterial challenge, animals were treated with a bolus intravenous injection of the humanized anti-FXI antibody 14E11, which blocks FXI activation by FXIIa (h14E11), or vehicle. Outcomes were measured as platelet count (Figure 6.9A) and circulating fibrinogen (Figure 6.9B) as percentage

of baseline values. Our results show that *S. aureus* challenge induced a drop in platelet count to 40% of baseline at 8 hours; this was partially rescued to 60% by pretreatment when FXI activation by FXIIa was inhibited with h14E11. *S. aureus* challenge also decreased plasma fibrinogen to 40% of baseline at 8 hours, which was rescued to 80% upon pretreatment with the anti-FXI antibody h14E11.



**Figure 6.9 Long-chain polyP-containing bacteria induce platelet and fibrinogen consumption *in vivo* in a FXIIa-dependent manner.**

In a non-human primate model of sepsis, *Papio anubis* baboons were pretreated with either normal saline or a single (1 mg/kg) bolus of anti-FXI antibody h14E11, followed by an intravenous two hour (T<sub>0</sub> to T<sub>120</sub> min) infusion of a lethal dose ( $1-2 \times 10^{10}$  cfu/kg) of *S. aureus*. Blood samples were obtained at times 0, 2, 4, 6 and 8 hours. Platelet levels were determined using a VetScan HM5 Hematology Analyzer (A) and plasma levels of fibrinogen were measured using Clauss clotting assay<sup>66</sup> (B). Data are shown as mean  $\pm$  SEM. LD<sub>100</sub> animals n = 2; LD<sub>100</sub> + h14E11 animals n = 2.

Taken together this pilot experiment suggests that long-chain polyP-containing bacteria promote platelet and fibrinogen consumption in the bloodstream in a contact activation pathway-dependent manner.

## 6.6 Discussion

Coagulation factor (F)XII is an abundant member of the intrinsic coagulation pathway with an elusive role in hemostasis yet mounting evidence for roles in thrombo-hemorrhagic complications in the presence of negatively charged molecules and surfaces artificial to the blood environment. Clinically, FXII-deficient patients have a prolonged activated partial thromboplastin time (aPTT) but do not suffer from abnormal bleeding and are otherwise asymptomatic.[405] Conversely, activation of FXII *in vivo* can lead to development of life-threatening consumptive coagulopathy similar to a complication associated with sepsis.[140] Our results suggest that FXII is activated by polyphosphate of the size produced by bacteria (long-chain polyP) in the bloodstream promoting platelet activation and consumption under shear. We show that inhibition of FXIIa activity neutralizes the effect of long-chain polyP on whole blood under shear and may be a viable target in preventing platelet consumption in the setting where long-chain polyP levels may be increased. We show in an initial proof-of-concept experiment using an established *in vivo* nonhuman primate model of bacterial sepsis that inhibition of FXI activation by FXIIa was found to inhibit platelet and fibrinogen consumption.

Sepsis is an infection-induced systemic inflammatory response syndrome (SIRS) that typically progresses to terminal hypotension, insufficient organ perfusion and death within hours to days when left untreated.[123,124] Timely and aggressive medical management, including treatment of the underlying cause or supportive care (volume/electrolyte supplementation, vasopressors, dialysis, oxygenation, and transfusion of blood products) reduce sepsis-associated mortality.[406,407] Yet, these measures often fail, and sepsis remains among the top leading causes of hospital mortality.[408] Thus, advanced sepsis presents a significant problem. Fulminant or rapidly-progressing disseminated

intravascular coagulopathy (DIC) is a deadly complication of sepsis that has no disease-specific effective antithrombotic treatment. Nevertheless, most patients in the later hemorrhagic phase of DIC are given transfusions of blood components, sometimes combined with anticoagulation, in an attempt to both reduce pathologic coagulation and support the failing hemostatic system.[128,129] However, the presumed efficacy of systemic anticoagulation with broad-spectrum antithrombotic agents such as heparin or activated protein C (no longer marketed) that target the extrinsic, intrinsic, and common pathways of thrombin generation has not been confirmed in large clinical trials.[409] There is a clear need for a better understanding of the molecular basis of sepsis/SIRS in order to develop safe and effective therapies to improve clinical outcomes and to identify druggable molecular targets and mechanisms that contribute to thrombin generation during early or advanced sepsis.

There is strong evidence that polyP in concert with FXII promotes thrombin generation. PolyP molecules  $\geq 30$  phosphates long directly promote FXII activation and fibrin formation, with increasing potency observed with increasing polyP chain length.[275] The majority of studies have focused on the effects of polyP of the size found in platelets (short-chain polyP) in the setting of closed systems using purified reagents or plasma. However, it is important to keep in mind that in circulating whole blood, the effects of polyP may be significantly reduced due to hydrolysis of polyP in the presence of red blood cells[410] and the effects of shear on the biodistribution of reactants and inhibitors.[268,277,411] At the same time, the enrichment of microbes within platelet aggregates[412–415] may increase the local concentration of polyP within the blood microenvironment. Along these lines, Zhu *et al.* demonstrated that inhibition of blood-borne short-chain polyP with recombinant exopolyphosphatase binding domain (PPXbd) decreases fibrin formation in thrombi formed on collagen *in vitro* and increases susceptibility of thrombi to lysis in the presence of tissue plasminogen activator.[416] Treatment of wild-type mice with PPXbd has been shown to be thromboprotective, while this effect is lost in FXII-deficient mice.[417] Our study confirms a role for long-chain polyP in promoting platelet deposition and fibrin formation in a FXII-dependent manner *in vivo* (Figure 6.10).

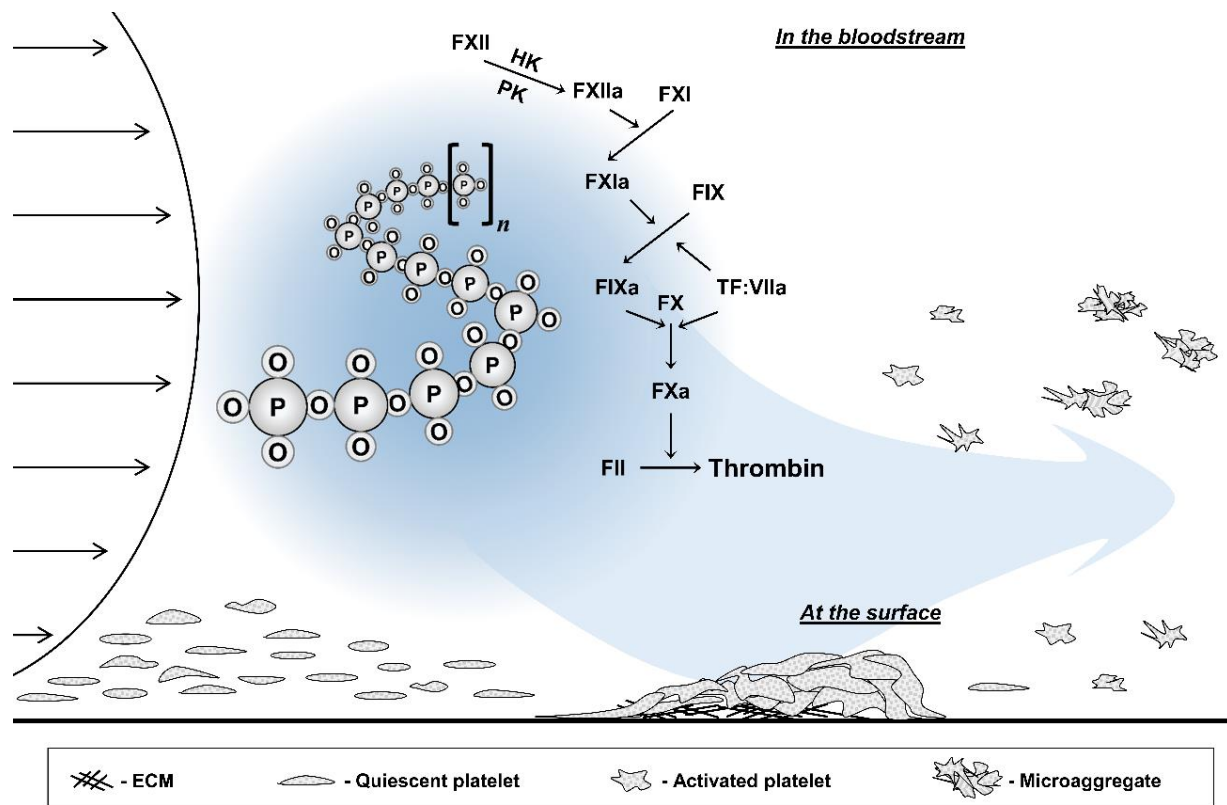


Figure 6.10 Cartoon of Hypothesis.

PolyP molecules may further derail and link multiple processes in an infected organism.[397,418] Inorganic polyP chains contain high energy phosphoanhydride bonds identical to ones found in adenosine triphosphate (ATP) molecules, which are hydrolyzed to fuel reactions in cells.[396,419] Notably, polyP chains have been shown to be utilized by select bacteria to generate ATP and ADP.[420] Furthermore, *Mycobacterium tuberculosis* and some other gram positive bacteria primarily depend on polyP for energy.[421–423] Hypophosphatemia is associated with sepsis severity and may represent an outcome of bacterial sequestering of phosphate for polyP production.[424] Moreover, microbes may release long-chain polyP upon cell damage or express long-chain polyP on their cell surfaces, promoting pathogenesis.[425] For instance, *Neisseria* expose as much as half of their polyP content on their cell surface, which may act as both an antiphagocytic capsule and a

promoter of virulence during infection.[426] Thus, we speculate that activation of the abundant levels of FXII found in the blood may be part of a physiological response aimed at containment of infectious agents, a strategy that unfortunately seems to fail at higher bacterial loads. In line with this thought, FXII activation in the presence of long-chain polyP can promote proteolysis of high molecular weight kininogen with concomitant bradykinin release,[388] pro-inflammatory responses[427–429] and complement system activation,[430–432] all of which can wreak havoc on an organism in the absence of balanced regulation. Thus, additional understanding of the crosstalk between polyP and FXII in the blood microenvironment may aid in the development of supportive therapeutics for sepsis management in the presence of bacteria that produce long-chain polyP.

## **Chapter 7. Effect of pneumatic tubing system transport on stored platelet concentrate units**

Jevgenia Zilberman-Rudenko, Frank Z. Zhao, Stephanie E. Reitsma, Annachiara Mitrugno,

Jiaqing Pang, Joseph J. Shatzel, Beth Rick, Christina Tyrrell, Wohaib Hasan,

Owen J.T. McCarty, Martin A. Schreiber

Chapter 7. was submitted for publication with the Biomedical Engineering Society,  
in *Cardiovascular Engineering and Technology*, Springer Publishing, January 2018.

### **7.1 Abstract**

*Purpose:* Platelet concentrate (PC) units are transfused into patients to mitigate or prevent bleeding. In a hospital, PC units are transported from the transfusion service to the healthcare teams via two methods: a pneumatic tubing system (PTS) or ambulatory transport. Whether PTS transport affects the activity and utility of platelets within PC units is unclear.

*Methods:* We quantified the gravitational forces and transport time associated with PTS and ambulatory transport within our hospital. Washed platelets and supernatants were prepared from PC units prior to transport as well as following ambulatory or PTS transport. For each group, we compared resting and agonist-induced platelet activity and platelet aggregate formation on collagen or von Willebrand factor (VWF) under shear, platelet VWF-receptor expression and VWF multimer levels.

*Results:* Subjection of PC units to rapid acceleration/deceleration forces during PTS transport did not pre-activate platelets or their ability to activate in response to platelet agonists as compared to ambulatory transport. Platelets within PC units transported via PTS retained their ability to adhere to surfaces of VWF and collagen under shear, although platelet aggregation on collagen and VWF was diminished as compared to ambulatory transport. VWF multimer levels and platelet GPIb receptor expression was unaffected by PTS transport as compared to ambulatory transport.

*Conclusions:* Subjection of PC units to PTS transport did not significantly affect the baseline or agonist-induced levels of platelet activation as compared to ambulatory transport. Our case study suggests that PTS transport may not significantly affect the hemostatic potential of platelets within PC units.

## **7.2 Introduction**

This chapter focuses on the study of the effect of PC unit handling during transport within a single hospital. We utilize assays described in previous chapters to assess the function of platelets in PC units following transport either via a pneumatic tubing system (PTS) or by a human courier and compare these to the basal function of platelets in this transfusion reagent. The objective of this study was to determine whether the biophysical forces encountered by platelets during transport of PC units via PTS used in hospitals has a deleterious effect. We have quantified the distinct forces and acceleration/deceleration transitions experienced by platelets in PC units during travel through PTS and compared these to ambulatory transport. We found that regardless of the transport method, platelets in PC units were refractory to a broad matrix of physiological stimuli as compared to freshly prepared platelets. In perfusion studies, we found that relative to ambulatory transport of stored platelet units, transport of PC units via PTS may diminish the ability of platelets to bind and aggregate on collagen and VWF under shear. However, PTS did not affect total platelet GPIb receptor or plasma VWF levels in PC unit samples. Results and an overview of the literature, discussed herein, raise a number of questions about PC unit collection, handling and platelet storage conditions.

## **7.3 Background**

Upon vessel injury, exposed extracellular matrix (ECM) proteins, such as fibrillar collagen, trigger a series of events that lead to the formation of a hemostatic plug to staunch blood loss.[150,151] The process of hemostasis depends on platelets tethering to the ECM in the presence of



shear, leading to platelet adhesion, rapid cellular activation and accumulation of additional platelets.[152] ECM-bound von Willebrand factor (VWF) plays a critical role in initial platelet deposition via shear-dependent platelet receptor glycoprotein (GP) Ib binding to VWF.[153–155] Platelet receptors GPVI and  $\alpha_2\beta_1$  mediate platelet activation leading to the release of secondary mediators and subsequent platelet aggregation. Platelet aggregation is enabled by platelet integrin  $\alpha_{IIb}\beta_3$  and fibrinogen.[156]

Platelet concentrate (PC) units are used for effective management and stabilization of patients with thrombocytopenia and clinically significant bleeding associated with a high morbidity and mortality. In the United States, PC units are most commonly collected by apheresis involving gentle centrifugation over a period of several hours from healthy adult volunteers. Guidelines have been established to ensure PC unit quality including storage duration, temperature and handling prior to release of this therapeutic blood product for patient transfusion.[433] However, once in the hospital setting, there are no universal or strict guidelines for PC unit delivery to care teams.

Pneumatic tubing systems (PTS) are widely used in hospitals to enable rapid and convenient transport of clinical samples, blood and therapeutic products, including PC units, within hospitals. Interestingly, the use of PTS has been discouraged for transport of clinical samples intended for platelet function testing.[434,435] Several studies have suggested that PTS transport of samples may affect the results of platelet functional tests including whole blood optical and electrode platelet aggregometry,[436–439] multiple parameters of rotational thromboelastometry (ROTEM)[438,440] and closure time within sheared platelet function test (PFA-100).[437,441,442] It is not clear however what effect if any PTS transport may have on the activity or function of platelets in PC units. The aim of this study was to determine whether exposure of PC units to changes in gravitational forces during PTS transport affects baseline platelet activity or response to agonists as compared to ambulatory transport of PC units.

## 7.4 Materials and Methods

### 7.4.1 *Materials and Reagents*

Cross-linked collagen-related protein/CRP-XL was purchased from University of Cambridge (Cambridge, England). Thromboxane A<sub>2</sub> analog/U46619 and PAR-1 agonist/TRAP6 were from Tocris (Bristol, England). Epinephrine and fibrillar collagen were from Chrono-Log (Havertown, PA). Human VWF was from Haematologic Technologies, Inc (Essex Junction, VT). Fibrinogen was from Enzyme Research Laboratories (South Bend, IN). PPACK, rabbit anti-human anti-VWF primary antibody and goat anti-human anti-Vinculin primary antibodies were from Santa Cruz (Dallas, TX). Anti-CD41-PE, anti-CD62P-APC and Cytotfix<sup>BD</sup> were from BD Pharmingen (Franklin Lakes, NJ). Anti-CD31-eFluor450 was from eBioscience (San Diego, CA). Mouse anti-human anti-GPIb/AK2 primary antibody was from GeneTex (Irvine, CA) and anti-mouse IgG -AF640 secondary was from Invitrogen (Carlsbad, CA). Seakem gold agarose was from Lonza (Basel, Switzerland). Recombinant rh-ADAMTS13 was from R&D Systems (Minneapolis, MN). SuperSignal West Dura Substrate was from Thermo Scientific (Waltham, MA). Other reagents were purchased from Sigma (St. Louis, MO).

### 7.4.2 *Procurement and handling of stored platelet concentrate units*

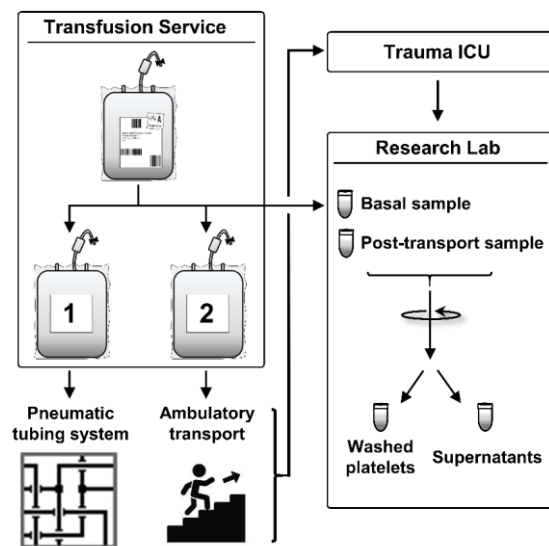
Single donor-per-unit platelet concentrate (PC) units were isolated by the American Red Cross, Pacific Northwest Blood Services Region, from citrated whole blood using a continuous-flow centrifugal apheresis machine Amicus (Fenwal Inc, Lake Zurich, IL), which utilizes a dual-stage separation technique with centrifugal force and belt-like geometrical configuration of separation and collection chambers (Table 7.1).[443] Each donor underwent a bilateral venipuncture allowing a simultaneous withdrawal of whole blood and reinfusion of returning blood products. Citrated whole blood was spun down at 1600rpm for an average of 10 minutes at RT to selectively isolate platelet rich plasma (PRP); red blood and white blood cells were reinfused back into the donor. PRP was then furthermore leuko-reduced by filtration and concentrated at 1600rpm for 10 minutes to remove a portion of the platelet-poor-plasma. PC units had an average concentration of  $7.6 \pm 0.5 \times 10^5$  plts/ $\mu$ L,

n=20. Stored PC units in apheresis bags were then received and stored by the OHSU Transfusion Medicine Services department. In accordance with USFDA guideline, stored PC units were taken out of the clinical inventory 5 days post-collection and released for research use. Stored PC units were collected from four ABO blood type donor groups: 7 from A, 7 from B, 3 from AB and 3 from O blood type; 4 PC units were from Rh<sup>-</sup> and 16 PC units were from Rh<sup>+</sup> donors.

On the day of an experiment, PC unit was handled according to the flow chart (Figure 7.1). Prior to transport, a basal sample was extracted from an apheresis bag containing a PC unit with a 15 Gauge needle and a 20mL syringe at the OHSU Transfusion Service and stored in a 15mL polypropylene conical Falcon® tube in the lab. Subsequently, the

remainder of the PC unit was split into two apheresis bags and transported to the OHSU Trauma and Surgical Intensive Care Unit via two parallel methods: pneumatic tubing system (PTS; Swisslog TransLogic, Apeldoorn, The Netherlands) or ambulatory (AMB) transport. Acceleration/ deceleration forces generated during these transport

methods were recorded using an accelerometer (Apple iPod touch, IOS 9, SensorLog v1.8); for reference we quantified the centrifugal forces experienced during a 1600rpm spin in a GPKR centrifuge outfitted with rotor SH 3.7 S/N 576 (Beckman Coulter, Inc, Brea, CA; Table 7.2 & Figure 7.2).



**Figure 7.1 A flow chart of an experimental PC unit handling procedure.**

A flow chart describing events on the day of an experiment. Prior to transport, a basal sample was extracted from an apheresis bag containing a platelet concentrate (PC) unit. Subsequently, the remainder of the PC unit was split into two apheresis bags and transported to the OHSU Trauma and Surgical Intensive Care Unit (ICU) via two parallel methods: pneumatic tubing system (PTS; Swisslog TransLogic, Apeldoorn, The Netherlands) or ambulatory (AMB) transport. All samples were subsequently processed at the research lab. When appropriate washed platelet and supernatants were purified from samples.

### 7.4.3 Human whole blood collection and preparation of concentrated platelet rich plasma and serum

To prepare fresh platelet-rich plasma (PRP), 40mL of human venous blood was drawn by venipuncture from healthy adult volunteers into 60mL syringe containing 1:10 3.8% sodium citrate in accordance with the OHSU Institutional Review Board. Whole blood was then transferred into a 50mL polypropylene conical Falcon® tube and spun down at 1600rpm for 10 minutes at RT; the acceleration/ deceleration profiles were recorded using an accelerometer as described above. After the first spin, PRP was transferred into new 50mL conical tube and spun down again at 1600rpm for 10 minutes; the plasma volume was adjusted to achieve a final concentration of  $4 \times 10^5$  plts/ $\mu$ L in concentrated (c)PRP (Table 7.1). The final yield was about 5mL of cPRP per 40mL whole blood donation.

| In text  | Blood drawn by             | Platelet concentrate preparation                | Intended use          | Stored at                           |
|--|----------------------------|---|-----------------------|-------------------------------------|
| <i>Platelet concentrate unit, PC unit</i>      | American Red Cross         | a continuous-flow centrifugal apheresis machine | Health care, clinical | OHSU Transfusion Service            |
| <i>Concentrated platelet rich plasma, cPRP</i> | OHSU Research Phlebotomist | Serial bench centrifugation                     | Research only         | Used within 2 hours from blood draw |

**Table 7.1 Description of platelet concentrate samples used in the study.**

Fresh serum was prepared by collection of human venous blood by venipuncture into a dry syringe. Non-anticoagulated blood was then left on a bench and allowed to clot for 30 minutes at room temperature. Serum was isolated by centrifugation at 2500rpm for 20 minutes in a Hermle Z300 centrifuge outfitted with rotor 221.12 V01 (Labnet, Edison, NJ).

### 7.4.4 Preparation of washed platelets and supernatants from stored PC units or fresh cPRP

Stored PC units or freshly prepared cPRP were divided into separate polypropylene tubes for select experimental procedures run in parallel. Prostacyclin (PGI<sub>2</sub>; 0.1  $\mu$ g/mL final) and acid/ citrate/ dextrose (ACD; 1:10 final volume ratio) were added to 200 $\mu$ L of PC units or fresh cPRP prior to pelleting to generate washed platelets. Samples were then spun down twice at 2500rpm for 10 minutes

to pellet the platelets; the final pellet was resuspended in 200 $\mu$ L of serum, counted and adjusted to a final count of  $4 \times 10^5$  plts/ $\mu$ L. Washed platelets were allowed to rest for 45 minutes before being evaluated for baseline and agonist-induced activation and microaggregation. To purify PC unit or cPRP supernatants, 20 $\mu$ L of PC units or cPRP were transferred into 1.7mL graduated copolymer polypropylene microcentrifuge and spun down at 2500rpm for 10 minutes.

#### 7.4.5 *Platelet activation and microaggregate detection*

PC units or freshly prepared cPRP were pelleted and resuspended in human serum to a final concentration of  $4 \times 10^5$  plts/ $\mu$ L. Samples were then added to tubes containing vehicle buffer, ADP (3, 10 and 200  $\mu$ M final), U46619 (1 and 10  $\mu$ M final), a combination of ADP and U46619 (10  $\mu$ M and 10  $\mu$ M final each), CRP-XL (0.3, 1 and 10  $\mu$ g/mL final), TRAP-6 (10 and 30  $\mu$ M final), a combination of CRP-XL and TRAP-6 (10  $\mu$ M and 30  $\mu$ M final each), 10  $\mu$ M epinephrine, or 100  $\mu$ g/mL fibrillar collagen in the absence or presence of 10  $\mu$ M ADP or 10  $\mu$ M epinephrine and incubated for 30 minutes at RT on a shaker agitated at 200rpm. Reactions were stopped by diluting samples 1:10 with a quenching solution consisting of modified HEPES-Tyroses with 40  $\mu$ M PPACK, 1.5% w/v Na-citrate (1:1, v:v).[277] Following this quenching step, 10 $\mu$ L of each sample was added to an additional 10 $\mu$ L of quenching solution containing the following anti-platelet antibodies: anti-CD41-PE, anti-CD62P-APC and anti-CD31-e450, to a final dilution of 1:50, and incubated for 30 minutes at RT in the dark. Samples were fixed by diluting 1:10 with quenching solution containing 12.5% Cytofix<sup>BD</sup>. 10,000 single platelets events were collected by quantifying a PE-conjugated platelet marker CD41 and the characteristic forward- and side-scatter scatter patterns using a fluorescence-activated cell sorter, FACS (Canto II; BD Biosciences). Platelet activation (%) was determined as the ratio of CD62P positive population of CD31/CD41 double-positive events as described previously.[277,313] Percent microaggregate formation was determined by the upshift in fluorescence intensity in CD31/CD41 double-positive events. To measure platelet GPIIb $\alpha$  levels, platelets were incubated with 1:50 dilution of mouse anti-human monoclonal AK2 primary antibody for 30 minutes at RT followed by 30 minutes

incubation with 1:50 final dilution of anti-CD41-PE and anti-CD31-eFluor450 and 1:1000 final dilution of anti-mouse IgG-AF640 secondary antibody.

#### 7.4.6 *Flow chamber assay*

Glass capillary tubes/chambers (0.2×2×200 mm; VitroCom) were coated with fibrillar collagen (100 µg/mL), VWF (100 µg/mL) or fibrinogen (100 µg/mL) for 1 hr at RT. Surfaces were blocked with 5 mg/mL denatured bovine serum albumin (BSA) for 1 hr at RT prior to assembly into a flow system as described previously.[277] Platelets content within PC unit samples was quantified. Final platelet counts were adjusted to  $4 \times 10^5$  plts/ $\mu$ L using autologous supernatants. PC units were then perfused through the chambers for 10 minutes at an initial wall shear rate ( $300 \text{ s}^{-1}$ ). Platelet aggregation was visualized with differential interference contrast microscopy and quantified using FlowJo software.

#### 7.4.7 *Immunoblot determination of VWF*

Fifty µg of plasma protein was loaded per well and run under non-reducing conditions as previously described.[444] A 1.5% low-to-medium resolution agarose gel was cast using Seakem gold agarose. Human VWF, incubated with or without rh-ADAMTS13, was used to confirm antibody specificity. After transfer to PVDF membrane, blots were incubated with an anti-VWF primary antibody followed by an HRP-conjugated secondary antibody. As a loading control, blots were probed for the high molecular weight housekeeping protein vinculin (117 kDa). Protein bands were visualized by chemiluminescence following incubation with SuperSignal West Dura Substrate. Quantitation of band area was performed with ImageJ (NIH).

#### 7.4.8 *Statistics*

Data are shown as means  $\pm$  SEM. Statistical significance of differences between means was determined by ANOVA. If means were shown to be significantly different, multiple comparisons were performed by the Tukey test. Probability values of  $P < 0.05$  were selected to be statistically significant.

## 7.5 Results

### 7.5.1 Physical parameters of platelet concentrate sample handling

After collection of a basal sample, platelet concentrate (PC) units were split into two transport study arms (Figure 7.1) and the gravitational forces and transit time experienced by PC units transported within the hospital at OHSU via PTS or AMB transport were examined (Figure 7.2). PC units were transported via PTS transport for  $144 \pm 8$  seconds, including passage through a redistribution center and experienced a maximum of  $7.96 \pm 0.08$ ,  $6.79 \pm 0.37$  and  $7.87 \pm 0.12$  G forces (n=16) in x-, y- and z-coordinate directions, respectively.

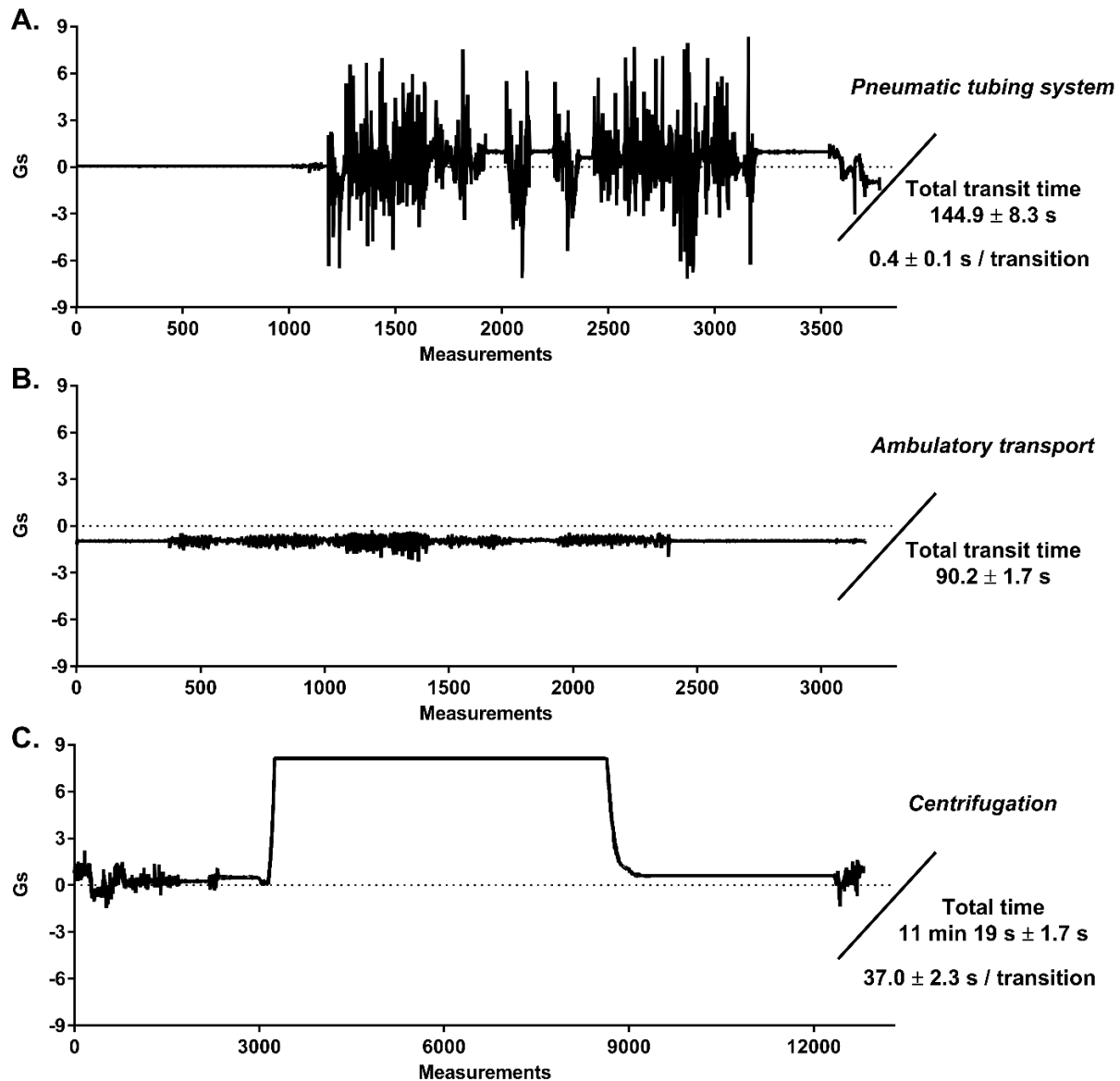
Samples transported via ambulatory (AMB) transport were transported for  $90 \pm 2$  seconds and experienced a maximum of  $0.64 \pm 0.10$ ,  $0.46 \pm 0.08$  and  $1.77 \pm 0.09$  G forces (n=16) in x-, y- and z-coordinate directions, respectively. Notably, PC units transported via PTS experienced frequent jolts of acceleration/deceleration amounting to  $547 \pm 77$  transitions in the z-coordinate direction, whilst AMB-transported platelets traveled steadily without z-coordinate transitions (Table 7.2 & Figure 7.2). PC units were subject to a similar degree of acceleration/deceleration transitions in the x- and y-coordinate directions during either PTS or AMB transport.

|  |   | Gs generated |   |      |    | Acceleration / Deceleration jolts |   |     |             |   |     |
|--|---|--------------|---|------|----|-----------------------------------|---|-----|-------------|---|-----|
|  |   | Max          | ± | SEM  | N  | Freq.                             | ± | SME | t(s) / jolt | ± | SEM |
| <b>Pneumatic tubing system transport</b> | x | 7.96         | ± | 0.08 | 16 | 269                               | ± | 54  | 1.0         | ± | 0.2 |
|  | y | 6.79         | ± | 0.37 | 16 | 205                               | ± | 26  | 1.1         | ± | 0.3 |
|  | z | 7.87         | ± | 0.12 | 16 | 547                               | ± | 77  | 0.4         | ± | 0.1 |
| <b>Ambulatory transport</b>              | x | 0.64         | ± | 0.10 | 16 | 164                               | ± | 49  | 17.5        | ± | 7.1 |
|  | y | 0.46         | ± | 0.08 | 16 | 257                               | ± | 106 | 6.8         | ± | 3.4 |
|  | z | 1.77         | ± | 0.09 | 16 | 1                                 | ± | -   | 90.2        | ± | 1.7 |
| <b>Centrifugation 1600 rpm</b>           | x | 7.57         | ± | 0.01 | 5  | 2                                 | ± | -   | 40.2        | ± | 2.6 |
|  | y | 7.99         | ± | 0.01 | 5  | 2                                 | ± | -   | 30.2        | ± | 3.4 |
|  | z | 8.16         | ± | 0.01 | 5  | 2                                 | ± | -   | 37.0        | ± | 2.3 |

**Table 7.2 Physical parameters of platelet concentrate sample handling.**

Acceleration/deceleration forces generated during each transport type and platelet centrifugation were measured using an accelerometer (Apple iPod touch 16gb, 6<sup>th</sup> gen., IOS 9, SensorLog v1.8). Frequency and duration per jolt of acceleration/deceleration transition points were quantified.

As a comparator, platelets were subjected to a sustained acceleration of  $8.16 \pm 0.01$  G forces ( $n=5$ ) in the z-coordinate direction during centrifugation at 1600 rpm with a smooth singular transition to baseline at the ‘low’ centrifuge brake setting (Table 7.2 & Figure 7.2).



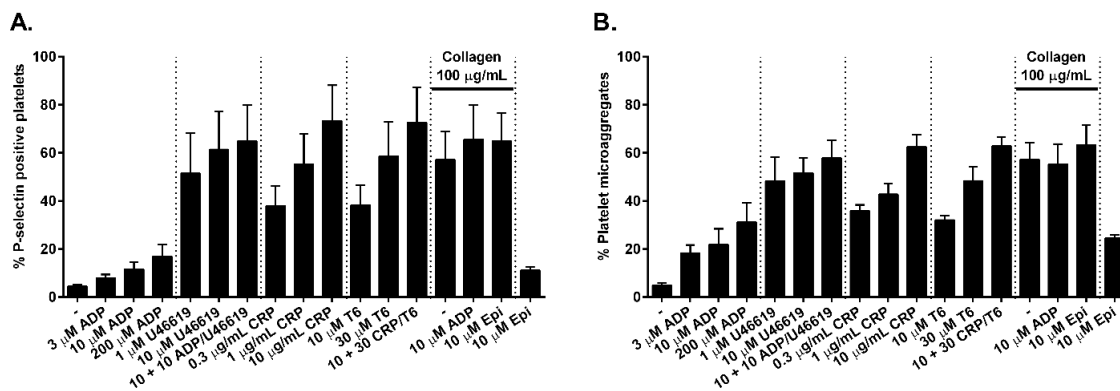
**Figure 7.2 Physical parameters of PC unit handling.**

Acceleration/deceleration profiles generated during transport via pneumatic tubing system (A;  $n = 16$ ), ambulatory transport (B;  $n = 16$ ) or platelet centrifugation (C;  $n = 5$ ) as measured using an accelerometer. Representative z-coordinate tracings are shown. Data are reported as mean  $\pm$  SEM.



### 7.5.2 Effect of transport on platelet activation and aggregation

We first designed experiments to determine whether PC unit transport had an effect on platelet activation or microaggregate formation. Washed platelets were isolated from stored PC units or freshly prepared concentrated (c)PRP (Table 7.1), and washed platelet activation was assessed by quantifying P-selectin (CD62P) expression (Figure 7.4A & Figure 7.3A). Platelet microaggregate formation was quantified by measuring a shift in mean fluorescence intensity of double-positive CD31 and CD41 events (Figure 7.4B & Figure 7.3B) as described previously.[277,313]

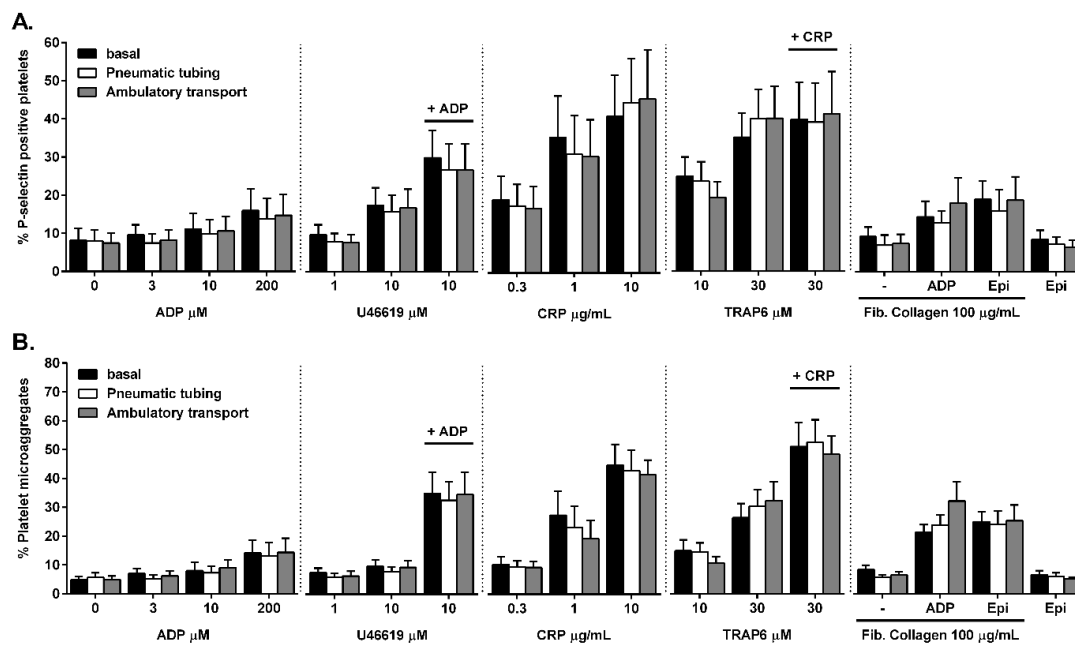


**Figure 7.3 Fresh platelet activation and microaggregation.**

Freshly prepared washed platelets were incubated with indicated agonists for 30 minutes, immunostained and evaluated by fluorescence-activated cell sorting (FACS) cytometry for percent platelet activation (CD41+/CD31+/CD62P+ events; A) or platelet microaggregate formation (high fluorescence intensity CD41+/CD31+ events; B). Mean  $\pm$  SEM, n = 3.

Consistent with previous reports, washed platelets purified from freshly prepared cPRP expressed significant levels of P-selectin from  $\alpha$ -granules in response to increasing concentrations of the GPCR agonists (TRAP-6, ADP, thromboxane A<sub>2</sub> analog U46619, epinephrine, or combinations of ADP and U46619), the ITAM-mediated (CRP-XL, fibrillar collagen) agonists, or combinations of these as compared to the vehicle control (Figure 7.3A). The percent CD62P-positive washed platelets increased up to 4-fold in response to ADP, up to 12-fold in the presence of the TxA<sub>2</sub> analog, 13-fold in the presence of the combination of ADP and U46619, up to 15-fold in the presence of CRP-XL or TRAP-6, 12-fold in the presence collagen alone, 30-fold in the presence of the combination of collagen and either ADP or epinephrine, and 3-fold in the presence epinephrine alone as compared to baseline.

Similarly, freshly prepared washed platelets formed microaggregates in response to increasing concentrations and combinations of agonists as compared to the vehicle control (Figure 7.3B). The degree of platelet microaggregation increased up to 6-fold in response to ADP, 10-fold in response to U46619, 11-fold in response to the combination of ADP and U46619, up to 12-fold in response to CRP-XL alone or in combination with TRAP-6, up to 9-fold in response to TRAP-6 alone, at least 11-fold in response to collagen alone or in combination with ADP or epinephrine, or 5-fold in response to epinephrine alone.



**Figure 7.4 Effect of transport on platelet activation and aggregation.** Washed platelets isolated from PC units were collected before (basal) or following transport via pneumatic tubing system transport (PTS) or by human courier, ambulatory transport (AMB). Samples were incubated with indicated agonists for 30 minutes, immunostained and evaluated by fluorescence-activated cell sorting (FACS) cytometry for percent platelet activation (CD41+/CD31+/CD62P+ events; A) or platelet microaggregate formation (high fluorescence intensity CD41+/CD31+ events; B). Mean±SEM, n = 7.

Notably, centrifugation of whole blood and cPRP during preparation of freshly washed platelets did not induce significant baseline platelet activation nor microaggregate formation. In contrast, platelets purified from PC units exhibited increased baseline platelet activation (Figure 7.4A) and microaggregate formation (Figure 7.4B) prior to either PTS or AMB transport.

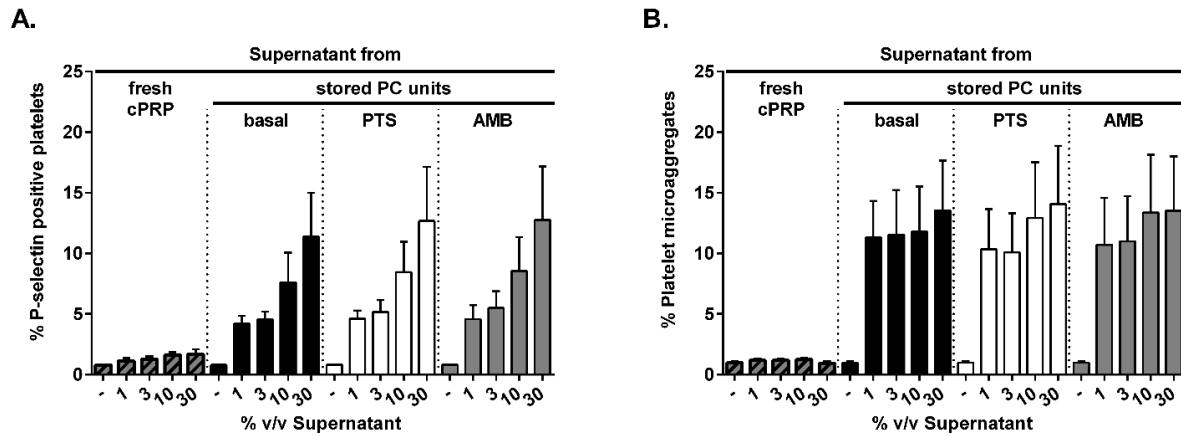
Furthermore, platelets isolated from PC units were refractory to low doses of the secondary mediators of platelet activation, ADP and U46619 at baseline. The percent platelet activation increased only 2-fold in response to 200  $\mu$ M ADP or 10  $\mu$ M U46619, while only a 3-fold increase was observed in response to a combination of 10  $\mu$ M ADP and 10  $\mu$ M U46619. The platelet agonists collagen or epinephrine alone failed to induce activation of washed platelets from PC units at baseline, while a 3-fold increase in CD62P expression was observed in response to the combination of collagen with ADP or epinephrine. Platelet activation reached a maximum of a 4-fold increase with increasing concentrations of CRP-XL, TRAP-6 or combinations of CRP-XL and TRAP-6. Similarly, the percent of platelet microaggregation increased only 2-fold in response to 200  $\mu$ M ADP, 7-fold in response to combination of U46619 and ADP, up to 8-fold in response to CRP-XL, 5-fold in response to TRAP-6, 10-fold in response to the combination of CRP-XL and TRAP-6 and up to 5-fold in response to the combinations of collagen and either ADP or epinephrine.

We did not observe a statistically significant difference in platelet activation or microaggregate formation after transport via PTS or AMB as compared to baseline for any of the agonists. Our data suggest that transport of PC units via either PTS or AMB routes does not affect agonist-induced platelet activation.

### *7.5.3 Effect of PC unit supernatant on freshly prepared platelet activation and aggregation*

Upon activation, platelets release secondary mediators including ADP to promote platelet activation via both paracrine and autocrine signaling. To test if supernatants from PC units contain secondary mediators which promote platelet activation, fresh washed platelets purified from cPRP were incubated with increasing levels of supernatants from PC units. Our data show that the presence of as low as 1% v/v PC unit supernatant was sufficient to induce an increase in P-selectin expression and microaggregate formation in freshly washed platelets at baseline (Figure 7.5A&B).

The transport of PC units via either PTS or AMB routes did not affect the ability of PC unit supernatant to induce activation of freshly washed platelets. In contrast, the supernatant from cPRP failed to elicit a response from freshly washed platelets, suggesting that the observed effects of the PC units on platelet reactivity was due to PC unit storage rather than the supernatant isolation method used herein.



**Figure 7.5 Effect of PC unit supernatant on fresh platelet activation and aggregation.**

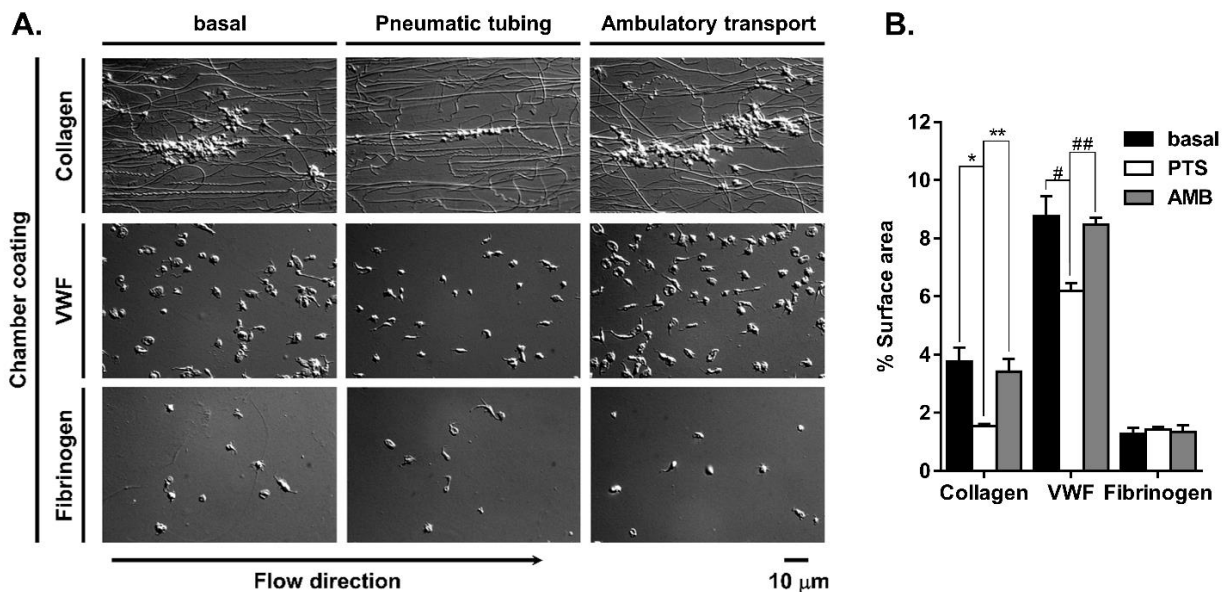
PC units were collected before (basal) or following transport via pneumatic tubing system transport (PTS) or by human courier, ambulatory transport (AMB) and pelleted by centrifugation to isolate supernatants. Freshly prepared washed platelets were resuspended in serum supplemented with indicated fraction (percent total volume) of PC unit supernatants. As a control, freshly washed platelets were resuspended in serum supplemented with supernatants isolated from cPRP. Fresh platelet activation (A) and microaggregate formation (B) in the presence of indicated levels of platelet supernatants were quantified by FACS; Mean±SEM, n = 4.

Together this data suggests that the supernatant from stored PC units may promote a baseline level of activation, which may dampen further agonist-induced platelet reactivity. This is in line with previous studies showing that ADP-stimulated platelets tend to become refractory to stimuli over time.[445,446]

#### 7.5.4 Effect of stored PC unit handling on platelet binding to collagen and VWF under shear

We next examined the effect of the transport of PC units on the platelet hemostatic function of binding to exposed ECM and adhesive proteins under shear. For each transport method, final platelet counts were adjusted to  $4 \times 10^5$  plts/ $\mu\text{L}$  using autologous supernatants. Platelet suspensions were perfused over immobilized fibrillar collagen, VWF or fibrinogen at a venous shear rate of  $300 \text{ s}^{-1}$ . We compared the degree of platelet adhesion (expressed as surface coverage) after 10 minutes.

Our data show that platelets in PC units prior to transport bound and aggregated on surfaces of collagen, VWF and fibrinogen (Figure 7.6A&B). Equivalent levels of platelet adhesion and aggregation were observed for platelets in PC units after AMB transport. Surprisingly, the degree of platelet adhesion and aggregation on collagen and VWF was reduced for platelets in PC units that had been transported via PTS. This raised the question of whether PTS transport effected the expression of the platelet VWF receptor, GPIb, in light of the fact that platelet activation was unaffected by transport of PC units via PTS.



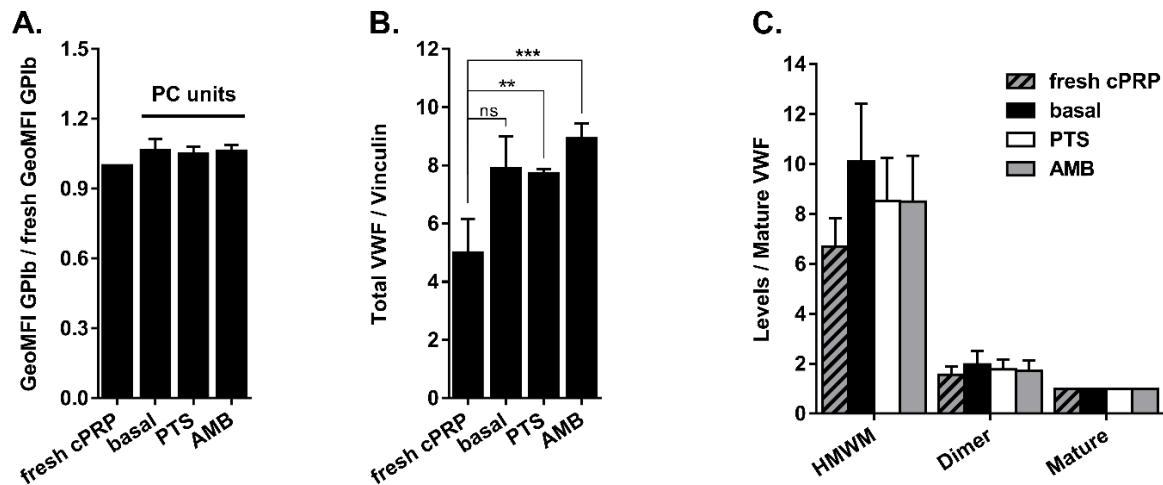
**Figure 7.6 Effect of PC unit handling on platelet binding to collagen and VWF under shear.**

PC units were collected before (basal) or following transport via pneumatic tubing system transport (PTS) or by human courier, ambulatory transport (AMB). Platelets content within PC units was quantified and final platelet counts were adjusted to  $4 \times 10^5$  plts/ $\mu\text{L}$  using autologous supernatants. Samples were perfused over surfaces of immobilized collagen, VWF or fibrinogen at a shear rate of  $300 \text{ s}^{-1}$  for 10 minutes. Differential interference contrast (DIC) microscopy of platelet adhesion and aggregation representative of three separate experiments (A) and surface area quantification mean $\pm$ SEM (B) are shown. \*, \*\*, # and ## indicate statistically different groups with corresponding p-values of 0.010, 0.013, 0.027 and 0.003, respectively.

### 7.5.5 Effect of PC unit handling on levels of platelet GPIb receptor and VWF forms

We next studied whether transport of PC units effected platelet GPIb receptor expression levels. Our results show that the expression level of GPIb was equivalent on platelets in PC units prior to and after transport via either PTS or AMB routes (Figure 7.7A). Moreover, GPIb levels on platelets in PC units were equivalent to GPIb levels measured on freshly washed platelets.

We next examined levels of VWF multimer forms in supernatants isolated from PC units prior to and following transport via either PTS or AMB routes. We found that when normalized to the housekeeping protein, vinculin, PC unit fractions isolated at baseline or following PTS or AMB transport contained similar levels of total VWF, although the levels were slightly higher than the levels observed in freshly prepared platelet-rich plasma (Figure 7.7B). The distribution of dimer and multimer forms of VWF was equivalent in the plasma of PC units prior to transport as compared to following transport via either PTS or AMB routes (Figure 7.7C). In summary, our data show that transport of PC units via either PTS or AMB methods does not affect either platelet GPIb receptor expression or VWF multimer distribution as compared to prior to transport.



**Figure 7.7 Effect of PC unit handling on levels of platelet GPIb receptor and VWF forms.**

PC units were collected before (basal) or following transport via pneumatic tubing system transport (PTS) or by human courier, ambulatory transport (AMB) and were immunostained for surface expression of GPIb and evaluated by FACS. Geometric mean fluorescent intensity (GeomFI) of GPIb levels were normalized to levels found in freshly prepared cPRP samples. Mean±SEM, n = 4. (A). In select experiments, PC units and cPRP samples were pelleted by centrifugation to isolate and test supernatants for VWF multimers by Western blot. Total levels of VWF forms were normalized to vinculin (B; ns = not statistically significant with p = 0.1173, \*\* p = 0.0331 and \*\*\* p = 0.0123; n = 4). Ratios of VWF forms, high molecular weight multimer (HMW), dimer and mature, were normalized to mature VWF forms (C; n = 4).

## 7.6 Discussion

Hemorrhage remains a major cause of death in trauma patients.[447–450] Inclusion of PC units as part of the early resuscitation strategy has been shown to promote survival of severely injured patients[451–453] and improve outcomes in patients with clinically relevant thrombocytopenia.[454] PC units are thus frequently rushed to the patient care teams as soon as the need is determined; commonly, pneumatic tubing systems (PTS) are used to accelerate and secure access of this vital transfusion product. Interestingly, several studies have indicated that transport of whole blood via PTS leads to abnormal platelet function test results as compared to AMB transport.[436–442,455] In fact, these collective findings have led to establishment of the international recommendation against the use of PTS for transport of clinical samples for platelet function testing.[434,435] It is puzzling that while PTS is no longer recommended for transport of clinical samples for platelet testing it is permitted and is frequently used for transport of PC units to be transfused into patients. Our case study was designed to examine whether transport of PC units via PTS transport effected platelet activation and function.

Donation of PC units involves a significant donor time involvement as well as a number of short-term and long-term risks to donor including compromise of immediate hematologic parameters, thrombopoiesis and bone demineralization.[456,457] Most of the studies looking at possible effects of PTS transport on platelet function have focused on the transport of whole blood sample via PTS and the use of a single concentration of a singular agonist or treatment coupled with platelet function tests.[458,459] In our study we quantified the acceleration/deceleration profiles that PC units experience within the OHSU PTS as compared to during ambulatory (AMB) transport. Our case study shows that subjecting PC units to rapid changes in gravitational forces during PTS transport does not affect platelet response to soluble platelet agonists, GPIb receptor expression or VWF multimer levels. A slight decrease was observed in the degree of platelet aggregation on collagen and VWF, and we are currently investigating the mechanism behind this reduction in aggregate formation. It is unclear

whether a slight decrease in aggregate formation is indicative of a clinically relevant loss of hemostatic function, however.

Our data indicate that platelets transported via PTS did not exhibit higher levels of activation or microaggregation as compared to platelets transported by an AMB method. This finding was consistent with Javela *et al.* who also showed that storage time rather than handling of PC units promoted baseline platelet CD62P-secretion.[460] Other groups have also shown that PTS had no effect on platelet metabolic activity, activation or secretion as a function of time of storage.[455,461,462] Moreover, recent work by Kelly *et al.*, showed that the ability of PC units to increase platelet count in non-bleeding cancer patients with thrombocytopenia was independent of the degree of platelet function as measured by aggregometry, P-selectin expression and fibrinogen binding.[463] Thus, perhaps as long as patients have a threshold concentration of functional platelets in circulation, the transfusion of additional platelets, even though they may exhibit reduced absolute activity, may be sufficient to stop bleeding. In this setting, the reactivity of the platelets within PC units may be secondary to the ability to rapidly transport PC units to patients at risk of hemorrhage. Conversely, in severely injured patients with thrombocytopenia and platelet dysfunction, the transfusion of PC units that retain platelet function may be paramount to promote hemostasis. Further studies are needed to properly assess the effect of transport on the stored PC units function in different patient populations to guide an appropriate utilization of this important therapeutic reagent.

Clinical assessment of platelet function is complicated by a number of variables; historically, platelet function tests are notorious for their technical complexity and limited utility due to potential effects of sample handling during transport, platelet fragility and use of purification steps.[438,458,464–467] The assessment of PC units is further complicated by platelet storage conditions during which platelets are prone to secrete secondary mediators, alter receptor availability, skew platelet response to stimuli and their ability to interact with certain ECM proteins.[445,446,462,468–472] Furthermore, others have found that storage combined with increased



frequency of the PTS transport dramatically decreases platelet function as assessed by aggregometry in the presence of collagen, ADP, TRAP-6 or arachidonic acid.[462] During the past two decades, significant strides have been made to improve and simplify platelet testing including taking it out of the niche testing labs and making tests more portable and predictive of clinical outcomes.[458,459] The potential commercialization of closed and open system methods using small volume whole blood samples hold the potential for the timely assessment of patient platelet function which may accelerate and simplify our understanding of patient-specific hemostatic capacity to guide potential interventions.[328,438,473–478]

This report focused on the study of the effect of PC unit handling during transport within a single hospital. We utilized PC units released from the clinical inventory in accordance with the American Red Cross guidelines. The timeframe for PC unit storage and expiration timeframe is set by the Red Cross to primarily prevent bacterial burden within blood component stored at RT. However, it is also likely that recently expired platelets maybe be less desirable for transfusion due to the accumulation of significant levels of platelet secondary mediators within the PC unit supernatant.[479] Furthermore, our data is in accord with the notion that PC unit storage may promote increased levels of high molecular weight VWF multimers (HMWM), which may be caused by stored platelet release of HMWM resistant to degradation by ADAMTS13.[480–483] With these limitations in mind it is important to note that we did not observe a difference in GPIb receptor expression between fresh and stored platelets.[484–489] While platelet transport via PTS had no effect on GPIb or VWF levels, we found that stored platelets exposed to high frequency of acceleration/deceleration jolts exhibited reduced aggregate formation on immobilized surfaces of collagen or VWF under shear. Future work using freshly isolated platelets will be focused on determining whether PTS plays a role in altering conformations of receptors and proteins that mediate these interactions, GPIb and VWF, and attempting to correlate these findings to clinical outcomes in patients who undergo platelet transfusion.[490,491]

## **Chapter 8. Design and utility of a point-of-care microfluidic platform to assess hematocrit and blood coagulation**

Jevgenia Zilberman-Rudenko, Rachel M. White, Dmitriy A. Zilberman,

Hari H.S. Lakshmanan, Joseph J. Shatzel, Jeevan Maddala, Owen J.T. McCarty

Chapter 8. was submitted for publication with the Biomedical Engineering Society, in *Cellular and Molecular Biomedical Engineering*, Springer Publishing, February 2018.

### **8.1 Abstract**

*Purpose:* To develop a small volume whole blood analyzer capable of measuring the hematocrit and coagulation kinetics of whole blood.

*Methods and Results:* A parallel-plate microfluidic chamber designed to facilitate self-driven capillary action across an internal electrical chip was developed and used to measure the electric parameters of whole human blood that had been anticoagulated or allowed to clot. To promote blood clotting, select chip surfaces were coated with tissue factor (TF), which activates the extrinsic pathway of coagulation to promote thrombin generation and fibrin formation. Whole human blood was added to the microfluidic device and voltage changes within the platform were measured and interpreted using basic RC circuit and fluid dynamics theory. Upon wetting of the sensing zone, the circuit between the two electrodes within sensing zone was closed to generate a rapid voltage drop from baseline. The voltage then rose due to sedimentation of red blood cells (RBC) in the sensing zone. The time for the voltage to return to the baseline level was dependent on hematocrit for anticoagulated blood samples. The initiation of fibrin formation in the presence of TF prevented the return of voltage to the baseline due to the reduced packing of RBCs in the sensing zone in the presence of coagulation.

*Conclusions:* The technology presented in this study has potential for monitoring the hematocrit and coagulation parameters of patient samples using a small volume of whole blood, suggesting it may hold clinical utility as a point-of-care test.

## **8.2 Introduction**

Clinically, it is vital to rapidly assess hemostasis in emergency situations especially when a patient is unresponsive and there is a suspicion of an intracranial bleeding. Point-of-care testing has the potential to quickly identify anticoagulated patients allowing providers to initiate appropriate reversal agents to promote stabilization of patients. The dynamic reactions in the blood that lead to hemostatic clot formation are dependent on levels and activity of blood plasma coagulation factors as well as cellular components, including platelets and red blood cells (RBC). Furthermore, detection of changes in RBC content may be useful in detection of an active bleed or dehydration and, together with other clinical findings (e.g. vitals), may help guide appropriate patient care. In this chapter we apply our understanding of coagulation dynamics as well as biorheology and describe development and potential utility of a point-of-care microfluidic platform to assess hematocrit and blood coagulation activity. Our results show that our platform is sensitive to the rate of RBC packing into the sensing zone in the presence or absence of coagulation pathway activation. We show that using RC and fluidics theory we can analyze electrical read-out from our platform to calculate hematocrit of a sample. Together, this platform has a potential for a multiplexed analysis of a small volume of whole blood, which may be of use in an emergency medicine situation.

## **8.3 Background**

Hemostasis is a vital physiological response to vessel injury, involving the dynamically regulated process of thrombus formation at the blood vessel wall to halt blood loss and maintain organ perfusion. Thrombosis is a pathophysiological process involving excessive thrombus formation within blood vessels that may progress to vessel occlusion and the threat of organ ischemia. Both processes, hemostasis and thrombosis, rely on the intermingled activation and inhibitory pathways of platelets and coagulation factors within the blood stream.

A wide range of basic clinical tests exist to assess coagulation parameters, platelet function and blood cellularity (complete blood cell count, CBC) separately. Yet, these tests fail in part to account for the interlink between the parameters as well as the complexities of blood reactions in the framework of blood biorheology. Specifically, the red blood cell content of blood, or hematocrit, can play a major role in platelet availability at the vessel wall[492] as well as the viscosity of blood.[493,494] Clinically, decreased hematocrit has been shown to be predictive of bleeding,[495] while increased hematocrit has been linked with thromboembolic complications.[312] Furthermore, blood behaves as a complex non-Newtonian particle suspension and blood rheology drastically differs in the setting of laminar or turbulent flows and varying shear flow gradients.

Clinical coagulation tests, such as the prothrombin time (PT) and activated partial thromboplastin time (aPTT) are used to assess blood clotting function in patients. These tests are performed by assessing clotting of isolated platelet poor plasma (PPP) in the presence of known activators of coagulation cascade via either the extrinsic pathway (lipidated tissue factor, TF, for PT) or the intrinsic pathway (silica or ellagic acid for aPTT) in a closed test system. These tests can provide useful information for pinpointing specific coagulation factor deficiency or monitor the drug effects of anticoagulant therapy. However, such tests currently require a sizable blood donation from a patient per test performed by trained personnel to collect blood, isolate and test plasma, all of which may be time consuming and costly.

A number of miniaturized technologies reliant on microfluidic engineering have been designed for use with whole blood or blood products. Some of these have become commercially available for use in the hospital setting and serve as popular means of bedside testing to facilitate a rapid assessment of specific patient parameters (metabolite and protein levels, coagulation tests etc.). These technologies have become increasingly user friendly and provide fast testing turn around, which can be vital for emergent situations or even at-home testing. However, additional considerations such as cost

and requirements of separate cartridges and sometimes even computational modules make this technology less accessible to the public at present.

In the study described within, we built upon our understanding of print electronics and microfluidic technology to create a microfluidic platform that only requires picoliters of whole blood. We aim to produce a cartridge technology that is compatible with home-based computational modules. The initial goal of this technology was to test blood flow dynamics for both anticoagulated blood as well as for blood in the presence of coagulation with a focus of assessing patient hematocrit and hematocrit-adjusted coagulation.

## **8.4 Materials and Methods**

### *Materials and Reagents*

Prothrombin time (PT)-reagent Dade® Innovin® was purchased from Siemens (Munich, Germany). Corn Trypsin Inhibitor (CTI) was purchased from Enzyme Research Laboratories, Inc. (South Bend, IN). Electronic chips were produced via a high-throughput silica printing process at HP, Inc (Corvallis, OR). All other materials were purchased from Sigma-Aldrich (St. Louis, MO) or previously cited sources.[268,496]

### *Microfluidic platform design and chip parameters*

The platform was designed as a parallel-plate microfluidic device with an internal electronic chip supplied by direct current (DC). The microfluidic device connected a sample inlet and the sensing zone with an outlet open to the air (Figure 8.1A-C). The sensing zone of the chip included two co-planar electrodes, where electrode 1 (E1) was connected to ground, while electrode 2 (E2) was connected to an input voltage via a pullup resistor (R1) and a DC switch (Figure 8.1D). E1 and E2 were designed to be separated by a physical gap and to remain electrically decoupled in a dry empty device. The electric

current path between E1 and E2 was expected to be established upon wetting of the sensing zone with a sample.

#### *Functionalization of microfluidic devices with an activator of the extrinsic pathway of coagulation*

Microfluidic devices were incubated with 1  $\mu\text{L}$  of stock solution of tissue factor (TF)-containing PT-time reagent (Dade<sup>®</sup> Innovin<sup>®</sup>) for 1 hour under rotation at room temperature. The introduction of Innovin<sup>®</sup> into the sensing zone corresponded with a drop in the measured voltage across the electrodes E2 to E1. Next, devices were rinsed with phosphate buffered saline (PBS) pH 7.4 and dried by vacuum-aspiration of liquid from the inlet and outlet. Surfaces were then blocked with 5 mg/mL denatured bovine serum albumin (BSA) for 1 hour at room temperature, followed by a rinse with PBS and drying of the device.

#### *Time constant approximation*

Using Ohm's Law, voltage contribution due to red blood cell (RBC) sedimentation within the sensing zone was treated as RBC membranes acting as leaky capacitors [497–502] leading to an increase of measured voltage over time with an exponential decay (Figure 8.3A&B). It was assumed that in the absence of coagulation, RBCs are free to flow and sediment within the sensing zone; thus, the measured  $\varepsilon$  would increase as a function of time until the maximal packing capacity of RBCs within the sensing zone was achieved. Thus, the time to maximal packing capacity is assumed to be a function of hematocrit (ratio of the volume of RBCs to the total volume of blood). Using this assumption, a basic approximation of the time constant,  $\tau_{H_x}$ , was derived for samples with different hematocrits.

Using experimentally acquired voltage profiles of a whole blood sample with hematocrit of 43 percent (Figure 8.2), the sample flow rate was estimated as:

$$Q_{H43} = \text{Volume}_{\text{sensing zone}} / t_{\varepsilon(H43)}, \quad (1)$$

where  $t_{\varepsilon(H43)}$  is the time required for the voltage to rise from transition #2 (Figure 8.2B) to final voltage plateau  $\varepsilon$ , transition #3.

$Volume_{sensing\ zone}$  was set as a constant volume of the sensing zone to be occupied by RBCs to achieve  $\varepsilon$ .

Knowing the fraction of RBCs within the sample, the bulk flow rate was estimated as:

$$Q = Q_{H43} * 100/43 \quad (2)$$

For ‘Approximation 1’ of  $\tau_x$ , flow rates ( $Q_{H_x}$ ) for samples with different hematocrits ( $H_x$ ) were calculated by multiplying the bulk flow rate by the percent hematocrit fraction (Figure 8.3C). Next,  $Volume_{sensing\ zone}$  was divided by respective  $Q_{H_x}$  to calculate  $t_{\varepsilon(H_x)}$ . Using RC circuit theory,  $\tau_x$  was approximated by dividing  $t_{\varepsilon(H_x)}$  by 5. This ‘Approximation 1’  $\tau_x$  vs.  $H_x$  is depicted in Figure 8.3D in grey.

For ‘Approximation 2’ of  $\tau_x$ , we accounted for the possible effect of hematocrit on blood viscosity.[493,503–505] Using Hatschet’s formula[503] modified by Pirofsky,[504] a relationship between hematocrit ( $H_x$ ) and blood viscosity ( $\mu_x$ ) was expressed as follows:

$$\mu_x = \frac{\mu_{plasma}}{1 - H_x^{1/3}} \quad (3)$$

Given that the flow rate of a particle is inversely proportional to the viscosity of the particle suspension, which in this case is blood, the relationship can be given as:

$$Q_{H43} \propto \frac{1}{\mu_x} \quad (4)$$

To arrive at an adjusted bulk flow  $Q'$ , bulk flow  $Q$  (derived in equation 2) was multiplied by the  $\mu_x$  for a hematocrit of 43. Subsequently,  $\mu_x$  and  $Q'_{H_x}$  for a range of hematocrits was derived and used to calculate adjusted  $t_{\varepsilon(H_x)}$  and  $\tau_x$  as above. This ‘Approximation 2’  $\tau_x$  vs.  $H_x$  is depicted in Figure 8.3D in black.

### *Human venous and capillary blood collection*

Venous whole human blood was drawn by venipuncture from healthy adult volunteers into either a dry syringe, a syringe containing a bivalent direct thrombin inhibitor (hirudin, 40  $\mu\text{g}/\text{mL}$  final) or trisodium citrate (0.38% w/v) in accordance with the Oregon Health & Science University Institutional Review Board. To isolate RBCs, whole blood was spun down at 1600 rpm for 10 minutes at RT in a Hermle Z300 centrifuge outfitted with rotor 221.12 V01 (Labnet, Edison, NJ). After the first spin, platelet rich plasma (PRP) was transferred into a new tube and, when appropriate, PRP was spun down again at 2500 rpm for 10 minutes to isolate platelet poor plasma (PPP). All blood products were used within 2 hours of the blood draw.

### *Statistics*

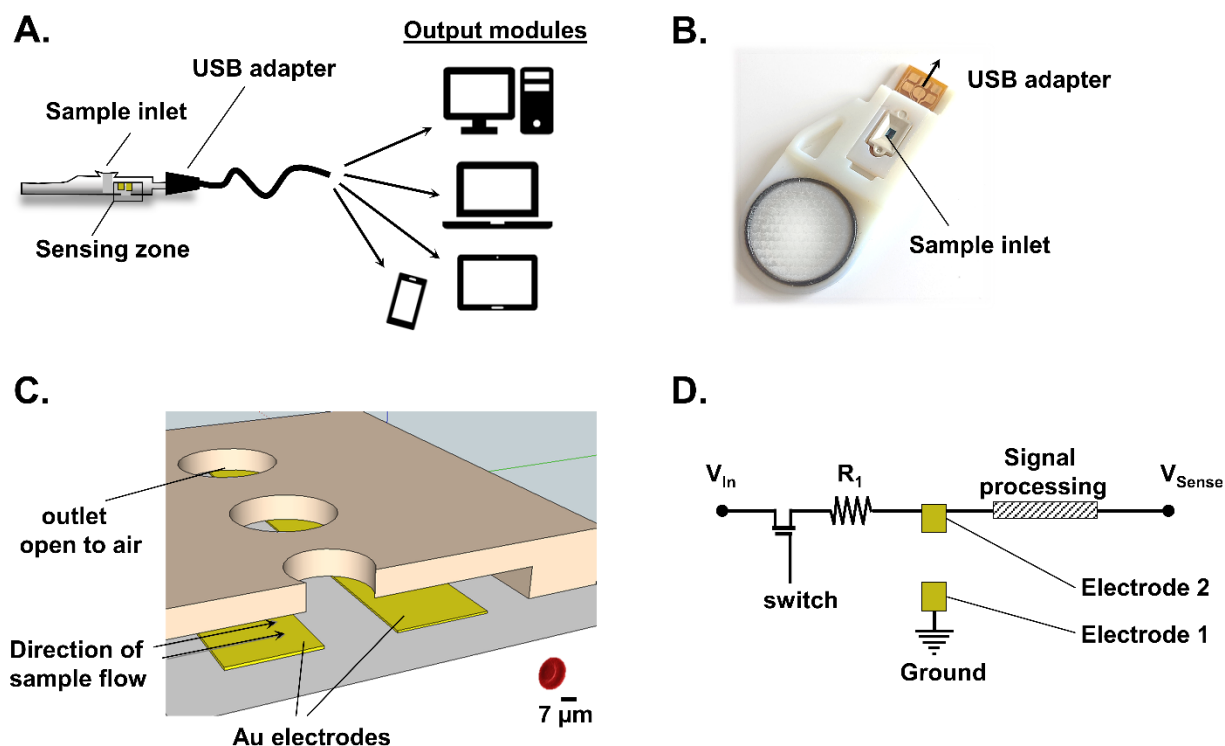
Data are shown as means  $\pm$  SEM. Statistical significance of differences between means where noted was determined by ANOVA. Probability values of  $P < 0.05$  were selected to be statistically significant.



## 8.5 Results

### 8.5.1 Design of a microfluidic platform for use with blood samples

The microfluidic blood analyzer platform was manufactured as a microfluidic device with an internal mass-printed electronic chip. The device was incased into an insulating plastic, which allowed handling and connection of the platform to a range of output modules via a USB adapter (Figure 8.1A&B). The parallel-plate microfluidic device connected a sample inlet to the sensing zone containing an outlet open to air (Figure 8.1A-C). The sensing zone of the chip included two co-planar gold (Au) electrodes physically separated by a gap and electronically uncoupled, with electrode 1 (E1) connected to ground, while electrode 2 (E2) connected to input voltage via a pullup resistor ( $R_1$ ) and a DC switch (Figure 8.1D).



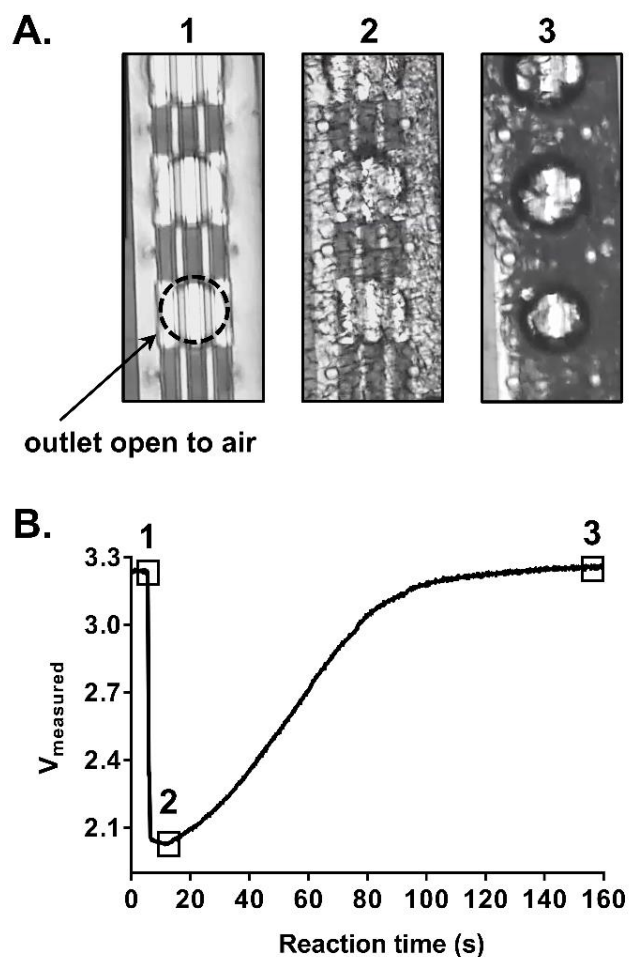
**Figure 8.1 Design of a microfluidic platform for use with blood samples.**

(A) Illustration of the experimental setup. (B) Photograph of the assembled device. (C) Illustration of the sensing zone with two gold (Au) electrodes. (D) Basic circuit design in the absence of blood sample.

### 8.5.2 Microfluidic platform with anticoagulated whole human blood sample

To study electrical parameters of anticoagulated whole human blood within our microfluidic platform, venous whole blood samples were collected from a healthy human donor (Hematocrit of 43) and anticoagulated with a bivalent direct thrombin inhibitor (40  $\mu\text{g}/\text{mL}$  hirudin). Microfluidic device surfaces were blocked with bovine serum albumin (BSA) and vacuum-aspirated prior to addition of the blood sample (Figure 8.2A, panel 1). Notably, addition of a buffer to the sensing zone resulted in a rapid if not instantaneous drop in voltage from  $V_{\text{max}}$  ( $\sim 3.3\text{ V}$ ) to  $\sim 2.1\text{ V}$ ; this voltage drop could be reversed by subsequent removal of buffer out of the device by vacuum-aspiration (data not shown).

Anticoagulated whole blood was added to the sample inlet and progressed quickly (within 5 seconds) by self-driven capillary action to the outlet within sensing zone (Figure 8.1); the presence of red blood cells (RBCs) within the sensing zone was visualized with light microscopy Figure 8.2A, panel 2). The wetting of the sensing zone with a blood sample produced a rapid drop in the voltage from  $V_{\text{max}}$  to  $\sim 2.1\text{ V}$  (corresponding to transition from point 1 to point 2 on the graph in Figure 8.2B). With increasing time, RBCs would enrich within the sensing zone resulting in decreased light transmittance through the sensing zone



**Figure 8.2 Microfluidic platform with anticoagulated whole human blood sample.**

Venous whole blood samples collected from a healthy human donor (Hematocrit of 43) were anticoagulated with bivalent direct thrombin inhibitor (40  $\mu\text{g}/\text{mL}$  hirudin) and applied to the inlet of the microfluidic device. Real-time progression of blood sample within microfluidic device was (A) visualized with light microscopy with pertinent transition points shown in panels (1-3) and (B) labeled on the voltage profile (1) dry sensing zone prior to blood entry, (2) entry of blood samples and (3) sedimentation of RBCs within sensing zone. Data representative of  $n > 30$ .

(Figure 8.2A, panel 3) and the increase in voltage measured (Figure 8.2B). Eventually, RBCs packing would near maximal capacity, as observed via microscopy as a lack of RBC movement; correspondingly, the voltage returned to near  $V_{\max}$  (Figure 8.2B, point 3).

### 8.5.3 *Estimation of microfluidic platform voltage sensitivity to hematocrit*

We next approximated the dependence of voltage on the concentration of RBCs (hematocrit). We used experimental observations of voltage measurements for a blood sample with a hematocrit of 43 percent (Figure 8.2) and adapted a previously validated three-element-model of blood;[506,507] where blood components were modeled as an RC circuit comprised of two resistor components, corresponding to resistive properties of blood plasma ( $R_p$ ) and intracellular components of blood cells ( $R_i$ ), and a capacitor ( $C_m$ ), corresponding to a collective capacitance of RBC membranes (Figure 8.3A).

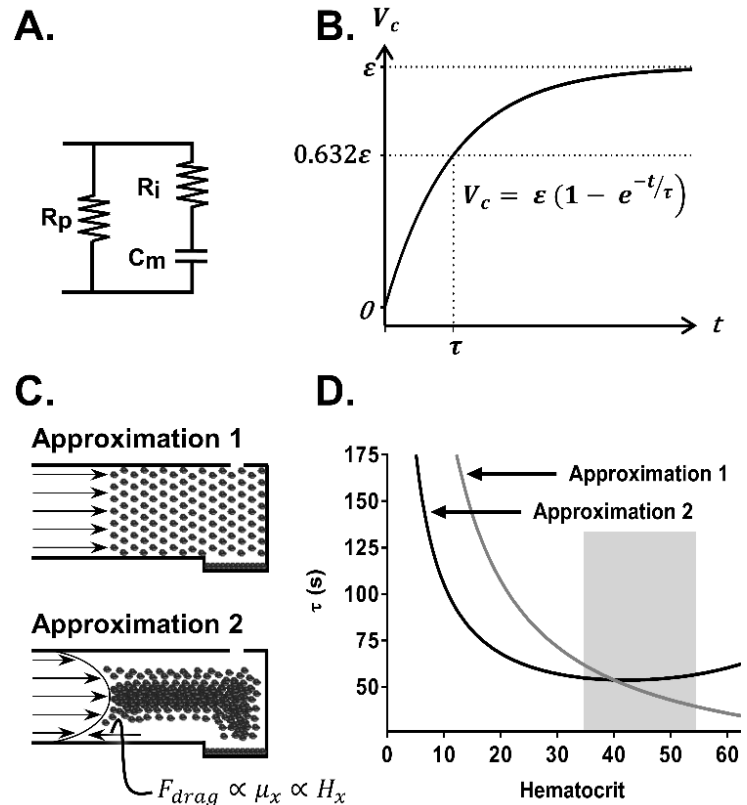
Human whole blood was assumed to be a non-Newtonian suspension of cells and proteins under laminar flow existing in a stable neutralized state facilitated by electrostatic repulsion of blood cells and proteins.[508,509] We assumed that the experimentally measured rise in voltage (transition from point 2 to point 3 in Figure 8.2B) corresponded with RBCs sedimentation into the sensing zone with RBCs acting as leaky capacitors,[497–502,510] resulting in an increase in measured voltage over time in accord to Ohm's law (Figure 8.3B). We further assumed that in the absence of coagulation, the maximal capacity of RBCs packing would be equivalent regardless of the initial hematocrit and thus leading to the same voltage rise ( $\varepsilon$ ) from  $\sim 2.1V$  to  $V_{\max}$ .

Using these assumptions, we were then able to model the time evolution of the RBC-dependent voltage rise and estimated time required to reach ( $\varepsilon$ ) for a sample with hematocrit of 43 percent ( $t_{\varepsilon(H43)}$ ). We also were able to model the time constant,  $\tau_{H43}$ , which corresponds to time required to reach  $0.632\varepsilon$  and equals to approximately  $1/5^{\text{th}}$  of the  $t_{\varepsilon(H43)}$ .

Knowing the total volume of the sensing zone, we derived a basic estimate of the flow rate of blood samples ( $Q_{H43}$ ) by dividing the sensing zone volume by  $t_{\varepsilon(H43)}$ .

For ‘Approximation 1’ of  $\tau_{H_x}$  as function of hematocrit ( $H_x$ ), RBCs in samples with different hematocrits were predicted to have equivalent flow profiles regardless of hematocrit (Figure 8.3C) and thus the bulk flow was estimated by dividing the sample flow rate ( $Q_{H43}$ ) by the RBC content (hematocrit percent).

The flow rates of samples with different hematocrits were then calculated by multiplying the bulk flow rate by hematocrit percent. These values were then used to predict the time to  $\varepsilon$  for select hematocrits and divided by 5 to estimate  $\tau_{H_x}$  as a function of hematocrit. The resultant ‘Approximation 1’  $\tau_{H_x}$  values were plotted (grey curve) as a function of hematocrit (Figure 8.3D).



**Figure 8.3 Estimation of microfluidic platform voltage sensitivity to hematocrit.** (A) Assumed three component blood circuit addition between two electrodes. (B) Voltage profile of a RBC-capacitor contribution based on Ohm’s Law. (C) Illustration of RBC flow rate assumptions for approximation of the time constant values ( $\tau_{H_x}$ ) as a function of hematocrit: approximation 1 accounted for bulk blood flow only and approximation 2 accounted for viscosity and blood flow profile change due to hematocrit increase. (D) Plot of approximated  $\tau_{H_x}$  values as a function of sample hematocrit using approximation 1 (grey line) and approximation 2 (black line). The normal hematocrit range for men (40 to 54%) and women (36 to 48%) is highlighted with a grey box.

For ‘Approximation 2’ of  $\tau_{H_x}$  as function of hematocrit ( $H_x$ ), the blood sample viscosity was modeled to be dependent upon the hematocrit (Figure 8.3C).[493,503–505] We divided the blood flow rate ( $Q_{H43}$ ) by a viscosity factor that accounts for changes in viscosity due to RBCs, [503,504] calculated for sample with a hematocrit of 43 percent. The resultant flow rate ( $Q'_{H43}$ ) was then used to calculate an adjusted bulk flow rate and ‘Approximation 2’ of  $\tau_{H_x}$  (black curve) as function of hematocrit (Figure 8.3D),

Both our approximations predict that  $\tau_{H_x}$  should decrease exponentially with increases in hematocrit.

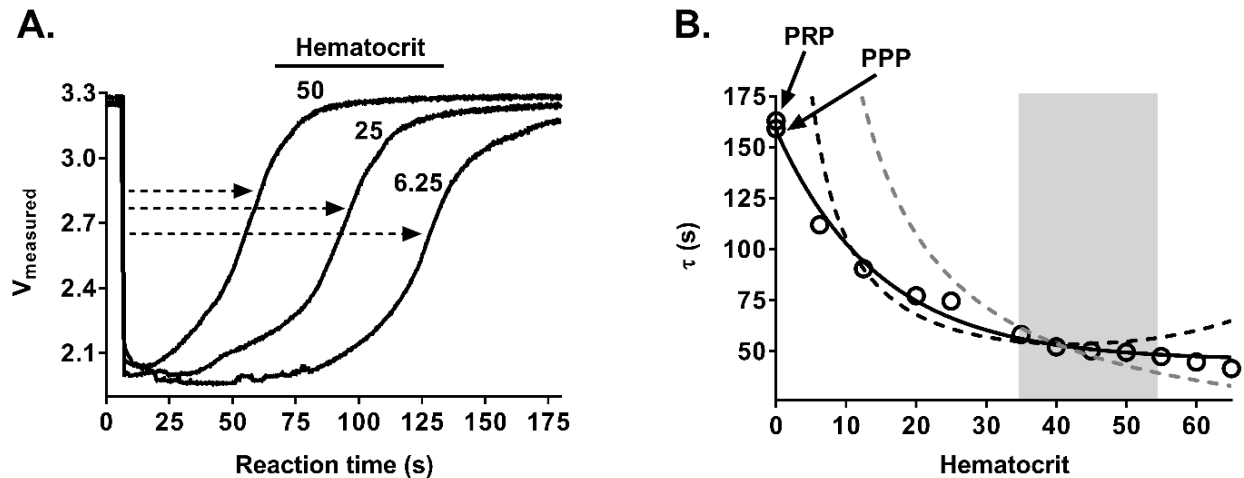
#### 8.5.4 Sensitivity of the microfluidic platform to hematocrit

We next evaluated the sensitivity of our device to hematocrit in order to compare our predicted values to experimental data. We therefore prepared whole human blood samples with select hematocrits. Fresh whole human blood was collected by venipuncture and anticoagulated with a bivalent direct thrombin inhibitor (40  $\mu\text{g}/\text{mL}$  hirudin). Blood was then subjected to a series of centrifugation steps to isolate RBC, platelet-rich plasma (PRP) and platelet-poor plasma (PPP) fractions. The RBC pellets were diluted with autologous PPP to select levels of hematocrit before use in the microfluidic devices. Our data shows that the time to reach  $0.632\varepsilon$ , or  $\tau_{H_x}$ , decreased as a function of hematocrit ( $H_x$ ), with a longer  $\tau_{H_x}$  observed with lower hematocrit (Figure 8.4A).

We next plotted  $\tau_{H_x}$  values, calculated from voltage profiles, as a function of hematocrit levels to study the relationship between  $\tau_{H_x}$  and hematocrit (Figure 8.4B). The  $\tau_{H_x}$  times calculated from experimental data exponentially decreased with hematocrit level. Approximated values of  $\tau_{H_x}$  approached the empirical values of  $\tau_{H_x}$  for the physiological ranges of hematocrit (36-54%).[511]

Notably,  $\tau_{H_x}$  values for samples with hematocrit range below 20 percent were significantly ( $p < 0.001$ ) higher as compared to the normal range, suggesting that this microfluidic platform may be

sensitive enough to identify patients with clinically unsafe low levels of hematocrit.[512] In the presence of elevated hematocrits outside the normal range, the approximations diverged into either lower or higher  $\tau_{H_x}$  values as compared to experimental values, suggesting additional forces may be affecting the flow of RBCs at elevated hematocrit levels.



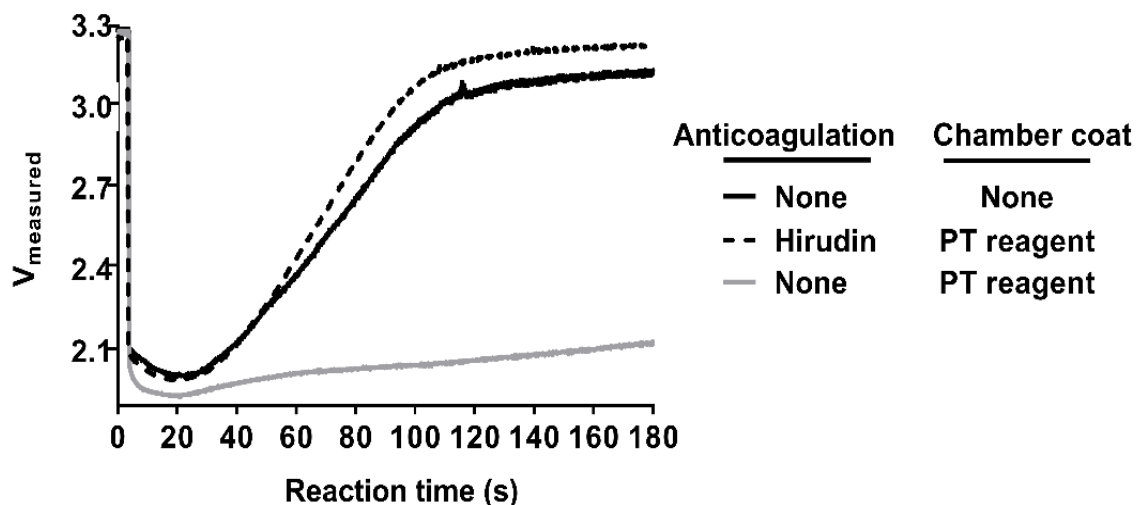
**Figure 8.4 Sensitivity of the microfluidic platform to hematocrit.**

Venous whole blood anticoagulated with bivalent direct thrombin inhibitor (hirudin) was subjected to series of centrifugation steps to isolate RBC, platelet-rich plasma (PRP) and platelet-poor plasma (PPP) fractions. RBC pellet was diluted with autologous PPP to indicated levels of hematocrit and samples were applied to BSA-coated microfluidic devices. (A) Real-time progression of blood cell suspension within microfluidic device was recorded using voltage measurement. The dashed arrows indicate calculation of empirical time constant values ( $\tau_{H_x}$ ) for samples with different hematocrits. (B) Plot of empirical  $\tau_{H_x}$  values for samples with different hematocrit content is shown as Mean  $\pm$  SEM,  $n \geq 3$ . Single points were fitted to an exponential decay curve (solid black line) and compared to approximated  $\tau_{H_x}$  values from Figure 8.3 (dashed lines). The normal hematocrit range for men (40 to 54%) and women (36 to 48%) is highlighted in grey.

#### 8.5.5 Sensitivity of the microfluidic platform to coagulation

We next assessed the sensitivity of our microfluidic platform to initiation of coagulation. Select microfluidic devices were functionalized with lipidated tissue factor (TF), which activates the extrinsic pathway of coagulation (Dade<sup>®</sup> Innovin<sup>®</sup>). Venous whole blood was collected into an empty syringe and pretreated with either vehicle buffer control, a bivalent direct thrombin inhibitor (hirudin) or an inhibitor of coagulation factor XIIIa (corn trypsin inhibitor, CTI). Samples were added to microfluidic devices and real-time voltage recordings were obtained.

Regardless of the anticoagulant, a near instantaneous drop in voltage was observed following introduction of blood into the device (Figure 8.5). For samples pretreated with hirudin, a similar change in voltage as a function of time was observed as compared to the profile observed for chambers coated with or without TF. In contrast, a sudden drop was observed upon entry of non-anticoagulated blood into TF-coated chambers, yet the voltage remained depressed throughout the observation period, presumably due to the fact that rapid fibrin formation slowed the blood flow and prevented RBCs from packing into the sensing zone. A slight recovery of voltage was observed when blood was pretreated with the FXIIa inhibitor CTI. Taken together our data demonstrates that this device platform is sensitive to both RBC content as well as the rate of fibrin formation.



**Figure 8.5 Sensitivity of the microfluidic platform to coagulation.**

Non-anticoagulated venous whole blood was pretreated with either vehicle buffer control, abivalent direct thrombin inhibitor (hirudin) or coagulation factor XIIa inhibitor (corn trypsin inhibitor, CTI) and added to either BSA-blocked or Innovin-coated microfluidic device. The real-time progression of blood cells within cartridge was recorded using voltage measurements. Graphs are representative of results from  $n \geq 4$  repeats.

## 8.6 Discussion

The target of this work was to establish a microfluidic platform utilizing an electrical chip design that allows testing of whole blood dynamics for hemostatic assessment. We have developed a rational microfluidic device design that allows a self-driven passive flow of a blood sample through the sensing zone coupled with a signal processing algorithm that helps to isolate a signature of red blood cell (RBC) sedimentation and packing. The platform allows for an evaluation of hematocrit using an RC circuit and fluid dynamic theory of RBC transport in whole blood. The platform is sensitive to the rate of thrombin generation and fibrin formation, when the chip is functionalized with an initiator of the extrinsic pathway of coagulation (tissue factor). Together, this platform has a potential for a multiplexed analysis of a small volume of whole blood.

Several portable small volume blood analyzer platform designs have proven to be successful in a clinical point-of-care setting. Notably, Abbott's iSTAT<sup>®</sup> technology allows for rapid testing of blood parameters in emergency medicine and surgical settings. The iSTAT<sup>®</sup>-specific computational module is compatible with a wide range of cartridges for bedside testing of basic coagulation as well as metabolic panels in naïve venous blood.[513,514] While use of these portable blood analyzers provides information used for immediate care, design of patient treatment plans typically requires analysis of blood samples in a routine clinical blood laboratory panel including but not limited to PT/INR, CBC and levels of specific coagulation markers.[513] Thus, there exists a need for a point-of-care technology that provides these values in emergency or surgical settings.

Roche and Alere have developed computational modules with cartridges compatible with capillary blood samples obtained via finger prick for the intended use by patients to assess their hemostatic state at home. However, since hemostasis is a complex process involving blood enzymes as well as cells, results from these designs may not account for flow-dependent parameters of blood clotting at distinct shear rates in different vessel beds. Specifically, when it comes to assessment of patients on anticoagulation therapy and other contributing factors to prothrombotic phenotypes such as



inflammation or cancer, failure to account for cellular components involved in whole blood clotting may underestimate the clotting kinetics which in turn may compromise the information patients use to adjust their therapy with potentially deleterious repercussions to their health; this is in part why the Alere INRatio2<sup>®</sup> home testing module-cartridge technology was recently recalled.[515]

Part of the goal of at-home testing devices is to reduce costs and exposures involved with frequent hospital visits for patients on chronic anticoagulation and other types of hemostatic irregularities. After appropriate patient coaching by a physician, access to data from home tests can further provide a sense of comfort for both the patient and the provider. Currently marketed technologies to measure coagulation range in cost from \$1000-\$2000 for the computational module itself; additional costs are incurred to purchase the test cartridges. These costs may in part prohibit the use of such technologies for fixed income patient population groups. The aim of this study was to develop a small-volume microfluidic platform design that is sensitive to cellular dynamics of blood samples which can be integrated with existing user computational modalities. Ideally this technology would be adapted for use with smart phone technologies to allow for both data collection and sharing as appropriate.

RBCs play a key role in the delivery of oxygen and nutrients to organs; thus, monitoring hematocrit levels is an essential part in patient management. Moreover, hematocrit levels affect clotting associated with thrombosis and hemostasis[494,516,517] and predict clinical bleeding.[495] Thus, the capability to both assess the hematocrit level and the hematocrit-adjusted clotting properties of a whole blood patient sample (Figure 8.6) maybe of utility in monitoring patients with procoagulant and/or hemorrhagic risks.[518,519] Moreover, requirement for a small volume (< 5  $\mu$ L) to perform these tests is compatible with blood collection procedures using a small lancet from a finger prick rather than venipuncture, further reducing the need for hospital visits for such patient populations, blood loss, and alternative testing routes for patients with limited venous access.

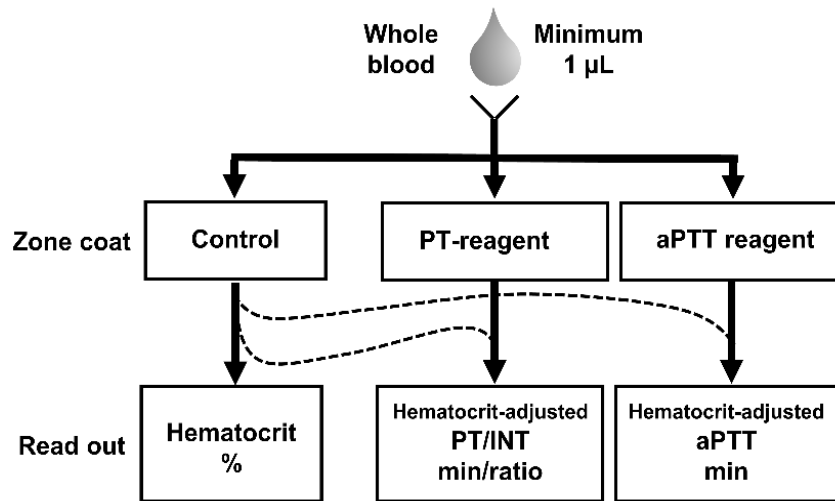


Figure 8.6 Schematic of possible blood measurements and result readouts.

Cancer patients undergoing chemotherapy frequently suffer from bone marrow suppression and thus a drop in hematocrit, platelets and other related aspects of hemostasis. Yet, cancer patients are also predisposed to potentially dangerous thrombus formation due to cancer itself, immobility, tissue damage and other confounding factors.[520,521] Thus, such populations, particularly when anticoagulation is needed, require continuous monitoring and therapy adjustment to mitigate potential thrombo-hemorrhagic complications. Importantly, due to bone marrow and thus immune system suppression, cancer patient populations are also vulnerable to the development of potentially lethal infections. Thus, the capability for home testing may be potentially beneficial from the perspective of limiting hospital visits and thus dangerous in-hospital exposures.

Whole blood is a complex sample to handle, study and quantify. Blood behaves as a non-Newtonian fluid, which means its viscosity changes with shear rate.[522] It is a colloid suspension that adheres to Stokes theory of particle motion in viscous solution but only with a hematocrit of up to one percent.[523] Some strides to understand particle motion in physiologically relevant hematocrit settings are coming from the field of study of silica slurries; however RBCs and other cells introduce other challenges that are difficult to account for in slurries. Whole blood in part follows the Fahraeus effect, which predicts that RBCs tend to migrate to the channel centerline and form a core that flows

faster as compared to the rest of the blood, thus contributing to higher ‘discharge’ hematocrit ( $H_d$ ) as compared to sample hematocrit ( $H_x$ ).[9,10] Yet, again this relationship falls apart at hematocrits above 45 percent.[524] Furthermore, RBC shape and potential shape changes, channel diameter and geometry, temperature and other aspects all play a role in flow dynamics of this viscoelastic and intricate fluid.[505,525–527]

Clinically, it is vital to rapidly assess hemostasis in emergency situations. While classically used anticoagulants, such as warfarin, could be monitored with traditional tests including PT and aPTT, the effects of newer direct oral anticoagulants cannot be easily assessed.[528] In patients presenting with acute major or central nervous system bleeding, point of care testing has the potential to quickly identify anticoagulated patients allowing providers to initiate appropriate reversal agents. Likewise, certain medical conditions such as end stage liver disease[529] and antiphospholipid antibodies[530] interfere with the accuracy of traditional coagulation tests. Point-of-care microfluidic platforms have the potential for utility to offer better assessment of these patients in real time.

## Chapter 9. Discussion and Future Directions

### 9.1 Discussion

#### 9.1.1 Limitations

Studies of blood reaction dynamics *in vitro*, *ex vivo* and *in vivo* allow approximation of physiological processes and have contributed many discoveries to the blood research and medical field. However, a full recapitulation of a systemic response in select disease states is a challenge both at the bench top and in a living organism.

Closed *in vitro* testing systems provide utility in studying blood reactions using a reductionist approach from reactions between purified proteins to physiological mixtures such as blood plasma and whole blood. These study systems facilitate identification of protein-protein binding, enzyme kinetics and other biochemical parameters as well studies of platelet activation in the presence of known agonists and the formation of a blood plasma clot in a tube.

Open *in vitro* and *ex vivo* testing systems, such as microfluidics, extend studies to include blood dynamics under shear flow, which further aid in understanding blood reaction dynamics in the vasculature while controlling the environment. For instance, open testing systems were paramount for identifying shear-dependent binding of the platelet receptor glycoprotein (GP)Ib to von Willebrand Factor (VWF), which is an initial step of platelet recruitment to exposed subendothelial extracellular matrix proteins essential for establishment of a hemostatic plug.[531–533] Further, open systems allow studies of platelet aggregation in the presence of fibrin formation under shear, where the extent of fibrin formation under shear flow is dependent on the flux of reactants as well as reaction rates in contrast to closed systems where the initial concentration of reactants (agonists, antagonists and other molecules) remains constant.[268,272,313,411] Open *in vitro* and *ex vivo* testing systems have been employed to elucidate a difference in the platelet to fibrin ratio in the presence of arterial versus venous shear rates (as further discussed in Chapter 3 and Chapter 4).[6,271,313]

Additional developments in microfluidic techniques have included the introduction of live vascular endothelial cells and malleability of channels (more on this in Section 9.3), as well as the scaling up and multiplexing of studies to screen concentration gradients of reagents (*in vitro* cell toxicity and/or drug potency), define mechanistic pathways and identify new potential therapeutic targets. Yet, ultimately, to validate the physiological relevance of findings of *in vitro* and *ex vivo* studies, data from *in vivo* and/or clinical studies are required.

Human cardiovascular and hematologic systems co-exist in a constantly changing state affected by many genetic, environmental and behavioral factors. Animal studies have been essential for many discoveries and at this time remain the only way to evaluate the safety of potential therapeutic agents prior to human studies. Some limitations of animal studies include differences in species' immune system, study environmental and the length of studies that frequently do not allow development of human conditions that add to comorbidities in different disease states. Similar limitations however also arise in clinical trials, design of which is important to be able to arrive at definitive data for the tested hypothesis, while limiting the bias of testing scenario.

The work described in this thesis utilized a number of established as well as newly developed *in vitro* and *ex vivo* closed and open testing systems as well as a number of the *in vivo* animal model studies. Limitations of study approaches were identified and leveraged by consulting clinical and research reports as well as follow up studies. The short-comings of each approach were minimized by employment of a combination of testing assays as well as rigorous approaches to judiciously utilize study materials, including freshly drawn whole human blood, washed platelets and blood plasma. Limitations and future directions to address these as well as limited utility of described findings were specified in discussion sections for each respective chapter as well as below.

### 9.1.2 *Conclusions*

The studies outlined in this dissertation have investigated the dynamics of blood biorheology, coagulation, platelet activation and thrombus formation in flowing blood. The overall aim of these studies was to design and test experimental approaches to gain a broad understanding of blood reactions with an ultimate goal of improving therapeutic approaches to mitigate thrombo-hemorrhagic complications in different clinically-relevant settings. In this section, I will summarize and draw brief conclusions from these.

The events that support physiological process of hemostasis versus pathological process of thrombosis are distinct in part due to the biorheology of blood flow and thrombin mass transfer that differentially distributes blood components and reactants inside and outside blood vessels. The biorheology of blood is dependent on red blood cell (RBC) content, blood plasma protein concentration and the properties of vasculature or microfluidic network which dictate wall shear stress and shear rates.[5,534] In Chapter 3 and Chapter 4, we investigated biorheological concepts of platelet activation and coagulation under shear.

Our results show that specific microvascular network geometries, shear gradients and local thrombus formation can lead to changes in blood biorheology in the flowing blood. Using an integrative computational and experimental approach, we identify specific conditions that promote the mass transfer and amplification of thrombin generated at the site of a local thrombus formation within flowing blood. This work may be of significance for the development of a potentially safer extracorporeal membrane oxygenator (ECMO) designs. Current state of the art oxygenator designs require significant priming volume (> 300 mL) and expose blood to a large area of artificial surface and pathologic blood flows as well as areas of stasis or recirculation, which can promote pathologic thrombin generation amplification and render these life-saving machines impractical. The microfluidic multi-bypass network designs hold potential for increasing the gas exchange rate and drastically reducing the priming volume. Our integrated approach (described in Chapter 3 and Chapter 4) may

help develop microfluidic network oxygenator designs that lower thrombogenicity of these devices thus increasing their safety.

Recent studies have supported the notion that coagulation factor (F)XI and FXIIa inhibitors may represent a therapeutic strategy to prevent cardiovascular thrombotic pathologies. Congenital FXI deficiency protects patients from strokes and venous thromboembolism, and is only associated with minor bleeding episodes.[535,536] In Chapter 5, we utilize an *ex vivo* flow system developed in Chapter 4 and examine the role of FXI in platelet activation and consumption in the bloodstream distal from the site of thrombus formation. Our results demonstrate that the activation of the FXI axis plays a key role in distal platelet activation and microaggregate formation in solution downstream of thrombus formation under both venous and arterial shear flow. I hypothesize that pharmacological targeting of FXI may be useful in mitigating platelet activation and therefore prevent platelet-driven amplification of platelet aggregate and thrombi formation in prothrombotic conditions involving direct contact pathway of the coagulation agonists. For instance, in operating rooms and intensive care units, patients' blood is exposed to a number of artificial materials (tubing, catheters, ECMO, hemodialyzer and etc.) and injury to the vasculature. It is possible that some of the thrombo-embolic complications seen during the treatment of these patients has to do with the distal effects of local thrombus formation and the role of FXI activation due to contact pathway activation and thrombin generation.

The polyanionic molecule, long-chain polyP, has been shown to accumulate in a variety of microorganisms, inducing a FXII-dependent pathological response in mice.[537] Our group has shown that activation of FXII in the presence of long-chain polyP can promote FIX and prothrombin activation independently of FXI,[538] thus suggesting a potentially important role of FXII in conditions where long-chain polyP may be enriched either in solution or on a surface e.g. as biofilm on a venous catheter. Additionally, blockade of FXII might be protective in microorganism-driven thrombotic complications accompanying sepsis, as inhibition of FXII activation of FXI reduced thrombotic complications in animal models of sepsis.[535,539]

In Chapter 6 we use closed and open experimental platforms to study the role of activated FXII(a) activity in the presence of bacterial-type long-chain polyP and showed that FXIIa activity promotes platelet consumption in the presence of long-chain polyP in blood flow *in vitro*. Long-chain polyP had no direct effect on platelet activation or adhesion to the extracellular matrix and instead primarily promoted platelet activation and consumption by fueling thrombin generation and fibrin formation in a FXII-dependent manner. FXII-deficiency was protective against occlusive platelet aggregate formation in the murine model of lethal pulmonary microvasculature occlusion. In a non-human primate model of bacterial sepsis, pretreatment of animals with an antibody blocking FXI activation by FXIIa diminished long-chain polyP-containing LD<sub>100</sub> *S. aureus*-induced platelet and fibrinogen consumption.

Thrombin amplification is implicated in the deadly complication of sepsis titled disseminated intravascular consumptive coagulopathy (DIC) and characterized by concomitant thrombotic complications and bleeding due to consumption of coagulation factors and platelets.[127]. Multiple approaches have been explored for the identification of safe and effective inhibition of thrombin generation inhibition. However, clinically the primarily focus has been on inhibiting the extrinsic and the common pathways of coagulation[142,286,535] or platelet aggregation via inhibition of GPIIb/IIIa.[177] In my opinion, which is supported by clinical reports, such approaches are at the risk of limiting the physiologically relevant functions of platelets and coagulation factors in hemostatic, immunologic and other processes which require the generation of thrombin. I believe our research described in Chapter 6 may aid in the identification of potentially safer anticoagulation therapies. My hypothesis is that development of targeted therapies against FXII-FXI axis, which does not seem vital for survival of humans or mice,[535,536] may help mitigate the development of DIC while maintaining extrinsic pathways-initiated thrombin generation and fibrin formation necessary to maintain blood-vessel barrier, bacterial clearance and healing.



The short-term goals for my PhD dissertation were to develop my skills in the effective design and execution of experiments that will succinctly address pertinent gaps in medical knowledge, maintain collaborative inter-disciplinary research investigations, and enhance my communication skills, all of which are required for my career as an independent researcher and a physician-scientist. To this effect, outside of the longer-term main projects, I have sought-out and completed two separate collaborative shorter pilot studies with surgical and transfusion medicine teams, Chapter 7, and an industry collaborator, Chapter 8.

As part of the clinical quality-control team, I used the knowledge gained and approaches developed to assess therapeutic utility of a transfusion reagent subjected to different physiological forces within the hospitals pneumatic tubing transport system, as described in Chapter 7. Through this time-pressed experience, I learned a significant amount about platelet concentrate preparation and storage at the American Red Cross as well as vital logistics within a hospital. While mostly negative, our data suggested that pneumatic tubing platelet concentrate transport may affect initial platelet-VWF recruitment (section 1.4.1). In my opinion, our findings and the lack of the exact guidelines for transport of this vital transfusion reagent, warrant a closer look at the practice of platelet concentrate units transport within different hospitals and at the clinical outcomes of using platelet concentrate units after different types of transport in vulnerable patient populations lacking platelet adhesion initiation.

Alongside a team of industry electrical and material engineers, I worked to develop a design of a new point-of-care microfluidic platform compatible with detection of blood flow with an internal electrical chip, Chapter 8. A number of design variations were tested, leveraging the speed of electrical read out versus physiologically-relevant blood reaction dynamics of blood pumped through the system by passive capillary flow. In Chapter 8 we report a potential utility of one of the designs to assess clinically important blood parameters of hemostasis and thrombosis. We believe this technology has potential in facilitating rapid testing of patient capillary blood hematocrit and coagulation properties at

bedside in a clinic or even at home and may be of use for chronic monitoring without necessitation of venous blood draws nor hospital visits.

Collectively, this dissertation provides new study platforms and insights into the blood reaction dynamics, such as contact activation of the coagulation cascade and platelet activation and aggregation under shear flow. In the next two sections, we describe future work directions focused on characterization of novel pro-coagulant molecules, Section 9.2, and blood reactions in the presence of normal and aberrant endogenous regulation, Section 9.3. These studies will serve as an elaboration of existing studies and microfluidic platform designs with the goal of discovering safer anti-coagulation therapies for different disease settings.

## 9.2 Discovery of novel pro-coagulant and pro-thrombotic molecules

Most of our mechanistic work described in this dissertation, has focused on the role of coagulation factor (F)XI activation by activated FXII and its role in thrombin generation and fibrin formation. Recently, Drs. John H. Griffin and Hiroshi Deguchi (The Scripps Research Institute, La Jolla, CA), have used exome genotyping to identify a potential link between a family of endogenous molecules, muscle myosins, and venous thrombo-embolic complications as pertinent to trauma population.[540]

As an MD/PhD student, my ultimate goal is to become an effective practicing physician-scientist and to add to the understanding of human disease pathophysiology, which can then be used to design and implement therapeutic interventions. Inspired by my personal interest in trauma and surgery and with the encouragement of my mentor, Dr. Owen McCarty, I pursued an opportunity to join the Griffin group in La Jolla for a 6-month fellowship where I got to actively contribute to this new direction of coagulation research as well as learn new techniques and concepts.

This prompted a series of ongoing collaborative studies combining collective expertise in blood reaction dynamics. Our future directions include using developed techniques and our joint effort to study blood reaction dynamics in the presence of different types and forms of myosins and related proteins. *Section 9.2.1* highlights our published manuscript studying the role of skeletal myosin in thrombin generation and *Section 9.2.2* describes our ongoing efforts in understanding the role of cardiac myosin in formation and stability of a fibrin-rich clot. This work may be of value to understanding and mitigating thrombo-embolic complications in the setting of trauma and heart disease.

9.2.1 *Prothrombotic skeletal muscle myosin directly enhances prothrombin activation by binding factors Xa and Va*

Hiroshi Deguchi, Ranjeet K. Sinha, Patrizia Marchese, Zaverio M. Ruggeri,

Jevgenia Zilberman-Rudenko, Owen J.T. McCarty, Mitchell J. Cohen, John H. Griffin

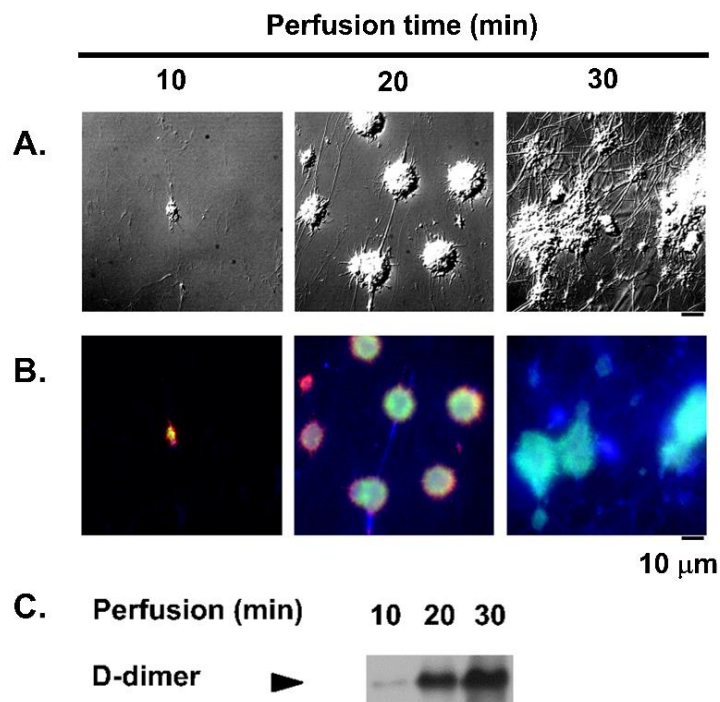
Part of Section 9.2.1 were published in *Blood*, Oct 2016;128(14):1870-1878

Permission is not required by the publisher for this type of use.

Thrombin is generated in blood by proteolytic activation of prothrombin by factor (F)Xa, FVa, and Ca<sup>2+</sup> assembled on a suitable surface.[45,541] Insufficient or excessive thrombin generation is associated with bleeding or thrombosis, respectively. Knowledge of the molecular surfaces that regulate thrombin generation is essential. Recent studies emphasize that thrombin generation primarily occurs at the site of damaged endothelium and exposed subendothelium, not primarily on the membranes of activated platelets.[542,543] Thus, damaged cells, subendothelial basement membranes, and damaged tissues may provide procoagulant surfaces that contribute to thrombin generation.

A variety of molecular and structural elements distinct from phosphatidylserine or phospholipid membranes are procoagulant, including collagens that are prothrombotic via both platelet activation[235,544,545] and contact activation mechanisms.[546,547] Murine and primate *in vivo* thrombosis model studies[140,548] are consistent with prothrombotic mechanism for collagens. Collagens bind FIX[549] and a mouse model with a variant of FIX defective in collagen binding manifests impaired hemostasis.[542] Laminins are procoagulant via both platelet activation and contact activation.[140,234,235,545–550] Polyphosphates and polynucleotides support contact activation and other procoagulant reactions,[45,551] but none of these enhances prothrombinase activity.

In a pilot exomics rare variant genotyping study targeting low frequency exomic variants for their potential association with venous thrombosis,[540] we linked a cluster of skeletal muscle myosin heavy chain gene rare missense variants to venous thrombosis. But myosin is not a member of any conventional pathway affecting thrombosis or hemostasis. Thus, here we tested the hypothesis that myosin can directly influence blood coagulation and thrombosis. *Ex vivo* studies of the effects of myosin on thrombogenesis in fresh human blood were conducted and showed that addition of myosin to blood augmented the thrombotic responses of human blood flowing over collagen-coated surfaces ( $300\text{ s}^{-1}$  shear rate). Perfusion of human blood over myosin-coated surfaces also caused fibrin and platelet deposition, evidencing myosin's thrombogenicity (Figure 9.1).

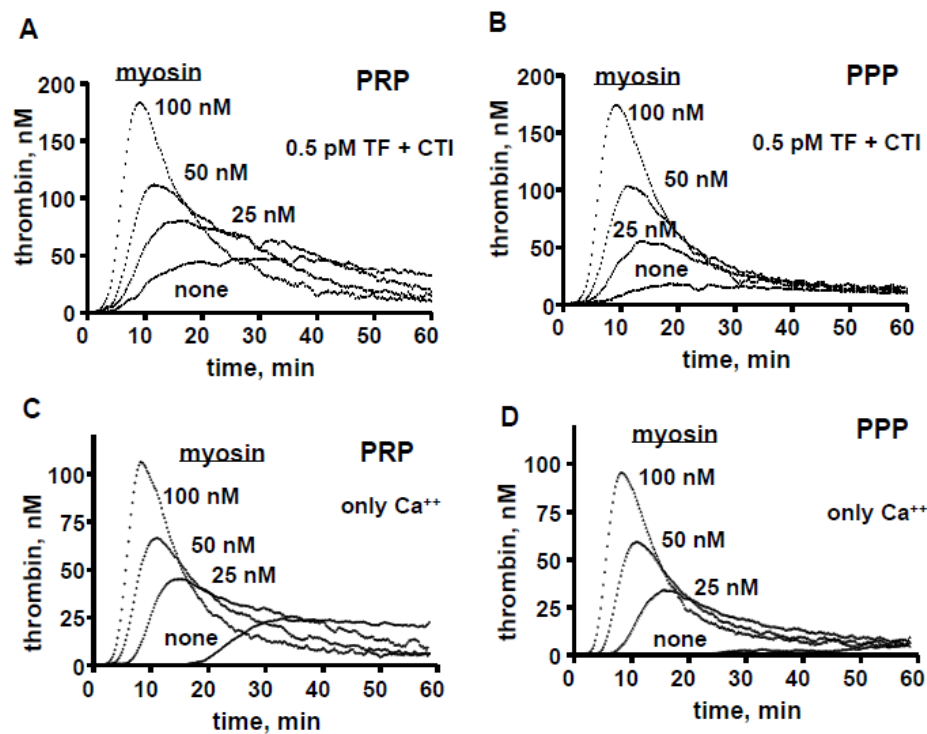


**Figure 9.1 Fibrin deposition and platelet aggregation on myosin.** Recalcified whole blood was perfused over myosin-coated chambers for indicated perfusion times at  $300\text{ s}^{-1}$  shear rate. Images of local thrombi formed at each time point were recorded using differential interference contrast (A) or fluorescent light microscopy (B) after staining for fibrin (blue), P-selectin (green) and integrin  $\alpha$ -IIb (red). In parallel experiments, thrombi formed by corresponding perfusion time points were lysed and immunoblotted for the fibrin degradation product, D-dimer (C).

Myosin markedly enhanced thrombin generation in both platelet rich plasma and platelet poor plasma, indicating that myosin promoted thrombin generation in plasma primarily independent of platelets (Figure 9.2). In purified reaction mixtures composed only of FXa, FVa, FII (prothrombin) and

calcium ions, myosin greatly enhanced prothrombinase activity. The GLA domain of FXa was not required for myosin's prothrombinase enhancement.

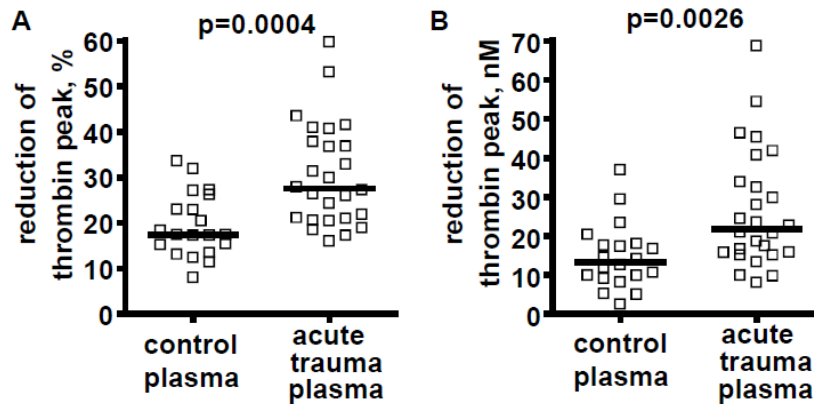
When binding of purified clotting factors to immobilized-myosin was monitored using Bio-Layer Interferometry, FXa and FVa each showed favorable binding interactions. FVa reduced by 100-fold the apparent  $K_d$  of myosin for FXa ( $K_d \sim 0.48$  nM), primarily by reducing  $k_{off}$ , indicating formation of a stable ternary complex of myosin:FXa:FVa.



**Figure 9.2 Skeletal muscle myosin promotes thrombin generation in platelet rich plasma and platelet poor plasma.**

Freshly prepared PRP and PPP (30  $\mu$ l) from the same donor was incubated with various indicated concentrations of myosin for 10 min at 37°C. Then, fluorogenic thrombin substrate solution (I-1140) either with TF (Innovin, final 0.5 pM) and CaCl<sub>2</sub> (final 11 mM) or with CaCl<sub>2</sub> alone (final 11 mM) was added to the plasma/myosin mixture (total final volume 110  $\mu$ l) to initiate thrombin generation at 37°C. For TF-induced thrombin generation assays using PRP and PPP, corn trypsin inhibitor (CTI) (final 50  $\mu$ g/mL) was added to freshly prepared PRP and PPP immediately after blood was processed to obtain PRP and PPP. Thrombin generation was followed continuously using a SPECTRAMax GEMINI XS fluorometer (Molecular Devices, Sunnyvale, CA) with excitation and emission wavelengths set at 360 and 460 nm, respectively. The first derivative of fluorescence versus time was used to produce thrombin generation curves with the correction for substrate consumption and inner filter effect.<sup>20</sup> Thrombin generation is shown for PRP plus 0.5 pM TF-Ca<sup>2+</sup> and CTI (A) or for only Ca<sup>2+</sup> addition (C), or for PPP plus 0.5 pM TF-Ca<sup>2+</sup> and CTI (B) or for only Ca<sup>2+</sup> addition (D). The same sets of experiments were done for four different adult healthy blood donors, and data for one donor's PRP and PPP are shown.

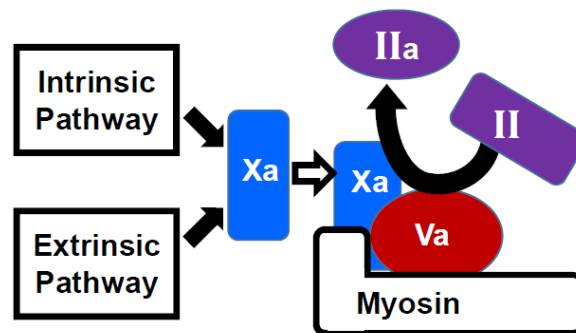
In studies to assess possible clinical relevance for this discovery, we found that anti-myosin antibodies inhibited thrombin generation in acute trauma patient plasmas more than in control plasmas, implying myosin might contribute to acute trauma coagulopathy (Figure 9.3).



**Figure 9.3 Anti-myosin antibody-induced reduction of thrombin peak values observed for acute trauma coagulopathy plasmas and normal control plasmas following tissue factor/ $\text{Ca}^{2+}$  ion addition.**

The effects of anti-myosin antibodies on the 0.1 pM TF-induced peak of thrombin generation in plasmas from acute traumatic coagulopathy patients (N=26) and healthy controls (N=20) were tested using either polyclonal antiserum against myosin heavy and light chains or nonimmune control antiserum, respectively (2 mg/mL protein). The graphs show the reduction of thrombin peak values by anti-myosin antibodies either as percent of control peak (A) or in absolute concentration of the thrombin peak (B). Bars indicate median values.

In summary, we report the remarkable direct effects of skeletal muscle myosin on thrombin generation and fibrin formation in *ex vivo* studies of flowing human blood and *in vitro* in thrombin generation assays using both plasma assays and purified prothrombinase assays due to myosin's ability to bind FXa and FVa (Figure 9.4). We posit that myosin enhancement of thrombin generation could contribute either to promote hemostasis or to augment thrombosis risk with consequent implications for myosin's possible contributions to pathophysiology in the setting of acute injuries.



**Figure 9.4 Thrombin generation can be driven by prothrombin activation on the surface of myosin which binds FXa & FVa.** The intrinsic and extrinsic coagulation pathways converge at the generation of factor (F)Xa which is the key enzyme that activates prothrombin. As depicted here, both FXa and its cofactor, FVa, bind to myosin which potently promotes prothrombin activation to generate thrombin. Extensive data in this report lead to this novel scheme for prothrombin activation which may occur on the surface of myosin independent of any particular cell surface.

### 9.2.2 *Role of cardiac myosin promoting thrombin generation and tissue plasminogen activator-induced plasma clot lysis*

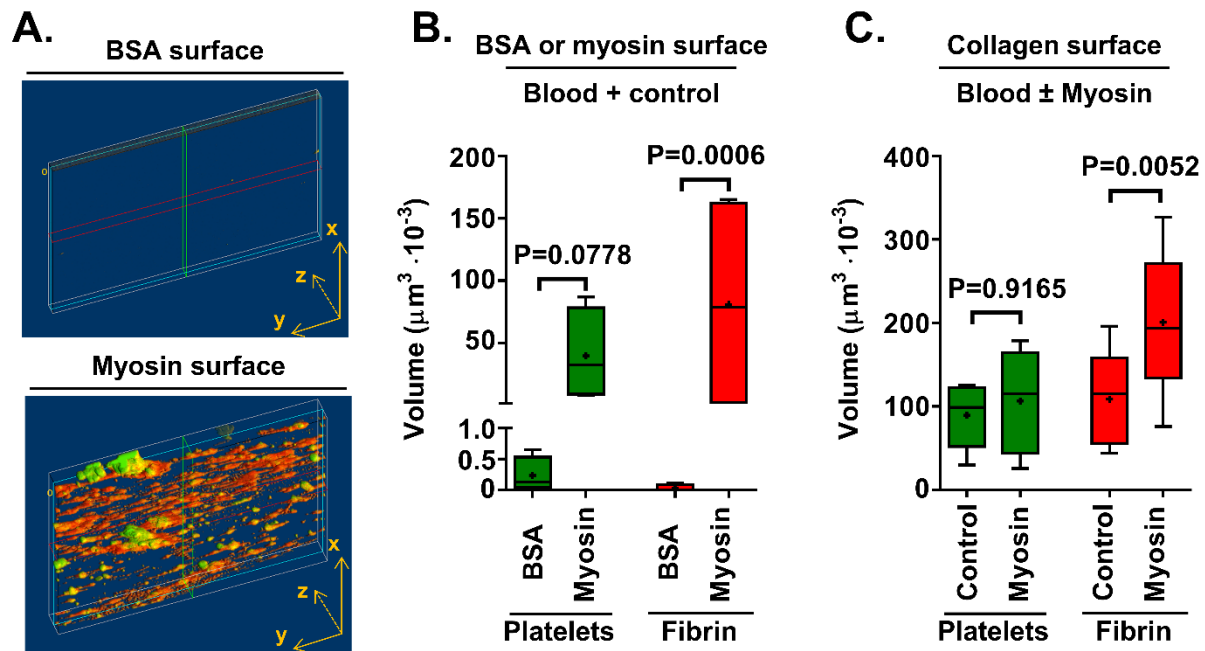
Studies during the past decades have identified cardiomyocytes as targets for the action of thrombin and in fact it has been shown that protease-activated receptor (PAR)-1, a high-affinity receptor for thrombin, is one of the most prevalent receptors expressed by cardiomyocytes.[552,553] Recently we discovered that skeletal muscle myosin, which is in the same family as cardiac myosin, exerts prothrombotic effects by binding factor (F)Xa and enhancing prothrombin activation and thrombin generation in the presence of FVa (Section 9.2.1).[279] Thus, it is possible that muscle myosin may play a role in increasing probability of trauma patients developing potentially deadly thrombotic complications affecting perfusion of the heart muscle (MI) or brain (stroke).

The timing of intervention to achieve organ reperfusion has been shown to be important. For MI, complex algorithms exist to weigh risk-to-benefit ratios for employing therapies for different patients to limit thrombin generation and platelet activation as well as lysis of fibrin mesh.[554,555] Thus, there is a need to identify markers and mechanisms to help stratify patient groups and increase safety of interventions in the setting of trauma and a potential for MI. Increased cardiac myosin gene expression has been previously associated with human heart failure.[556] Increased serum levels of cardiac myosin are found in patients with MI[557] and among these higher levels of cardiac myosin are associated with worse outcomes.[558,559] Furthermore, muscle myosins molecules have been implicated in fibrinolysis inhibition,[560] which may furthermore play a role in MI interventions involving fibrinolytics such as tissue plasminogen activator (tPA) infusion.

Our current and future efforts are focusing on testing the influence of cardiac myosin on thrombus formation and fibrinolysis. We first studied the effects of cardiac myosin on thrombogenesis *ex vivo* using fresh human flowing blood; our results show that perfusion of blood over cardiac myosin-coated surfaces at  $300 \text{ s}^{-1}$  shear rate caused extensive fibrin deposition on myosin surface (Figure 9.5A top & B). Addition of cardiac myosin to blood also promoted the thrombotic responses of



human blood flowing over collagen-coated surfaces, evidence of myosin's thrombogenicity (Figure 9.5 A bottom & C).

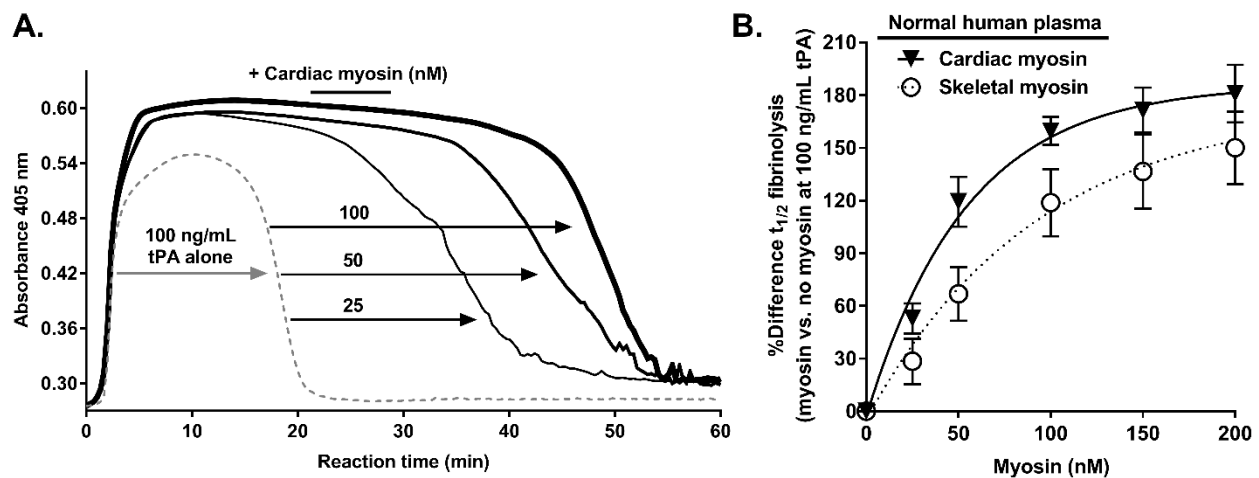


**Figure 9.5 Cardiac myosin promotes *ex vivo* thrombus formation in flowing blood.**

The thrombogenicity of myosin was studied either (A&B) when whole blood without myosin addition flowed over BSA-coated or myosin-coated surfaces or (C) when myosin (or control vehicle) was added to whole blood that then flowed over collagen-coated surfaces. Data represent observations at 4 min after flow initiation at  $300 \text{ s}^{-1}$  wall shear rate. (A) Recalcified human blood was perfused over either immobilized myosin or BSA-coated control surfaces. Three-dimensional reconstruction of platelet aggregates and fibrin on myosin or BSA coated coverslip was generated from confocal z-sections serially collected after blood perfusion. Recalcified flowing human blood contained mepacrine (green) to visualize platelets and Alexa 546-labeled anti-fibrin antibody (red) to visualize fibrin. Yellow represents superposition of corresponding images at 4 min. (B) Volumes of fibrin and platelet aggregates are shown in the box and whisker graphs (min to max values from four positions within the channel from four experiments). (C) Either cardiac muscle myosin (50 nM) or control buffer was added to recalcified blood before its perfusion over collagen-coated surface. Volumes of platelet aggregates and fibrin on collagen-coated coverslip was generated as described for panel (B) and are shown in the box and whisker graphs (min to max values from four positions within the channel from four experiments).

Our further studies showed that cardiac myosin enhanced thrombin generation in whole blood, platelet rich plasma (PRP) and platelet poor plasma (PPP), indicating that myosin promotes thrombin generation in plasma primarily independently of platelets or other blood cell components. In a purified system, composed of FXa, FVa, prothrombin and calcium ions, cardiac myosin greatly enhanced prothrombinase activity. Experiments using GLA-domainless FXa showed that the GLA domain of FXa was not required for cardiac myosin's prothrombinase enhancement in contrast to phospholipid-enhanced prothrombinase activity which requires that GLA domain.

We next studied the effect of cardiac and skeletal myosin on tPA-induced fibrin lysis in PPP. In 96-well plate static plasma clot lysis studies, increasing concentrations of cardiac and skeletal muscle myosin attenuated tPA-mediated clot lysis (Figure 9.6A & B). The ability of cardiac myosin to inhibit tPA-induced plasma clot lysis was ablated in the presence of the carboxypeptidase inhibitor (CPI) from tubers, an inhibitor of thrombin activatable fibrinolysis inhibitor (TAFI). Clot lysis assays using TAFI-deficient plasma confirmed the requirement for TAFI for the antifibrinolytic action of cardiac myosin.



**Figure 9.6 Cardiac myosin attenuates tPA-induced plasma clot lysis.**

A mixture of 100  $\mu$ L of thrombin (5 nM final),  $\text{CaCl}_2$  (17 mM final), phospholipid vesicles (60% PC: 20% PS: 20% PE; final concentration 10  $\mu$ M) diluted with HBS (20 mM HEPES, 147 mM NaCl, 3 mM KCl, pH7.4) 0.1% BSA and tPA (100 ng/mL final), was added to 100  $\mu$ L citrated normal human pooled plasma, which was pre-incubated for 30 min at 37C in the presence of vehicle buffer (HBS 0.1% BSA) or different amounts of cardiac myosin. The turbidity at 405 nm was measured at 37C for 180 min in a Thermomax microplate reader (A) and percent difference in plasma clot lysis  $t_{1/2}$  in the presence of either cardiac or skeletal myosin as compared to no myosin control condition was quantified (B).

Trauma-induced coagulopathy and fibrinolytic shutdown is frequently detected on clinical thromboelastography (TEG; Section 1.3.5) tests in severely injured patients. Fibrinolysis shutdown, as detected by decreased percent of lysis within a set time post maximum clot amplitude (MA) on TEG, has been associated with an increased incidence of thrombotic complications and mortality,[561] but the mechanism of inhibition of fibrinolysis remains unclear. We next examined whether the effects of skeletal and cardiac muscle myosins on coagulation and fibrinolysis *in vitro* using TEG. Whole blood was collected from healthy volunteers and citrated native TEGs were performed to evaluate the global

coagulation response (reaction, R, time, coagulation angle, MA) and percent of lysis 30 and 60 minutes after MA (LY30 and LY60 respectively) in the presence of skeletal or cardiac muscle myosin (100 nM). This was performed in the presence or absence of 50 ng/mL of tPA and compared with a control buffer. Our preliminary results showed that cardiac and skeletal muscle myosins were able to significantly shorten the R time in line with enhanced prothrombinase activity. Myosins did not significantly affect clot angle (dependent on fibrinogen levels) nor MA (platelet-dependent value). While the lysis percent decrease in the presence of myosin varied among donors, both cardiac and skeletal myosins produced a tendency towards lower percent clot lysis in the presence of tPA. Of note, in both experimental set ups (96-well PPP fibrin formation and lysis as well as whole blood TEGs) tPA was added at the beginning of the reaction. Thus, findings from these studies would not necessarily predict an existing thrombus susceptibility to tPA-induced lysis.

Due to complexity of human physiology and different comorbid factors, the link between trauma and heart disease has been debated for over a century.[562] Blunt trauma to the chest has been associated with myocardial infarction (MI; thrombotic occlusion of coronary arteries supplying the heart muscle) in healthy adults.[563,564] Furthermore, there is mounting evidence that any traumatic incapacitation of a patient can increase the probability of a patient developing potentially deadly thrombotic complications such as MI and stroke.

Our work thus far shows that cardiac myosin is both procoagulant and anti-fibrinolytic due to its ability to bind FXa and strongly promote thrombin generation. We hypothesize that cardiac myosin-dependent thrombin generation increases TAFI activation and subsequent inhibition of clot lysis, which may potentiate the clot stability and resistance to pharmacological lysis by tPA in injured coronary arteries. This line of work raises new questions about potential procoagulant functions for cardiac myosin in coronary health and disease.

### 9.3 Development of microfluidic platforms to study blood reaction dynamics at the vessel wall

The shear-dependent binding of the platelet receptor glycoprotein (GP)Ib to von Willebrand Factor (VWF) is requisite for the initial step of platelet recruitment to damaged vessel wall under flow.[531,532] The production of VWF as well as other important pro- and anti-thrombotic proteins by endothelial cells is a highly regulated process *in vivo* (Section 1.5). Our future directions include development of a range of endothelialized flow chamber designs to study complex dynamics of cells and proteins at the blood-vessel interface and within the subendothelial compartment. *Section 9.3.1* highlights primary data collected using techniques developed during this ongoing effort and *Section 9.3.2* describes technical aspects and study potential for the endothelialized flow platforms.

#### 9.3.1 *Removal of the C-terminal domains of ADAMTS13 by activated coagulation factor FXI induces platelet adhesion on endothelial cells under flow conditions*

Kathleen S. Garland, Stephanie Reitsma, Toshiaki Shirai, Jevgenia Zilberman-Rudenko, Erik I. Tucker, David Gailani, András Gruber, Owen J.T. McCarty, Cristina Puy

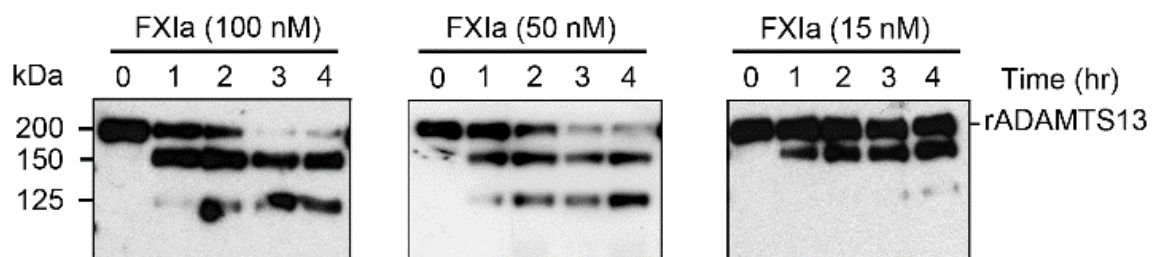
Parts of Section 9.3.1 were published in *Frontiers Medicine*, Dec 2017;4:232[eCollection]

Permission is not required by the publisher for this type of use.

Platelet recruitment to sites of vascular injury is mediated by von Willebrand factor (VWF). The shear-induced unravelling of ultra-large VWF multimers causes the formation of a “stringlike” conformation, which rapidly recruits platelets from the bloodstream. A disintegrin and metalloproteinase with a thrombospondin type 1 motif, member 13 (ADAMTS13) regulates this process by cleaving VWF to prevent aberrant platelet adhesion; it is unclear whether ADAMTS13 itself is regulated.

The serine proteases  $\alpha$ -thrombin and plasmin have been shown to cleave ADAMTS13. Based on sequence homology, we hypothesized that the activated coagulation factor XI (FXIa) would likewise

cleave ADAMTS13. Our results show that FXIa cleaves ADAMTS13 at the C-terminal domains, generating a truncated ADAMTS13 with a deletion of part of the thrombospondin type-1 domain and the CUB1-2 domains (Figure 9.7), while thrombin cleaved ADAMTS13 near the CUB1-2 domains and plasmin cleaved ADAMTS13 at the metalloprotease domain and at the C-terminal domain. Using a cell surface immunoassay, we observed that FXIa induced the deletion of the CUB1-2 domains from ADAMTS13 on the endothelial cell surface.

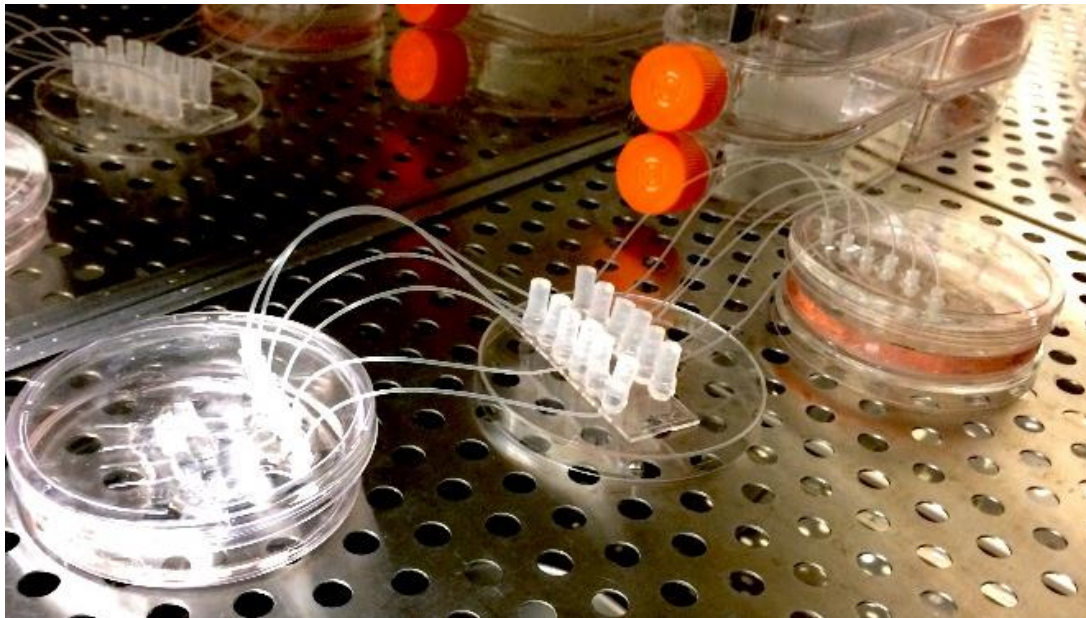


**Figure 9.7 Proteolysis of ADAMTS13 by FXIa.**

rADAMTS13 (250 nM) was incubated with FXIa (100-15 nM) for selected times (0-4 hours) at 37°C. MTS13 forms was analyzed by western blotting using an anti-ADAMTS13 MET domain antibody.

Prior studies have shown that ADAMTS13 binds endothelial cells in a specific manner and that the cleavage of VWF by ADAMTS13 occurs mainly at the EC surface.[565] It has further been proposed that the binding of the ADAMTS13 TSP7-CUB2 domain to the VWF D4CK domains induces a conformational activation of ADAMTS13, causing ADAMTS13 to unfold fully and expose the spacer domain.[566] The spacer domain can then directly interact with the VWF A2 domain, enhancing the cleavage of VWF by ADAMTS13 under flow conditions. Removal of the C-terminal of ADAMTS13 domains was also shown to abrogate the capacity of ADAMTS13 to bind and cleave VWF under flow conditions *ex vivo*[567] and *in vivo*.[568] Thus we next studied whether cleavage of the TSP6-8 and the two C-terminal CUB domains of ADAMTS13 by FXIa, or the cleavage of the CUB 1-2 domains of ADAMTS13 by  $\alpha$ -thrombin might abrogate ADAMTS13 activity under flow by assessing the length of VWF that had been released by activated endothelial cells under shear.

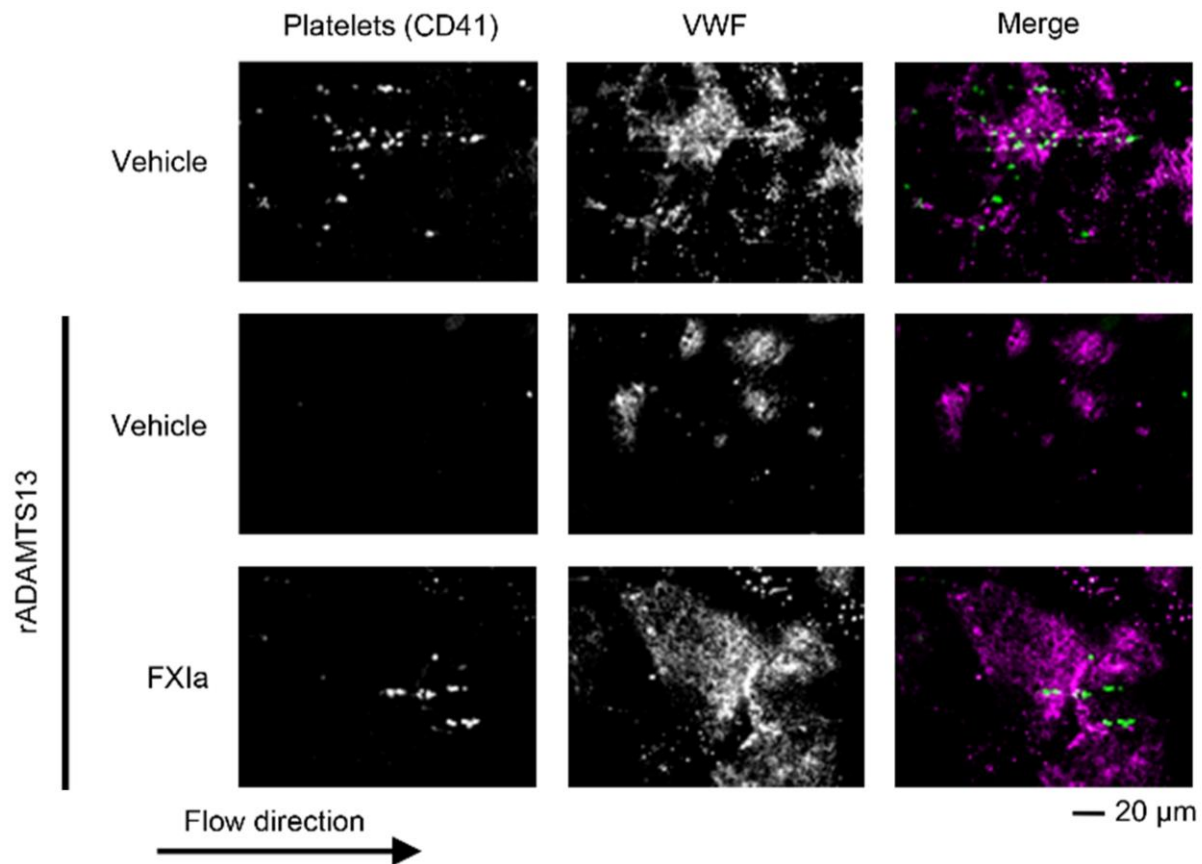
To study ADAMTS13 regulation in the presence of endothelial cells under shear flow, HUVECs were cultured in the parallel-plate flow chamber (ibidi  $\mu$ -slide VI<sup>0.1</sup>) under shear conditions ( $1000 \text{ s}^{-1}$ ) beginning 48 hours before the flow experiment. Devices were incubated with cells for 30 minutes prior to induction of passive flow by adding growth medium to the inflow port of each channel. Passive flow was maintained by emptying the outflow and refilling the inflow for 1 hour or until morphology changes of HUVECs, from round to elongated, was noted. Inflow ports of the flow devices were then connected to a growth medium well and the outflow ports were connected to a waste well. All six channels were connected to the same growth medium well and the outflowing growth medium was recirculated in a specially-designed Spider<sup>JZR</sup> culture system to achieve comparable EC confluency in each channel (Figure 9.8). The height of the medium well was maintained to achieve an initial flow rate of  $20 \mu\text{L}/\text{min}$  for 48 hours or until confluence. The day of the experiments, HUVECs were starved in serum free media (SFM) for 2 hours, and then stimulated with  $10 \text{ ng}/\text{mL}$  TNF $\alpha$  in SFM supplemented with 3% fatty acid-free bovine serum albumin (BSA) for 4 hrs to induce VWF release.



**Figure 9.8 Spider<sup>JZR</sup> culture system.**

All channels seeded with endothelial cells are simultaneously cultured under shear with flow of media promoted by gravity.

Human whole blood was drawn by venipuncture into 3.8% sodium citrate from a healthy donor per institutional IRB protocol and washed platelets were purified as previously described.[569] Washed platelets ( $3 \times 10^8/\text{mL}$ ) in the presence or absence of rADAMTS13 (2.5 nM) were perfused through the flow chamber for 10 minutes at  $2.5 \text{ dyne}/\text{cm}^2$  and platelet-VWF string formation was visualized by staining for CD41 (green) and VWF (far red). Using this endothelialized flow study set up, we were able to observe that the addition of 2.5 nM full-length rADAMTS13 abrogated platelet-VWF string formation (Figure 9.9 and Figure 9.10).



**Figure 9.9 FXIa inhibits ADAMTS13 cleavage of VWF.**

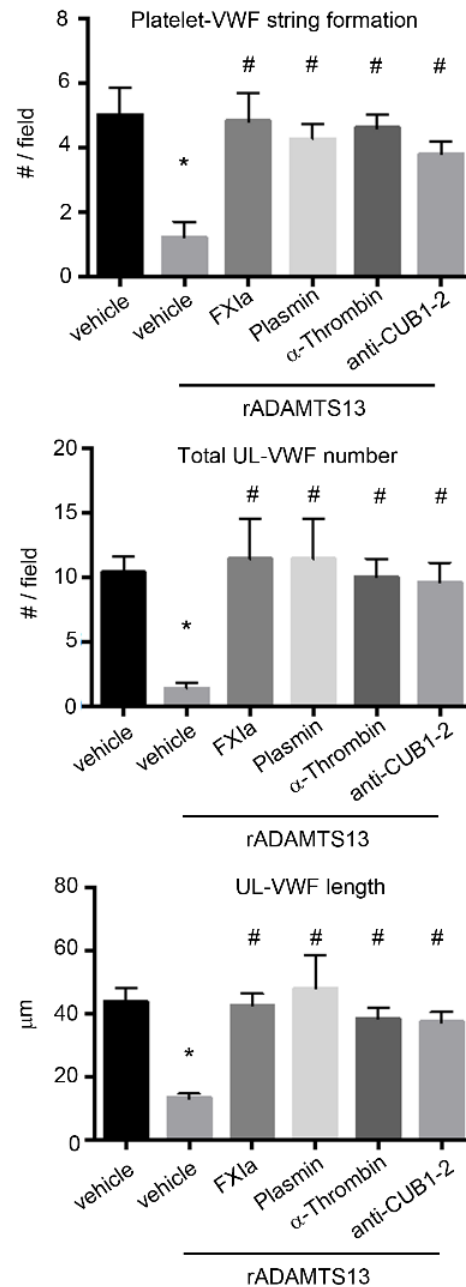
rADAMTS13 (250 nM) was incubated at  $37^\circ\text{C}$  for 4 hours with the following: FXIa (50 nM),  $\alpha$ -thrombin (50 nM) and plasmin (50 nM) in HBS with 5 mM  $\text{CaCl}_2$ . Reactions were stopped with aprotinin (50  $\mu\text{M}$ ) and hirudin (10  $\mu\text{g}/\text{mL}$ ). Endothelialized parallel-plate flow chambers were prepared and EC's were stimulated with  $\text{TNF}\alpha$  to release VWF. VWF string formation and platelet adhesion depicted with fluorescence following perfusion of washed platelets at a venous flow rate of  $2.5 \text{ dyne}/\text{cm}^2$  in the absence or presence of rADAMTS13 (2.5 nM) incubated with either vehicle, FXIa,  $\alpha$ -thrombin, plasmin, or an anti-ADAMTS13 CUB domain antibody (20  $\text{ng}/\text{mL}$ ).



In contrast, the incubation of rADAMTS13 with FXIa reversed ability of ADAMTS13 to cleave VWF, resulting in an increase in the formation of platelet-VWF strings. A similar effect was observed when rADAMTS13 was incubated with either  $\alpha$ -thrombin or plasmin. Interestingly, the addition of an anti-ADAMTS13 CUB1-2 domain antibody also blocked ADAMTS13 activity under flow (Figure 9.9 and Figure 9.10).

This data suggests, that removal of the C-terminal domain of ADAMTS13 by FXIa or thrombin caused an increase in ADAMTS13 activity as measured by using a fluorogenic substrate and blocked the ability of ADAMTS13 to cleave VWF on the endothelial cell surface, resulting in persistence of VWF strands and causing significant increase in platelet adhesion under flow conditions (Figure 9.9 and Figure 9.10).

Utilizing this *in-vitro* endothelialized flow chamber technique, we were able to demonstrate a novel mechanism for coagulation proteinases including FXIa in regulating ADAMTS13 activity and function. This may represent an additional hemostatic function by which FXIa promotes local platelet deposition at sites of vessel injury (Section 1.3.5).



**Figure 9.10 FXIa, thrombin and plasmin inhibit ADAMTS13 cleavage of VWF.** TNF $\alpha$ -stimulated ECs were perfused and visualized as above (Figure 9.9). Platelet string formation, total VWF number, and VWF length were quantified and compared between noted substrates. Using Dunnett's multiple comparison test, \* and # indicate statistical significance ( $p < 0.05$ ) between vehicle groups and vehicle-rADAMTS13 and treatment groups, respectively. Data are mean  $\pm$  SEM ( $n = 3$ ).



### 9.3.2 *Development of a new 3D-endothelialized microfluidic model to study hemostasis*

Jevgenia Zilberman-Rudenko, Joanna L. Sylman, Kathleen S. Garland, Cristina Puy,

Andrew D. Wong, Peter C. Searson, Owen J.T. McCarty

Parts of Section 9.3.2 were published in *Platelets* March 2017;28(5):449-456

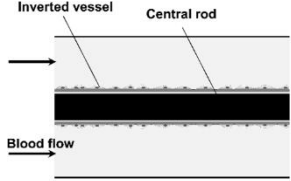
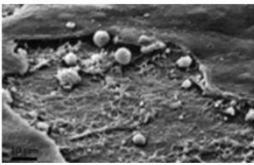
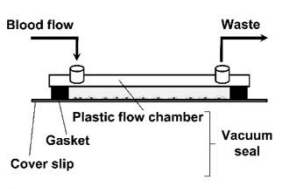

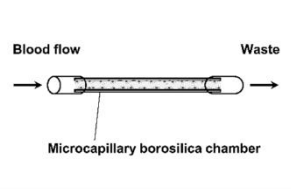

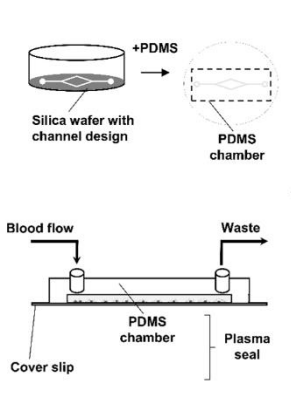


Permission is not required by the publisher for this type of use.

Microfluidic device technologies are useful for the studies of the dynamic interactions of platelets and ECs under flow conditions.[272,570,571] Current and developing flow chamber design models (Table 9.1) allow for mechanistic studies of platelet adhesion to the vessel wall at sites of injury or inflammation. Endothelialized microfluidic devices have been utilized to demonstrate that shear stress is an important factor in regulating endothelial barrier integrity and vessel patency. In these models, the parameters of geometry, compliance, biorheology and cellular complexity can be varied to recapitulate the physical biology of platelet recruitment and activation under physiologically relevant conditions of blood flow.

Advances in microfluidic device design allow for high-throughput and dynamic real-time studies of cellular and molecular mechanisms that regulate platelet-endothelium interactions in disease states ranging from atherosclerotic plaque formation to sepsis and cancer angiogenesis and metastasis (Table 1.7). In section 9.3.1 we used one of the commercially available parallel-flow 6-channel devices (Table 9.1). Our future directions include development of new polydimethylsiloxane (PDMS)-based endothelialized platforms for studies that may provide insight into the (patho)physiology of different disease states and serve as an expedient platform for therapy design and testing.

## Basic set up

## Notes

|  |   |   |
|--|---|---|
| <p><b>Annular</b></p>                     |    | <p><b>Advantages:</b> Use of native vessel layers to study the platelet-endothelium interface.</p> <p><b>Limitations:</b> Visualization requires histologic processing; use requires large volumes.</p> <p><b>Major findings:</b> von Willebrand Factor (VWF)-VIII complex mediates platelet adhesion to denuded vessels under shear.[531,532,572]</p> <p>Platelet internalization of recombinant coagulation factor VII.[573]</p>  |
| <p><b>Parallel-plate</b></p>              | <p><b>Chambers</b></p>   | <p><b>Advantages:</b> Real-time studies of platelet-endothelium interaction under shear; simple set-up.[270,574–576]</p> <p><b>Limitations:</b> Non-compliant, non-gas permeable, macroscopic scale, expensive fabrication of microvessel network geometry.[577–579]</p> <p><b>Major findings:</b> Identification of the roles for platelet receptors under shear, for instance a shear-dependent role for the platelet receptor GPIb in the pathophysiology of Bernard-Soulier syndrome (BSS);[152,155,158–160,580]</p>  |
| <p><b>Microcapillaries</b></p>            |    | <p>VWF multimer processing by ADAMTS13 under shear.[163,164,166–168]</p> <p>Effect of shear on endothelial barrier function and receptor expression.[265,272,581,582]</p>   |
| <p><b>Compliant chambers (PDMS)</b></p>  | <p><b>Single channel</b></p>  <p><b>Network</b></p>  | <p><b>Advantages:</b> Compliant, gas permeable and cost-effective material; ability to form microscale vessels; study of 3D cylindrical channels surrounded by an ECM layer; study complex blood vessel network biorheology, shear gradients and platelet distribution.[225,314,571,583–593]</p> <p><b>Limitations:</b> Potential for the absorption of hydrophobic or toxic substances by PDMS after prolonged use;[594,595] limitation in high Reynold number flow designs.[22]</p> <p><b>Major findings:</b> Role of shear on VWF multimer expression and processing and VWF-mediated platelet aggregation on an intact endothelium immediately downstream of a region of high shear stress.[266,596,597]</p> <p>Identification of specific ADAMTS13 domains required for VWF processing.[598]</p> <p>Study of endothelial barrier leak under (patho)physiological conditions.[599–602]</p> <p>Effect of vessel geometry and flow disturbance on EC morphology,[603] EC receptor expression profile.[264,604] and thrombus formation.[267,605,606]</p> <p>Study of complex microvasculature networks and bioreactors.[226,607–610]</p> |

**Table 9.1 Summary of perfusable endothelialized models.**

Diagrams and photographs of the basic set up for various microfluidic techniques are summarized. Advantages, limitations, and major findings are listed for each platform. For annular perfusion model, an electron microscopy image of a processed vessel section post perfusion is shown.[166]

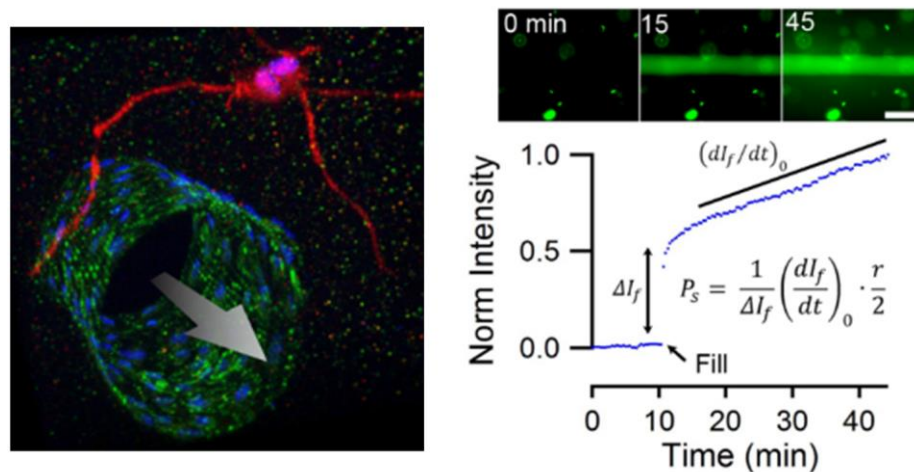
The advent of the use of an optically-clear, inert, non-toxic, gas permeable and cost-effective polydimethylsiloxane (PDMS) polymer for the production of flow chambers in the 1990s expanded device design capabilities to nanometer dimensions.[583–586] Building on a broad knowledge of biorheology, channels were designed to achieve specified shear and specific flow dynamics, and printed onto a master mold using photolithographic techniques. Microfluidic devices are typically prepared by plasma or vacuum bonding the PDMS chambers, made by curing PDMS over master molds, onto a microscope cover slip.[314] The use of a compliant material such as PDMS helped to mimic vessel deformation and changes in blood viscosity due to shear thinning and pressure drops found in the microvasculature *in vivo* under high-flow conditions.[587–589]

Endothelialized PDMS microfluidic devices have facilitated simultaneous studies of multiple shear conditions from high physiologic to pathologic rates of  $500 - 30,000 \text{ s}^{-1}$ , regimes which have been shown to promote VWF multimer formation.[596,597] A channel design mimicking vessel narrowing, such as occurs due to atherosclerotic plaque formation, tested in parallel to an *in vivo* murine model of atherosclerosis has shown that vessel constriction leads to increased VWF release and VWF-dependent platelet aggregation to the intact endothelium immediately downstream of the constriction.[266] Mechanistic studies have utilized PDMS-based platforms to define the ADAMTS13 domains required for VWF cleavage.[598] PDMS microfluidic platforms offer a great potential for development of targeted therapies for the treatment of patients with debilitating chronic TTP by allowing high throughput screening of known ADAMTS13 mutations.[611]

Another advantage of PDMS microfluidic technology is the ability to have user-defined spatial control of the microenvironment properties. For instance, these platforms allow for the control of the spatial organization of surface coatings of adhesive or ECM proteins, cells and the controlled release of agonists and inhibitors.[225,590–593] As an example, in one study human umbilical ECs were focally injured by an electrode in order to study the interaction of platelets with activated and adjacent healthy ECs.[612] The results showed that while activated ECs lost their tight junctions and released

their Weibel-Palade bodies to promote platelet recruitment and adhesion, ECs upstream and downstream of the site of focal injury maintained their quiescence state and barrier function under physiological flow conditions.

ECs play an important role in the progression of many diseases including sepsis and cancer, both of which are multi-faceted dynamic processes. In sepsis, the dysfunction of vascular ECs has been correlated with multiple organ failure and poorer outcomes.[613] Thus our goal was to borrow from the field of oncology (and specifically Drs. Peter C. Searson and Andrew Wong, Johns Hopkins, Whiting School of Engineering, Baltimore, MD) and develop a 3D perfusable, cylindrical microvessel embedded in an ECM material[571,599] to study endothelial barrier leak in the presence of blood in a quantitative and kinetic manner (Figure 9.11) with direct observations of a role for platelets in immunity-related processes within the vasculature.[599–602]



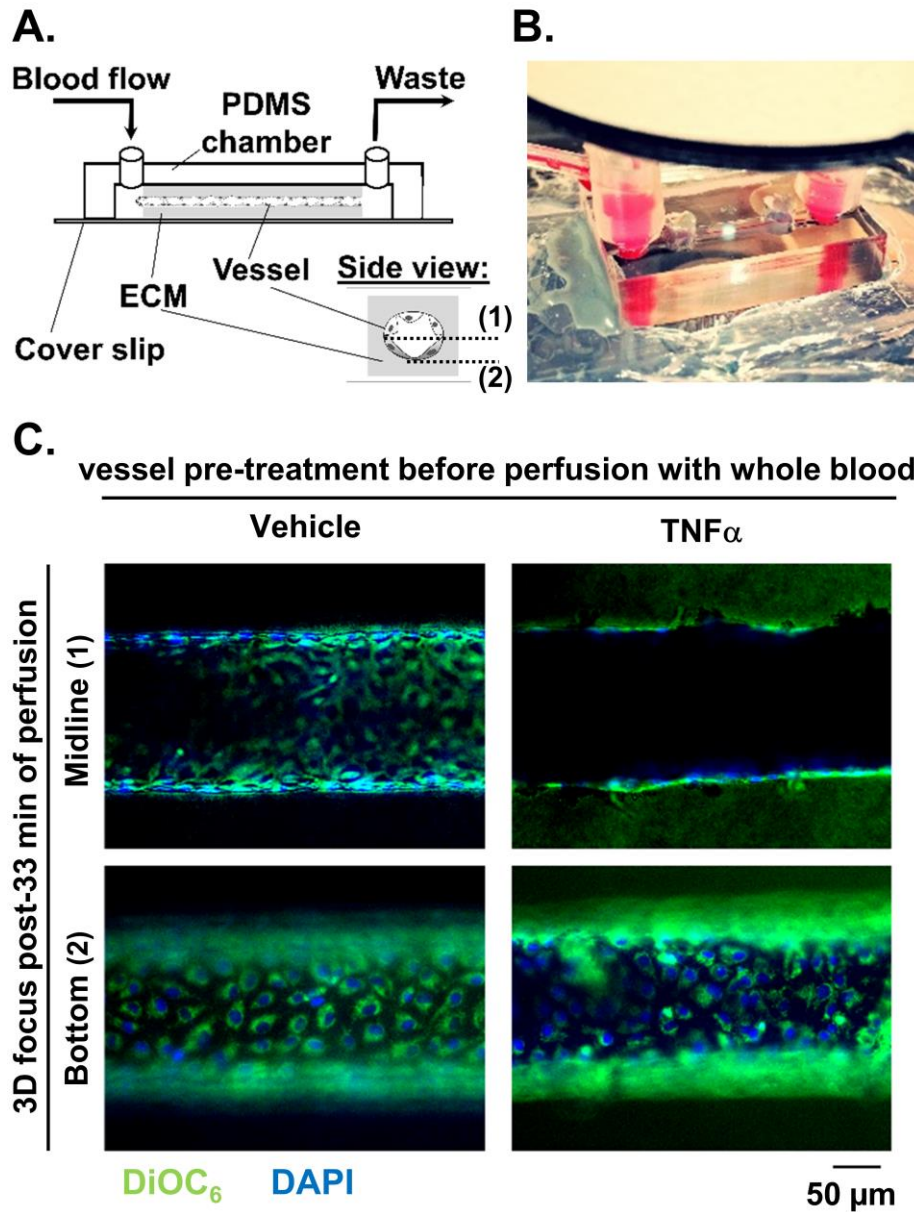
**Figure 9.11 Quantitative permeability studies.** Cylindrical perfuseable embedded vessel to study cancer cell intravasation. Early loss of EC integrity and barrier leak development can be quantitatively assessed with fluorescently-labeled BSA. Figure adapted from Wong and Searson *Cancer Research* 2014.

Due to my past work studying pathogenesis of hyperinflammatory complications in children with rare immunodeficiencies with Drs. Eric P. Hanson and Richard M. Siegel (National Institutes of Health, NIAMS), sepsis and inflammation have always been an interest of mine. Disseminated loss of barrier and vascular leak, a serious sequela of sepsis progression, leads to hypotension, hypoperfusion, tissue edema and multiorgan failure which are only temporarily attenuated with aggressive fluid

resuscitation.[240,241] Thrombin acts as a direct activator of local EC signaling including promotion of platelet aggregation on the surface of the activated endothelium and activation of ADAM10-dependent VE-cadherin proteolysis leading to endothelial cell dissociation and gap formation.[238,239] Complete inhibition of thrombin generation however has proven ineffective and dangerous, as thrombin generation and fibrin formation are important for pathogen clearance. Thus, further studies are needed to develop safer alternative anticoagulation therapies (Section 1.3.6).

As a future physician-scientist I am inspired by studies with potential to mitigate thrombo-hemorrhagic complications in patients with such complicated diseases such as sepsis. Thus, I see a tremendous need for study platforms to aid in understanding of blood-endothelium interface and I truly believe that Drs. McCarty and Gruber have an extensive expertise and great tools to study this topic. As a budding biomedical engineer I am further interested in the potential expanded capacity of incorporating a subendothelial matrix compartment in these 3D microvessel devices to further investigate metastatic cancer cell and lymphocyte intravasation and extravasation, respectively,[253,255,571] and enable the control of physical parameters such as transmural pressure and interstitial flow through the ECM[614] to study platelet-endothelium dynamics. Lastly, these microvessel chambers will exhibit a physiologically relevant cylindrical geometry, which may prove useful for the modeling of smaller diameter microvessels where curvature has been shown to affect endothelial morphology and response to shear stress.[603]

To bring the 3D perfusable microvessel technology to Oregon Health & Science University, I have ventured out to Johns Hopkins to learn the basics of this technology from Dr. Wong in one week, which is an approximate needed time (from start to finish) to construct the chamber set-up and establish a non-leaky ‘microvessel’ suspended in ECM. I then sourced the necessary equipment and materials and worked with the group to set up shop on our lucky 13<sup>th</sup> floor. Figure 9.12 depicts our preliminary results from a study looking at the role of thrombin generation and platelet aggregation in endothelial barrier leak development and repair in healthy as well as inflamed ‘microvessels’.



**Figure 9.12 The role of inflammation on platelet-endothelium interface under shear flow in 3D chamber**  
 A 3D-chamber device design (A) and experimental prototype (B) with a perfuseable cylindrical microvessel embedded in an extracellular matrix (ECM) material. Microvessel phenotype (following treatment with vehicle or 10 ng/mL TNF $\alpha$  for 4 hrs in starvation media) pre- and post- perfusion with recalcified whole blood for 33 min as visualized by differential interference contrast, DIC, (A) and fluorescence microscopy (B).

These future investigations in the presence of endothelium will extend our previous studies of the role of contact activation coagulation pathway in thrombin generation and platelet consumption to the blood-endothelium interface, providing clinically relevant insights for attenuating thrombo-hemorrhagic complications in sepsis and other disease states.

## REFERENCES

- 1 Westerhof N, Stergiopoulos N, Noble MIM. Law of Poiseuille. *Snapshots of Hemodynamics*. Boston, MA: Springer US; 2010. p. 9–14.
- 2 Klabunde RE. Cardiovascular physiology concepts. 2nd ed. Philadelphia, PA: Lippincott Williams & Wilkins/Wolters Kluwer; 2012.
- 3 Dzierzak E, Philipsen S. Erythropoiesis: development and differentiation. *Cold Spring Harb Perspect Med* 2013; **3**: a011601.
- 4 Aarts PA, Bolhuis PA, Sakariassen KS, Heethaar RM, Sixma JJ. Red blood cell size is important for adherence of blood platelets to artery subendothelium. *Blood* 1983; **62**: 214–7.
- 5 Brass LF, Diamond SL. Transport physics and biorheology in the setting of hemostasis and thrombosis. *J Thromb Haemost* 2016; **14**: 906–17.
- 6 Fogelson AL, Neeves KB. Fluid Mechanics of Blood Clot Formation. *Annu Rev Fluid Mech* 2015; **47**: 377–403.
- 7 Vahidkhan K, Diamond SL, Bagchi P. Platelet dynamics in three-dimensional simulation of whole blood. *Biophys J* 2014; **106**: 2529–40.
- 8 Yeh C, Eckstein EC. Transient lateral transport of platelet-sized particles in flowing blood suspensions. *Biophys J* 1994; **66**: 1706–16.
- 9 Fahraeus R. The suspension stability of the blood. *Physiol Rev* 1929; **9**: 241–74.
- 10 Pries AR, Neuhaus D, Gaehtgens P. Blood viscosity in tube flow: dependence on diameter and hematocrit. *Am J Physiol* 1992; **263**: H1770-1778.
- 11 Woldhuis B, Tangelder GJ, Slaaf DW, Reneman RS. Concentration profile of blood platelets differs in arterioles and venules. *Am J Physiol* 1992; **262**: H1217-1223.
- 12 Rott N. Note on the History of the Reynolds Number. *Annu Rev Fluid Mech* 1990; **22**: 1–12.
- 13 Burch GE, DePasquale NP. Hematocrit, viscosity and coronary blood flow. *Dis Chest* 1965; **48**: 225–32.
- 14 Gad-El-Hak M, Morton JB, Kutchal H. Turbulent flow of red cells in dilute suspensions. Effect on kinetics of O<sub>2</sub> uptake. *Biophys J* 1977; **18**: 289–300.
- 15 Caro CG. Transport of <sup>14</sup>C-4-cholesterol between perfusing serum and dog common carotid artery: a shear dependent process. *Cardiovasc Res* 1974; **8**: 194–203.
- 16 Kroll MH, Hellums JD, McIntire LV, Schafer AI, Moake JL. Platelets and shear stress. *Blood* 1996; **88**: 1525–41.
- 17 Lipowsky HH. Microvascular rheology and hemodynamics. *Microcirc N Y N* 1994 2005; **12**: 5–15.

- 18 Papaioannou TG, Stefanadis C. Vascular wall shear stress: basic principles and methods. *Hell J Cardiol HJC Hellēnikē Kardiologikē Epitheōrēsē* 2005; **46**: 9–15.
- 19 Yang W-J. *Biothermal-fluid Sciences: Principles and Applications*. Garland Science; 1989.
- 20 Poelmann RE, Gittenberger-de Groot AC, Hierck BP. The development of the heart and microcirculation: role of shear stress. *Med Biol Eng Comput* 2008; **46**: 479–84.
- 21 Adamo L, Naveiras O, Wenzel PL, McKinney-Freeman S, Mack PJ, Gracia-Sancho J, Suchy-Dacey A, Yoshimoto M, Lensch MW, Yoder MC, García-Cardena G, Daley GQ. Biomechanical forces promote embryonic haematopoiesis. *Nature* 2009; **459**: 1131–5.
- 22 McCarty OJT, Ku D, Sugimoto M, King MR, Cosemans JMEM, Neeves KB, Subcommittee on Biorheology. Dimensional analysis and scaling relevant to flow models of thrombus formation: communication from the SSC of the ISTH. *J Thromb Haemost* 2016; **14**: 619–22.
- 23 Ottino JM. *The kinematics of mixing: stretching, chaos, and transport*. Cambridge ; New York: Cambridge University Press; 1989.
- 24 Aref H. Stirring by chaotic advection. *J Fluid Mech* 1984; **143**: 1.
- 25 Wiggins S, Ottino JM. Foundations of chaotic mixing. *Philos Transact A Math Phys Eng Sci* 2004; **362**: 937–70.
- 26 Carson L, Doctor VM. Mechanism of potentiation of antithrombin III and heparin cofactor II inhibition by sulfated xylans. *Thromb Res* 1990; **58**: 367–81.
- 27 Liu L, Dewar L, Song Y, Kulczycky M, Blajchman MA, Fenton JW, Andrew M, Delorme M, Ginsberg J, Preissner KT. Inhibition of thrombin by antithrombin III and heparin cofactor II in vivo. *Thromb Haemost* 1995; **73**: 405–12.
- 28 Walker CPR, Royston D. Thrombin generation and its inhibition: a review of the scientific basis and mechanism of action of anticoagulant therapies. *Br J Anaesth* 2002; **88**: 848–63.
- 29 Davie EW. A Brief Historical Review of the Waterfall/Cascade of Blood Coagulation. *J Biol Chem* 2003; **278**: 50819–32.
- 30 Schmidt A. Neue Untersuchungen über die Faserstoffgerinnung. *Pflüg Arch Für Gesamte Physiol Menschen Thiere* 1872; **6**: 413–538.
- 31 Schmidt A. *Zur Blutlehre*. Vogel: Leipzig; 1892.
- 32 Arthur M, Pagès C. Nouvelle theorie chimique de la coagulation du sang. *Arch Physiol Norm Pathol* 1890; **5**: 739–46.
- 33 Shapiro SS. Treating thrombosis in the 21st century. *N Engl J Med* 2003; **349**: 1762–4.
- 34 Semple JW, Italiano JE, Freedman J. Platelets and the immune continuum. *Nat Rev Immunol* 2011; **11**: 264–74.



- 35 Engelmann B, Massberg S. Thrombosis as an intravascular effector of innate immunity. *Nat Rev Immunol* 2013; **13**: 34–45.
- 36 Pallister C, Watson M. Haematology. Banbury: Scion; 2011.
- 37 Rapaport SI, Schiffman S, Patch MJ, Ames SB. The importance of activation of antihemophilic globulin and proaccelerin by traces of thrombin in the generation of intrinsic prothrombinase activity. *Blood* 1963; **21**: 221–36.
- 38 Eaton D, Rodriguez H, Vehar GA. Proteolytic processing of human factor VIII. Correlation of specific cleavages by thrombin, factor Xa, and activated protein C with activation and inactivation of factor VIII coagulant activity. *Biochemistry (Mosc)* 1986; **25**: 505–12.
- 39 Friedman PA, Przysiecki CT. Vitamin K-dependent carboxylation. *Int J Biochem* 1987; **19**: 1–7.
- 40 Vermeer C. Gamma-carboxyglutamate-containing proteins and the vitamin K-dependent carboxylase. *Biochem J* 1990; **266**: 625–36.
- 41 Hoffbrand AV, Pettit JE, Moss PAH. Essential haematology. Oxford: Blackwell Science; 2002.
- 42 Carson SD, Brozna JP. The role of tissue factor in the production of thrombin. *Blood Coagul Fibrinolysis Int J Haemost Thromb* 1993; **4**: 281–92.
- 43 Mackman N, Taubman M. Tissue Factor: Past, Present, and Future. *Arterioscler Thromb Vasc Biol* 2009; **29**: 1986–8.
- 44 Mackman N, Tilley RE, Key NS. Role of the extrinsic pathway of blood coagulation in hemostasis and thrombosis. *Arterioscler Thromb Vasc Biol* 2007; **27**: 1687–93.
- 45 Smith SA, Travers RJ, Morrissey JH. How it all starts: Initiation of the clotting cascade. *Crit Rev Biochem Mol Biol* 2015; **50**: 326–36.
- 46 Esmon CT, Owen WG. Identification of an endothelial cell cofactor for thrombin-catalyzed activation of protein C. *Proc Natl Acad Sci U S A* 1981; **78**: 2249–52.
- 47 Kurosawa S, Stearns-Kurosawa DJ, Hidari N, Esmon CT. Identification of functional endothelial protein C receptor in human plasma. *J Clin Invest* 1997; **100**: 411–8.
- 48 Morton I, Hall J. Concise dictionary of pharmacological agents: properties and synonyms. Boston: Kluwer Academic; 1999.
- 49 Nicolaes GAF, Dahlbäck B. Congenital and acquired activated protein C resistance. *Semin Vasc Med* 2003; **3**: 33–46.
- 50 Rosendaal FR. [Recently discovered frequent cause of venous thrombosis: factor V Leiden, a mutated factor V, resistant against protein C inactivation]. *Ned Tijdschr Geneesk* 1994; **138**: 1944–8.
- 51 Alhenc-Gelos M, Gandrille S, Aubry ML, Emmerich J, Flessinger JN, Aiach M. Unexplained thrombosis and factor V Leiden mutation. *Lancet Lond Engl* 1994; **344**: 555–6.

- 52 Tanturi CA, Wetzel NC. Studies upon the relation between plasma antithrombin and heparin; influence of plasma antithrombin on prothrombin time. *Am J Med Sci* 1949; **217**: 410–20.
- 53 Rao LV, Rapaport SI, Hoang AD. Binding of factor VIIa to tissue factor permits rapid antithrombin III/heparin inhibition of factor VIIa. *Blood* 1993; **81**: 2600–7.
- 54 Lawson JH, Butenas S, Ribarik N, Mann KG. Complex-dependent inhibition of factor VIIa by antithrombin III and heparin. *J Biol Chem* 1993; **268**: 767–70.
- 55 Jordan RE, Oosta GM, Gardner WT, Rosenberg RD. The kinetics of hemostatic enzyme-antithrombin interactions in the presence of low molecular weight heparin. *J Biol Chem* 1980; **255**: 10081–90.
- 56 Griffith MJ. Kinetics of the heparin-enhanced antithrombin III/thrombin reaction. Evidence for a template model for the mechanism of action of heparin. *J Biol Chem* 1982; **257**: 7360–5.
- 57 Olson ST, Björk I. Predominant contribution of surface approximation to the mechanism of heparin acceleration of the antithrombin-thrombin reaction. Elucidation from salt concentration effects. *J Biol Chem* 1991; **266**: 6353–64.
- 58 Olson ST, Björk I, Sheffer R, Craig PA, Shore JD, Choay J. Role of the antithrombin-binding pentasaccharide in heparin acceleration of antithrombin-proteinase reactions. Resolution of the antithrombin conformational change contribution to heparin rate enhancement. *J Biol Chem* 1992; **267**: 12528–38.
- 59 Bedsted T, Swanson R, Chuang Y-J, Bock PE, Björk I, Olson ST. Heparin and calcium ions dramatically enhance antithrombin reactivity with factor IXa by generating new interaction exosites. *Biochemistry (Mosc)* 2003; **42**: 8143–52.
- 60 Franchini M, Frattini, Crestani, Sissa, Bonfanti. Treatment of hemophilia B: focus on recombinant factor IX. *Biol Targets Ther* 2013; : 33.
- 61 Franchini M, Mannucci PM. Inhibitors of propagation of coagulation (factors VIII, IX and XI): a review of current therapeutic practice: Inhibitors of factors VIII, IX and XI. *Br J Clin Pharmacol* 2011; **72**: 553–62.
- 62 Seligsohn U. Factor XI deficiency in humans. *J Thromb Haemost* 2009; **7 Suppl 1**: 84–7.
- 63 Ridker PM, Miletich JP, Hennekens CH, Buring JE. Ethnic distribution of factor V Leiden in 4047 men and women. Implications for venous thromboembolism screening. *JAMA* 1997; **277**: 1305–7.
- 64 Gregg JP, Yamane AJ, Grody WW. Prevalence of the factor V-Leiden mutation in four distinct American ethnic populations. *Am J Med Genet* 1997; **73**: 334–6.
- 65 De Stefano V, Chiusolo P, Paciaroni K, Leone G. Epidemiology of factor V Leiden: clinical implications. *Semin Thromb Hemost* 1998; **24**: 367–79.

- 66 Kujovich JL. Factor V Leiden Thrombophilia. In: Adam MP, Ardinger HH, Pagon RA, Wallace SE, Bean LJ, Stephens K, Amemiya A, editors. *GeneReviews*®. Seattle (WA): University of Washington, Seattle; 1993.
- 67 Holbrook A, Schulman S, Witt DM, Vandvik PO, Fish J, Kovacs MJ, Svensson PJ, Veenstra DL, Crowther M, Guyatt GH. Evidence-Based Management of Anticoagulant Therapy. *Chest* 2012; **141**: e152S–e184S.
- 68 Pollack CV. Coagulation assessment with the new generation of oral anticoagulants. *Emerg Med J* 2016; **33**: 423–30.
- 69 Wysowski DK, Nourjah P, Swartz L. Bleeding Complications With Warfarin Use: A Prevalent Adverse Effect Resulting in Regulatory Action. *Arch Intern Med* 2007; **167**: 1414.
- 70 Hylek EM, Go AS, Chang Y, Jensvold NG, Henault LE, Selby JV, Singer DE. Effect of Intensity of Oral Anticoagulation on Stroke Severity and Mortality in Atrial Fibrillation. *N Engl J Med* 2003; **349**: 1019–26.
- 71 Ageno W, Gallus AS, Wittkowsky A, Crowther M, Hylek EM, Palareti G. Oral Anticoagulant Therapy. *Chest* 2012; **141**: e44S–e88S.
- 72 Budnitz DS, Lovegrove MC, Shehab N, Richards CL. Emergency Hospitalizations for Adverse Drug Events in Older Americans. *N Engl J Med* 2011; **365**: 2002–12.
- 73 Hylek EM. Risk Factors for Intracranial Hemorrhage in Outpatients Taking Warfarin. *Ann Intern Med* 1994; **120**: 897.
- 74 You JJ, Singer DE, Howard PA, Lane DA, Eckman MH, Fang MC, Hylek EM, Schulman S, Go AS, Hughes M, Spencer FA, Manning WJ, Halperin JL, Lip GYH. Antithrombotic Therapy for Atrial Fibrillation. *Chest* 2012; **141**: e531S–e575S.
- 75 Fuster V, Rydén LE, Cannom DS, Crijns HJ, Curtis AB, Ellenbogen KA, Halperin JL, Kay GN, Le Huezey J-Y, Lowe JE, Olsson SB, Prystowsky EN, Tamargo JL, Wann LS, Smith SC, Priori SG, Estes NAM, Ezekowitz MD, Jackman WM, January CT, et al. 2011 ACCF/AHA/HRS focused updates incorporated into the ACC/AHA/ESC 2006 guidelines for the management of patients with atrial fibrillation: a report of the American College of Cardiology Foundation/American Heart Association Task Force on practice guidelines. *Circulation* 2011; **123**: e269-367.
- 76 Connolly SJ, Pogue J, Eikelboom J, Flaker G, Commerford P, Franzosi MG, Healey JS, Yusuf S, on behalf of the ACTIVE W Investigators. Benefit of Oral Anticoagulant Over Antiplatelet Therapy in Atrial Fibrillation Depends on the Quality of International Normalized Ratio Control Achieved by Centers and Countries as Measured by Time in Therapeutic Range. *Circulation* 2008; **118**: 2029–37.
- 77 McKnight JT, Maxwell AJ, Anderson RL. Warfarin necrosis. *Arch Fam Med* 1992; **1**: 105–8.
- 78 Ageno W, Garcia D, Aguilar MI, Douketis J, Finazzi G, Imberti D, Iorio A, Key NS, Lim W, Marietta M, Prisco D, Sarode R, Testa S, Tositto A, Crowther M. Prevention and treatment of

- bleeding complications in patients receiving vitamin K antagonists, part 2: Treatment. *Am J Hematol* 2009; **84**: 584–8.
- 79 Morgenstern LB, Hemphill JC, Anderson C, Becker K, Broderick JP, Connolly ES, Greenberg SM, Huang JN, Macdonald RL, Messe SR, Mitchell PH, Selim M, Tamargo RJ, on behalf of the American Heart Association Stroke Council and Council on Cardiovascular Nursing. Guidelines for the Management of Spontaneous Intracerebral Hemorrhage: A Guideline for Healthcare Professionals From the American Heart Association/American Stroke Association. *Stroke* 2010; **41**: 2108–29.
- 80 Connolly SJ, Ezekowitz MD, Yusuf S, Eikelboom J, Oldgren J, Parekh A, Pogue J, Reilly PA, Themeles E, Varrone J, Wang S, Alings M, Xavier D, Zhu J, Diaz R, Lewis BS, Darius H, Diener H-C, Joyner CD, Wallentin L. Dabigatran versus Warfarin in Patients with Atrial Fibrillation. *N Engl J Med* 2009; **361**: 1139–51.
- 81 Connolly SJ, Ezekowitz MD, Yusuf S, Reilly PA, Wallentin L. Newly Identified Events in the RE-LY Trial. *N Engl J Med* 2010; **363**: 1875–6.
- 82 Boehringer Ingelheim Pharmaceuticals I. Pradaxa prescribing information. Boehringer Ingelheim Pharmaceuticals, Inc.; 2015. p. 1–16.
- 83 Janssen Pharmaceuticals I. Xarelto prescribing information. Titusville, NJ:Janssen Pharmaceuticals, Inc.; 2014. p. 1–13.
- 84 Bristol-Meyers Squibb I. Eliquis prescribing information. Bristol-Meyers Squibb Company.; 2014. p. 1–30.
- 85 Bauer KA, Eriksson BI, Lassen MR, Turpie AG, Steering Committee of the Pentasaccharide in Major Knee Surgery Study. Fondaparinux compared with enoxaparin for the prevention of venous thromboembolism after elective major knee surgery. *N Engl J Med* 2001; **345**: 1305–10.
- 86 Eriksson BI, Bauer KA, Lassen MR, Turpie AG, Steering Committee of the Pentasaccharide in Hip-Fracture Surgery Study. Fondaparinux compared with enoxaparin for the prevention of venous thromboembolism after hip-fracture surgery. *N Engl J Med* 2001; **345**: 1298–304.
- 87 Lassen MR, Bauer KA, Eriksson BI, Turpie AGG, European Pentasaccharide Elective Surgery Study (EPHESUS) Steering Committee. Postoperative fondaparinux versus preoperative enoxaparin for prevention of venous thromboembolism in elective hip-replacement surgery: a randomised double-blind comparison. *Lancet Lond Engl* 2002; **359**: 1715–20.
- 88 Turpie AGG, Bauer KA, Eriksson BI, Lassen MR, PENTATHALON 2000 Study Steering Committee. Postoperative fondaparinux versus postoperative enoxaparin for prevention of venous thromboembolism after elective hip-replacement surgery: a randomised double-blind trial. *Lancet Lond Engl* 2002; **359**: 1721–6.
- 89 Agnelli G, Bergqvist D, Cohen AT, Gallus AS, Gent M, PEGASUS investigators. Randomized clinical trial of postoperative fondaparinux versus perioperative dalteparin for prevention of venous thromboembolism in high-risk abdominal surgery. *Br J Surg* 2005; **92**: 1212–20.

- 90 Guyton AC, Hall JE. Textbook of medical physiology. 11th ed. Philadelphia: Elsevier Saunders; 2006.
- 91 Haines S, Racine E, Zeolla M. Venous thromboembolism. *Pharmacotherapy: a Pathophysiologic Approach*. 5th ed. New York, NY, USA: DiPiro J, Talbert R, Yee G et al. (editors). McGraw-Hill Companies, Inc.; 2002. p. 337–73.
- 92 Leclerc JR, Geerts WH, Desjardins L, Laflamme GH, L'Espérance B, Demers C, Kassis J, Cruickshank M, Whitman L, Delorme F. Prevention of venous thromboembolism after knee arthroplasty. A randomized, double-blind trial comparing enoxaparin with warfarin. *Ann Intern Med* 1996; **124**: 619–26.
- 93 Palmer AJ, Koppenhagen K, Kirchhof B, Weber U, Bergemann R. Efficacy and safety of low molecular weight heparin, unfractionated heparin and warfarin for thrombo-embolism prophylaxis in orthopaedic surgery: a meta-analysis of randomised clinical trials. *Haemostasis* 1997; **27**: 75–84.
- 94 Street JT, McGrath M, O'Regan K, Wakai A, McGuinness A, Redmond HP. Thromboprophylaxis Using a Low Molecular Weight Heparin Delays Fracture Repair: *Clin Orthop* 2000; **381**: 278–89.
- 95 Ahmed I, Majeed A, Powell R. Heparin induced thrombocytopenia: diagnosis and management update. *Postgrad Med J* 2007; **83**: 575–82.
- 96 Handschin AE, Trentz OA, Hoerstrup SP, Kock HJ, Wanner GA, Trentz O. Effect of low molecular weight heparin (dalteparin) and fondaparinux (Arixtra) on human osteoblasts in vitro. *Br J Surg* 2005; **92**: 177–83.
- 97 Quader MA, Stump LS, Sumpio BE. Low molecular weight heparins: current use and indications. *J Am Coll Surg* 1998; **187**: 641–58.
- 98 Cesarman-Maus G, Hajjar KA. Molecular mechanisms of fibrinolysis. *Br J Haematol* 2005; **129**: 307–21.
- 99 Mosnier LO, Bouma BN. Regulation of fibrinolysis by thrombin activatable fibrinolysis inhibitor, an unstable carboxypeptidase B that unites the pathways of coagulation and fibrinolysis. *Arterioscler Thromb Vasc Biol* 2006; **26**: 2445–53.
- 100 Marler JR, Goldstein LB. Medicine. Stroke--tPA and the clinic. *Science* 2003; **301**: 1677.
- 101 Collen D, Lijnen HR. Basic and clinical aspects of fibrinolysis and thrombolysis. *Blood* 1991; **78**: 3114–24.
- 102 Watts G. Utako Okamoto. *Lancet* 2016; **387**: 2286.
- 103 Dunn CJ, Goa KL. Tranexamic acid: a review of its use in surgery and other indications. *Drugs* 1999; **57**: 1005–32.
- 104 Sandrock K, Zieger B. Current Strategies in Diagnosis of Inherited Storage Pool Defects. *Transfus Med Hemotherapy* 2010; **37**: 4–4.

- 105 Huizing M, Pederson B, Hess RA, Griffin A, Helip-Wooley A, Westbroek W, Dorward H, O'Brien KJ, Golas G, Tsilou E, White JG, Gahl WA. Clinical and cellular characterisation of Hermansky-Pudlak syndrome type 6. *J Med Genet* 2009; **46**: 803–10.
- 106 Kirchmaier CM, Pillitteri D. Diagnosis and Management of Inherited Platelet Disorders. *Transfus Med Hemotherapy* 2010; **37**: 3–3.
- 107 WOMAN Trial Collaborators. Effect of early tranexamic acid administration on mortality, hysterectomy, and other morbidities in women with post-partum haemorrhage (WOMAN): an international, randomised, double-blind, placebo-controlled trial. *Lancet Lond Engl* 2017; **389**: 2105–16.
- 108 Napolitano LM, Cohen MJ, Cotton BA, Schreiber MA, Moore EE. Tranexamic acid in trauma: how should we use it? *J Trauma Acute Care Surg* 2013; **74**: 1575–86.
- 109 Ker K, Roberts I, Shakur H, Coats TJ. Antifibrinolytic drugs for acute traumatic injury. *Cochrane Database Syst Rev* 2015; : CD004896.
- 110 Müller MC, Meijers JC, Vroom MB, Juffermans NP. Utility of thromboelastography and/or thromboelastometry in adults with sepsis: a systematic review. *Crit Care* 2014; **18**: R30.
- 111 da Luz LT, Nascimento B, Rizoli S. Thrombelastography (TEG®): practical considerations on its clinical use in trauma resuscitation. *Scand J Trauma Resusc Emerg Med* 2013; **21**: 29.
- 112 Salomon O, Steinberg DM, Zucker M, Varon D, Zivelin A, Seligsohn U. Patients with severe factor XI deficiency have a reduced incidence of deep-vein thrombosis. *Thromb Haemost* 2011; **105**: 269–73.
- 113 Salomon O, Steinberg DM, Koren-Morag N, Tanne D, Seligsohn U. Reduced incidence of ischemic stroke in patients with severe factor XI deficiency. *Blood* 2008; **111**: 4113–7.
- 114 Yang DT, Flanders MM, Ascp MT, Kim H. Elevated Factor XI Activity Levels Are Associated With an Increased Odds Ratio for Cerebrovascular Events. *Am J Clin Pathol* 2006; **126**: 411–5.
- 115 Puy C, Rigg RA, McCarty OJT. The hemostatic role of factor XI. *Thromb Res* 2016; **141**: S8–11.
- 116 Whelihan MF, Orfeo T, Gissel MT, Mann KG. Coagulation procofactor activation by factor XIa. *J Thromb Haemost JTH* 2010; **8**: 1532–9.
- 117 Matafonov A, Cheng Q, Geng Y, Verhamme IM, Umunakwe O, Tucker EI, Sun M-F, Serebrov V, Gruber A, Gailani D. Evidence for factor IX-independent roles for factor XIa in blood coagulation. *J Thromb Haemost* 2013; **11**: 2118–27.
- 118 Puy C, Tucker EI, Matafonov A, Cheng Q, Zientek KD, Gailani D, Gruber A, McCarty OJT. Activated factor XI increases the procoagulant activity of the extrinsic pathway by inactivating tissue factor pathway inhibitor. *Blood* 2015; **125**: 1488–96.
- 119 Puy C, Tucker EI, Wong ZC, Gailani D, Smith SA, Choi SH, Morrissey JH, Gruber A, McCarty OJT. Factor XII promotes blood coagulation independent of factor XI in the presence of long chain polyphosphate. *J Thromb Haemost* 2013; **11**: 1341–52.

- 120 Whelihan MF, Orfeo T, Gissel MT, Mann KG. Coagulation procofactor activation by factor XIa. *J Thromb Haemost* 2010; **8**: 1532–9.
- 121 Puy C, Tucker EI, Matafonov A, Cheng Q, Zientek KD, Gailani D, Gruber A, McCarty OJT. Activated factor XI increases the procoagulant activity of the extrinsic pathway by inactivating tissue factor pathway inhibitor. *Blood* 2015; **125**: 1488–96.
- 122 Wang X, Cheng Q, Xu L, Feuerstein GZ, Smith PL, Seiffert DA. Effects of factor IX or factor XI deficiency on ferric chloride-induced carotid artery occlusion in mice. *J Thromb Haemost* 2005; **3**: 695–702.
- 123 Angus DC, van der Poll T. Severe sepsis and septic shock. *N Engl J Med* 2013; **369**: 840–51.
- 124 Wiersinga WJ. Current insights in sepsis: from pathogenesis to new treatment targets. *Curr Opin Crit Care* 2011; **17**: 480–6.
- 125 Angus DC, Sirio CA, Clermont G, Bion J. International comparisons of critical care outcome and resource consumption. *Crit Care Clin* 1997; **13**: 389–407.
- 126 Mayr FB, Yende S, Angus DC. Epidemiology of severe sepsis. *Virulence* 2014; **5**: 4–11.
- 127 Levi M, Schultz M, Poll T van der. Disseminated Intravascular Coagulation in Infectious Disease. *Semin Thromb Hemost* 2010; **36**: 367–77.
- 128 Dellinger RP, Levy MM, Rhodes A, Annane D, Gerlach H, Opal SM, Sevransky JE, Sprung CL, Douglas IS, Jaeschke R, Osborn TM, Nunnally ME, Townsend SR, Reinhart K, Kleinpell RM, Angus DC, Deutschman CS, Machado FR, Rubenfeld GD, Webb S, et al. Surviving Sepsis Campaign: international guidelines for management of severe sepsis and septic shock, 2012. *Intensive Care Med* 2013; **39**: 165–228.
- 129 Zeerleder S, Hack CE, Wuillemin WA. Disseminated intravascular coagulation in sepsis. *Chest* 2005; **128**: 2864–75.
- 130 Davis RP, Miller-Dorey S, Jenne CN. Platelets and coagulation in infection. *Clin Transl Immunol* 2016; **5**: e89.
- 131 Taylor FB, Chang A, Esmon CT, D’Angelo A, Vigano-D’Angelo S, Blick KE. Protein C prevents the coagulopathic and lethal effects of Escherichia coli infusion in the baboon. *J Clin Invest* 1987; **79**: 918–25.
- 132 Bernard GR, Vincent J-L, Laterre P-F, LaRosa SP, Dhainaut J-F, Lopez-Rodriguez A, Steingrub JS, Garber GE, Helterbrand JD, Ely EW, Fisher CJ. Efficacy and Safety of Recombinant Human Activated Protein C for Severe Sepsis. *N Engl J Med* 2001; **344**: 699–709.
- 133 Faust AC, Chung T, Feldman M. Stopping trials early for benefit--not so fast! *Ann Pharmacother* 2012; **46**: 1564–7.
- 134 Poole D, Bertolini G, Garattini S. Withdrawal of “Xigris” from the market: old and new lessons. *J Epidemiol Community Health* 2012; **66**: 571–2.

- 135 Lai PS, Thompson BT. Why Activated Protein C Was Not Successful in Severe Sepsis and Septic Shock: Are We Still Tilting at Windmills? *Curr Infect Dis Rep* 2013; **15**: 407–12.
- 136 Luo D, Szaba FM, Kummer LW, Johnson LL, Tucker EI, Gruber A, Gailani D, Smiley ST. Factor XI-deficient mice display reduced inflammation, coagulopathy, and bacterial growth during listeriosis. *Infect Immun* 2012; **80**: 91–9.
- 137 Tucker EI, Verbout NG, Leung PY, Hurst S, McCarty OJT, Gailani D, Gruber A. Inhibition of factor XI activation attenuates inflammation and coagulopathy while improving the survival of mouse polymicrobial sepsis. *Blood* 2012; **119**: 4762–8.
- 138 Luo D, Lin J-S, Parent MA, Mullarky-Kanevsky I, Szaba FM, Kummer LW, Duso DK, Tighe M, Hill J, Gruber A, Mackman N, Gailani D, Smiley ST. Fibrin facilitates both innate and T cell-mediated defense against *Yersinia pestis*. *J Immunol Baltim Md 1950* 2013; **190**: 4149–61.
- 139 Kravtsov DV, Matafonov A, Tucker EI, Sun M-F, Walsh PN, Gruber A, Gailani D. Factor XI contributes to thrombin generation in the absence of factor XII. *Blood* 2009; **114**: 452–8.
- 140 Cheng Q, Tucker EI, Pine MS, Sisler I, Matafonov A, Sun M-F, White-Adams TC, Smith SA, Hanson SR, McCarty OJT, Renné T, Gruber A, Gailani D. A role for factor XIIa-mediated factor XI activation in thrombus formation in vivo. *Blood* 2010; **116**: 3981–9.
- 141 Puy C, Tucker EI, Wong ZC, Gailani D, Smith SA, Choi SH, Morrissey JH, Gruber A, McCarty OJT. Factor XII promotes blood coagulation independent of factor XI in the presence of long-chain polyphosphates. *J Thromb Haemost* 2013; **11**: 1341–52.
- 142 Tucker EI, Marzec UM, White TC, Hurst S, Rugonyi S, McCarty OJT, Gailani D, Gruber A, Hanson SR. Prevention of vascular graft occlusion and thrombus-associated thrombin generation by inhibition of factor XI. *Blood* 2009; **113**: 936–44.
- 143 Büller HR, Bethune C, Bhanot S, Gailani D, Monia BP, Raskob GE, Segers A, Verhamme P, Weitz JI. Factor XI Antisense Oligonucleotide for Prevention of Venous Thrombosis. *N Engl J Med* 2014; **372**: 232–40.
- 144 Lupu F. Inhibition of Factor XI Activation By Factor XIIa Blocks Coagulopathy And Provides Organ Protection And Survival Benefit In a Baboon Model of *S. Aureus* Sepsis. Berlin, Germany; 2017.
- 145 Polanowska-Grabowska R, Raha S, Gear AR. Adhesion efficiency, platelet density and size. *Br J Haematol* 1992; **82**: 715–20.
- 146 Schubert S, Weyrich AS, Rowley JW. A tour through the transcriptional landscape of platelets. *Blood* 2014; **124**: 493–502.
- 147 Lannan KL, Sahler J, Kim N, Spinelli SL, Maggirwar SB, Garraud O, Cognasse F, Blumberg N, Phipps RP. Breaking the Mold: Transcription Factors in the Anucleate Platelet and Platelet-Derived Microparticles. *Front Immunol* 2015; **6**.
- 148 Weyrich AS, Schwertz H, Kraiss LW, Zimmerman GA. Protein synthesis by platelets: historical and new perspectives. *J Thromb Haemost* 2009; **7**: 241–6.



- 149 Daly ME. Determinants of platelet count in humans. *Haematologica* 2011; **96**: 10–3.
- 150 Jackson SP. The growing complexity of platelet aggregation. *Blood* 2007; **109**: 5087–95.
- 151 Jackson SP, Nesbitt WS, Kulkarni S. Signaling events underlying thrombus formation. *J Thromb Haemost* 2003; **1**: 1602–12.
- 152 Watson SP, Auger JM, McCarty OJT, Pearce AC. GPVI and integrin  $\alpha$ IIb $\beta$ 3 signaling in platelets. *J Thromb Haemost* 2005; **3**: 1752–62.
- 153 McCarty OJT, Calaminus SDJ, Berndt MC, Machesky LM, Watson SP. von Willebrand factor mediates platelet spreading through glycoprotein Ib and alpha(IIb)beta3 in the presence of botrocetin and ristocetin, respectively. *J Thromb Haemost* 2006; **4**: 1367–78.
- 154 Ozaki Y, Asazuma N, Suzuki-Inoue K, Berndt MC. Platelet GPIb-IX-V-dependent signaling. *J Thromb Haemost* 2005; **3**: 1745–51.
- 155 Ruggeri ZM. Platelets in atherothrombosis. *Nat Med* 2002; **8**: 1227–34.
- 156 Jurk K, Kehrel BE. Platelets: physiology and biochemistry. *Semin Thromb Hemost* 2005; **31**: 381–92.
- 157 D’Andrea G, Chetta M, Margaglione M. Inherited platelet disorders: thrombocytopenias and thrombocytopathies. *Blood Transfus* 2009; .
- 158 Konstantopoulos K, Chow TW, Turner NA, Hellums JD, Moake JL. Shear stress-induced binding of von Willebrand factor to platelets. *Biorheology* 1997; **34**: 57–71.
- 159 Alevriadou BR, Moake JL, Turner NA, Ruggeri ZM, Folie BJ, Phillips MD, Schreiber AB, Hrinda ME, McIntire LV. Real-time analysis of shear-dependent thrombus formation and its blockade by inhibitors of von Willebrand factor binding to platelets. *Blood* 1993; **81**: 1263–76.
- 160 Yago T, Lou J, Wu T, Yang J, Miner JJ, Coburn L, López JA, Cruz MA, Dong J-F, McIntire LV, McEver RP, Zhu C. Platelet glycoprotein Ibalph forms catch bonds with human WT vWF but not with type 2B von Willebrand disease vWF. *J Clin Invest* 2008; **118**: 3195–207.
- 161 Zwaginga JJ, Sixma JJ, de Groot PG. Activation of endothelial cells induces platelet thrombus formation on their matrix. Studies of new in vitro thrombosis model with low molecular weight heparin as anticoagulant. *Arterioscler Dallas Tex* 1990; **10**: 49–61.
- 162 Blann A. von Willebrand factor and the endothelium in vascular disease. *Br J Biomed Sci* 1993; **50**: 125–34.
- 163 Dong J, Moake JL, Nolasco L, Bernardo A, Arceneaux W, Shrimpton CN, Schade AJ, McIntire LV, Fujikawa K, López JA. ADAMTS-13 rapidly cleaves newly secreted ultralarge von Willebrand factor multimers on the endothelial surface under flowing conditions. *Blood* 2002; **100**: 4033–9.

- 164 Dong J, Moake JL, Bernardo A, Fujikawa K, Ball C, Nolasco L, López JA, Cruz MA. ADAMTS-13 metalloprotease interacts with the endothelial cell-derived ultra-large von Willebrand factor. *J Biol Chem* 2003; **278**: 29633–9.
- 165 South K, Luken BM, Crawley JTB, Phillips R, Thomas M, Collins RF, Deforche L, Vanhoorelbeke K, Lane DA. Conformational activation of ADAMTS13. *Proc Natl Acad Sci* 2014; **111**: 18578–83.
- 166 McCarty OJT, Conley RB, Shentu W, Tormoen GW, Zha D, Xie A, Qi Y, Zhao Y, Carr C, Belcik T, Keene DR, de Groot PG, Lindner JR. Molecular imaging of activated von Willebrand factor to detect high-risk atherosclerotic phenotype. *JACC Cardiovasc Imaging* 2010; **3**: 947–55.
- 167 Huo Y, Schober A, Forlow SB, Smith DF, Hyman MC, Jung S, Littman DR, Weber C, Ley K. Circulating activated platelets exacerbate atherosclerosis in mice deficient in apolipoprotein E. *Nat Med* 2003; **9**: 61–7.
- 168 Theilmeier G, Michiels C, Spaepen E, Vreys I, Collen D, Vermynen J, Hoylaerts MF. Endothelial von Willebrand factor recruits platelets to atherosclerosis-prone sites in response to hypercholesterolemia. *Blood* 2002; **99**: 4486–93.
- 169 Brass LF, Zhu L, Stalker TJ. Minding the gaps to promote thrombus growth and stability. *J Clin Invest* 2005; **115**: 3385–92.
- 170 Brass LF, Tomaiuolo M, Stalker TJ. Harnessing the Platelet Signaling Network to Produce an Optimal Hemostatic Response. *Hematol Oncol Clin North Am* 2013; **27**: 381–409.
- 171 Coughlin SR. Protease-activated receptors in hemostasis, thrombosis and vascular biology. *J Thromb Haemost* 2005; **3**: 1800–14.
- 172 Coughlin SR. Thrombin signalling and protease-activated receptors. *Nature* 2000; **407**: 258–64.
- 173 Nieman MT. Protease-activated receptors in hemostasis. *Blood* 2016; **128**: 169–77.
- 174 Nakanishi-Matsui M, Zheng YW, Sulciner DJ, Weiss EJ, Ludeman MJ, Coughlin SR. PAR3 is a cofactor for PAR4 activation by thrombin. *Nature* 2000; **404**: 609–13.
- 175 Sambrano GR, Weiss EJ, Zheng YW, Huang W, Coughlin SR. Role of thrombin signalling in platelets in haemostasis and thrombosis. *Nature* 2001; **413**: 74–8.
- 176 Vassallo RR, Kieber-Emmons T, Cichowski K, Brass LF. Structure-function relationships in the activation of platelet thrombin receptors by receptor-derived peptides. *J Biol Chem* 1992; **267**: 6081–5.
- 177 Jackson SP, Schoenwaelder SM. Antiplatelet therapy: in search of the “magic bullet.” *Nat Rev Drug Discov* 2003; **2**: 775–89.
- 178 Nieman MT, Schmaier AH. Interaction of thrombin with PAR1 and PAR4 at the thrombin cleavage site. *Biochemistry (Mosc)* 2007; **46**: 8603–10.

- 179 Vu TK, Wheaton VI, Hung DT, Charo I, Coughlin SR. Domains specifying thrombin-receptor interaction. *Nature* 1991; **353**: 674–7.
- 180 Arora P, Ricks TK, Trejo J. Protease-activated receptor signalling, endocytic sorting and dysregulation in cancer. *J Cell Sci* 2007; **120**: 921–8.
- 181 Smith TH, Coronel LJ, Li JG, Dores MR, Nieman MT, Trejo J. Protease-activated Receptor-4 Signaling and Trafficking Is Regulated by the Clathrin Adaptor Protein Complex-2 Independent of  $\beta$ -Arrestins. *J Biol Chem* 2016; **291**: 18453–64.
- 182 Duvernay M, Young S, Gailani D, Schoenecker J, Hamm HE, Hamm H. Protease-activated receptor (PAR) 1 and PAR4 differentially regulate factor V expression from human platelets. *Mol Pharmacol* 2013; **83**: 781–92.
- 183 Covic L, Singh C, Smith H, Kuliopulos A. Role of the PAR4 thrombin receptor in stabilizing platelet-platelet aggregates as revealed by a patient with Hermansky-Pudlak syndrome. *Thromb Haemost* 2002; **87**: 722–7.
- 184 Cerrito F, Lazzaro MP, Gaudio E, Arminio P, Aloisi G. 5HT<sub>2</sub>-receptors and serotonin release: their role in human platelet aggregation. *Life Sci* 1993; **53**: 209–15.
- 185 Ziu E, Hadden C, Li Y, Lowery CL, Singh P, Ucer SS, Mercado CP, Gu HH, Kilic F. Effect of serotonin on platelet function in cocaine exposed blood. *Sci Rep* 2015; **4**.
- 186 Coppinger JA, Cagney G, Toomey S, Kislinger T, Belton O, McRedmond JP, Cahill DJ, Emili A, Fitzgerald DJ, Maguire PB. Characterization of the proteins released from activated platelets leads to localization of novel platelet proteins in human atherosclerotic lesions. *Blood* 2004; **103**: 2096–104.
- 187 Heijnen HF, Debili N, Vainchencker W, Breton-Gorius J, Geuze HJ, Sixma JJ. Multivesicular bodies are an intermediate stage in the formation of platelet alpha-granules. *Blood* 1998; **91**: 2313–25.
- 188 Michelson AD, editor. Platelets. 2nd ed. Amsterdam ; Boston: Academic Press/Elsevier; 2007.
- 189 Ozgonenel B, Rajpurkar M, Lusher JM. How do you treat bleeding disorders with desmopressin? *Postgrad Med J* 2007; **83**: 159–63.
- 190 Eapen M, DeLaat CA, Baker KS, Cairo MS, Cowan MJ, Kurtzberg J, Steward CG, Veys PA, Filipovich AH. Hematopoietic cell transplantation for Chediak-Higashi syndrome. *Bone Marrow Transplant* 2007; **39**: 411–5.
- 191 Schrör K. Aspirin and platelets: the antiplatelet action of aspirin and its role in thrombosis treatment and prophylaxis. *Semin Thromb Hemost* 1997; **23**: 349–56.
- 192 Lange RA, Hillis LD. The duel between dual antiplatelet therapies. *N Engl J Med* 2013; **368**: 1356–7.
- 193 Levine GN, Bates ER, Bittl JA, Brindis RG, Fihn SD, Fleisher LA, Granger CB, Lange RA, Mack MJ, Mauri L, Mehran R, Mukherjee D, Newby LK, O’Gara PT, Sabatine MS, Smith PK,

- Smith SC. 2016 ACC/AHA Guideline Focused Update on Duration of Dual Antiplatelet Therapy in Patients With Coronary Artery Disease. *J Am Coll Cardiol* 2016; **68**: 1082–115.
- 194 Musumeci G, Di Lorenzo E, Valgimigli M. Dual antiplatelet therapy duration: what are the drivers? *Curr Opin Cardiol* 2011; **26 Suppl 1**: S4-14.
- 195 Cannon CP, Harrington RA, James S, Ardissino D, Becker RC, Emanuelsson H, Husted S, Katus H, Keltai M, Khurmi NS, Kontny F, Lewis BS, Steg PG, Storey RF, Wojdyla D, Wallentin L, PLATElet inhibition and patient Outcomes Investigators. Comparison of ticagrelor with clopidogrel in patients with a planned invasive strategy for acute coronary syndromes (PLATO): a randomised double-blind study. *Lancet Lond Engl* 2010; **375**: 283–93.
- 196 Rubboli A, Patti G. What is the role for Glycoprotein IIb/IIIa inhibitor use in the catheterisation laboratory in the current era? *Curr Vasc Pharmacol* 2018; .
- 197 Lozano I, Rondan J, Vegas JM, Segovia E. Cangrelor or Abciximab as First Choice in Cardiogenic Shock. *JACC Cardiovasc Interv* 2017; **10**: 2467–8.
- 198 Vaduganathan M, Qamar A, Badreldin HA, Faxon DP, Bhatt DL. Reply: Cangrelor or Abciximab as First Choice in Cardiogenic Shock. *JACC Cardiovasc Interv* 2017; **10**: 2468–9.
- 199 Kastrati A, Mehilli J, Schühlen H, Dirschinger J, Dotzer F, ten Berg JM, Neumann F-J, Bollwein H, Volmer C, Gawaz M, Berger PB, Schömig A, Intracoronary Stenting and Antithrombotic Regimen-Rapid Early Action for Coronary Treatment Study Investigators. A clinical trial of abciximab in elective percutaneous coronary intervention after pretreatment with clopidogrel. *N Engl J Med* 2004; **350**: 232–8.
- 200 Nishijima DK, Zehtabchi S, Berrong J, Legome E. Utility of platelet transfusion in adult patients with traumatic intracranial hemorrhage and preinjury antiplatelet use: A systematic review. *J Trauma Acute Care Surg* 2012; **72**: 1658–63.
- 201 McMillian WD, Rogers FB. Management of prehospital antiplatelet and anticoagulant therapy in traumatic head injury: a review. *J Trauma* 2009; **66**: 942–50.
- 202 Lindblad C, Thelin EP, Nekludov M, Frostell A, Nelson DW, Svensson M, Bellander B-M. Assessment of Platelet Function in Traumatic Brain Injury-A Retrospective Observational Study in the Neuro-Critical Care Setting. *Front Neurol* 2018; **9**: 15.
- 203 Vartanian KB, Berny MA, McCarty OJT, Hanson SR, Hinds MT. Cytoskeletal structure regulates endothelial cell immunogenicity independent of fluid shear stress. *Am J Physiol - Cell Physiol* 2010; **298**: C333–41.
- 204 Vartanian KB, Kirkpatrick SJ, McCarty OJT, Vu TQ, Hanson SR, Hinds MT. Distinct extracellular matrix microenvironments of progenitor and carotid endothelial cells. *J Biomed Mater Res A* 2009; **91**: 528–39.
- 205 Toshner M, Dunmore BJ, McKinney EF, Southwood M, Caruso P, Upton PD, Waters JP, Ormiston ML, Skepper JN, Nash G, Rana AA, Morrell NW. Transcript Analysis Reveals a Specific HOX Signature Associated with Positional Identity of Human Endothelial Cells. Bishopric NH, editor. *PLoS ONE* 2014; **9**: e91334.

- 206 Lin Y, Weisdorf DJ, Solovey A, Hebbel RP. Origins of circulating endothelial cells and endothelial outgrowth from blood. *J Clin Invest* 2000; **105**: 71–7.
- 207 Medina RJ, Barber CL, Sabatier F, Dignat-George F, Melero-Martin JM, Khosrotehrani K, Ohneda O, Randi AM, Chan JKY, Yamaguchi T, Van Hinsbergh VWM, Yoder MC, Stitt AW. Endothelial Progenitors: A Consensus Statement on Nomenclature: Endothelial Progenitors Nomenclature. *STEM CELLS Transl Med* 2017; **6**: 1316–20.
- 208 Lidington EA, Moyes DL, McCormack AM, Rose ML. A comparison of primary endothelial cells and endothelial cell lines for studies of immune interactions. *Transpl Immunol* 1999; **7**: 239–46.
- 209 Vartanian KB, Berny MA, McCarty OJT, Hanson SR, Hinds MT. Cytoskeletal structure regulates endothelial cell immunogenicity independent of fluid shear stress. *Am J Physiol Cell Physiol* 2010; **298**: C333–341.
- 210 Lam RHW, Sun Y, Chen W, Fu J. Elastomeric microposts integrated into microfluidics for flow-mediated endothelial mechanotransduction analysis. *Lab Chip* 2012; **12**: 1865.
- 211 Sato M, Saito N, Sakamoto N, Ohashi T. High wall shear stress gradient suppress morphological responses of endothelial cells to fluid flow world congress on medical physics and biomedical engineering. *IFMBE Proceedings*. Munich, Germany: Springer; 2010. p. 312–3.
- 212 Ostrowski MA, Huang NF, Walker TW, Verwijlen T, Poplawski C, Khoo AS, Cooke JP, Fuller GG, Dunn AR. Microvascular Endothelial Cells Migrate Upstream and Align Against the Shear Stress Field Created by Impinging Flow. *Biophys J* 2014; **106**: 366–74.
- 213 Steward R, Tambe D, Hardin CC, Krishnan R, Fredberg JJ. Fluid shear, intercellular stress, and endothelial cell alignment. *Am J Physiol-Cell Physiol* 2015; **308**: C657–64.
- 214 Okamoto T, Kawamoto E, Takagi Y, Akita N, Hayashi T, Park EJ, Suzuki K, Shimaoka M. Gap junction-mediated regulation of endothelial cellular stiffness. *Sci Rep* 2017; **7**.
- 215 Metallo CM, Vodyanik MA, de Pablo JJ, Slukvin II, Palecek SP. The response of human embryonic stem cell-derived endothelial cells to shear stress. *Biotechnol Bioeng* 2008; **100**: 830–7.
- 216 Estrada R, Giridharan GA, Nguyen M-D, Roussel TJ, Shakeri M, Parichehreh V, Prabhu SD, Sethu P. Endothelial cell culture model for replication of physiological profiles of pressure, flow, stretch, and shear stress in vitro. *Anal Chem* 2011; **83**: 3170–7.
- 217 Urbaczek AC, Leão PAGC, Souza FZR de, Afonso A, Vieira Alberice J, Cappelini LTD, Carlos IZ, Carrilho E. Endothelial Cell Culture Under Perfusion On A Polyester-Toner Microfluidic Device. *Sci Rep* 2017; **7**.
- 218 Garland KS, Reitsma SE, Shirai T, Zilberman-Rudenko J, Tucker EI, Gailani D, Gruber A, McCarty OJT, Puy C. Removal of the C-Terminal Domains of ADAMTS13 by Activated Coagulation Factor XI induces Platelet Adhesion on Endothelial Cells under Flow Conditions. *Front Med* 2017; **4**: 232.

- 219 Marcus AJ, Broekman MJ, Drosopoulos JHF, Olson KE, Islam N, Pinsky DJ, Levi R. Role of CD39 (NTPDase-1) in thromboregulation, cerebroprotection, and cardioprotection. *Semin Thromb Hemost* 2005; **31**: 234–46.
- 220 de Graaf JC, Banga JD, Moncada S, Palmer RM, de Groot PG, Sixma JJ. Nitric oxide functions as an inhibitor of platelet adhesion under flow conditions. *Circulation* 1992; **85**: 2284–90.
- 221 Higgs EA, Higgs GA, Moncada S, Vane JR. Prostacyclin (PGI<sub>2</sub>) inhibits the formation of platelet thrombi in arterioles and venules of the hamster cheek pouch. 1977. *Br J Pharmacol* 1997; **120**: 439–43; discussion 437-438.
- 222 Michiels C. Endothelial cell functions. *J Cell Physiol* 2003; **196**: 430–43.
- 223 Woulfe D, Yang J, Brass L. ADP and platelets: the end of the beginning. *J Clin Invest* 2001; **107**: 1503–5.
- 224 Gerlach H, Esposito C, Stern DM. Modulation of Endothelial Hemostatic Properties: An Active Role in the Host Response. *Annu Rev Med* 1990; **41**: 15–24.
- 225 Sylman JL, Lantvit SM, Vedepo MC, Reynolds MM, Neeves KB. Transport limitations of nitric oxide inhibition of platelet aggregation under flow. *Ann Biomed Eng* 2013; **41**: 2193–205.
- 226 Thon JN, Mazutis L, Wu S, Sylman JL, Ehrlicher A, Machlus KR, Feng Q, Lu S, Lanza R, Neeves KB, Weitz DA, Italiano JE. Platelet bioreactor-on-a-chip. *Blood* 2014; **124**: 1857–67.
- 227 Yeom E, Park JH, Kang YJ, Lee SJ. Microfluidics for simultaneous quantification of platelet adhesion and blood viscosity. *Sci Rep* 2016; **6**: 24994.
- 228 Reitsma S, Slaaf DW, Vink H, van Zandvoort MAMJ, oude Egbrink MGA. The endothelial glycocalyx: composition, functions, and visualization. *Pflug Arch Eur J Physiol* 2007; **454**: 345–59.
- 229 Weinbaum S, Tarbell JM, Damiano ER. The structure and function of the endothelial glycocalyx layer. *Annu Rev Biomed Eng* 2007; **9**: 121–67.
- 230 Chappell D, Jacob M, Paul O, Rehm M, Welsch U, Stoeckelhuber M, Conzen P, Becker BF. The glycocalyx of the human umbilical vein endothelial cell: an impressive structure ex vivo but not in culture. *Circ Res* 2009; **104**: 1313–7.
- 231 Becker BF, Jacob M, Leipert S, Salmon AHJ, Chappell D. Degradation of the endothelial glycocalyx in clinical settings: searching for the sheddases. *Br J Clin Pharmacol* 2015; **80**: 389–402.
- 232 Pries AR, Secomb TW, Jacobs H, Sperandio M, Osterloh K, Gaehtgens P. Microvascular blood flow resistance: role of endothelial surface layer. *Am J Physiol* 1997; **273**: H2272-2279.
- 233 Bergmeier W, Hynes RO. Extracellular Matrix Proteins in Hemostasis and Thrombosis. *Cold Spring Harb Perspect Biol* 2012; **4**.

- 234 White-Adams TC, Berny MA, Patel IA, Tucker EI, Gailani D, Gruber A, McCarty OJT. Laminin promotes coagulation and thrombus formation in a factor XII-dependent manner. *J Thromb Haemost* 2010; **8**: 1295–301.
- 235 Chen J, López JA. Interactions of platelets with subendothelium and endothelium. *Microcirculation* 2005; **12**: 235–46.
- 236 Frenette PS, Moyna C, Hartwell DW, Lowe JB, Hynes RO, Wagner DD. Platelet-endothelial interactions in inflamed mesenteric venules. *Blood* 1998; **91**: 1318–24.
- 237 Mody NA, King MR. Influence of Brownian Motion on Blood Platelet Flow Behavior and Adhesive Dynamics near a Planar Wall. *Langmuir ACS J Surf Colloids* 2007; **23**: 6321–8.
- 238 Rabiet MJ, Plantier JL, Rival Y, Genoux Y, Lampugnani MG, Dejama E. Thrombin-induced increase in endothelial permeability is associated with changes in cell-to-cell junction organization. *Arterioscler Thromb Vasc Biol* 1996; **16**: 488–96.
- 239 Schulz B, Pruessmeyer J, Maretzky T, Ludwig A, Blobel CP, Saftig P, Reiss K. ADAM10 Regulates Endothelial Permeability and T-Cell Transmigration by Proteolysis of Vascular Endothelial Cadherin. *Circ Res* 2008; **102**: 1192–201.
- 240 Lee WL, Slutsky AS. Sepsis and Endothelial Permeability. *N Engl J Med* 2010; **363**: 689–91.
- 241 Marx G. Fluid therapy in sepsis with capillary leakage. *Eur J Anaesthesiol* 2003; **20**: 429–42.
- 242 Mackman N. The many faces of tissue factor. *J Thromb Haemost* 2009; **7 Suppl 1**: 136–9.
- 243 Gailani D, Broze GJ. Factor XI activation in a revised model of blood coagulation. *Science* 1991; **253**: 909–12.
- 244 Renné T, Pozgajová M, Grüner S, Schuh K, Pauer H-U, Burfeind P, Gailani D, Nieswandt B. Defective thrombus formation in mice lacking coagulation factor XII. *J Exp Med* 2005; **202**: 271–81.
- 245 White-Adams TC, Berny MA, Tucker EI, Gertz JM, Gailani D, Urbanus RT, de Groot PG, Gruber A, McCarty OJT. Identification of coagulation factor XI as a ligand for platelet apolipoprotein E receptor 2 (ApoER2). *Arterioscler Thromb Vasc Biol* 2009; **29**: 1602–7.
- 246 Puy C, Tucker EI, Matafonov A, Cheng Q, Zientek KD, Gailani D, Gruber A, McCarty OJT. Activated factor XI increases the procoagulant activity of the extrinsic pathway by inactivating tissue factor pathway inhibitor. *Blood* 2015; **125**: 1488–96.
- 247 Chung DW, Chen J, Ling M, Fu X, Blevins T, Parsons S, Le J, Harris J, Martin TR, Konkle BA, Zheng Y, López JA. High-density lipoprotein modulates thrombosis by preventing von Willebrand factor self-association and subsequent platelet adhesion. *Blood* 2016; **127**: 637–45.
- 248 Glaser CB, Morser J, Clarke JH, Blasko E, McLean K, Kuhn I, Chang RJ, Lin JH, Vilander L, Andrews WH, Light DR. Oxidation of a specific methionine in thrombomodulin by activated neutrophil products blocks cofactor activity. A potential rapid mechanism for modulation of coagulation. *J Clin Invest* 1992; **90**: 2565–73.

- 249 Prieto JH, Sampoli Benitez BA, Melacini G, Johnson DA, Wood MJ, Komives EA. Dynamics of the fragment of thrombomodulin containing the fourth and fifth epidermal growth factor-like domains correlate with function. *Biochemistry (Mosc)* 2005; **44**: 1225–33.
- 250 Kaneider NC, Egger P, Dunzendorfer S, Noris P, Balduini CL, Gritti D, Ricevuti G, Wiedermann CJ. Reversal of Thrombin-Induced Deactivation of CD39/ATPDase in Endothelial Cells by HMG-CoA Reductase Inhibition Effects on Rho-GTPase and Adenosine Nucleotide Metabolism. *Arterioscler Thromb Vasc Biol* 2002; **22**: 894–900.
- 251 Gu SX, Stevens JW, Lentz SR. Regulation of thrombosis and vascular function by protein methionine oxidation. *Blood* 2015; **125**: 3851–9.
- 252 Dayal S, Wilson KM, Motto DG, Miller FJ, Chauhan AK, Lentz SR. Hydrogen peroxide promotes aging-related platelet hyperactivation and thrombosis. *Circulation* 2013; **127**: 1308–16.
- 253 Ed Rainger G, Chimen M, Harrison MJ, Yates CM, Harrison P, Watson SP, Lordkipanidzé M, Nash GB. The role of platelets in the recruitment of leukocytes during vascular disease. *Platelets* 2015; **26**: 507–20.
- 254 Kirchhofer D, Tschopp TB, Hadváry P, Baumgartner HR. Endothelial cells stimulated with tumor necrosis factor- $\alpha$  express varying amounts of tissue factor resulting in inhomogenous fibrin deposition in a native blood flow system. Effects of thrombin inhibitors. *J Clin Invest* 1994; **93**: 2073–83.
- 255 Wirtz D, Konstantopoulos K, Searson PC. The physics of cancer: the role of physical interactions and mechanical forces in metastasis. *Nat Rev Cancer* 2011; **11**: 512–22.
- 256 Sato N, Beitz JG, Kato J, Yamamoto M, Clark JW, Calabresi P, Raymond A, Frackelton AR. Platelet-derived growth factor indirectly stimulates angiogenesis in vitro. *Am J Pathol* 1993; **142**: 1119–30.
- 257 Slungaard A, Fernandez JA, Griffin JH, Key NS, Long JR, Piegors DJ, Lentz SR. Platelet factor 4 enhances generation of activated protein C in vitro and in vivo. *Blood* 2003; **102**: 146–51.
- 258 Nash GF, Turner LF, Scully MF, Kakkar AK. Platelets and cancer. *Lancet Oncol* 2002; **3**: 425–30.
- 259 Baimukanova G, Miyazawa B, Potter DR, Muench MO, Bruhn R, Gibb SL, Spinella PC, Cap AP, Cohen MJ, Pati S. Platelets regulate vascular endothelial stability: assessing the storage lesion and donor variability of apheresis platelets. *Transfusion (Paris)* 2016; **56**: S65–75.
- 260 Nieswandt B, Hafner M, Echtenacher B, Männel DN. Lysis of tumor cells by natural killer cells in mice is impeded by platelets. *Cancer Res* 1999; **59**: 1295–300.
- 261 Palumbo JS, Talmage KE, Massari JV, La Jeunesse CM, Flick MJ, Kombrinck KW, Jirousková M, Degen JL. Platelets and fibrin(ogen) increase metastatic potential by impeding natural killer cell-mediated elimination of tumor cells. *Blood* 2005; **105**: 178–85.
- 262 Kwak BR, Mulhaupt F, Veillard N, Gros DB, Mach F. Altered pattern of vascular connexin expression in atherosclerotic plaques. *Arterioscler Thromb Vasc Biol* 2002; **22**: 225–30.



- 263 Tzima E, Irani-Tehrani M, Kiosses WB, Dejana E, Schultz DA, Engelhardt B, Cao G, DeLisser H, Schwartz MA. A mechanosensory complex that mediates the endothelial cell response to fluid shear stress. *Nature* 2005; **437**: 426–31.
- 264 Khan OF, Sefton MV. Endothelial cell behaviour within a microfluidic mimic of the flow channels of a modular tissue engineered construct. *Biomed Microdevices* 2011; **13**: 69–87.
- 265 Ensley AE, Nerem RM, Anderson DEJ, Hanson SR, Hinds MT. Fluid shear stress alters the hemostatic properties of endothelial outgrowth cells. *Tissue Eng Part A* 2012; **18**: 127–36.
- 266 Westein E, van der Meer AD, Kuijpers MJE, Frimat J-P, van den Berg A, Heemskerk JWM. Atherosclerotic geometries exacerbate pathological thrombus formation poststenosis in a von Willebrand factor-dependent manner. *Proc Natl Acad Sci U S A* 2013; **110**: 1357–62.
- 267 Holme PA, Orvim U, Hamers MJ, Solum NO, Brosstad FR, Barstad RM, Sakariassen KS. Shear-induced platelet activation and platelet microparticle formation at blood flow conditions as in arteries with a severe stenosis. *Arterioscler Thromb Vasc Biol* 1997; **17**: 646–53.
- 268 Zilberman-Rudenko J, Sylman JL, Lakshmanan HHS, McCarty OJT, Maddala J. Dynamics of blood flow and thrombus formation in a multi-bypass microfluidic ladder network. *Cell Mol Bioeng* 2016; : 1–14.
- 269 Konstantopoulos K, Kukreti S, McIntire LV. Biomechanics of cell interactions in shear fields. *Adv Drug Deliv Rev* 1998; **33**: 141–64.
- 270 Lawrence MB, McIntire LV, Eskin SG. Effect of flow on polymorphonuclear leukocyte/endothelial cell adhesion. *Blood* 1987; **70**: 1284–90.
- 271 Ruggeri ZM. Platelet Adhesion under Flow. *Microcirculation* 2009; **16**: 58–83.
- 272 Colace TV, Tormoen GW, McCarty OJT, Diamond SL. Microfluidics and coagulation biology. *Annu Rev Biomed Eng* 2013; **15**: 283–303.
- 273 Neeves KB, Onasoga AA, Wufsus AR. The use of microfluidics in hemostasis: clinical diagnostics and biomimetic models of vascular injury. *Curr Opin Hematol* 2013; **20**: 417–23.
- 274 Sakariassen KS, Turitto VT, Baumgartner HR. Recollections of the development of flow devices for studying mechanisms of hemostasis and thrombosis in flowing whole blood. *J Thromb Haemost* 2004; **2**: 1681–90.
- 275 Smith SA, Choi SH, Davis-Harrison R, Huyck J, Boettcher J, Rienstra CM, Morrissey JH. Polyphosphate exerts differential effects on blood clotting, depending on polymer size. *Blood* 2010; **116**: 4353–9.
- 276 Choi SH, Smith SA, Morrissey JH. Polyphosphate is a cofactor for the activation of factor XI by thrombin. *Blood* 2011; **118**: 6963–70.
- 277 Zilberman-Rudenko J, Itakura A, Wiesenekker CP, Vetter R, Maas C, Gailani D, Tucker EI, Gruber A, Gerdes C, McCarty OJT. Coagulation Factor XI Promotes Distal Platelet Activation

- and Single Platelet Consumption in the Bloodstream Under Shear Flow. *Arterioscler Thromb Vasc Biol* 2016; **36**: 510–7.
- 278 Hemker HC, Kremers R. Data management in thrombin generation. *Thromb Res* 2013; **131**: 3–11.
- 279 Deguchi H, Sinha RK, Marchese P, Ruggeri ZM, Zilberman-Rudenko J, McCarty OJT, Cohen MJ, Griffin JH. Prothrombotic skeletal muscle myosin directly enhances prothrombin activation by binding factors Xa and Va. *Blood* 2016; .
- 280 Mosnier LO, von dem Borne PA, Meijers JC, Bouma BN. Plasma TAFI levels influence the clot lysis time in healthy individuals in the presence of an intact intrinsic pathway of coagulation. *Thromb Haemost* 1998; **80**: 829–35.
- 281 von dem Borne PA, Meijers JC, Bouma BN. Feedback activation of factor XI by thrombin in plasma results in additional formation of thrombin that protects fibrin clots from fibrinolysis. *Blood* 1995; **86**: 3035–42.
- 282 Mosnier LO, Meijers JC, Bouma BN. The role of protein S in the activation of thrombin activatable fibrinolysis inhibitor (TAFI) and regulation of fibrinolysis. *Thromb Haemost* 2001; **86**: 1040–6.
- 283 Baker SM, Phillips KG, McCarty OJT. Development of a Label-free Imaging Technique for the Quantification of Thrombus Formation. *Cell Mol Bioeng* 2012; **5**: 488–92.
- 284 McCarty OJT, Abulencia JP, Mousa SA, Konstantopoulos K. Evaluation of Platelet Antagonists in In Vitro Flow Models of Thrombosis. *Anticoagulants, Antiplatelets, and Thrombolytics*. New Jersey: Humana Press; 2003. p. 21–34.
- 285 Hanson S, Griffin J, Harker L, Kelly A, Esmon C, Gruber A. Antithrombotic Effects of Thrombin-Induced Activation of Endogenous Protein-C in Primates. *J Clin Invest* 1993; **92**: 2003–12.
- 286 Gruber A, Hanson SR. Factor XI–dependence of surface- and tissue factor–initiated thrombus propagation in primates. *Blood* 2003; **102**: 953–5.
- 287 Angliker H, Wikström P, Rauber P, Stone S, Shaw E. Synthesis and properties of peptidyl derivatives of arginylfluoromethanes. *Biochem J* 1988; **256**: 481–6.
- 288 Clauss A. Rapid physiological coagulation method in determination of fibrinogen. *Acta Haematol* 1957; **17**: 237–46.
- 289 Stavrou EX, Fang C, Merkulova A, Alhalabi O, Grobe N, Antoniak S, Mackman N, Schmaier AH. Reduced thrombosis in Klkb1<sup>-/-</sup> mice is mediated by increased Mas receptor, prostacyclin, Sirt1, and KLF4 and decreased tissue factor. *Blood* 2015; **125**: 710–9.
- 290 Diamond SL. New Microfluidic Paths to Test for Bleeding or Clotting. *Cell Mol Bioeng* 2017; **10**: 1–2.

- 291 Yeager T, Roy S. Evolution of Gas Permeable Membranes for Extracorporeal Membrane Oxygenation: EVOLUTION OF ECMO MEMBRANES. *Artif Organs* 2017; **41**: 700–9.
- 292 Gimbel AA, Flores E, Koo A, García-Cardena G, Borenstein JT. Development of a biomimetic microfluidic oxygen transfer device. *Lab Chip* 2016; **16**: 3227–34.
- 293 Morris PD, Narracott A, von Tengg-Kobligk H, Silva Soto DA, Hsiao S, Lungu A, Evans P, Bressloff NW, Lawford PV, Hose DR, Gunn JP. Computational fluid dynamics modelling in cardiovascular medicine. *Heart* 2016; **102**: 18–28.
- 294 Rana K, Timmer BJ, Neeves KB. A combined microfluidic-microstencil method for patterning biomolecules and cells. *Biomicrofluidics* 2014; **8**: 056502.
- 295 Hansen RR, Wufsus AR, Barton ST, Onasoga AA, Johnson-Paben RM, Neeves KB. High content evaluation of shear dependent platelet function in a microfluidic flow assay. *Ann Biomed Eng* 2013; **41**: 250–62.
- 296 Zheng Y, Chen J, López JA. Flow-driven assembly of VWF fibres and webs in in vitro microvessels. *Nat Commun* 2015; **6**: 7858.
- 297 Lei M, Kleinstreuer C, Truskey GA. Numerical investigation and prediction of atherogenic sites in branching arteries. *J Biomech Eng* 1995; **117**: 350–7.
- 298 Popel AS, Johnson PC. Microcirculation and Hemorheology. *Annu Rev Fluid Mech* 2005; **37**: 43–69.
- 299 Mackman N. New insights into the mechanisms of venous thrombosis. *J Clin Invest* 2012; **122**: 2331–6.
- 300 Tousi N, Wang B, Pant K, Kiani MF, Prabhakarpanidian B. Preferential adhesion of leukocytes near bifurcations is endothelium independent. *Microvasc Res* 2010; **80**: 384–8.
- 301 Nesbitt WS, Westein E, Tovar-Lopez FJ, Tolouei E, Mitchell A, Fu J, Carberry J, Fouras A, Jackson SP. A shear gradient-dependent platelet aggregation mechanism drives thrombus formation. *Nat Med* 2009; **15**: 665–73.
- 302 Bark DL, Ku DN. Platelet Transport Rates and Binding Kinetics at High Shear over a Thrombus. *Biophys J* 2013; **105**: 502–11.
- 303 Tsai M, Kita A, Leach J, Rounsevell R, Huang JN, Moake J, Ware RE, Fletcher DA, Lam WA. In vitro modeling of the microvascular occlusion and thrombosis that occur in hematologic diseases using microfluidic technology. *J Clin Invest* 2012; **122**: 408–18.
- 304 Flamm MH, Diamond SL. Multiscale Systems Biology and Physics of Thrombosis Under Flow. *Ann Biomed Eng* 2012; **40**: 2355–64.
- 305 Hathcock JJ. Flow Effects on Coagulation and Thrombosis. *Arterioscler Thromb Vasc Biol* 2006; **26**: 1729–37.

- 306 Turitto VT, Baumgartner HR. Platelet interaction with subendothelium in a perfusion system: Physical role of red blood cells. *Microvasc Res* 1975; **9**: 335–44.
- 307 Turitto VT, Weiss HJ. Red blood cells: their dual role in thrombus formation. *Science* 1980; **207**: 541–3.
- 308 Replogle RL, Meiselman HJ, Merrill EW. Clinical implications of blood rheology studies. *Circulation* 1967; **36**: 148–60.
- 309 Perkkiö J, Wurzinger LJ, Schmid-Schönbein H. Plasma and platelet skimming at T-junctions. *Thromb Res* 1987; **45**: 517–26.
- 310 Jønsson V, Bock JE, Nielsen JB. Significance of plasma skimming and plasma volume expansion. *J Appl Physiol Bethesda Md* 1985 1992; **72**: 2047–51.
- 311 Pearson TC, Wetherley-Mein G. Vascular occlusive episodes and venous haematocrit in primary proliferative polycythaemia. *Lancet Lond Engl* 1978; **2**: 1219–22.
- 312 Brækkan SK, Mathiesen EB, Njølstad I, Wilsgaard T, Hansen J-B. Hematocrit and risk of venous thromboembolism in a general population. The Tromsø study. *Haematologica* 2010; **95**: 270–5.
- 313 Zilberman-Rudenko J, Itakura A, Maddala J, Baker-Groberg SM, Vetter R, Tucker EI, Gruber A, Gerdes C, McCarty OJT. Biorheology of Platelet Activation in the Bloodstream Distal to Thrombus Formation. *Cell Mol Bioeng* 2016; **9**: 496–508.
- 314 McDonald JC, Duffy DC, Anderson JR, Chiu DT, Wu H, Schueller OJ, Whitesides GM. Fabrication of microfluidic systems in poly(dimethylsiloxane). *Electrophoresis* 2000; **21**: 27–40.
- 315 Maddala J, Wang WS, Vanapalli SA, Rengaswamy R. Traffic of pairs of drops in microfluidic ladder networks with fore-aft structural asymmetry. *Microfluid Nanofluidics* 2013; **14**: 337–44.
- 316 Zilberman-Rudenko J, Itakura A, Wiesenekker CP, Vetter R, Maas C, Gailani D, Tucker EI, Gruber A, Gerdes C, McCarty OJT. Coagulation Factor XI Promotes Distal Platelet Activation and Single Platelet Consumption in the Bloodstream Under Shear Flow. *Art Thromb Vasc Biol* 2016; **36**: 510–7.
- 317 Baker-Groberg SM, Cianchetti FA, Phillips KG, McCarty OJT. Development of a method to quantify platelet adhesion and aggregation under static conditions. *Cell Mol Bioeng* 2014; **7**: 285–90.
- 318 Bird RB, Stewart WE, Lightfoot EN. Transport phenomena. New York: John Wiley & Sons; 1960.
- 319 Hussain MA, Kar S, Puniyani RR. Relationship between power law coefficients and major blood constituents affecting the whole blood viscosity. *J Biosci* 1999; **24**: 329–37.
- 320 Johnston BM, Johnston PR, Corney S, Kilpatrick D. Non-Newtonian blood flow in human right coronary arteries: steady state simulations. *J Biomech* 2004; **37**: 709–20.

- 321 Runyon MK, Kastrup CJ, Johnson-Kerner BL, Van Ha TG, Ismagilov RF. Effects of Shear Rate on Propagation of Blood Clotting Determined Using Microfluidics and Numerical Simulations. *J Am Chem Soc* 2008; **130**: 3458–64.
- 322 Holme PA, Ørvim U, Hamers MJAG, Solum NO, Brosstad FR, Barstad RM, Sakariassen KS. Shear-Induced Platelet Activation and Platelet Microparticle Formation at Blood Flow Conditions as in Arteries With a Severe Stenosis. *Arterioscler Thromb Vasc Biol* 1997; **17**: 646–53.
- 323 Shankaran H, Alexandridis P, Neelamegham S. Aspects of hydrodynamic shear regulating shear-induced platelet activation and self-association of von Willebrand factor in suspension. *Blood* 2003; **101**: 2637–45.
- 324 Chang JY. Thrombin specificity. Requirement for apolar amino acids adjacent to the thrombin cleavage site of polypeptide substrate. *Eur J Biochem FEBS* 1985; **151**: 217–24.
- 325 Lee AM, Tormoen GW, Kanso E, McCarty OJT, Newton PK. Modeling and simulation of procoagulant circulating tumor cells in flow. *Front Oncol* 2012; **2**: 108.
- 326 Jain A, Graveline A, Waterhouse A, Vernet A, Flaumenhaft R, Ingber DE. A shear gradient-activated microfluidic device for automated monitoring of whole blood haemostasis and platelet function. *Nat Commun* 2016; **7**: 10176.
- 327 Jackson SP, Nesbitt WS, Westein E. Dynamics of platelet thrombus formation. *J Thromb Haemost* 2009; **7**: 17–20.
- 328 Baker-Groberg SM, Lattimore S, Recht M, McCarty OJT, Haley KM. Assessment of neonatal platelet adhesion, activation, and aggregation. *J Thromb Haemost* 2016; **14**: 815–27.
- 329 Phillips KG, Velasco CR, Li J, Kolatkar A, Luttgen M, Bethel K, Duggan B, Kuhn P, McCarty OJT. Optical quantification of cellular mass, volume, and density of circulating tumor cells identified in an ovarian cancer patient. *Front Oncol* 2012; **2**: 72.
- 330 Zimmerman WBJ. Microfluidics: History, Theory and Applications. Springer Science & Business Media; 2006.
- 331 Hammon JW. Extracorporeal Circulation. *Cardiac Surgery in the Adult*. 4th ed. New York: McGraw-Hill Medical; 2008. p. 350–370.
- 332 Kniazeva T, Hsiao JC, Charest JL, Borenstein JT. A microfluidic respiratory assist device with high gas permeance for artificial lung applications. *Biomed Microdevices* 2011; **13**: 315–23.
- 333 Meyer A, Strüber M, Fischer S. Advances in Extracorporeal Ventilation. *Anesthesiol Clin* 2008; **26**: 381–91.
- 334 Vollmer AP, Probststein RF, Gilbert R, Thorsen T. Development of an integrated microfluidic platform for dynamic oxygen sensing and delivery in a flowing medium. *Lab Chip* 2005; **5**: 1059–66.

- 335 Wu W-I, Rochow N, Chan E, Fusch G, Manan A, Nagpal D, Selvaganapathy PR, Fusch C. Lung assist device: development of microfluidic oxygenators for preterm infants with respiratory failure. *Lab Chip* 2013; **13**: 2641–50.
- 336 Jain A, Munn LL. Biomimetic postcapillary expansions for enhancing rare blood cell separation on a microfluidic chip. *Lab Chip* 2011; **11**: 2941–7.
- 337 Johnson-Chavarria EM, Tanyeri M, Schroeder CM. A Microfluidic-based Hydrodynamic Trap for Single Particles. *J Vis Exp* 2011; : e2517.
- 338 Kang E, Lee DH, Kim C-B, Yoo SJ, Lee S-H. A hemispherical microfluidic channel for the trapping and passive dissipation of microbubbles. *J Micromechanics Microengineering* 2010; **20**: 045009.
- 339 Liberale C, Cojoc G, Bragheri F, Minzioni P, Perozziello G, La Rocca R, Ferrara L, Rajamanickam V, Di Fabrizio E, Cristiani I. Integrated microfluidic device for single-cell trapping and spectroscopy. *Sci Rep* 2013; **3**.
- 340 Boyer CJ, Swartz RD. Severe Clotting During Extracorporeal Dialysis Procedures. *Semin Dial* 1991; **4**: 69–71.
- 341 Burgin T, Johnson D, Chung H, Clark A, McGrath J. Analytical and Finite Element Modeling of Nanomembranes for Miniaturized, Continuous Hemodialysis. *Membranes* 2015; **6**.
- 342 Aird WC. Vascular bed-specific thrombosis. *J Thromb Haemost* 2007; **5**: 283–91.
- 343 Lasheras JC. The Biomechanics of Arterial Aneurysms. *Annu Rev Fluid Mech* 2007; **39**: 293–319.
- 344 Han X, Bibb R, Harris R. Artificial Vascular Bifurcations – Design and Modelling. *Procedia CIRP* 2016; **49**: 14–8.
- 345 Lee SYK, Wong M, Zohar Y. Pressure losses in microchannels with bends. *The 14th IEEE International Conference on Micro Electro Mechanical Systems, 2001. MEMS 2001*. 2001. p. 491–4.
- 346 You J, Flores L, Packirisamy M, Stiharu I. Modeling the Effect of Channel Bends on Microfluidic Flow. *IASME Transactions*. Udine, Italy; 2005. p. 144–51.
- 347 Khandelwal V, Dhiman A, Baranyi L. Laminar flow of non-Newtonian shear-thinning fluids in a T-channel. *Comput Fluids* 2015; **108**: 79–91.
- 348 Doshi N, Orje JN, Molins B, Smith JW, Mitragotri S, Ruggeri ZM. Platelet mimetic particles for targeting thrombi in flowing blood. *Adv Mater Deerfield Beach Fla* 2012; **24**: 3864–9.
- 349 Eckstein EC, Belgacem F. Model of platelet transport in flowing blood with drift and diffusion terms. *Biophys J* 1991; **60**: 53–69.

- 350 Watts T, Barigou M, Nash GB. Comparative rheology of the adhesion of platelets and leukocytes from flowing blood: why are platelets so small? *Am J Physiol Heart Circ Physiol* 2013; **304**: H1483-1494.
- 351 Madershahian N, Nagib R, Wippermann J, Strauch J, Wahlers T. A simple technique of distal limb perfusion during prolonged femoro-femoral cannulation. *J Card Surg* 2006; **21**: 168–9.
- 352 Chiu W-C, Slepian MJ, Bluestein D. Thrombus formation patterns in the HeartMate II ventricular assist device: clinical observations can be predicted by numerical simulations. *ASAIO J Am Soc Artif Intern Organs* 1992 2014; **60**: 237–40.
- 353 Nosovitsky VA, Ilegbusi OJ, Jiang J, Stone PH, Feldman CL. Effects of Curvature and Stenosis-Like Narrowing on Wall Shear Stress in a Coronary Artery Model with Phasic Flow. *Comput Biomed Res* 1997; **30**: 61–82.
- 354 Andrews RK, Berndt MC. Platelet physiology and thrombosis. *Thromb Res* 2004; **114**: 447–53.
- 355 Samuel M, Pixley RA, Villanueva MA, Colman RW, Villanueva GB. Human factor XII (Hageman factor) autoactivation by dextran sulfate. Circular dichroism, fluorescence, and ultraviolet difference spectroscopic studies. *J Biol Chem* 1992; **267**: 19691–7.
- 356 Jones CM, Baker-Groberg SM, Cianchetti FA, Glynn JJ, Healy LD, Lam WY, Nelson JW, Parrish DC, Phillips KG, Scott-Drechsel DE, Tagge IJ, Zelaya JE, Hinds MT, McCarty OJT. Measurement science in the circulatory system. *Cell Mol Bioeng* 2014; **7**: 1–14.
- 357 Roehrig S, Straub A, Pohlmann J, Lampe T, Pernerstorfer J, Schlemmer K-H, Reinemer P, Perzborn E. Discovery of the novel antithrombotic agent 5-chloro-N-((5S)-2-oxo-3-[4-(3-oxomorpholin-4-yl)phenyl]-1,3-oxazolidin-5-yl)methyl)thiophene-2-carboxamide (BAY 59-7939): an oral, direct factor Xa inhibitor. *J Med Chem* 2005; **48**: 5900–8.
- 358 Itakura A, Verbout NG, Phillips KG, Insall RH, Gailani D, Tucker EI, Gruber A, McCarty OJT. Activated factor XI inhibits chemotaxis of polymorphonuclear leukocytes. *J Leukoc Biol* 2011; **90**: 923–7.
- 359 Jonnalagadda D, Izu LT, Whiteheart SW. Platelet secretion is kinetically heterogeneous in an agonist-responsive manner. *Blood* 2012; **120**: 5209–16.
- 360 Abulencia JP, Tien N, McCarty OJ, Plymire D, Mousa SA, Konstantopoulos K. Comparative antiplatelet efficacy of a novel, nonpeptide GPIIb/IIIa antagonist (XV454) and abciximab (c7E3) in flow models of thrombosis. *Arterioscler Thromb Vasc Biol* 2001; **21**: 149–56.
- 361 Mousa SA, Abulencia JP, McCarty OJT, Turner NA, Konstantopoulos K. Comparative efficacy between the glycoprotein IIb/IIIa antagonists roxifiban and orbofiban in inhibiting platelet responses in flow models of thrombosis. *J Cardiovasc Pharmacol* 2002; **39**: 552–60.
- 362 Goodeve AC, Pavlova A, Oldenburg J. Genomics of bleeding disorders. *Haemoph Off J World Fed Hemoph* 2014; **20 Suppl 4**: 50–3.
- 363 Tormoen GW, Rugonyi S, Gruber A, McCarty OJT. The role of carrier number on the procoagulant activity of tissue factor in blood and plasma. *Phys Biol* 2011; **8**: 066005.

- 364 Maas C, Meijers JCM, Marquart JA, Bakhtiari K, Weeterings C, de Groot PG, Urbanus RT. Activated factor V is a cofactor for the activation of factor XI by thrombin in plasma. *Proc Natl Acad Sci U S A* 2010; **107**: 9083–7.
- 365 Oliver JA, Monroe DM, Roberts HR, Hoffman M. Thrombin Activates Factor XI on Activated Platelets in the Absence of Factor XII. *Arterioscler Thromb Vasc Biol* 1999; **19**: 170–7.
- 366 Lavigne G, Mercier E, Queré I, Dauzat M, Gris J-C. Thrombophilic families with inheritably associated high levels of coagulation factors VIII, IX and XI. *J Thromb Haemost* 2003; **1**: 2134–9.
- 367 Meijers JC, Tekelenburg WL, Bouma BN, Bertina RM, Rosendaal FR. High levels of coagulation factor XI as a risk factor for venous thrombosis. *N Engl J Med* 2000; **342**: 696–701.
- 368 Salomon O, Steinberg DM, Seligshon U. Variable bleeding manifestations characterize different types of surgery in patients with severe factor XI deficiency enabling parsimonious use of replacement therapy. *Haemophilia* 2006; **12**: 490–3.
- 369 Gailani D, Renné T. The intrinsic pathway of coagulation: a target for treating thromboembolic disease? *J Thromb Haemost* 2007; **5**: 1106–12.
- 370 Naito K, Fujikawa K. Activation of human blood coagulation factor XI independent of factor XII. Factor XI is activated by thrombin and factor XIa in the presence of negatively charged surfaces. *J Biol Chem* 1991; **266**: 7353–8.
- 371 Renné T, Gailani D. Role of Factor XII in hemostasis and thrombosis: clinical implications. *Expert Rev Cardiovasc Ther* 2007; **5**: 733–41.
- 372 Matafonov A, Cheng Q, Geng Y, Verhamme IM, Umunakwe O, Tucker EI, Sun M, Serebrov V, Gruber A, Gailani D. Evidence for factor IX-independent roles for factor XIa in blood coagulation. *J Thromb Haemost* 2013; **11**: 2118–27.
- 373 Whelihan MF, Orfeo T, Gissel MT, Mann KG. Coagulation procofactor activation by factor XIa. *J Thromb Haemost* 2010; **8**: 1532–9.
- 374 Büller HR, Bethune C, Bhanot S, Gailani D, Monia BP, Raskob GE, Segers A, Verhamme P, Weitz JI, FXI-ASO TKA Investigators. Factor XI antisense oligonucleotide for prevention of venous thrombosis. *N Engl J Med* 2015; **372**: 232–40.
- 375 Zhang H, Löwenberg EC, Crosby JR, MacLeod AR, Zhao C, Gao D, Black C, Revenko AS, Meijers JCM, Strokes ES, Levi M, Monia BP. Inhibition of the intrinsic coagulation pathway factor XI by antisense oligonucleotides: a novel antithrombotic strategy with lowered bleeding risk. *Blood* 2010; **116**: 4684–92.
- 376 Stalker TJ, Welsh JD, Tomaiuolo M, Wu J, Colace TV, Diamond SL, Brass LF. A systems approach to hemostasis: 3. Thrombus consolidation regulates intrathrombus solute transport and local thrombin activity. *Blood* 2014; **124**: 1824–31.



- 377 Tomaiuolo M, Stalker TJ, Welsh JD, Diamond SL, Sinno T, Brass LF. A systems approach to hemostasis: 2. Computational analysis of molecular transport in the thrombus microenvironment. *Blood* 2014; **124**: 1816–23.
- 378 Leung PY, Hurst S, Berny-Lang MA, Verbout NG, Gailani D, Tucker EI, Wang RK, McCarty OJT, Gruber A. Inhibition of Factor XII-Mediated Activation of Factor XI Provides Protection Against Experimental Acute Ischemic Stroke in Mice. *Transl Stroke Res* 2012; **3**: 381–9.
- 379 Chesnutt JKW, Han H-C. Tortuosity Triggers Platelet Activation and Thrombus Formation in Microvessels. *J Biomech Eng* 2011; **133**: 121004-121004–11.
- 380 Casa LDC, Ku DN. Geometric design of microfluidic chambers: platelet adhesion versus accumulation. *Biomed Microdevices* 2014; **16**: 115–26.
- 381 Zhang J, Bergeron AL, Yu Q, Sun C, McIntire LV, López JA, Dong J. Platelet Aggregation and Activation under Complex Patterns of Shear Stress\*. *Thromb Haemost* 2002; **88**: 817–21.
- 382 Shen F, Kastrup CJ, Liu Y, Ismagilov RF. Threshold response of initiation of blood coagulation by tissue factor in patterned microfluidic capillaries is controlled by shear rate. *Arterioscler Thromb Vasc Biol* 2008; **28**: 2035–41.
- 383 Wong RK, Sleep JR, Visner AJ, Raasch DJ, Lanza LA, DeValeria PA, Torloni AS, Arabia FA. Thrombography reveals thrombin generation potential continues to deteriorate following cardiopulmonary bypass surgery despite adequate hemostasis. *J Extra Corpor Technol* 2011; **43**: 19–25.
- 384 Levi M, Ten Cate H. Disseminated intravascular coagulation. *N Engl J Med* 1999; **341**: 586–92.
- 385 van der Poll T, Levi M. Crosstalk between inflammation and coagulation: the lessons of sepsis. *Curr Vasc Pharmacol* 2012; **10**: 632–8.
- 386 Abraham E. Coagulation abnormalities in acute lung injury and sepsis. *Am J Respir Cell Mol Biol* 2000; **22**: 401–4.
- 387 Delvaeye M, Conway EM. Coagulation and innate immune responses: can we view them separately? *Blood* 2009; **114**: 2367–74.
- 388 Müller F, Mutch NJ, Schenk WA, Smith SA, Esterl L, Spronk HM, Schmidbauer S, Gahl WA, Morrissey JH, Renné T. Platelet polyphosphates are proinflammatory and procoagulant mediators in vivo. *Cell* 2009; **139**: 1143–56.
- 389 Karlsrud TS, Buø L, Aasen AO, Johansen HT. Cleavage of plasma high molecular weight kininogen in surgical ICU patients. *Intensive Care Med* 1996; **22**: 760–5.
- 390 Karlsrud TS, Buø L, Aasen AO, Johansen HT. Bradykinin release from high molecular weight kininogen in surgical ICU patients. *Immunopharmacology* 1996; **33**: 365–8.
- 391 Kaufman N, Page JD, Pixley RA, Schein R, Schmaier AH, Colman RW. Alpha 2-macroglobulin-kallikrein complexes detect contact system activation in hereditary angioedema and human sepsis. *Blood* 1991; **77**: 2660–7.

- 392 Fredenburgh JC, Gross PL, Weitz JI. Emerging anticoagulant strategies. *Blood* 2016; : Epub ahead of print.
- 393 Salomon O, Steinberg DM, Dardik R, Rosenberg N, Zivelin A, Tamarin I, Ravid B, Berliner S, Seligsohn U. Inherited factor XI deficiency confers no protection against acute myocardial infarction. *J Thromb Haemost* 2003; **1**: 658–61.
- 394 Tucker EI, Verbout NG, Leung PY, Hurst S, McCarty OJT, Gailani D, Gruber A. Inhibition of factor XI activation attenuates inflammation and coagulopathy while improving the survival of mouse polymicrobial sepsis. *Blood* 2012; **119**: 4762–8.
- 395 Ruiz FA, Lea CR, Oldfield E, Docampo R. Human platelet dense granules contain polyphosphate and are similar to acidocalcisomes of bacteria and unicellular eukaryotes. *J Biol Chem* 2004; **279**: 44250–7.
- 396 Kornberg A, Rao NN, Ault-Riché D. Inorganic Polyphosphate: A Molecule of Many Functions. *Annu Rev Biochem* 1999; **68**: 89–125.
- 397 Morrissey JH, Choi SH, Smith SA. Polyphosphate: an ancient molecule that links platelets, coagulation, and inflammation. *Blood* 2012; **119**: 5972–9.
- 398 Choi SH, Smith SA, Morrissey JH. Polyphosphate accelerates factor V activation by factor XIa. *Thromb Haemost* 2015; **113**: 599–604.
- 399 Matafonov A, Leung PY, Gailani AE, Grach SL, Puy C, Cheng Q, Sun M -f., McCarty OJT, Tucker EI, Kataoka H, Renne T, Morrissey JH, Gruber A, Gailani D. Factor XII inhibition reduces thrombus formation in a primate thrombosis model. *Blood* 2014; **123**: 1739–46.
- 400 Hansson KM, Nielsen S, Elg M, Deinum J. The effect of corn trypsin inhibitor and inhibiting antibodies for FXIa and FXIIa on coagulation of plasma and whole blood. *J Thromb Haemost* 2014; **12**: 1678–86.
- 401 Korneeva VA, Trubetskov MM, Korshunova AV, Lushchekina SV, Kolyadko VN, Sergienko OV, Lunin VG, Panteleev MA, Ataulakhanov FI. Interactions outside the proteinase-binding loop contribute significantly to the inhibition of activated coagulation factor XII by its canonical inhibitor from corn. *J Biol Chem* 2014; **289**: 14109–20.
- 402 Hamad BK, Pathak M, Manna R, Fischer PM, Emsley J, Dekker LV. Assessment of the protein interaction between coagulation factor XII and corn trypsin inhibitor by molecular docking and biochemical validation. *J Thromb Haemost* 2017; **15**: 1818–28.
- 403 Konoshenko GI, Polin AN. Inorganic polyphosphate metabolism in *Staphylococcus aureus* and the action on it of antibiotics. *Antibiotiki* 1978; **23**: 403–5.
- 404 Gonzalez H, Jensen TE. Nickel sequestering by polyphosphate bodies in *Staphylococcus aureus*. *Microbios* 1998; **93**: 179–85.
- 405 Ratnoff OD, Colopy JE. A familial hemorrhagic trait associated with a deficiency of a clot-promoting fraction of plasma. *J Clin Invest* 1955; **34**: 602–13.

- 406 Russell JA. Management of sepsis. *N Engl J Med* 2006; **355**: 1699–713.
- 407 Levinson AT, Casserly BP, Levy MM. Reducing mortality in severe sepsis and septic shock. *Semin Respir Crit Care Med* 2011; **32**: 195–205.
- 408 McEvoy C, Kollef MH. Determinants of hospital mortality among patients with sepsis or septic shock receiving appropriate antibiotic treatment. *Curr Infect Dis Rep* 2013; **15**: 400–6.
- 409 Thachil J, Toh CH, Levi M, Watson HG. The withdrawal of Activated Protein C from the use in patients with severe sepsis and DIC [Amendment to the BCSH guideline on disseminated intravascular coagulation]. *Br J Haematol* 2012; **157**: 493–4.
- 410 Arkowitz R, Gersonde K. Effect of cadmium ions on dioxygen affinity and polyphosphate activity of human red blood cells. *Blut* 1988; **56**: 185–90.
- 411 Diamond SL. Tissue factor activity under flow. *Thromb Res* 2010; **125**: S29–30.
- 412 Colace T, Muthard R, Diamond SL. Thrombus growth and embolism on tissue factor-bearing collagen surfaces under flow: Role of thrombin with and without fibrin. *Arterioscler Thromb Vasc Biol* 2012; **32**: 1466–76.
- 413 Maloney SF, Brass LF, Diamond SL. P2Y12 or P2Y1 inhibitors reduce platelet deposition in a microfluidic model of thrombosis while apyrase lacks efficacy under flow conditions. *Integr Biol Quant Biosci Nano Macro* 2010; **2**: 183–92.
- 414 Fogelson AL, Hussain YH, Leiderman K. Blood clot formation under flow: the importance of factor XI depends strongly on platelet count. *Biophys J* 2012; **102**: 10–8.
- 415 Fitzgerald JR, Foster TJ, Cox D. The interaction of bacterial pathogens with platelets. *Nat Rev Microbiol* 2006; **4**: 445–57.
- 416 Zhu S, Travers RJ, Morrissey JH, Diamond SL. FXIa and platelet polyphosphate as therapeutic targets during human blood clotting on collagen/tissue factor surfaces under flow. *Blood* 2015; **126**: 1494–502.
- 417 Labberton L, Kenne E, Long AT, Nickel KF, Di Gennaro A, Rigg RA, Hernandez JS, Butler L, Maas C, Stavrou EX, Renné T. Neutralizing blood-borne polyphosphate in vivo provides safe thromboprotection. *Nat Commun* 2016; **7**: 12616.
- 418 Smith SA, Choi SH, Collins JNR, Travers RJ, Cooley BC, Morrissey JH. Inhibition of polyphosphate as a novel strategy for preventing thrombosis and inflammation. *Blood* 2012; **120**: 5103–10.
- 419 Phillips NF, Hsieh PC, Kowalczyk TH. Polyphosphate glucokinase. *Prog Mol Subcell Biol* 1999; **23**: 101–25.
- 420 Nocek B, Kochinyan S, Proudfoot M, Brown G, Evdokimova E, Osipiuk J, Edwards AM, Savchenko A, Joachimiak A, Yakunin AF. Polyphosphate-dependent synthesis of ATP and ADP by the family-2 polyphosphate kinases in bacteria. *Proc Natl Acad Sci U S A* 2008; **105**: 17730–5.

- 421 Mukai T, Kawai S, Mori S, Mikami B, Murata K. Crystal structure of bacterial inorganic polyphosphate/ATP-glucomannokinase. Insights into kinase evolution. *J Biol Chem* 2004; **279**: 50591–600.
- 422 Kawai S, Mori S, Mukai T, Suzuki S, Yamada T, Hashimoto W, Murata K. Inorganic Polyphosphate/ATP-NAD kinase of *Micrococcus flavus* and *Mycobacterium tuberculosis* H37Rv. *Biochem Biophys Res Commun* 2000; **276**: 57–63.
- 423 Mukai T, Kawai S, Matsukawa H, Matuo Y, Murata K. Characterization and Molecular Cloning of a Novel Enzyme, Inorganic Polyphosphate/ATP-Glucomannokinase, of *Arthrobacter* sp. Strain KM. *Appl Environ Microbiol* 2003; **69**: 3849–57.
- 424 Shor R, Halabe A, Rishver S, Tilis Y, Matas Z, Fux A, Boaz M, Weinstein J. Severe hypophosphatemia in sepsis as a mortality predictor. *Ann Clin Lab Sci* 2006; **36**: 67–72.
- 425 Tinsley CR, Manjula BN, Gotschlich EC. Purification and characterization of polyphosphate kinase from *Neisseria meningitidis*. *Infect Immun* 1993; **61**: 3703–10.
- 426 Noegel A, Gotschlich EC. Isolation of a high molecular weight polyphosphate from *Neisseria gonorrhoeae*. *J Exp Med* 1983; **157**: 2049–60.
- 427 Hassanian SM, Dinarvand P, Smith SA, Rezaie AR. Inorganic polyphosphate elicits pro-inflammatory responses through activation of the mammalian target of rapamycin complexes 1 and 2 in vascular endothelial cells. *J Thromb Haemost* 2015; **13**: 860–71.
- 428 Dinarvand P, Hassanian SM, Qureshi SH, Manithody C, Eissenberg JC, Yang L, Rezaie AR. Polyphosphate amplifies proinflammatory responses of nuclear proteins through interaction with receptor for advanced glycation end products and P2Y1 purinergic receptor. *Blood* 2014; **123**: 935–45.
- 429 Renne T, Schmaier AH, Nickel KF, Blomback M, Maas C. In vivo roles of factor XII. *Blood* 2012; **120**: 4296–303.
- 430 Saito H, Matsushita T, Kojima T. Historical perspective and future direction of coagulation research. *J Thromb Haemost* 2011; **9 Suppl 1**: 352–63.
- 431 Ghebrehiwet B, Randazzo BP, Dunn JT, Silverberg M, Kaplan AP. Mechanisms of activation of the classical pathway of complement by Hageman factor fragment. *J Clin Invest* 1983; **71**: 1450–6.
- 432 Wijeyewickrema LC, Lameignere E, Hor L, Duncan RC, Shiba T, Travers RJ, Kapopara PR, Lei V, Smith SA, Kim H, Morrissey JH, Pike RN, Conway EM. Polyphosphate is a novel cofactor for regulation of complement by a serpin, C1 inhibitor. *Blood* 2016; **128**: 1766–76.
- 433 AABB. Standards for Blood Banks and Transfusion Services. 29th ed. American Association of Blood Banks; 2014.
- 434 Harrison P, Mackie I, Mumford A, Briggs C, Liesner R, Winter M, Machin S, British Committee for Standards in Haematology. Guidelines for the laboratory investigation of heritable disorders of platelet function. *Br J Haematol* 2011; **155**: 30–44.

- 435 Magnette A, Chatelain M, Chatelain B, Ten Cate H, Mullier F. Pre-analytical issues in the haemostasis laboratory: guidance for the clinical laboratories. *Thromb J* 2016; **14**: 49.
- 436 Bolliger D, Seeberger MD, Tanaka KA, Dell-Kuster S, Gregor M, Zenklusen U, Grapow M, Tsakiris DA, Filipovic M. Pre-analytical effects of pneumatic tube transport on impedance platelet aggregometry. *Platelets* 2009; **20**: 458–65.
- 437 Hübner U, Böckel-Frohnhofer N, Hummel B, Geisel J. The effect of a pneumatic tube transport system on platelet aggregation using optical aggregometry and the PFA-100. *Clin Lab* 2010; **56**: 59–64.
- 438 Glas M, Mauer D, Kassas H, Volk T, Kreuer S. Sample transport by pneumatic tube system alters results of multiple electrode aggregometry but not rotational thromboelastometry. *Platelets* 2013; **24**: 454–61.
- 439 Thalén S, Forsling I, Eintrei J, Söderblom L, Antovic JP. Pneumatic tube transport affects platelet function measured by multiplate electrode aggregometry. *Thromb Res* 2013; **132**: 77–80.
- 440 Amann G, Zehntner C, Marti F, Colucci G. Effect of acceleration forces during transport through a pneumatic tube system on ROTEM® analysis. *Clin Chem Lab Med* 2012; **50**: 1335–42.
- 441 Dyszkiewicz-Korpanty A, Quinton R, Yassine J, Sarode R. The effect of a pneumatic tube transport system on PFA-100 trade mark closure time and whole blood platelet aggregation. *J Thromb Haemost* 2004; **2**: 354–6.
- 442 Wallin O, Söderberg J, Grankvist K, Jonsson PA, Hultdin J. Preanalytical effects of pneumatic tube transport on routine haematology, coagulation parameters, platelet function and global coagulation. *Clin Chem Lab Med* 2008; **46**: 1443–9.
- 443 Tenorio GC, Strauss RG, Wieland MJ, Behlke TA, Ludwig GA. A randomized comparison of plateletpheresis with the same donors using four blood separators at a single blood center. *J Clin Apheresis* 2002; **17**: 170–6.
- 444 Schoner A, Tyrrell C, Wu M, Gelow JM, Hayes AA, Lindner JR, Thornburg KL, Hasan W. Endocardial Endothelial Dysfunction Progressively Disrupts Initially Anti then Pro-Thrombotic Pathways in Heart Failure Mice. *PLoS One* 2015; **10**: e0142940.
- 445 Baurand A, Eckly A, Bari N, Léon C, Hechler B, Cazenave JP, Gachet C. Desensitization of the platelet aggregation response to ADP: differential down-regulation of the P2Y1 and P2cyc receptors. *Thromb Haemost* 2000; **84**: 484–91.
- 446 Hardy AR, Conley PB, Luo J, Benovic JL, Poole AW, Mundell SJ. P2Y1 and P2Y12 receptors for ADP desensitize by distinct kinase-dependent mechanisms. *Blood* 2005; **105**: 3552–60.
- 447 Hess JR, Brohi K, Dutton RP, Hauser CJ, Holcomb JB, Kluger Y, Mackway-Jones K, Parr MJ, Rizoli SB, Yukioka T, Hoyt DB, Bouillon B. The coagulopathy of trauma: a review of mechanisms. *J Trauma* 2008; **65**: 748–54.
- 448 Sobrino J, Shafi S. Timing and causes of death after injuries. *Proc Bayl Univ Med Cent* 2013; **26**: 120–3.

- 449 Sauaia A, Moore FA, Moore EE, Moser KS, Brennan R, Read RA, Pons PT. Epidemiology of trauma deaths: a reassessment. *J Trauma* 1995; **38**: 185–93.
- 450 Kauvar DS, Lefering R, Wade CE. Impact of hemorrhage on trauma outcome: an overview of epidemiology, clinical presentations, and therapeutic considerations. *J Trauma* 2006; **60**: S3-11.
- 451 Perkins JG, Cap AP, Andrew CP, Spinella PC, Blackburne LH, Grathwohl KW, Repine TB, Ketchum L, Waterman P, Lee RE, Beekley AC, Sebesta JA, Shorr AF, Wade CE, Holcomb JB. An evaluation of the impact of apheresis platelets used in the setting of massively transfused trauma patients. *J Trauma* 2009; **66**: S77-84; discussion S84-85.
- 452 Pidcoke HF, Aden JK, Mora AG, Borgman MA, Spinella PC, Dubick MA, Blackburne LH, Cap AP. Ten-year analysis of transfusion in Operation Iraqi Freedom and Operation Enduring Freedom: increased plasma and platelet use correlates with improved survival. *J Trauma Acute Care Surg* 2012; **73**: S445-452.
- 453 Yonge JD, Schreiber MA. The pragmatic randomized optimal platelet and plasma ratios trial: what does it mean for remote damage control resuscitation? *Transfusion (Paris)* 2016; **56 Suppl 2**: S149-156.
- 454 Stanworth SJ, Estcourt LJ, Powter G, Kahan BC, Dyer C, Choo L, Bakrania L, Llewelyn C, Littlewood T, Soutar R, Norfolk D, Coppelstone A, Smith N, Kerr P, Jones G, Raj K, Westerman DA, Szer J, Jackson N, Bardy PG, et al. A No-Prophylaxis Platelet-Transfusion Strategy for Hematologic Cancers. *N Engl J Med* 2013; **368**: 1771–80.
- 455 Enko D, Mangge H, Münch A, Niedrist T, Mahla E, Metzler H, Prüller F. Pneumatic tube system transport does not alter platelet function in optical and whole blood aggregometry, prothrombin time, activated partial thromboplastin time, platelet count and fibrinogen in patients on anti-platelet drug therapy. *Biochem Medica* 2017; : 217–24.
- 456 Winters JL. Complications of donor apheresis. *J Clin Apheresis* 2006; **21**: 132–41.
- 457 Das SS, Chaudhary R, Verma SK, Ojha S, Khetan D. Determinants of transfusion decisions in a mixed medical-surgical intensive care unit – A prospective cohort study. *Blood Transfus* 2009; **7**: 188–92.
- 458 Cardigan R, Turner C, Harrison P. Current methods of assessing platelet function: relevance to transfusion medicine. *Vox Sang* 2005; **88**: 153–63.
- 459 Holme S. Storage and Quality Assessment of Platelets. *Vox Sang* 1998; **74**: 207–16.
- 460 Javela K, Eronen J, Sarna S, Kekomäki R. Soluble glycoprotein V as a quality marker of platelet concentrates stressed by transportation. *Transfusion (Paris)* 2005; **45**: 1504–11.
- 461 Sandgren P, Larsson S, Wai-San P, Aspevall-Diedrich B. The effects of pneumatic tube transport on fresh and stored platelets in additive solution. *Blood Transfus* 2014; **12**: 85–90.
- 462 Lancé MD, Marcus M a. E, van Oerle R, Theunissen HMS, Henskens YMC. Platelet concentrate transport in pneumatic tube systems--does it work? *Vox Sang* 2012; **103**: 79–82.

- 463 Kelly AM, Garner SF, Foukaneli T, Godec TR, Herbert N, Kahan BC, Deary A, Bakrania L, Llewelyn C, Ouwehand WH, Williamson LM, Cardigan RA. The effect of variation in donor platelet function on transfusion outcome: a semirandomized controlled trial. *Blood* 2017; **130**: 214–20.
- 464 Bartels A, Sarpong Y, Coberly J, Hughes N, Litt J, Quick J, Kessel J, Nelson C, Coughenour J, Barnes SL, Litofsky NS, Hammer RD, Ahmad S. Failure of the Platelet Function Assay (PFA)-100 to detect antiplatelet agents. *Surgery* 2015; **158**: 1012–8; discussion 1018-1019.
- 465 Favaloro EJ. Diagnosing von Willebrand disease: a short history of laboratory milestones and innovations, plus current status, challenges, and solutions. *Semin Thromb Hemost* 2014; **40**: 551–70.
- 466 De Rossi SS, Glick M. Bleeding time: an unreliable predictor of clinical hemostasis. *J Oral Maxillofac Surg Off J Am Assoc Oral Maxillofac Surg* 1996; **54**: 1119–20.
- 467 Ling L-Q, Liao J, Niu Q, Wang X, Jia J, Zuo C-H, Jiang H, Zhou J. Evaluation of an automated light transmission aggregometry. *Platelets* 2017; : 1–8.
- 468 Devine DV, Serrano K. The Platelet Storage Lesion. *Clin Lab Med* 2010; **30**: 475–87.
- 469 Boomgaard MN, Gouwerok CW, Homburg CH, de Groot G, IJsseldijk MJ, de Korte D. The platelet adhesion capacity to subendothelial matrix and collagen in a flow model during storage of platelet concentrates for 7 days. *Thromb Haemost* 1994; **72**: 611–6.
- 470 Gitz E, Koekman CA, van den Heuvel DJ, Deckmyn H, Akkerman JW, Gerritsen HC, Urbanus RT. Improved platelet survival after cold storage by prevention of glycoprotein Iba clustering in lipid rafts. *Haematologica* 2012; **97**: 1873–81.
- 471 Kicken CH, Roest M, Henskens YMC, de Laat B, Huskens D. Application of an optimized flow cytometry-based quantification of Platelet Activation (PACT): Monitoring platelet activation in platelet concentrates. *PLoS One* 2017; **12**: e0172265.
- 472 Kicken C, Poucke SV, Marcus AE, Lancé MD, Henskens Y. Response of platelet concentrates to pressure and temperature changes without impairment of the in vitro function. *Thromb Res* 2015; **135**: 679–83.
- 473 Li R, Elmongy H, Sims C, Diamond SL. Ex vivo recapitulation of trauma-induced coagulopathy and preliminary assessment of trauma patient platelet function under flow using microfluidic technology. *J Trauma Acute Care Surg* 2016; **80**: 440–9.
- 474 Jeger V, Zimmermann H, Exadaktylos AK. The Role of Thrombelastography in Multiple Trauma. *Emerg Med Int* 2011; **2011**: 1–4.
- 475 Moore HB, Moore EE, Chapman MP, Gonzalez E, Slaughter AL, Morton AP, D'Alessandro A, Hansen KC, Sauaia A, Banerjee A, Silliman CC. Viscoelastic measurements of platelet function, not fibrinogen function, predicts sensitivity to tissue-type plasminogen activator in trauma patients. *J Thromb Haemost* 2015; **13**: 1878–87.

- 476 Tisherman SA, Schmicker RH, Brasel KJ, Bulger EM, Kerby JD, Minei JP, Powell JL, Reiff DA, Rizoli SB, Schreiber MA. Detailed description of all deaths in both the shock and traumatic brain injury hypertonic saline trials of the Resuscitation Outcomes Consortium. *Ann Surg* 2015; **261**: 586–90.
- 477 Schreiber MA, Differding J, Thorborg P, Mayberry JC, Mullins RJ. Hypercoagulability is most prevalent early after injury and in female patients. *J Trauma* 2005; **58**: 475–80; discussion 480–481.
- 478 Jain A, van der Meer AD, Papa A-L, Barrile R, Lai A, Schlechter BL, Otieno MA, Loudon CS, Hamilton GA, Michelson AD, Frelinger AL, Ingber DE. Assessment of whole blood thrombosis in a microfluidic device lined by fixed human endothelium. *Biomed Microdevices* 2016; **18**.
- 479 Kreuger AL, Caram-Deelder C, Jacobse J, Kerkhoffs J-L, van der Bom JG, Middelburg RA. Effect of storage time of platelet products on clinical outcomes after transfusion: a systematic review and meta-analyses. *Vox Sang* 2017; **112**: 291–300.
- 480 Luo G-P, Ni B, Yang X, Wu Y-Z. von Willebrand factor: more than a regulator of hemostasis and thrombosis. *Acta Haematol* 2012; **128**: 158–69.
- 481 Lenting PJ, Denis CV. Platelet von Willebrand factor: sweet resistance. *Blood* 2013; **122**: 4006–7.
- 482 Kanaji S, Fahs SA, Shi Q, Haberichter SL, Montgomery RR. Contribution of platelet vs. endothelial VWF to platelet adhesion and hemostasis. *J Thromb Haemost* 2012; **10**: 1646–52.
- 483 McGrath RT, van den Biggelaar M, Byrne B, O’Sullivan JM, Rawley O, O’Kennedy R, Voorberg J, Preston RJS, O’Donnell JS. Altered glycosylation of platelet-derived von Willebrand factor confers resistance to ADAMTS13 proteolysis. *Blood* 2013; **122**: 4107–10.
- 484 Leytin V, Allen DJ, Gwozdz A, Garvey B, Freedman J. Role of platelet surface glycoprotein Ib $\alpha$  and P-selectin in the clearance of transfused platelet concentrates. *Transfusion (Paris)* 2004; **44**: 1487–95.
- 485 Canault M, Duerschmied D, Brill A, Stefanini L, Schatzberg D, Cifuni SM, Bergmeier W, Wagner DD. p38 mitogen-activated protein kinase activation during platelet storage: consequences for platelet recovery and hemostatic function in vivo. *Blood* 2010; **115**: 1835–42.
- 486 Liang X, Russell SR, Estelle S, Jones LH, Cho S, Kahn ML, Berndt MC, Bunting ST, Ware J, Li R. Specific inhibition of ectodomain shedding of glycoprotein Ib $\alpha$  by targeting its juxtamembrane shedding cleavage site. *J Thromb Haemost* 2013; **11**: 2155–62.
- 487 Tao Y, Zhang X, Liang X, Zang J, Mo X, Li R. Structural basis for the specific inhibition of glycoprotein Ib $\alpha$  shedding by an inhibitory antibody. *Sci Rep* 2016; **6**: 24789.
- 488 Liang X, Syed AK, Russell SR, Ware J, Li R. Dimerization of glycoprotein Ib $\alpha$  is not sufficient to induce platelet clearance. *J Thromb Haemost* 2016; **14**: 381–6.



- 489 Chen W, Liang X, Syed AK, Jessup P, Church WR, Ware J, Josephson CD, Li R. Inhibiting GPIIb/IIIa Shedding Preserves Post-Transfusion Recovery and Hemostatic Function of Platelets After Prolonged Storage. *Arterioscler Thromb Vasc Biol* 2016; **36**: 1821–8.
- 490 Auton M, Zhu C, Cruz MA. The mechanism of VWF-mediated platelet GPIIb/IIIa binding. *Biophys J* 2010; **99**: 1192–201.
- 491 Singh I, Themistou E, Porcar L, Neelamegham S. Fluid shear induces conformation change in human blood protein von Willebrand factor in solution. *Biophys J* 2009; **96**: 2313–20.
- 492 Aarts PA, van den Broek SA, Prins GW, Kuiken GD, Sixma JJ, Heethaar RM. Blood platelets are concentrated near the wall and red blood cells, in the center in flowing blood. *Arterioscler Dallas Tex* 1988; **8**: 819–24.
- 493 Trevan JW. The Viscosity of Blood. *Biochem J* 1918; **12**: 60–71.
- 494 Walton BL, Lehmann M, Skorczewski T, Holle LA, Beckman JD, Cribb JA, Mooberry MJ, Wufsus AR, Cooley BC, Homeister JW, Pawlinski R, Falvo MR, Key NS, Fogelson AL, Neeves KB, Wolberg AS. Elevated hematocrit enhances platelet accumulation following vascular injury. *Blood* 2017; **129**: 2537–46.
- 495 Westenbrink BD, Alings M, Granger CB, Alexander JH, Lopes RD, Hylek EM, Thomas L, Wojdyla DM, Hanna M, Keltai M, Steg PG, De Caterina R, Wallentin L, van Gilst WH. Anemia is associated with bleeding and mortality, but not stroke, in patients with atrial fibrillation: Insights from the Apixaban for Reduction in Stroke and Other Thromboembolic Events in Atrial Fibrillation (ARISTOTLE) trial. *Am Heart J* 2017; **185**: 140–9.
- 496 Zilberman-Rudenko J, Itakura A, Wiesenekker CP, Vetter R, Maas C, Gailani D, Tucker EI, Gruber A, Gerdes C, McCarty OJT. Coagulation Factor XI Promotes Distal Platelet Activation and Single Platelet Consumption in the Bloodstream Under Shear Flow. *Arterioscler Thromb Vasc Biol* 2016; **36**: 510–7.
- 497 Ashrafuzzaman M, Tuszynski J. Structure of Membranes. *Membrane Biophysics*. Berlin, Heidelberg: Springer Berlin Heidelberg; 2012. p. 9–30.
- 498 Fricke H. The electric capacity of suspensions with special reference to blood. *J Gen Physiol* 1925; **9**: 137–52.
- 499 McClendon J. Colloidal properties of the surface of the living cell. II. Electrical conductivity and capacity of blood to alternating currents of long duration and varying in frequency from 260 to 2,000,000 cycles per second. *J Biol Chem* 1926; **69**: 733–54.
- 500 Gaw RL, Cornish BH, Thomas BJ. The electrical impedance of pulsatile blood flowing through rigid tubes: a theoretical investigation. *IEEE Trans Biomed Eng* 2008; **55**: 721–7.
- 501 Hoetink AE, Faes TJC, Visser KR, Heethaar RM. On the flow dependency of the electrical conductivity of blood. *IEEE Trans Biomed Eng* 2004; **51**: 1251–61.
- 502 Zhao TX, Jacobson B, Ribbe T. Triple-frequency method for measuring blood impedance. *Physiol Meas* 1993; **14**: 145–56.

- 503 Hatschek E. The viscosity of liquids. London: G. Bell and Sons Ltd.; 1928.
- 504 Pirofsky B. The determination of blood viscosity in man by a method based on Poiseuille's law. *J Clin Invest* 1953; **32**: 292–8.
- 505 Gidaspow D, Huang J. Kinetic theory based model for blood flow and its viscosity. *Ann Biomed Eng* 2009; **37**: 1534–45.
- 506 Maha AA. Effect of glucose-6-phosphate dehydrogenase deficiency on some biophysical properties of human erythrocytes. *Hematol Amst Neth* 2009; **14**: 38–45.
- 507 Lei KF, Chen K-H, Tsui P-H, Tsang N-M. Real-time electrical impedimetric monitoring of blood coagulation process under temperature and hematocrit variations conducted in a microfluidic chip. *PloS One* 2013; **8**: e76243.
- 508 Fernandes HP, Cesar CL, Barjas-Castro M de L. Electrical properties of the red blood cell membrane and immunohematological investigation. *Rev Bras Hematol E Hemoter* 2011; **33**: 297–301.
- 509 Ciciliano JC, Sakurai Y, Myers DR, Fay ME, Hechler B, Meeks S, Li R, Dixon JB, Lyon LA, Gachet C, Lam WA. Resolving the multifaceted mechanisms of the ferric chloride thrombosis model using an interdisciplinary microfluidic approach. *Blood* 2015; **126**: 817–24.
- 510 Parsegian A. Energy of an ion crossing a low dielectric membrane: solutions to four relevant electrostatic problems. *Nature* 1969; **221**: 844–6.
- 511 Billett HH. Hemoglobin and Hematocrit. In: Walker HK, Hall WD, Hurst JW, editors. *Clinical Methods: The History, Physical, and Laboratory Examinations*. 3rd ed. Boston: Butterworths; 1990.
- 512 Fakhry SM, Fata P. How low is too low? Cardiac risks with anemia. *Crit Care* 2004; **8 Suppl 2**: S11–14.
- 513 Moreno M, Schwartz A, Dvorkin R. The Accuracy of Point-of-Care Creatinine Testing in the Emergency Department. *Adv Emerg Med* 2015; **2015**: 1–5.
- 514 Steinfeldt-Visscher J, Teerenstra S, Gunnewiek JMTK, Weerwind PW. Evaluation of the i-STAT point-of-care analyzer in critically ill adult patients. *J Extra Corpor Technol* 2008; **40**: 57–60.
- 515 FDA Class I recall. Alere Recalls INRatio and INRatio2 PT/INR Monitoring System Due to Incorrect Test Results. U.S. Food & Drug Administration; 2016.
- 516 Chebbi R. Dynamics of blood flow: modeling of the Fåhræus-Lindqvist effect. *J Biol Phys* 2015; **41**: 313–26.
- 517 Ogawa S, Szlam F, Bolliger D, Nishimura T, Chen EP, Tanaka KA. The impact of hematocrit on fibrin clot formation assessed by rotational thromboelastometry. *Anesth Analg* 2012; **115**: 16–21.

- 518 Hum J, Shatzel JJ, Jou JH, Deloughery TG. The efficacy and safety of direct oral anticoagulants vs traditional anticoagulants in cirrhosis. *Eur J Haematol* 2017; **98**: 393–7.
- 519 Mangaonkar AA, Hoversten KP, Gangat N. Prognostic risk model for patients with high-risk polycythemia vera and essential thrombocythemia. *Expert Rev Hematol* 2018; : 1–6.
- 520 Kyriazi V, Theodoulou E. Assessing the risk and prognosis of thrombotic complications in cancer patients. *Arch Pathol Lab Med* 2013; **137**: 1286–95.
- 521 Khorana AA, Carrier M, Garcia DA, Lee AYY. Guidance for the prevention and treatment of cancer-associated venous thromboembolism. *J Thromb Thrombolysis* 2016; **41**: 81–91.
- 522 Merrill EW. Rheology of blood. *Physiol Rev* 1969; **40**: 863–84.
- 523 Nagasawa Y, Kato Z, Tanaka S. Particle sedimentation monitoring in high-concentration slurries. *AIP Adv* 2016; **6**: 115206.
- 524 Fedosov DA, Caswell B, Popel AS, Karniadakis GE. Blood flow and cell-free layer in microvessels. *Microcirculation* 2010; **17**: 615–28.
- 525 Thurston GB. Plasma release-cell layering theory for blood flow. *Biorheology* 1989; **26**: 199–214.
- 526 Thurston GB. Rheological parameters for the viscosity viscoelasticity and thixotropy of blood. *Biorheology* 1979; **16**: 149–62.
- 527 Thurston GB, Henderson NM. Effects of flow geometry on blood viscoelasticity. *Biorheology* 2006; **43**: 729–46.
- 528 Samuelson BT, Cuker A. Measurement and reversal of the direct oral anticoagulants. *Blood Rev* 2017; **31**: 77–84.
- 529 Kujovich JL. Coagulopathy in liver disease: a balancing act. *Hematol Am Soc Hematol Educ Program* 2015; **2015**: 243–9.
- 530 Ortel TL. Antiphospholipid syndrome: laboratory testing and diagnostic strategies. *Am J Hematol* 2012; **87 Suppl 1**: S75-81.
- 531 Sakariassen KS, Bolhuis PA, Sixma JJ. Human blood platelet adhesion to artery subendothelium is mediated by factor VIII-Von Willebrand factor bound to the subendothelium. *Nature* 1979; **279**: 636–8.
- 532 Sixma JJ, Sakariassen KS, Bolhuis PA. The Role of Factor VIII-von Willebrand Factor in Adhesion of Platelets to the Vessel Wall. *Pathobiology of the Endothelial Cell*. Elsevier; 1982. p. 139–52.
- 533 von Willebrand E. Hereditar pseudoheemofili,. *Fin Laekaresaellsk Hand* 1926; **68**: 87–112.
- 534 Marossy A, Svorc P, Kron I, Gresová S. Hemorheology and circulation. *Clin Hemorheol Microcirc* 2009; **42**: 239–58.

- 535 Gailani D, Bane CE, Gruber A. Factor XI and contact activation as targets for antithrombotic therapy. *J Thromb Haemost JTH* 2015; **13**: 1383–95.
- 536 Gailani D, Gruber A. Factor XI as a Therapeutic Target. *Arterioscler Thromb Vasc Biol* 2016; : ATVBAHA.116.306925.
- 537 Smith SA, Choi SH, Collins JNR, Travers RJ, Cooley BC, Morrissey JH. Inhibition of polyphosphate as a novel strategy for preventing thrombosis and inflammation. *Blood* 2012; **120**: 5103–10.
- 538 Puy C, Tucker EI, Wong ZC, Gailani D, Smith SA, Choi SH, Morrissey JH, Gruber A, McCarty OJT. Factor XII promotes blood coagulation independent of factor XI in the presence of long-chain polyphosphates. *J Thromb Haemost JTH* 2013; **11**: 1341–52.
- 539 Cheng Q, Tucker EI, Pine MS, Sisler I, Matafonov A, Sun M-F, White-Adams TC, Smith SA, Hanson SR, McCarty OJT, Renné T, Gruber A, Gailani D. A role for factor XIIa-mediated factor XI activation in thrombus formation in vivo. *Blood* 2010; **116**: 3981–9.
- 540 Deguchi H, Sinha RK, Elias D, Griffin JH. Exome genotyping links Venous thrombosis risk with the myosin gene cluster and leads to discovery of new family of procoagulant factors. 2015.
- 541 Davie EW, Fujikawa K, Kisiel W. The coagulation cascade: initiation, maintenance, and regulation. *Biochemistry (Mosc)* 1991; **30**: 10363–70.
- 542 Flaumenhaft R. Thrombus formation reimagined. *Blood* 2014; **124**: 1697–8.
- 543 Ivanciu L, Krishnaswamy S, Camire RM. New insights into the spatiotemporal localization of prothrombinase in vivo. *Blood* 2014; **124**: 1705–14.
- 544 Watson SP. Platelet activation by extracellular matrix proteins in haemostasis and thrombosis. *Curr Pharm Des* 2009; **15**: 1358–72.
- 545 Berndt MC, Metharom P, Andrews RK. Primary haemostasis: newer insights. *Haemoph Off J World Fed Hemoph* 2014; **20 Suppl 4**: 15–22.
- 546 Wilner GD, Nossel HL, LeRoy EC. Activation of Hageman factor by collagen. *J Clin Invest* 1968; **47**: 2608–15.
- 547 Cochrane CG, Griffin JH. The biochemistry and pathophysiology of the contact system of plasma. *Adv Immunol* 1982; **33**: 241–306.
- 548 van der Meijden PEJ, Munnix ICA, Auger JM, Govers-Riemslog JWP, Cosemans JMEM, Kuijpers MJE, Spronk HM, Watson SP, Renné T, Heemskerk JWM. Dual role of collagen in factor XII-dependent thrombus formation. *Blood* 2009; **114**: 881–90.
- 549 Gailani D. Factor IX binding to collagen. *J Thromb Haemost* 2009; **7**: 1840–2.
- 550 Gui T, Reheman A, Ni H, Gross PL, Yin F, Monroe D, Monahan PE, Stafford DW. Abnormal hemostasis in a knock-in mouse carrying a variant of factor IX with impaired binding to collagen type IV. *J Thromb Haemost* 2009; **7**: 1843–51.

- 551 Smith SA, Mutch NJ, Baskar D, Rohloff P, Docampo R, Morrissey JH. Polyphosphate modulates blood coagulation and fibrinolysis. *Proc Natl Acad Sci U S A* 2006; **103**: 903–8.
- 552 Sabri A, Muske G, Zhang H, Pak E, Darrow A, Andrade-Gordon P, Steinberg SF. Signaling properties and functions of two distinct cardiomyocyte protease-activated receptors. *Circ Res* 2000; **86**: 1054–61.
- 553 Smid M, Dielis AWJH, Spronk HMH, Rumley A, van Oerle R, Woodward M, ten Cate H, Lowe G. Thrombin Generation in the Glasgow Myocardial Infarction Study. Kiechl S, editor. *PLoS ONE* 2013; **8**: e66977.
- 554 WRITING COMMITTEE MEMBERS\*, O’Gara PT, Kushner FG, Ascheim DD, Casey DE, Chung MK, de Lemos JA, Ettinger SM, Fang JC, Fesmire FM, Franklin BA, Granger CB, Krumholz HM, Linderbaum JA, Morrow DA, Newby LK, Ornato JP, Ou N, Radford MJ, Tamis-Holland JE, et al. 2013 ACCF/AHA Guideline for the Management of ST-Elevation Myocardial Infarction: A Report of the American College of Cardiology Foundation/American Heart Association Task Force on Practice Guidelines. *Circulation* 2013; **127**: e362–425.
- 555 Reddy K. Recent advances in the diagnosis and treatment of acute myocardial infarction. *World J Cardiol* 2015; **7**: 243.
- 556 Nakao K, Minobe W, Roden R, Bristow MR, Leinwand LA. Myosin heavy chain gene expression in human heart failure. *J Clin Invest* 1997; **100**: 2362–70.
- 557 Hirayama A, Arita M, Takagaki Y, Tsuji A, Kodama K, Inoue M. Clinical assessment of specific enzyme immunoassay for the human cardiac myosin light chain II (MLC II) with use of monoclonal antibodies. *Clin Biochem* 1990; **23**: 515–22.
- 558 Yamada T, Matsumori A, Tamaki S, Sasayama S. Myosin light chain I grade: a simple marker for the severity and prognosis of patients with acute myocardial infarction. *Am Heart J* 1998; **135**: 329–34.
- 559 Hillis GS, Taggart P, Wardlaw D, Hillis L, Zhao N, Dalsey WC, Mangione A. The relative utility of cardiac troponin I, creatine kinase-MBmass, and myosin light chain-1 in the long-term risk stratification of patients with chest pain. *Clin Cardiol* 2003; **26**: 147–52.
- 560 Kolev K, Tenekedjiev K, Ajtai K, Kovalszky I, Gombas J, Váradi B, Machovich R. Myosin: a noncovalent stabilizer of fibrin in the process of clot dissolution. *Blood* 2003; **101**: 4380–6.
- 561 Moore HB, Moore EE, Liras IN, Gonzalez E, Harvin JA, Holcomb JB, Sauaia A, Cotton BA. Acute Fibrinolysis Shutdown after Injury Occurs Frequently and Increases Mortality: A Multicenter Evaluation of 2,540 Severely Injured Patients. *J Am Coll Surg* 2016; **222**: 347–55.
- 562 Moritz A. Trauma and Heart Disease. *Case Western Reserve Law Review* 1954; **5**: 133–49.
- 563 Wei T, Wang L, Chen L, Wang C, Zeng C. Acute myocardial infarction and congestive heart failure following a blunt chest trauma. *Heart Vessels* 2002; **17**: 77–9.
- 564 Lolay GA, Abdel-Latif AK. Trauma induced myocardial infarction. *Int J Cardiol* 2016; **203**: 19–21.

- 565 Dong J, Moake JL, Nolasco L, Bernardo A, Arceneaux W, Shrimpton CN, Schade AJ, McIntire L V, Fujikawa K, Lo A. ADAMTS-13 rapidly cleaves newly secreted ultralarge von Willebrand factor multimers on the endothelial surface under flowing conditions. *Hem Thromb Vasc Biol* 2002; **100**: 4033–9.
- 566 Zanardelli S, Chion ACK, Groot E, Lenting PJ, Mckinnon T a. J, Laffan M a., Tseng M, Lane D a. A novel binding site for ADAMTS13 constitutively exposed on the surface of globular VWF THROMBOSIS AND HEMOSTASIS A novel binding site for ADAMTS13 constitutively exposed on the surface of globular VWF. *Thromb Haemost* 2009; **114**: 2819–28.
- 567 Zhang P, Pan W, Rux AH, Sachais BS, Zheng XL. The cooperative activity between the carboxyl-terminal TSP1 repeats and the CUB domains of ADAMTS13 is crucial for recognition of von Willebrand factor under flow. *Blood* 2007; **110**: 1887–94.
- 568 Banno F, Chauhan AK, Kokame K, Yang J, Miyata S, Wagner DD, Miyata T. The distal carboxyl-terminal domains of ADAMTS13 are required for regulation of in vivo thrombus formation. *Blood* 2009; **113**: 5323–9.
- 569 Ngo ATP, Thierheimer MLD, Babur Ö, Rocheleau AD, Huang T, Pang J, Rigg RA, Mitrugno A, Theodorescu D, Burchard J, Nan X, Demir E, McCarty OJT, Aslan JE. Assessment of roles for the Rho-specific guanine nucleotide dissociation inhibitor Ly-GDI in platelet function: a spatial systems approach. *Am J Physiol - Cell Physiol* 2017; **312**: C527–36.
- 570 Zwaginga JJ, Sakariassen KS, Nash G, King MR, Heemskerk JW, Frojmovic M, Hoylaerts MF, Biorheology Subcommittee of the SSC of the Isth. Flow-based assays for global assessment of hemostasis. Part 2: current methods and considerations for the future. *J Thromb Haemost* 2006; **4**: 2716–7.
- 571 Bogorad MI, DeStefano J, Karlsson J, Wong AD, Gerecht S, Searson PC. Review: in vitro microvessel models. *Lab Chip* 2015; **15**: 4242–55.
- 572 Baumgartner HR. The role of blood flow in platelet adhesion, fibrin deposition, and formation of mural thrombi. *Microvasc Res* 1973; **5**: 167–79.
- 573 Lopez-Vilchez I, Hedner U, Altisent C, Diaz-Ricart M, Escolar G, Galan AM. Redistribution and Hemostatic Action of Recombinant Activated Factor VII Associated with Platelets. *Am J Pathol* 2011; **178**: 2938–48.
- 574 Jaffe EA, Nachman RL, Becker CG, Minick CR. Culture of human endothelial cells derived from umbilical veins. Identification by morphologic and immunologic criteria. *J Clin Invest* 1973; **52**: 2745–56.
- 575 Sakariassen KS, Aarts PA, de Groot PG, Houdijk WP, Sixma JJ. A perfusion chamber developed to investigate platelet interaction in flowing blood with human vessel wall cells, their extracellular matrix, and purified components. *J Lab Clin Med* 1983; **102**: 522–35.
- 576 Cooke BM, Usami S, Perry I, Nash GB. A simplified method for culture of endothelial cells and analysis of adhesion of blood cells under conditions of flow. *Microvasc Res* 1993; **45**: 33–45.

- 577 Chiu J-J, Chien S. Effects of Disturbed Flow on Vascular Endothelium: Pathophysiological Basis and Clinical Perspectives. *Physiol Rev* 2011; **91**: 327–87.
- 578 Halldorsson S, Lucumi E, Gómez-Sjöberg R, Fleming RMT. Advantages and challenges of microfluidic cell culture in polydimethylsiloxane devices. *Biosens Bioelectron* 2015; **63**: 218–31.
- 579 Whitesides GM, Stroock AD. Flexible methods for microfluidics. *Phys Today* 2001; **54**: 42–8.
- 580 Cranmer SL, Ulsemer P, Cooke BM, Salem HH, de la Salle C, Lanza F, Jackson SP. Glycoprotein (GP) Ib-IX-transfected cells roll on a von Willebrand factor matrix under flow. Importance of the GPIb/actin-binding protein (ABP-280) interaction in maintaining adhesion under high shear. *J Biol Chem* 1999; **274**: 6097–106.
- 581 Hsu PP, Li S, Li YS, Usami S, Ratcliffe A, Wang X, Chien S. Effects of flow patterns on endothelial cell migration into a zone of mechanical denudation. *Biochem Biophys Res Commun* 2001; **285**: 751–9.
- 582 Chiu JJ, Wang DL, Chien S, Skalak R, Usami S. Effects of disturbed flow on endothelial cells. *J Biomech Eng* 1998; **120**: 2–8.
- 583 Duffy DC, McDonald JC, Schueller OJ, Whitesides GM. Rapid Prototyping of Microfluidic Systems in Poly(dimethylsiloxane). *Anal Chem* 1998; **70**: 4974–84.
- 584 Whitesides GM. The origins and the future of microfluidics. *Nature* 2006; **442**: 368–73.
- 585 Berthier E, Young EWK, Beebe D. Engineers are from PDMS-land, Biologists are from Polystyrenia. *Lab Chip* 2012; **12**: 1224–37.
- 586 Sia SK, Whitesides GM. Microfluidic devices fabricated in poly(dimethylsiloxane) for biological studies. *Electrophoresis* 2003; **24**: 3563–76.
- 587 Han H-C, Chesnutt JKW, Garcia JR, Liu Q, Wen Q. Artery Buckling: New Phenotypes, Models, and Applications. *Ann Biomed Eng* 2013; **41**: 1399–410.
- 588 Raj A, Sen AK. Flow-induced deformation of compliant microchannels and its effect on pressure–flow characteristics. *Microfluid Nanofluidics* 2016; **20**.
- 589 Gervais T, El-Ali J, Günther A, Jensen KF. Flow-induced deformation of shallow microfluidic channels. *Lab Chip* 2006; **6**: 500.
- 590 Neeves KB, Maloney SF, Fong KP, Schmaier AA, Kahn ML, Brass LF, Diamond SL. Microfluidic focal thrombosis model for measuring murine platelet deposition and stability: PAR4 signaling enhances shear-resistance of platelet aggregates. *J Thromb Haemost* 2008; **6**: 2193–201.
- 591 De Silva MN, Desai R, Odde DJ. Micro-patterning of animal cells on PDMS substrates in the presence of serum without use of adhesion inhibitors. *Biomed Microdevices* 2004; **6**: 219–22.

- 592 Tseng P-Y, Rele SS, Sun X-L, Chaikof EL. Membrane-mimetic films containing thrombomodulin and heparin inhibit tissue factor-induced thrombin generation in a flow model. *Biomaterials* 2006; **27**: 2637–50.
- 593 Hansen RR, Wufsus AR, Barton ST, Onasoga AA, Johnson-Paben RM, Neeves KB. High content evaluation of shear dependent platelet function in a microfluidic flow assay. *Ann Biomed Eng* 2013; **41**: 250–62.
- 594 Wang JD, Douville NJ, Takayama S, ElSayed M. Quantitative analysis of molecular absorption into PDMS microfluidic channels. *Ann Biomed Eng* 2012; **40**: 1862–73.
- 595 Sackmann EK, Fulton AL, Beebe DJ. The present and future role of microfluidics in biomedical research. *Nature* 2014; **507**: 181–9.
- 596 Li M, Ku DN, Forest CR. Microfluidic system for simultaneous optical measurement of platelet aggregation at multiple shear rates in whole blood. *Lab Chip* 2012; **12**: 1355–62.
- 597 Colace TV, Diamond SL. Direct observation of von Willebrand factor elongation and fiber formation on collagen during acute whole blood exposure to pathological flow. *Arterioscler Thromb Vasc Biol* 2013; **33**: 105–13.
- 598 Bao J, Xiao J, Mao Y, Zheng XL. Carboxyl terminus of ADAMTS13 directly inhibits platelet aggregation and ultra large von Willebrand factor string formation under flow in a free-thiol-dependent manner. *Arterioscler Thromb Vasc Biol* 2014; **34**: 397–407.
- 599 Chrobak KM, Potter DR, Tien J. Formation of perfused, functional microvascular tubes in vitro. *Microvasc Res* 2006; **71**: 185–96.
- 600 Wong AD, Searson PC. Live-cell imaging of invasion and intravasation in an artificial microvessel platform. *Cancer Res* 2014; **74**: 4937–45.
- 601 Wong AD, Ye M, Levy AF, Rothstein JD, Bergles DE, Searson PC. The blood-brain barrier: an engineering perspective. *Front Neuroengineering* 2013; **6**: 7.
- 602 Zheng Y, Chen J, Craven M, Choi NW, Totorica S, Diaz-Santana A, Kermani P, Hempstead B, Fischbach-Teschl C, López JA, Stroock AD. In vitro microvessels for the study of angiogenesis and thrombosis. *Proc Natl Acad Sci U S A* 2012; **109**: 9342–7.
- 603 Ye M, Sanchez HM, Hultz M, Yang Z, Bogorad M, Wong AD, Searson PC. Brain microvascular endothelial cells resist elongation due to curvature and shear stress. *Sci Rep* 2014; **4**.
- 604 Mannino RG, Myers DR, Ahn B, Wang Y, Margo Rollins, Gole H, Lin AS, Guldborg RE, Giddens DP, Timmins LH, Lam WA. “Do-it-yourself in vitro vasculature that recapitulates in vivo geometries for investigating endothelial-blood cell interactions.” *Sci Rep* 2015; **5**: 12401.
- 605 Zheng Y, Chen J, López JA. Flow-driven assembly of VWF fibres and webs in in vitro microvessels. *Nat Commun* 2015; **6**: 7858.
- 606 Zheng Y, Chen J, López JA. Microvascular platforms for the study of platelet-vessel wall interactions. *Thromb Res* 2014; **133**: 525–31.



- 607 Tsai J-C, Lin Y-W, Huang C-Y, Lin C-Y, Tsai Y-T, Shih C-M, Lee C-Y, Chen Y-H, Li C-Y, Chang N-C, Lin F-Y, Tsai C-S. The role of calpain-myosin 9-Rab7b pathway in mediating the expression of Toll-like receptor 4 in platelets: a novel mechanism involved in  $\alpha$ -granules trafficking. *PloS One* 2014; **9**: e85833.
- 608 Zheng Y, Roberts MA. Tissue engineering: Scalable vascularized implants. *Nat Mater* 2016; **15**: 597–9.
- 609 Roberts MA, Tran D, Coulombe KLK, Razumova M, Regnier M, Murry CE, Zheng Y. Stromal Cells in Dense Collagen Promote Cardiomyocyte and Microvascular Patterning in Engineered Human Heart Tissue. *Tissue Eng Part A* 2016; **22**: 633–44.
- 610 Park J, Li Y, Berthiaume F, Toner M, Yarmush ML, Tilles AW. Radial flow hepatocyte bioreactor using stacked microfabricated grooved substrates. *Biotechnol Bioeng* 2008; **99**: 455–67.
- 611 Zhang P, Pan W, Rux AH, Sachais BS, Zheng XL. The cooperative activity between the carboxyl-terminal TSP1 repeats and the CUB domains of ADAMTS13 is crucial for recognition of von Willebrand factor under flow. *Blood* 2007; **110**: 1887–94.
- 612 Sylman JL, Artzer DT, Rana K, Neeves KB. A vascular injury model using focal heat-induced activation of endothelial cells. *Integr Biol* 2015; **7**: 801–14.
- 613 Peters K, Unger RE, Brunner J, Kirkpatrick CJ. Molecular basis of endothelial dysfunction in sepsis. *Cardiovasc Res* 2003; **60**: 49–57.
- 614 Price GM, Wong KHK, Truslow JG, Leung AD, Acharya C, Tien J. Effect of mechanical factors on the function of engineered human blood microvessels in microfluidic collagen gels. *Biomaterials* 2010; **31**: 6182–9.

## Biographical Sketch

Jevgenia (Jenya) Zilberman-Rudenko was born in post-Soviet Union Estonia in 1983 to Irina and Aleksei Rudenko. She has spent her formative years studying at the Tallinna Juhkentali Gymnasium alongside her four sisters and competing at Estopen Kickboxing meets with her teammates. Shortly following graduation from high school, Jenya moved to United States and worked in different capacities at an accounting company in San Diego, CA, while taking classes at the San Diego Community College and volunteering at the tutoring center and a local hospital.

In 2008, Jenya transferred to University of California Berkeley where she studied Chemical Biology. During this time, she participated in research projects in labs of Dr. Eva Nogales, in the Molecular and Cell Biology department/HHMI, and Dr. Buford Price, in the department of Physics/Space Science Laboratories. Additionally, Jenya was actively involved in scientific educational outreach led by Lawrence Labs and practice of Yongmudo discipline. Jenya earned her Bachelor of Science degree in Chemical Biology in June of 2010.

Building on her interests in research and medicine, Jenya pursued an intramural postbaccalaureate research position at National Institutes of Health, NIAMS, joining the lab of Drs. Eric Hanson and Richard Siegel in August of 2010. Here she worked on translational research combining mechanistic and clinical work with the aim to understand pathophysiology of regulatory processes implicated in inflammatory diseases and immunodeficiencies. This solidified her passion for a career as a physician scientist, prompting her to apply and secure a position with the MD-PhD program at Oregon Health & Science University (OHSU).

In August of 2012, Jenya has started medical school at OHSU and completed the first two years of the medical curriculum as well as a published research project in the lab of Dr. Brian Johnstone. In August 2014, Jenya continued her education by joining the lab of Dr. Owen McCarty in which she pursued a number of biomedical engineering projects with clinically-relevant topics. During her time at OHSU, Jenya submitted a successfully funded grant proposal to receive a Ruth L. Kirschstein National Research Service Award (NRSA, F31HL13623001). Additionally, Jenya was awarded a Chas Patrick Award to sponsor her participation in the Surgical Innovation program (July – October, 2016), combining her interests in medical technology development with the goal of improving patient care. To build on her interest in trauma surgery, Jenya has worked as part of the clinical research team of Dr. Martin Schreiber at OHSU and completed a six months research fellowship in the lab of Dr. John Griffin at the Scripps Research Institute, La Jolla, CA.

Jenya's research has been published in a number of peer-reviewed journals and presented at academic conferences including the Keystone Symposia Clinical Immunology conference, American Physician Scientist Association meetings, International Society of Thrombosis and Hemostasis conferences, Gordon conference, Arteriosclerosis Thrombosis and Vascular Biology conferences and Biomedical Engineering Society conference. During the last year of her PhD, Jenya and her husband of over 13 years, Dmitriy Zilberman, have biked 564 miles, ran 252 miles and dug out and relocated over a 1000 of cubic feet of dirt out of the backyard of their newly acquired house.

Training, funding, achievements, current publications and select presentations are listed on the next four pages in Curriculum Vitae.

## Curriculum Vitae

### EDUCATION / TRAINING

- 2012 – Oregon Health & Science University, MD-PhD Candidate, Biomed Engineering  
2010 – 2012 National Institutes of Health, NIAMS, Postbac Fellow/IRTA, Autoimmunity/MCB  
2005 – 2010 University of California, Berkeley, BS Chemical Biology

### RESEARCH EXPERIENCE

- 2014 – Coagulation / Thrombosis / Fluid dynamics, Biomedical Engineering department,  
PI: Owen J.T. McCarty, PhD, Oregon Health & Science University, Portland, OR  
Co-mentor: András Gruber, MD, Oregon Health & Science University, OR
- 2017 Trauma-induced coagulopathy, Department of Molecular Medicine,  
PIs: John H. Griffin, PhD, Hiroshi Deguchi, MD, PhD, The Scripps Res. Instit., CA  
Co-PIs: Mitchell J. Cohen, MD, Ernest Moore, MD, Trauma, UC Denver, CO
- 2016 – Trauma / Coagulation / Critical and Acute care, Department of Surgery,  
PI: Martin Schreiber, MD, Oregon Health & Science University, Portland, OR
- 2016 Surgical Innovation Internship, Department of Surgery and OCTRI joint program,  
Lead by: John Hunter, MD/ Sharon Kryger, Oregon Health & Science University
- 2013 HIF3 / Articular cartilage formation, Orthopaedics and Rehabilitation,  
PI: Brian Johnstone, PhD, Oregon Health & Science University, Portland, OR
- 2010 – 2012 Rare immunodeficiencies and hyperinflammatory diseases / NF- $\kappa$ B, NIAMS,  
PIs: Eric P. Hanson, MD and Richard Siegel, MD, PhD, NIH, Bethesda, MD
- 2009 – 2010 Microtubule assembly / Proteomics, Molecular Cell Biology Department,  
PI: Eva Nogales, PhD, University of California, Berkeley/HHMI, Berkeley, CA
- 2010 Cryobiology / Ice-core extractor design, Space Science Laboratory, Physics,  
PI: Buford Price, PhD, University of California, Berkeley/SSL, Berkeley, CA
- 2008 Compound synthesis and analysis / Diabetes research, Medicinal chemistry,  
PI: Mihai Azimioara, MA, Novartis Research Foundation, San Diego, CA

### REVIEWER

- 2016 – Platelets

### TEACHING & OUTREACH

- 2013– OHSU Med. curriculum steering / Allied health anatomy course / GIE tutoring.  
2013– Outreach, VirtuOHSU, MedStars, Saturday Academy, OMSI, Johnson Scholars  
2012–2014 Medical volunteer, SW Community Health Center, Portland, OR.  
2011–2012 Medical volunteer, Oncology ICU, Johns Hopkins Medicine, Bethesda, MD.  
2011–2012 Science outreach, Scientific Director Office / IRP, NIAMS, NIH, Bethesda, MD.  
2010 K8 science mod. developer & instructor, Lawrence Hall of Science, Berkeley, CA  
2009 Co-founder and Dir. of Recruitment and Community Outreach, Fruitful Minds  
2007–2008 TA/Science outreach, Chem. Department, SD Mesa Community College, CA  
2006–2008 Senior Math/Physics/Chemistry Tutor, SD Mesa Community College, CA.

## **MENTOR**

- 2014 – OHSU: Chantal Wiesenekker, Jeevan Maddala, Stephanie Reitsma, Daniel Sallee, Tal Eshel, Hari Lakshmanan  
2010 – 2012 NIH: Lamine Aloui, Alex Wessel  
2009 – 2010 UC Berkeley: Vivek Musinipally, Sara Sun

## **OTHER WORK EXPERIENCE**

- 2005 – 2007 Accountant I, National Franchise Financial Services, San Diego, CA  
2004 – 2005 Corporate Purchasing Manager, VP Market: Maxima/T-market, Tallinn, ESTONIA

## **PROFESSIONAL MEMBERSHIPS**

- 2017– American Heart Association  
2017– American College of Surgeons  
2017– Wilderness Medicine Society  
2016– Biomedical Engineering Society  
2015– International Society of Thrombosis and Hemostasis  
2012– American Physician Scientist Association  
2010 US Immunodeficiency Society

## **GRANTS**

- 2016 – 2020 Ruth L. Kirschstein National Research Service Award (NRSA)

## **AWARDS & HONORS**

- 2017 Biomedical Engineering Society Travel Award to CMBE Conference  
2017 Graduate Student Organization Award  
2016 – 2017 N. L. Tartar Trust Fellowship  
2016 Chas Patrick Award  
2015 – 2016 June & Robert Koler Travel Award  
2013 ASM Raymond W. Sarber Award  
2012 Keystone Symposia Scholarship Future of Science Fund Scholarship  
2011 US Immunodeficiency Network (USIDNET) Travel Award for CIS meeting  
2010 – 2012 Intramural Research Training Award, the National Institutes of Health  
2008 – 2010 UC Berkeley Undergraduate Grant  
2009 – 2010 Space Sciences Laboratory (SSL) Work-Study Award  
2009 – 2010 Federal S.M.A.R.T. Grant  
2009 – 2010 Federal Pell Grant  
2008 – 2009 Rodkey Scholarship  
2008 – 2009 Phoebe A. Hearst Memorial Scholarship for women in science  
2008 – 2009 E & V Esberg Scholarship  
2006 – 2008 Outstanding Contributions to the Math and Science Tutoring Center  
2006 – 2008 Dean's Honor List & The Honors Book Award (4 semesters)  
2008 W. J. Agnello Memorial Scholarship for Academic Excellence in Science  
2008 M&M Dietschman Academic Achievement and Leadership Award  
2008 Chemistry Department Award for Outstanding Scholarship and Leadership  
2007 Val and Ron Ontell Future Teacher Scholarship  
2007 Academic Senate Award  
2007 Whitney M. Young Memorial Award

## RESEARCH PUBLICATIONS

1. Rigg RA, Healy LD, Chu TT, Ngo ATP, Mitrugno A, **Zilberman-Rudenko J**, Aslan JE, Hinds MT, Vecchiarelli LD, Morgan TK, Gruber A, Temple KJ, Lindsley CW, Duvernay MT, Hamm HE, McCarty OJ. Protease-activated receptor 4 (PAR4) activity promotes platelet granule release and platelet-leukocyte interactions. *Platelets* 2018; Accepted for publication Nov 2017.
2. Garland KS, Reitsma S, Shirai T, **Zilberman-Rudenko J**, Tucker EI, Gailani D, Gruber A, McCarty OJ, Puy C. Removal of the C-terminal domains of ADAMTS13 by activated coagulation factor XI induces platelet adhesion on endothelial cells under flow conditions. *Front Med* 2017 Dec[Epub ahead of print].
3. **Zilberman-Rudenko J**, McCarty OJT. Utility and development of microfluidic platforms for platelet research. *Platelets*, 2017;28(5):425-426.
4. **Zilberman-Rudenko J**, Sylman LJ, Garland KS, Puy C, Wong AD, Searson PC, McCarty OJT. Utility of microfluidic devices to study the platelet-endothelium interface. *Platelets*, 2017;28(5): 449-456.
5. **Zilberman-Rudenko J**, Sylman LJ, Lakshmanan HHS, McCarty OJT, Maddala J. Dynamics of blood flow and thrombus formation in a multi-bypass microfluidic ladder network. *Cell Mol Bioeng*, 2017;10(1): 16-29. (with Editorial)
6. Sylman LJ, Daalkhaikav U, Zhang Y, Gray EM, Farhang PA, Chu TT, **Zilberman-Rudenko J**, Puy C, Tucker EI, Smith SA, Morrissey JH, Walker TW, Nan XL, Gruber A, McCarty OJT. Differential roles for the coagulation factors XI and XII in regulating the physical biology of fibrin. *Ann Biomed Eng*, 2017;45(5):1328-1340.
7. **Zilberman-Rudenko J**, Itakura A, Maddala J, Baker-Groberg SM, Vetter R, Tucker EI, Gruber A, Gerdes C, McCarty OJT. Biorheology of platelet activation in the bloodstream distal to thrombus formation. *Cell Mol Bioeng*, 2016;9(4):496-508.
8. Deguchi H, Sinha RK, Marxhese P, Ruggeri ZM, **Zilberman-Rudenko J**, McCarty OJT, Cohen MJ, Griffin JH. Prothrombotic skeletal muscle myosin directly enhances prothrombin activation by binding factors Xa and Va. *Blood*, 2016;128(14):1870-1878.
9. **Zilberman-Rudenko J**, Itakura A, Wiesenekker CP, Ralf Vetter, Maas C, Gailani D, Tucker EI, Gruber A, Gerdes C, McCarty OJT. Coagulation factor XI promotes distal platelet activation and consumption under shear flow. *Arter Thromb Vasc Biol*, 2016;36(3):510-7.
10. **Zilberman-Rudenko J**, Monaco-Shawver L, Wessel A, Luo Y, Pelletier M, Tsai WL, Lee Y, Vonortas S, Cheng L, Ashwell JD, Orange J, Siegel RM, Hanson EP. Recruitment of A20 by the C-terminal ubiquitin-binding domain of NEMO suppresses NF- $\kappa$ B activation and autoinflammatory disease. *Proc Nat Acad Sci U S A*, 2016;113(6):1612-7.
11. Baker-Groberg SM,\* Bornstein S,\* **Zilberman-Rudenko J**, Schmidt M, Tormoen GW, Kernan C, Thomas CR Jr, Wong MH, Phillips KG, McCarty OJT. Effect of ionizing radiation on the physical biology of head and neck squamous cell carcinoma cells. *Cell Mol Bioeng*, 2015;8(3):517-525; \*-equally contributing first authors.
12. Markway BD, Cho H, **Zilberman-Rudenko J**, Holden P, McAlinden A, and Johnstone B. Hypoxia-inducible factor 3-alpha expression is associated with the stable chondrocyte phenotype. *J Orthop Res*, 2015;33(11):1561-70.

## MANUSCRIPTS UNDER REVIEW/ PENDING

1. **Zilberman-Rudenko J**, Reitsma SE, Puy C, Rigg RA, Smith SA, Tucker EI, Silasi R, Maas C, Urbanus RT, Gailani D, Morrissey JH, Gruber A, Lupu F, Schmaier AH, McCarty OJT. Coagulation factor XII activity promotes platelet consumption in the presence of bacterial-type long-chain polyphosphate in blood flow *in vitro* and bacteria *in vivo*. *Arter Thromb Vasc Biol*, 2018; Responding to reviewers.
2. **Zilberman-Rudenko J**, Zhao FZ, Reitsma SE, Mitrugno A, Pang J, Shatzel JJ, Rick B, Tyrrell C, Hasan W, McCarty OJT, Schreiber MA. Effect of pneumatic tubing system transport on stored platelet concentrate units. *Cardiovasc Eng Tech*, 2018; Submitted for Review Jan 2018.
3. **Zilberman-Rudenko J**, White RM, Zilberman DA, Lakshmanan HHS, Schatzel JJ, Maddal J, McCarty OJT. Design and utility of a point-of-care microfluidic platform to assess hematocrit and blood coagulation. *Cell Mol Bioeng*, 2018; Submitted for Review Feb 2018.

## (SELECTED) RESEARCH PRESENTATIONS

1. **Zilberman-Rudenko J**, Reitsma SE, Puy C, Anh N, Wiesenekker CP, Smith SA, Travers TJ, Morrissey JH, Maas C, Tucker EI, Gruber A, McCarty OJT. Long-chain Polyphosphate Promotes FXII-dependent Platelet Consumption under Shear Flow. ISTH 2017 Congress and 63rd Annual SSC Meeting, Berlin, Germany, July 2017 [Poster]
2. **Zilberman-Rudenko J**, Wong AD, Sallee DE, Reitsma SE, Puy C, Shirai T, Mitrugno A, Searson PC and McCarty OJT. Design and Utility of Extracellular Matrix-embedded Microvessels to Study the Platelet-endothelium Interface. ISTH 2017 Congress and 63rd Annual SSC Meeting, Berlin, Germany, July 2017 [Poster]
3. **Zilberman-Rudenko J**, Zhao FZ, Reitsma SE, Pang J, Tyrrell C, Hasan W, Schreiber MA and McCarty OJT. Effect of Handling on the Functional Utility of Stored Platelet Units. ISTH 2017 Congress and 63rd Annual SSC Meeting, Berlin, Germany, July 2017 [Poster]
4. **Zilberman-Rudenko J**, Reitsma SE, Puy C, Anh N, Wiesenekker CP, Smith SA, Travers TJ, Morrissey JH, Maas C, Tucker EI, Gruber A, McCarty OJT. Coagulation Factor XII Promotes Platelet Consumption in the Presence of Microbial Polyphosphate Under Shear Flow. ATVB/PVD 2017 Scientific Sessions, Minneapolis, MN, May 2017 [Poster]
5. **Zilberman-Rudenko J**, Wong AD, Searson PC, McCarty OJT. *In Vitro* Microvessels to Study the Platelet-Endothelium Interface. ATVB/PVD 2017 Scientific Sessions, Minneapolis, MN, May 2017 [Poster]
6. **Zilberman-Rudenko J**, Sylman LJ, Lakshmanan HHS, Maddala J, McCarty OJT. Dynamics of blood flow and thrombus formation in a multi-bypass microfluidic ladder network. Cellular and Molecular Biomedical Engineering Conference, Kona, HI, January 2017 [Talk].
7. **Zilberman-Rudenko J**, Puy C, Anh N, Wiesenekker CP, Smith SA, Travers TJ, Morrissey JH, Maas C, Tucker EI, Gruber A, McCarty OJT. Coagulation factor XI promotes platelet consumption in the presence of microbial polyphosphate under shear flow. 2016 Hemostasis Gordon Research Conference, Stowe, VT, July 2016 [Poster]

8. **Zilberman-Rudenko J**, Gruber A, and McCarty OJT. Coagulation factor XI promotes distal platelet activation and single platelet consumption in the bloodstream under shear flow. 2016 joint ASCI/AAP Meeting, Chicago, IL, 2016 [Poster]
9. **Zilberman-Rudenko J**, Itakura A, Tucker EI, Gailani D, Smith SA, Choi SH, Morrissey JH, Gruber A, and McCarty OJT. Role of the coagulation factor XI in promoting distal platelet aggregation and thrombus formation in whole blood under flow. ISTH 2015 Congress and 61st Annual SSC Meeting, Toronto, BC, Canada, 2015 [Poster]
10. **Rudenko J**, Hanson EP. Ubiquitin Binding Specificity Plays an Important Role in the  $\Delta$ CT-NEMO Syndrome Pathogenesis. NF- $\kappa$ B Signaling and Biology, Keystone Symposium, Whistler, BC, Canada, March 2012. [Talk]

### **ATHLETIC ACKNOWLEDGMENTS**

- |      |  |
|------|--|
| 2010 | Silver, Groundwork and Sparring, UC Berkeley Young Mu Do Martial Arts Friendly   |
| 2006 | Silver, UC San Diego Electrical Engineering School Rowing Team, Dragon Boat Race |
| 2000 | Gold, ESTOPEN International Kickboxing Competition, Tallinn, ESTONIA             |
| 1999 | Silver, ESTOPEN International Kickboxing Competition, Tallinn, ESTONIA           |
| 1997 | Bronze, ESTOPEN International Kickboxing Competition, Narva, ESTONIA             |